

HEAT TRANSFER IN A MOTORED
RECIPROCATING ENGINE

by

ABDULNABI AL-SUDANI

A thesis submitted to the University of Liverpool for the degree
of Doctor in Philosophy.

Department of Mechanical Engineering

December, 1985



IMAGING SERVICES NORTH

Boston Spa, Wetherby
West Yorkshire, LS23 7BQ
www.bl.uk

Text close to edge of page in
original.

Some text is cut off.



ETHOS

Boston Spa, Wetherby
West Yorkshire, LS23 7BQ
www.bl.uk

This thesis contains overlays - each have been scanned over three images.

D E D I C A T I O N

In order to express his sincere thanks to his Wife and sons, for their encouragement and patience throughout this work the author wishes to dedicate his thesis to them.

S U M M A R Y

Investigation of non steady heat transfer in a reciprocating internal combustion engine under motoring condition at different compression and speed have been undertaken.

Instantaneous local velocity and turbulence as measured by hot wire anemometers and gas temperature measured by resistance thermometer together with pressure are correlated with heat flux measured by a rapid response surface thermocouple. The turbulence is included in the correlation.

All data collection and processing was by a mini computer system.

Significant dimensionless numbers used in the correlation are Reynold, total velocity ratio, gas temperature ratio, and energy.

A C K N O W L E D G E M E N T S

The author wishes to express his gratitude to his supervisor MR. C. P. WALKER for guidance, contribution and encouragement, and also to MR. J. HARDCASTLE for his effort in preparing the necessary electronic equipment, MR. J. BOYES for his help with data logging and MR. J. HAUGHIE for his assistance with the apparatus.

Thanks are also extended to all workshop staff, and in particular MR. T. HOBSON.

The author is deeply grateful to his Government for giving him the opportunity, along with their financial support and of course to his parents brothers, sisters and friends for their support and understanding.

Finally, thanks are due to MISS T. BENSON for her careful typing of this thesis.

N O T A T I O N

A	Surface area in m^2
B	Constant in hot-wire equation
C_1, C_2	Constants used in hot-wire equations
CC	Conversion factor for hot-wire equation
C_p	Specific heat
D	Cylinder bore diameter in m
E.M.F	Electric Motive Force
h	Heat transfer coefficient $W/m^2.K^\circ$
k	Thermal conductivity $W/m.K^\circ$
L	Connecting rod length m also the thickness of cylinder head wall
M	Mass of the thermometer wire Kg
n	Index in hot wire equation
N	Engine speed R.P.M.
Nu	Nusselt number = hD/K
P	Pressure N/M^2
Pr	Prandtel number = $\mu C_p/K$
q	Heat transfer in Kw
Q	Heat flux per unit area Kw/m^2
R	Gas constant $J/Kg.K^\circ$ also hot-wire resistance ohm
S	Engine stroke in m
t	Time in Sec.
T	Temperature in K°
U	Ensembl average gas velocity m/sec
U	Turbulence intensity m/sec
V	Volume in m^3
V_p	Mean piston speed m/sec

GREEK LETTERS

α	Thermal diffusivity
ϵ	Correction factor in pressure equation
θ	Angle about the cylinder axis
μ	Coefficient of dynamic viscosity
ν	Kinematic viscosity
ρ	Gas density Kg/m ³
σ	Specific heat of wire material

SUBSCRIPTS

a	Atmospheric conditions
bdc	Conditions at bottom dead centre
g	Gas
hw	Hot-wire
m	Refers to conditions at the maximum thermometer wire temperature, also maximum
o	Reference condition
tw	Thermometer wire
W	Wall Temperature

ABBREVIATIONS

ATDC	After top dead centre
BDC	Bottom dead centre
BTDC	Before top dead centre
CA	Crank angle
CR	Compression ratio
EV	Exhaust valve
EVC	Exhaust valve closed
EVO	Exhaust valve open

IV	Inlet valve
IVC	Inlet valve closed
IVO	Inlet valve open
FRST	Fast response surface thermocouple
TDC	Top dead centre

C O N T E N T S

	<u>Page No.</u>
SUMMARY	i
ACKNOWLEDGEMENTS	ii
NOTATION	iii
CHAPTER 1 INTRODUCTION	1
CHAPTER 2 THERMAL FLUXMETERS AND SURFACE THERMOCOUPLES	15
2.1 Introduction	
2.2 Wakefield's Design	
2.3 Requirements specification of Surface Thermocouple Design	
2.4 First Design	
2.5 Existing Solution	
CHAPTER 3 THEORY OF THE SURFACE THERMOCOUPLE	27
3.1 Theory of E.M.F. Induced by the Surface Thermocouple	
3.2 Time response theory of the Surface Thermocouple	
3.3 Theory of the Surface Thermocouple	
3.4 The Effect of the Cement	
CHAPTER 4 SURFACE THERMOCOUPLE DESIGN	33
4.1 Introduction	
4.2 Manufacturing Process	
4.3 Calibration	
CHAPTER 5 THEORY OF UNSTEADY HEAT TRANSFER IN I.C. ENGINE	40
5.1 Introduction	
5.2 Theory of Turbulence	
5.3 Methods of Predictions	
5.4 Present Prediction	

- 6.1 Introduction
- 6.2 The Engines
 - 6.2.1 Austin - Ricardo Engine
 - 6.2.2 Ricardo E6 Engine
- 6.3 Crank angle Marker and Coupling Device arrangement
 - 6.3.1 Existing Crank Angle Markers
 - 6.3.2 Crank Angle Marker System
 - 6.3.3 Coupling Device Arrangement
- 6.4 Instrumentation Theory
 - 6.4.1 Analysis of the hot wire signal
 - 6.4.2 Analysis of Gas Temperature Resistance Thermometer
 - 6.4.3 Pressure Correction Method
- 6.5 In Cylinder: Instrumentation
 - 6.5.1 Introduction
 - 6.5.2 Pressure
 - 6.5.3 Surface Wall Temperature
 - 6.5.4 Probes Construction
 - 6.5.5 Hot-Wire Anemometer
 - 6.5.6 Gas Thermometer Temperature
 - 6.5.7 Other Equipments
- 6.6 In Cylinder: Calibration
 - 6.6.1 Pressure
 - 6.6.2 Gas Temperature
 - 6.6.3 Velocity

CHAPTER 7	EXPERIMENTAL PROCEDURE	70
7.1	Introduction	
7.2	General Procedure	
7.3	First Stage of the Experiments	
7.4	Second Stage of the Experiments	
CHAPTER 8	DATA LOGGING AND CALCULATION	75
8.1	Introduction	
8.2	Instrumentation	
8.3	DATA Collection Procedure	
8.4	DATA Processing Method	
8.5	Calculation	
8.5.1	Calculating Gas Temperature from Gas Pressure	
8.5.2	Calculating Heat Flux from Surface Temperature	
8.5.3	Calculation of Re and Nu Numbers	
8.5.4	Correlation	
CHAPTER 9	DISCUSSION OF RESULTS	87
9.1	Introduction	
9.2	Primary Results	
9.2.1	Surface Wall Temperature	
9.2.2	Pressure	
9.2.3	Gas Temperature	
9.2.4	Hat Wire Signal	
9.3	Derived Results	
9.3.1	Heat Flux	
9.3.2	Reynold Number	
9.3.3	Energy Number	
9.3.4	Nusselt Number	
9.3.5	Gas Temperature Ratio	
9.3.6	Total Velocity Ratio	

9.4 Correlation

CHAPTER 10 CONCLUSION AND SUGGESTION FOR FURTHER WORK 107

10.1 Conclusion

10.2 Suggestion for Further Work

REFERENCES 111

APPENDICES

CHAPTER 1

INTRODUCTION

It is very important to have an understanding of the unsteady heat transfer during the operation of an internal combustion engine for design and improvement in performance purposes.

Many attempts have been made to provide an empirical formula for the estimation of instantaneous heat transfer rate. Because of large variations in the magnitude of the convective component of heat transfer from engine to engine, or even from point to point in the same engine cycle, this is because of variations in flow pattern, the existing formula ragain improvement.

The exact solution for predicting the heat transfer does not exist yet, an approximation and simplification must be considered to give reasonable agreement with the experiment evidence. For steady flow the heat transfer coefficient is usually used ($h = q/A(T_g - T_w)$ where T_g is fluid temperature and T_w is surface temperature). The condition in an internal combustion engine is different, it is unsteady, and one assumption then can be made is that the heat transfer is regarded as quasi-steady so that instantaneous heat transfer rate is proportional to the temperature difference and surface area existing at that instant. From experimental and theoretical investigation Ref. (8) the condition in an Internal combustion engine is not quasi-steady, because of the thermal capacity of the boundary fluid, there is a phase lag between driving temperature difference and resulting flux at the surface i.e. the temperature difference and the heat transfer rate are not zero simultaneously Refs. (44, 107). These are very difficult considerations and the difficulty of finding a useful approach is severe.

Heat transfer problems in an internal combustion engines have been of interest to many research workers. An early approach was made by Nusselt Ref. (103), his formula was built up on the basis of measurements of the heat loss from cylindrical bombs after the ignition of a quiescent air-fuel mixture. The formula, which consists of two components of heat transfer convection and radiation, tested by comparing time-average heat loss calculated from it with some early measurements. The conclusion made was the formula is satisfactory for the compression stroke but for the remainder cycle was less satisfactory. In addition to that the radiant heat transfer term was small compared with convective term. This formula is now little used, but Briling used the same expression but he replaced the constant of the piston-speed bracket with a different one, this formula reported in Ref. (28). This formula is dimensionally incorrect and it does not predict a sufficiently large radiative contribution to heat transfer Ref. (28).

Eichelberg Refs. (39, 40, 41) attempted direct measurement of instantaneous heat transfer in an operating engine by choosing a point in the combustion chamber, such that the heat flux through the wall may be expected to be substantially normal to the surface. The temperature variation with the time of the metal surface at the location was observed. From experimental data, apparently based on the experimental work reported by Hug Ref.(68) Eichelberg published his formula in 1939. Quite good agreement with measurements of Elser Ref.(44) and Oguri Ref. (104) was also found.

Moss Ref. (99) carried out experiments on a Benz single cylinder petrol engine motored at speeds from 600 to 1400 r.p.m. The heat transfer from gas to walls by convection when running under power was found to be

about one half of the total heat transfer, the remainder being due to radiation unlike Nusselts small quantity. The total heat transfer are also proportional to the square root of the gas density, temperature difference and $\text{Log}(1 + Cn)$ (where C is a constant and n is engine speed rps). The coefficient of heat transfer also found greater for induction stroke than for the remainder of the cycle.

Many workers have been involved with the analogy between certain aspects of heat transmission in internal-combustion engines, and heat transmission by forced convection between fluids and solid surfaces Refs. (22, 72, 81, 110, 111, 112, 131)

Taylor Ref. (132) discussed the limitations of the analogies of the previous workers, and pointed out how its usefulness can be extended, provided these limitations are observed. The conclusion obtained was that a limited current of data, properly correlated, can be used to give useful information on heat flow and temperatures in internal combustion engines.

Overbye et al Ref. (107) carried out experimental work with suitable mathematical analysis to give instantaneous heat transfer rates through the gas-metal interface. The heat transfer coefficients in unsteady heat transfer were evaluated. A theoretical analysis and correlation of experimental data were obtained. The experiments were carried out with two CFR engine in petrol engine form with fired and motored conditions in two different procedures. The result obtained did not correlate well with Eichelberg Ref. (40). The experimental detail was different (thermo-couple positioning etc) and Eichelberg used a diesel and Overbye a petrol engine. Also a correlation, obtained for heat transfer in a

motored engine, showed a good result when applied to experimental data.

Pflaum Ref. (109) attempted to improve the Eichelberg (Ref. 2) formula by amending the mean piston speed dependant term, and applying a correction factor which is dependant upon intake-manifold pressure. These were obtained by measurements of time-mean heat transfer rate on a four-stroke, prechamber-type diesel engine. The factor was intended by Pflaum to cover differences in transfer conditions to different parts of the engine. The conclusion was obtained on the basis of estimates that about half of this difference resulted from different flow conditions over the various parts and the other half from differences in radiative transfer to the polished liner and to the carbon-covered head and piston crown.

Annand Ref. (8) criticised the formulas reported in Refs. (28, 40, 44, 103, 104, 107, 109) in that they fail in one way or another to meet important requirements, and tried to construct a new relation to describe the instantaneous heat transfer. The data of Elser Ref. (44) and Overbye Ref. (107) were re-analysed. The conclusion obtained was that inspite of the phase lag between gas temperature change and heat flux variation the instantaneous heat transfer coefficient used in a quasi-steady manner can be used successfully in the analysis of heat transfer in reciprocating engines. The gas properties were evaluated at the average charge temperature derived from cylinder pressure, cylinder volume, and molal charge contents.

Ebersole et al Ref. (38) studied the relative magnitude of the time-averaged radiant and convective heat fluxes in diesel engine. The transient effect of the surface temperatures was neglected and a time-averaged surface temperature was observed. The conclusion obtained was the time-averaged radiant heat transfer accounts for 5 - 10% of the total heat transfer at low engine load, and 35 - 45% at near maximum load. It seemed to be that a higher per cent of radiant heat transfer occurs during the combustion and expansion portion of the cycle than during intake and exhaust, and the type of fuel and combustion could significantly affect the radiant heat transfer.

Knight Ref. (78) carried out estimations of the heat transfer in a diesel engine. The calculation was based on the analogy of the heat transfer coefficients for flow in pipes and this approach was used by French and Hartless Ref.(46). The instantaneous heat fluxes measured by surface thermocouple were compared with theory.

Henein Ref. (62) used the calculated velocity instead of mean piston velocity which is used by many workers Refs. (40, 103, 107, 109). The total heat transfer was calculated and a comparison showed the result due to Eichelberg Ref. (40) were lower than the results obtained by Henein for the heat transfer coefficients. It was suggested to divide the cycle into parts according to the turbulence present during each part. The highest values of heat transfer occur during combustion, not only due to high pressures and temperatures reached by the gas but also because of the high turbulent gas velocities produced.

Detailed simulations by computation and theory for the heat transfer in internal combustion engine have been carried out by many research workers Refs. (12, 52, 54, 80, 129).

Woschni Ref. (152) has introduced a method for determining the heat transfer coefficient for internal combustion engines. An equation has been derived containing two convective terms, one of which takes into account the piston motion and the other the convection due to combustion. These terms, expressed as constants, relate fluid flow conditions during the induction period (including scavenging) and take into consideration the type of combustion system. The result was a universally applicable equation designed for evaluating heat transfer coefficients. This equation can be valid if different constants are introduced for different engine designs, which are valid for geometrically similar engines. These constants must be determined experimentally by a statistical evaluation of heat balances. The work of Woschni discussed by many workers, and they raised many points missing from the work without consideration, this reported in Ref. (152).

Whitehouse Ref. (146) carried out many tests to obtain the instantaneous and mean values of heat transfer at various positions in the combustion chamber for different load and speed and comparing these with those obtained theoretically from synthesized cycle calculations using Annand's and Woschni's formulas. The conclusion obtained was that the concept of a mean gas temperature used in the formulas by many workers can not be realistic, and that development was needed in flux measurement.

Annand Ref. (9) in 1970 measured of instantaneous heat transfer rate from the working fluid to the cylinder head of a small open-chamber, four stroke compression - ignition engine at five points on the surface. The conclusion obtained was that the magnitude and the form of the heat flux variation during the cycle depend greatly on local conditions, the heat flux analysis was in terms of the bulk mean properties of the working fluid and the time derivative of the bulk mean temperature was added to the quasi-steady relation for the non-steady condition.

Hassan Ref.(59) used an approach based on the correlations used in flat plate turbulent flow and the agreement with the experimental result was within 20 per cent. Direct measurements of gas velocity , gas pressure, gas temperature and surface wall temperature were obtained. Further work is reported in Ref. (60).

Dao et al Ref. (31) studied the instantaneous heat transfer rates at the interface of the working gas and the walls of a motored engine. The effect of engine speed, compression ratio, intake pressure, swirl ratio, location on the cylinder head surface, and the shape of the piston top were studied. Relations were developed between heat transfer and the engine variables.

More recently many research workers Refs. (35, 47, 64, 71, 102, 125 140, 143, 153, 154), have been involved in heat transfer investigations with extensive experimental results and new correlations based on the earlier methods. These studies were carried out for both diesel and spark ignition engines.

In 1980 Borgnakke et al Ref. (19) developed a model for the instantaneous heat transfer and turbulence in a spark ignition engine. The model is in terms of an unsteady boundary layer, which has been affected by the free stream turbulence level and the rate of flame propagation in the combustion chamber of an engine having a simple pancake geometry. The turbulent Reynold number and the integral length scale have been used to describe the turbulent field effect on the heat transfer rate. This has been compared with the Annand and Woschni correlations which have less sensitivity, to the geometry and operating conditions, than the model result. This model was a further development of previous work in this field Refs. (25, 51, 63, 113, 120) what was new in this model was the introduction of the length scale, and compressibility effects in the calculation of kinetic energy.

Alkidas Refs. (3-6) carried out many experiments to measure the transient heat flux at different positions in a spark ignition engine. The influence of many parameters, engine speed, air fuel ratio and volumetric efficiency, on heat flux have been investigated. The load and injection timing effects on the distribution of heat rejection to the coolant of a single-cylinder diesel engine were carried out. Most of his work was experimental. Conclusions were made that; the peak heat flux increases with increasing engine speed; if the volumetric efficiency increased from 40 - 60 percent there is an increase by 30 percent in peak heat flux; and the peak heat flux reach a maximum near-stoichio metric mixture composition.

In order to aid the understanding of the heat transfer problem in the cylinder of an internal combustion engine, it is important to measure the air motion characteristics inside the cylinder. In addition to the

air motion effects on the heat transfer other parameters that change gas properties are significant (volumetric efficiency, scavenging, mixing, fuel evaporation, the combustion, friction, efficiencies, energy conversion, etc).

During the valve open period the gas motion in the cylinder is as a result of two motions, piston movement and the motion induced by the valves being open and these persist during closed periods. During the valve closed period the gas motion is generated are complex and unsteady, the complexity and the unsteadiness is due to the large change in the density and temperature of the gases in the cylinder and the periodic motion of the piston respectively.

Gas motion studies have been a topic of interest for a long time. An early simple experiment was set by Clark Ref. (18), showed the importance of the effect of gas motion on combustion.

Ricardo Ref. (116) used a vane anemometer for measuring the swirl and developments of this method have continued to be used by Refs. (1, 97, 133, 142). The vane anemometer is not adequate for measuring the detail of gas motion in the cylinder, but the method is used to produce a swirl parameter of use in engine design.

More recently the introduction of the hot-wire anemometer provides a suitable and reliable measurement for air motion investigation. Since the geometrical size of the probe is small and this allows the measurement to be carried out in boundary layer regions. The time constant of the anemometer is small and permits high-frequency velocity variation such as turbulence to be measured.

The first research of using the hot-wire technique in an internal combustion engine was carried out in 1939 by Wenger Ref. (145). Many workers have since been involved of using the hot wire technique in an engine Refs. (11, 43, 49, 61, 66, 67, 73, 83, 124, 136, 139, 148, 149). Since the condition in the cylinder is complex, it needs to be simplified into number of separate areas to be studied separately in order to have better understanding. Wenger carried out his investigation for the flow in a 4-stroke engine, and the effects of engine variables speed, compression ratio, throttle opening and jacket water temperatures were studied for different strokes. The result found was the maximum air velocity occurred during the induction stroke and this agreed with Ref. (124). The readings were also averaged over the entire stroke. The mean velocity increased linearly with increasing engine speed and a 20% increase in the compression ratio lead to a 10% increase in the air velocity.

Semenov Ref. (124) carried out measurements on a motored CFR engine. An automatic compensation for gas temperature and pressure variation Refs. (27, 123) was employed. The turbulence and the effect, of crank angle, the radius of the point of measurement, engine speed, compression ratio and the volumetric efficiency were studied for both induction and compression strokes.

The result obtained shows that if the engine speed increased the flow parameters increased linearly, during induction stroke. The average and the rms velocity were found to drop suddenly after IVC (inlet valve closed). During the compression stroke, the average velocity was found to decrease as the middle of the stroke was approached and to generally increase with the square of the engine speed. The flow parameters were

found to depend on the radius of the point of measurement (disagree with Wenger's result Ref. (145)). As the time rate of change of velocity increased (due to a change in throttle setting or engine speed) the turbulent intensity increased. It was suggested that the jet nature of the flow during induction stroke was the main source of turbulence.

Dent and Salama Refs. (33, 34) measured turbulence parameters on two motored spark-ignition engines at the spark plug location. The results showed good agreement with those of Semenov.

Tindal Ref. (135) used a hot-wire anemometer to measure the flow downstream of a central orifice in the cylinder head of a single stroke apparatus. The results compared well with those calculated from pressure difference readings.

Horvatin and Hussmann Ref. (66) carried out their investigation by using hot-wire anemometer probes at 5 locations in the cylinder head. A method to correct the output from the anemometer for gas temperature and pressure was employed. The result shows the gas velocity was proportional to engine speed.

Lobo Ref. (88, 89) examined the hot-wire validity in an engine in details. The limitations of wire dimensions, operating conditions, sensitivity and calibration stability were studied. The result showed that the hot-wire is sensitive to direction, having a high frequency response, stable calibration and satisfactory mechanical strength.

El-Khafaji Ref. (42) carried experiments in the combustion chamber and swept volume of a motored diesel engine. The temperature changes on the output of the anemometer was compensated automatically Ref. (42, 43). The result showed the axial component of the flow to diminish after IVC, as expected, swirl was found to increase with increasing engine speed or increasing pressure though the flow pattern was unaffected. Predicting the swirl in the induction stroke from steady flow tests on the cylinder head was carried out.

Dent and Derham Ref. (32) used a three-wire anemometer probe in order to measure both velocity magnitude and direction of the air flow. In this type of probe, the three wires are mutually perpendicular to each other. The swirl process was studied throughout the induction and compression stroke. A theoretical model for mean air swirl was developed and showed a good agreement with the experiment.

Many workers have carried out experiments in a fired engine Refs. (2, 70, 74, 75, 76, 105, 106). An electric discharge method was used to measure gas velocities under fired conditions in a 4-stroke diesel engine Refs. (105, 106). The electric discharge produce an ion cloud in the gas and the cloud moves down stream with the gas and is detected by a probe. The time taken by the ion cloud to move from the electrodes to the probe is inversely proportional to the gas velocity.

Flow visualization and photography was used in internal combustion engine to study the complete cycle but with little success as far as air movements are concerned. Many workers have used different methods of flow visualization Refs. (2, 49, 86, 100, 101, 119, 150).

A schlieren method was used for flow visualization in internal combustion engine Refs. (20, 91, 134).

The hot-wire anemometer has many disadvantages, such as fragile nature of the wire, a single wire is unable to detect the directions of the flow, the flow field is disturbed, it requires preliminary calibration, it does not allow a point measurement and it is difficult to use in a fired engine. The laser doppler velocimeter has been developed for flow measurement investigations. The first application of laser doppler to fluid mechanics was made by Ref. (155).

The laser doppler has been used by many workers in internal combustion engines Refs. (29, 53, 69, 95, 98, 114, 122, 147). The laser doppler anemometer has many disadvantages, such as the complication of the optical access to the chamber, seeding must be added to most gaseous flows. Whatever the method large amounts of data need to be collected rapidly and modern data logging systems have made this possible. A computer memory becomes cheaper the capability is improving continuously with on line computers, processing may also be immediately carried out.

Apart from the experimental techniques for flow measurement and heat transfer in an internal combustion engine theoretical and computation analysis has been carried out to aid the understanding and many workers have been involved in this direction Refs. (12, 13, 17, 48, 51, 52, 54, 80, 129, 137).

From the work described here in both diesel and spark-ignition engines, it can be classified into three main categories according to the type of the work carried out:-

1. Heat transfer investigations
2. In cylinder flow investigations
3. Heat transfer and in cylinder flow together.

In the present work the heat transfer and in cylinder flow adjacent to the heat transfer surface were studied experimentally in a motored E₆ four stroke engine in a petrol form. A surface thermocouple was developed, having time response of 0.5 m sec., 20 μsec for 5 micron and 1 micron film thickness respectively, for measuring instantaneous heat transfer. The hot-wire anemometer was used for velocity and turbulence measurement. Gas temperature and pressure were measured by a fine resistance wire and kistler transducer respectively. A mini computer was used to log and process the data.

CHAPTER 2

THERMAL FLUXMETERS AND SURFACE THERMOCOUPLES

- 2.1 Introduction
- 2.2 Wakefield's Design
- 2.3 Requirements Specifications of Surface
Thermocouple Design
- 2.4 First Design
- 2.5 Existing Solution

2.1 Introduction

The heat transfer between the working fluid of a reciprocating internal combustion engine and its combustion chamber walls has long been a topic of interest because of the problem of cyclic thermal loading and because of its effect on engine thermodynamics performance. The investigation of heat transfer during the cycle in an internal combustion engine needs the use of a temperature measuring device with a particularly fast response to temperature change.

The basic principles of the surface thermocouple were reported by Hackemann Ref. (56) who described a special thermocouple, developed in Germany during World War II, for gun barrel surface temperature measurement. The early development for internal combustion engine work was carried out by Bendersky Ref. (14) 1953, whose surface thermocouple design is shown in Fig. 2.1a.

The surface thermocouple has since been used for gunbarrel temperature measurements Refs. (10, 50, 96) and for surface temperature measurements in internal combustion engines.

In 1961 Overbye and his colleagues at University of Wisconsin Ref. (107) constructed a thermocouple with a one micron thermal junction below the surface of the combustion chamber wall of an engine, Fig 2.1b shows the construction which was different in shape to the Bendersky design but used the same principles. Ebersol and Myers Ref. (38) constructed a fast acting nickel-steel surface thermocouple Ref. (14), with the modification of including a sapphire window for radiation measurement as in Fig. 2.1c. The temperature of the surface beneath the window was

at a considerably lower temperature than the exposed wall surface. This temperature difference along the wall will cause multidimensional heat transfer, but their analysis was one-dimensional. An experiment was performed by replacing the window with a disk of opaque material and the result showed only a small decrease in the temperature recorded by the thermocouple, when compared with those measured with a window in the holder. This confirmed that the multidimensional component of heat transfer in this holder were significant. Fig. 2.1d shows the addition of air as a thermal insulation to reduce the multidimensional heat transfer. It was reduced to less than 4% of the total heat transfer at full load.

Fig. 2.1e shows the design of a surface thermocouple by Knight Ref. (78), experiments were carried out for different thickness of the thermal junction (0.005, 0.0025 and 0.001 inches). Extrapolation of the results to zero thickness shows that the actual surface temperature is less than the surface temperature registered by a surface thermocouple of finite thickness. The thermocouple element materials were platinum-13% Rhodium of 0.010 in diameter.

The properties of platinum are such that its thermal conductivity and heat capacity on a volume basis are not very different from that of steel. The electrical insulation of the thermocouple was glass and it was found that despite a correction for thermocouple thickness, the thermal insulation of the glass resulted in an over estimate of the temperature fluctuations.

Later attempts were made to improve the Bendersky thermocouple Ref. (62, 127, 87) and these are shown in figures 2.2a,b,c, respectively

In 1970 Annand & Ma Ref. (9) criticized these designs for two main reasons: firstly, after a certain stage in manufacture it becomes impossible to verify the integrity of the insulation of the wire; and secondly, they can be situated in the engine only where direct drilling through to the coolant side is possible. In addition, they suffer a high failure rate in service. A new method was developed to construct the new surface thermocouple as shown in Fig. 2.2e. First a lead was laid down on the iron cylinder head surface from the point at which measurement was wanted to a suitable terminal point. This was done by vacuum deposition of three successive films: first, a layer of aluminium to provide a bond; second, a layer of magnesium flouride as insulator; and finally, a layer of antimony. The total thickness was less than 0.005 mm. After the insulation was checked the thermocouple was completed by laying down a small section of antimony film to connect the existing film to the iron surface at the desired point. The result shows that the surface temperature is place dependent and its variable from cycle to cycle.

Hassan Ref. (59) and Whitehouse Ref. (146) carried out experiments by using the surface thermocouples shown in Figures 2.3a,b, respectively which use the same design principle as Bendersky Ref.(14). Hassan showed that the experimental results were adequate when compared with those data based on a flat plate heat transfer theory. Whitehouse concluded that to obtain actual instantaneous heat transfer, three-dimensional analysis should be used or to ensure the heatflow through the surface thermocouple is one-dimensional.

In 1973 Dao Ref. (31) had constructed a new fluxmeter to measure the heat flux in a motored piston engine. The cylinder head was modified and the valve system was replaced by the heat fluxmeter as shown in Fig. 2.3c. The heat fluxmeter shown in Fig. 2.3d which consists of a thin pyrex substrate having a thermistor deposited on both faces. The thickness of the thermistor and pyrex was 3×10^{-6} in, 0.005 in respectively. The problem of heat transfer was considered one-dimensional and solved by using electrical analogy. An observation was obtained that the heat fluxes would be the same at the same distance from the cylinder center. The effect of the oil contamination on the fluxmeter surface was investigated.

In 1974 Mattavi Ref. (92) had designed a miniature sensor to measure the heat transfer rates in engines. The sensor consists, basically of two thermocouples which are precisely positioned within a stepped cavity.. Each thermocouple is made up of a cylindrical contact which contains sheathed thermocouple wires. A thermocouple junction is located on the front and rear face as shown in Fig. 2.4a. A special technique was used by measuring the temperature simultaneously at two locations whose separation distance is accurately known. Fig. 2.4b shows the sensor installed in the wall of a liquid-cooled combustion chamber.

In 1977 Dent and Suliaman Ref. (35) tried to produce and use a surface thermocouple of the Bendersky type but they were not successful, because the surface thermocouples produced a high level of electrical noise. Therefore a new design of surface thermocouple was developed as shown in Fig. 2.4c. The use of a final layer of magnesium flouride over the film thermocouple produced a detector which was capable of withstanding the arduous conditions encountered during the firing of the engine, and also, a protective layer against catalytic reaction.

A major improvement to the signal output from the surface thermocouple was achieved.

In 1979 Kamel and Watson Ref. (71) used a surface thermocouple of the coaxial type, manufactured by ASEA and having a response time of $180 \mu\text{s}$. as shown in Fig. 2.5a. The sensor incorporates a second thermocouple 6 mm from the surface. In addition, a traversing thermocouple of the Ricardo type was used to obtain some correspondence with published data measured with this technique, in the area of the connecting passage. Fourier analysis of the surface temperatures was used for heat transfer calculation.

Hohenberg Ref. (64) developed a special design of surface thermocouple as shown in Fig. 2.5b. The measuring element consists of a mineral insulated thermocouple material of 0.5 mm diameter which is installed slightly protruding over the surface. For reasons of strength the insulating ceramic material has been replaced by a highly temperature resistant cement to a depth of approximately 1 mm. All measuring points are refaced by grinding to provide a smooth surface, which is coated by a thin layer of gold to establish the electrical connection between the Nicr and Ni-wires and is decisive for the function and the response of the thermocouples. The output from the surface thermocouple was adequate for heat transfer prediction.

Sihling and Woschni Ref. (126) used Bendersky type thermocouple, with vacuum deposited chrome plating of one micron thickness, in the form of a screw as shown in Fig. 2.5c. The heat transfer result does not agree with the calculated one because of the one-dimensional assumption, a method was used for correction.

In 1980 Alkidas Ref. (4) designed a heat flux probe from commercially available surface thermocouples, but with certain modification to minimize distortion of isotherms in the cylinder head as shown in Fig. 2.5d. The surface junction was formed by abrading the exposed thermocouple ribbon elements at the probe tip with a very fine carborundum stone to produce contacts among the microscopic fibres of the ribbons, furthermore, the in-depth thermocouple was placed as close as possible to the tip of the probe to reduce two-dimensional effects. One-dimensional analysis for heat transfer calculation was used. The surface thermocouple was used for fire and motored engine tests.

Guernigou and his colleagues (Ref, 55) have designed surface temperature fluxmeters for measuring convective and radiation heat transfer. Small dimensions were looked for and obtained with techniques that ensured a good repeatability of the characteristics of the thermometric component. The operating principle of surface temperature fluxmeters is based upon the diffusion of heat in a semi-infinite medium, the flux at the surface being linked with the evolution of surface temperature. Figs. 2.5e, f1, f2, show the construction of sensitive element, convective fluxmeters and radiation fluxmeter respectively.

In 1981 and 1982 Refs. (3, 6) Alkidas and Myers carried out research on the internal combustion engine using the surface thermocouple designed by Alkidas (4).

Law Ref. (85) designed a piston surface thermocouple as shown in Fig. 2.2d which consists of a mild steel body into which an oxide coated nickel wire was inserted. A wire drawing process on the body was then used to retain the wire. The wire was allowed to protrude at one

end, and the other end was polished and a thin nickel film was deposited. Law observed a high frequency noise on the output of the surface thermocouple thought due to magnetostrictive e.m.f. produced by the vibration of the Ni-wire. Hence a complicated method of connection to the wire was used.

Falcus Ref. (45) later concluded that the noise which was observed by Law was due to bad connection or shorting between wires. Falcus modified the surface thermocouple made by Law as shown in Fig. 2.6 to avoid the complicated wiring system. The backing thermocouple was mounted on the same axis.

Both Law and Flacus surface thermocouples designs suffered from an error caused by the presence of protuberance at the back of the surface thermocouple and this called the "Fin" problem. The magnitude of the error caused by Fin presence can be calculated by steady state analysis and if the diameter/length ratio of the Fin is small then it may be assumed that there are no radial temperature gradients within the Fin, and one-dimensional analysis may be applied Ref. (138).

2.2 Wakefield's Design

Wakefield Ref. (138) attempted to reduce the effect of sideways heat flux by insulating the outside diameter of the surface thermocouple to provide a thermal barrier against it, in order to achieve the ideal one-dimensional heat transfer case. Wakefield's surface thermocouple design for piston was based on the design used by Law Ref. (85) and Falcus Ref. (45) with improved techniques, for manufacturing both surface thermocouples and insulated surface thermocouples, in order to reduce the overall scrap rate and the process time. The modification made

was to utilize hypodermic needle tubing made from A.I.S.I. Type 304 austenitic stainless steel. The surface thermocouple can be manufactured by inserting the Ni-wire insulated by a surface oxide layer into the hypodermic tube (which is annealed first) and then dieing the main body onto the wire and tube to form a composite arrangement as shown in Fig. 2.7.

The Fin problem on Law's and Falcus's surface thermocouple was reduced by Wakefield, by spot welding the wires directly onto the back of the surface thermocouple.

Three different methods were investigated for insulating the surface thermocouple in order to reduce the sideways heat flux effect:

1. Ceramic Cement - The surface thermocouple is cemented directly into the piston, and cement will be the insulator as shown in Fig. 2.8b.
2. Ceramic Spraying - The surface thermocouple is sprayed with a ceramic insulating coat before being fitted into piston as shown in Fig. 2.8a.
3. Ceramic Sleeving - The surface thermocouple is bonded inside a ceramic cleave and then fitted in an outer metal tube within the piston as shown in Fig. 2.8c.

The adequate surface thermocouple design should satisfy a certain specification in order to obtain an accurate result (see next section).

2.3 Requirements Specifications of Surface Thermocouple Design

2.3.1 System Requirements

Any temperature measuring device should have little or no effect on the system under consideration. So in order to satisfy the condition the following aspects required for ideal surface thermocouple:

1. The surface thermocouple should be made of the same material as the component to avoid any discontinuities, particularly in the thermal conductivity.
2. The thermal junction of the surface thermocouple should form a continuation of the surface, so that the boundary layer is undisturbed.
3. The wire must be electrically insulated from the main body, and the technique used should produce a good insulation.
4. The rear of the surface thermocouple should be flush with the rear surface of the component, to avoid any "Fin effect".
5. The surface thermocouple should have a response compatible with the imposed temperature time dependent.
6. The surface thermocouple leads should be insulated in such a way as to avoid additional heat transfer by conduction along the thermocouple wire.

7. The nickel wire must be held tightly in order to overcome any frequency noise caused by the vibration of the nickel wire.

2.3.2 Backing Temperature

A standard thermocouple is used to measure the backing temperature of the surface thermocouple because the backing temperature does not vary significantly during the internal combustion engine cycle. In order to calculate the heat transfer one of the assumptions made is that one-dimensional heat flow, it is obviously a better calculation to measure the backing temperature on, or very near to, the axis of the surface temperature thermal junction. This axis lies along the central nickel wire. Most of the previous design the backing temperature were measured a way from the axis of the surface temperature thermal junction.

2.3.3 Sideways Heat Flux

It is quite obvious that, in practice a three-dimensional heat flow exists, so for one-dimensional analysis an error introduced due to sideways heat flux flow, and this can be reduced by a thermal insulation as described in Ref. (138). The result showed that the magnitude of sideways heat flux was small compared with the total heat transfer.

2.4 First Design

2.4.1 Introduction

An attempt was made to reproduce the surface thermocouple design by Law Ref. (85) and Falcus Ref. (45) and modified by Wakefield Ref. (138) without success. It was found impossible with the available equipment to produce a satisfactory oxide film on the Ni-wire whose integrity was preserved throughout the following manufacturing processes.

2.4.2 Wire Surface Oxidization Process

The Wakefield design required the first process to be the Ni-wire surface oxidation, the Falcus's rig, modified by Wakefield, as shown in Fig. 2.9a and Fig. 2.9b respectively, was built in order to oxidize the Ni-wire surface, the following difficulties were found with the oxidization process:

1. Initially trouble was found with freezing of the regulator valve. To overcome this problem a 150 watt CO₂ heater was used and connected directly to the gas cylinder as shown in Fig. 2.10. This possible is not mentioned in Refs. (45, 138).
2. By using the variac to apply 65 volts over 5 minutes period as recommended by Ref. (138) the Ni-wire melted. A transformer was used to reduce the voltage to a maximum 30 volts. The maximum voltage applied to the Ni-wire was finally found to be 15 volts if the wire was not to break. After the oxidization process the insulation of the Ni-wire was tested carefully with a low current meter, this will be describe in Chapter 4 (see figure 4.1.b), immersing the wire in a mercury container to avoid breaking the insulation. It was found that some parts of the Ni-wire surface has not been oxidized, and all attempts of varying voltage and gas flow rate were unsuccessful, although some short lengths were produced.

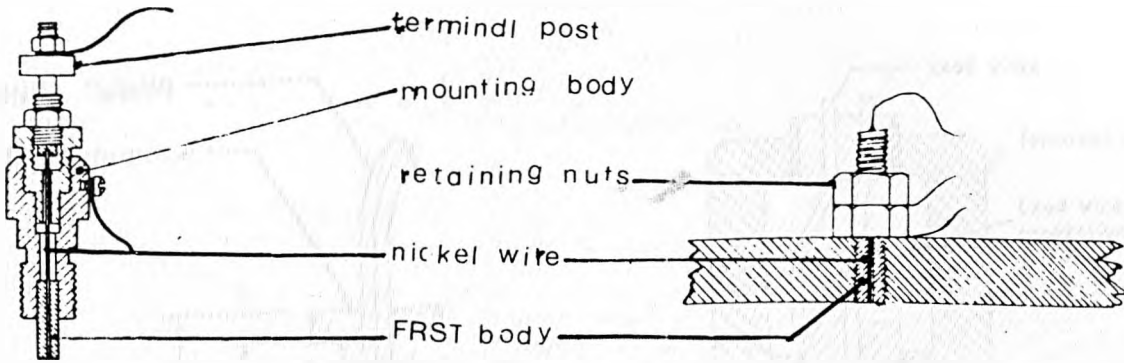
2.4.3 Dieing Process

The next process was dieing of the body and tube onto the Ni-wire. This process did not succeed for three reasons:

1. The body was broken during the dieing process.
2. The electrical insulation became damaged during the process.
3. It proved impossible to rigidly hold the wire after dieing.

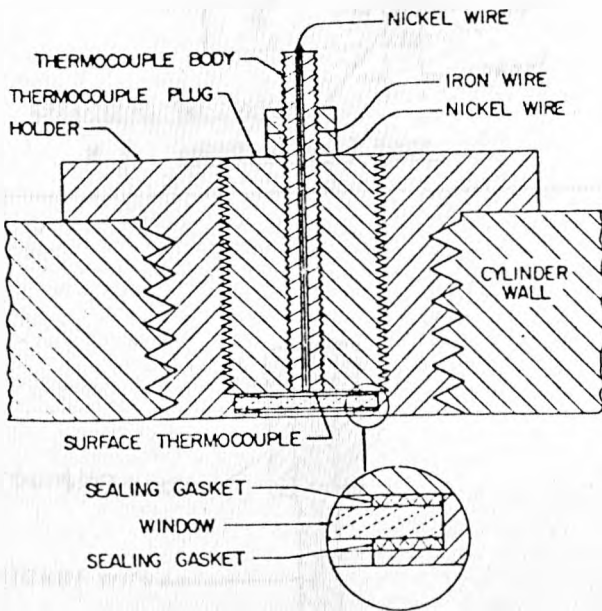
2.5 Existing Solution

The difficulties were too great and rather than persisting with attempts with this design an alternative more easily manufactured design was used. The major difference from the previous design is that chemical set cements are used as electrical insulation and holder for the Ni-wire. This design will be describe in Chapter 4.

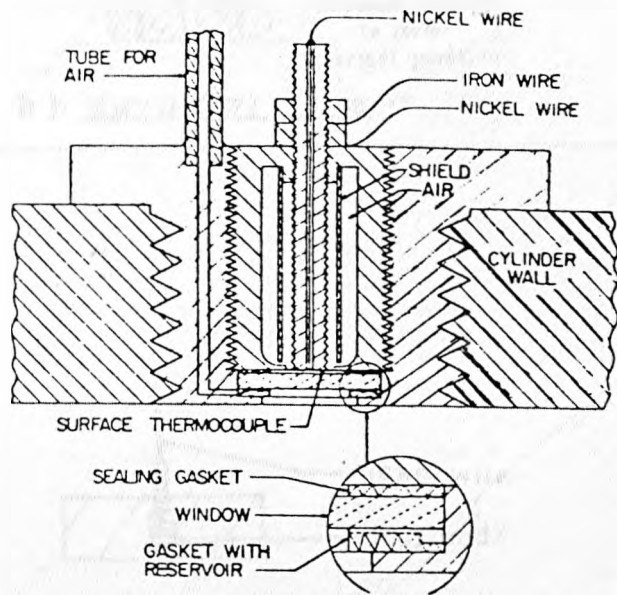


a) BENDERSKY (2) 1953

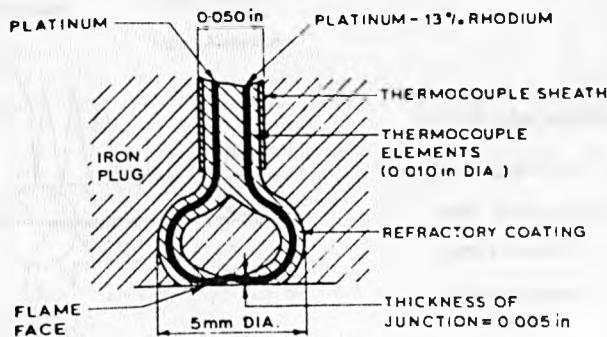
b) OVERBYE (3) 1961



c) EBERSOLE (8) 1963

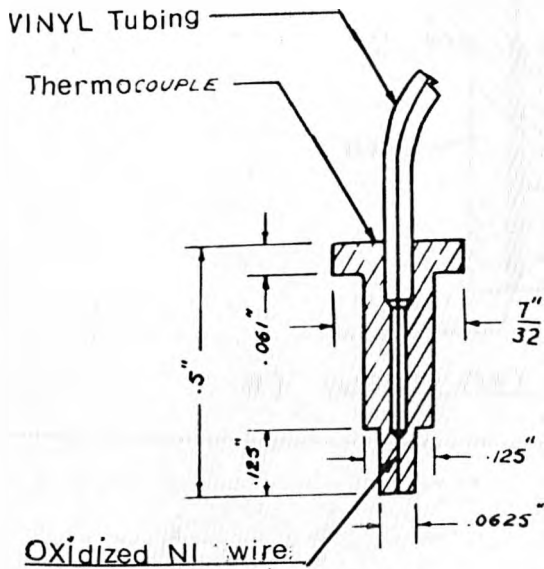


d) EBERSOLE (8) 1963

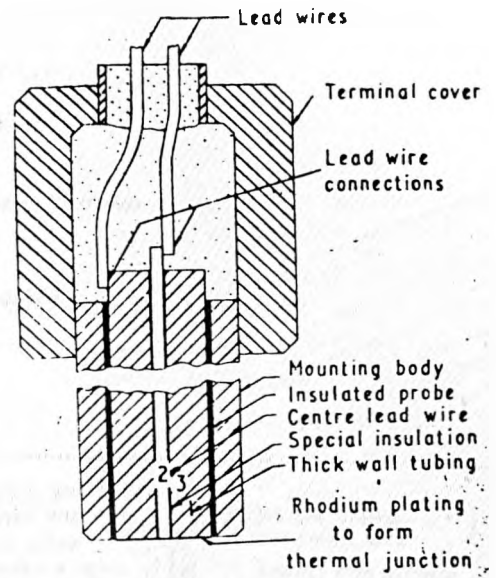


e) KNIGHT (9) 1964

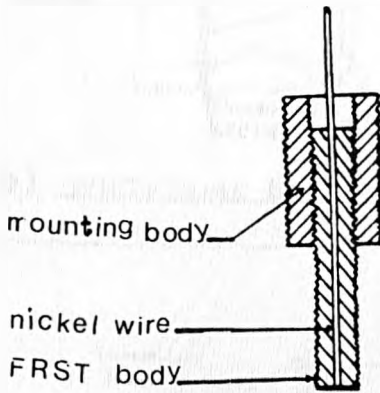
VARIOUS FRST DESIGNS



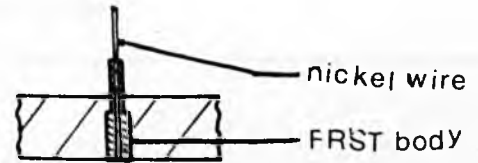
a) HENEIN (62) 1965



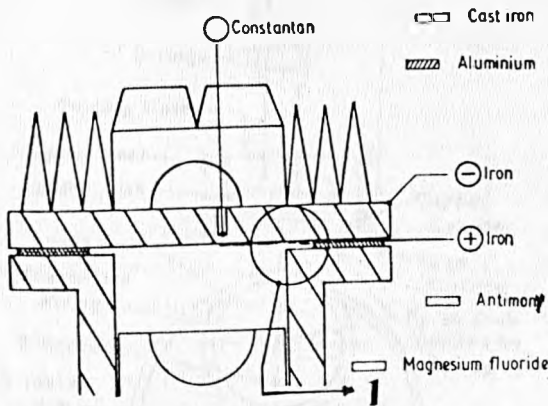
b) SMYTH (127) 1968



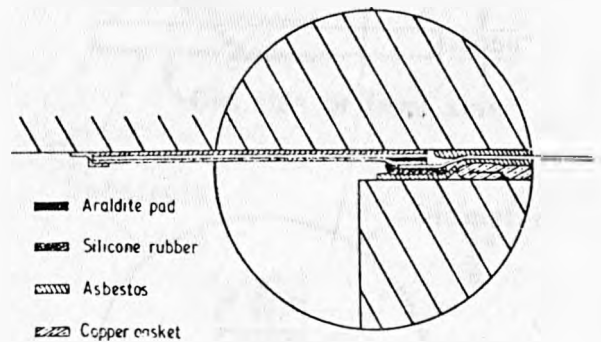
c) LEFEUVRE (87) 1969



d) LAW (85) 1968

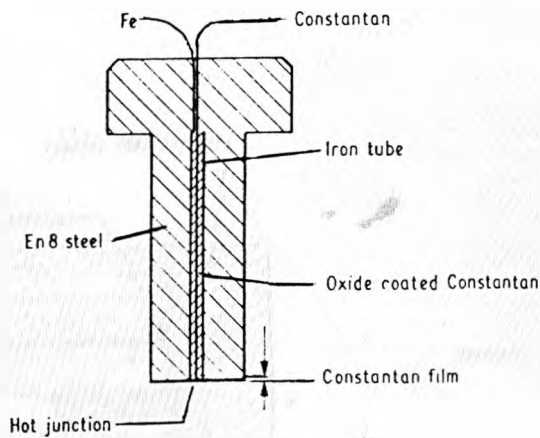


e) ANNAND (9) 1970

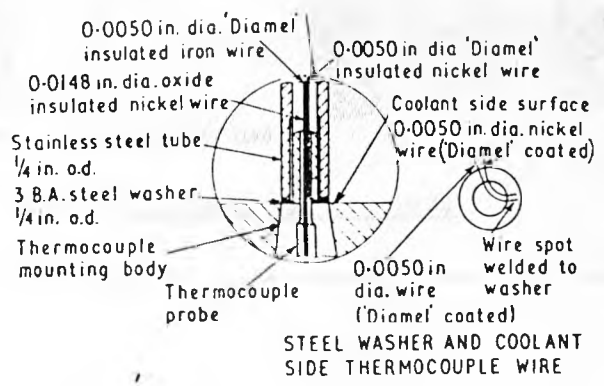
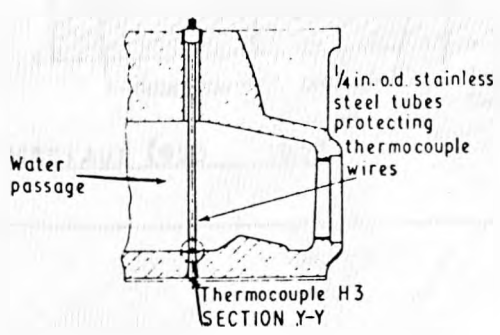


SECTION (1)

VARIOUS FRST DESIGNS

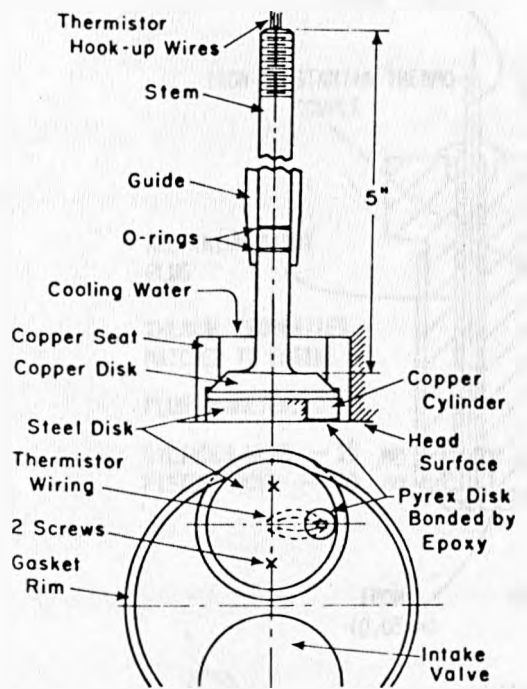


a) HASSAN (59) 1970

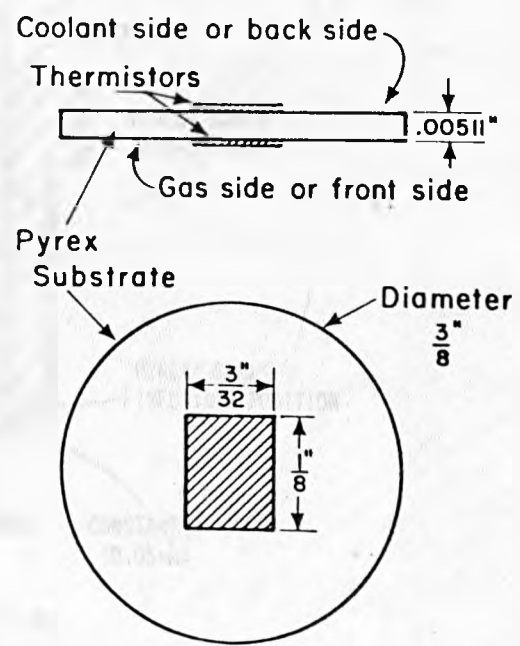


b) WHITHOUSE (46) 1970

SECTION Y-Y

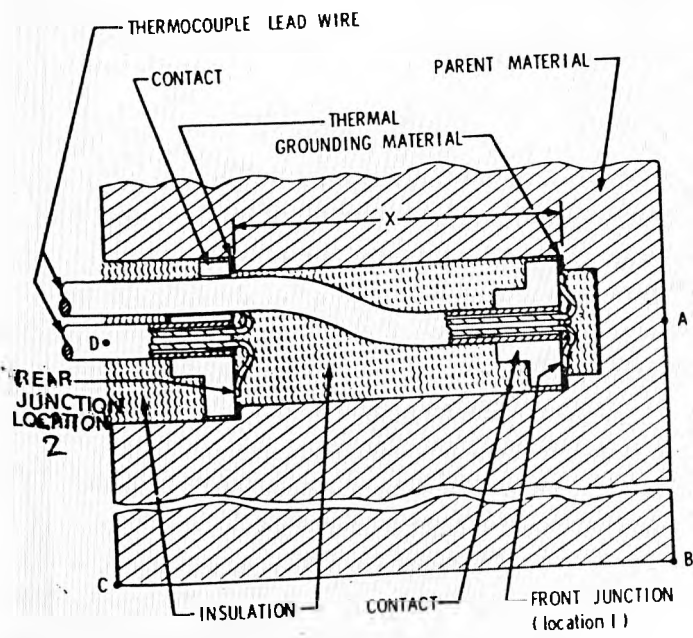


c) DAO (31) 1973

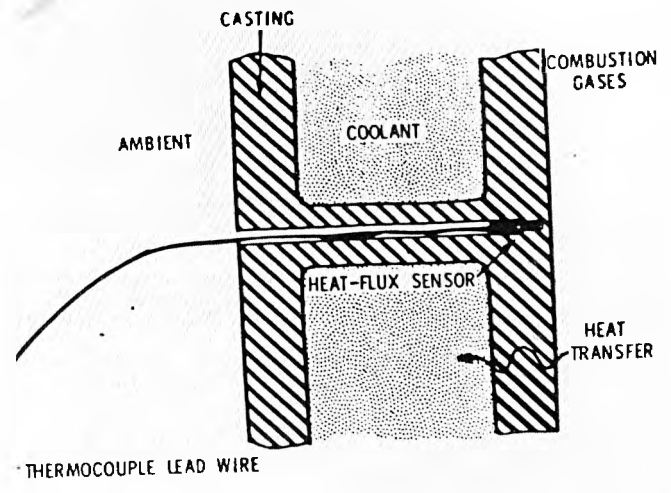


d) DAO'S FLUX METER

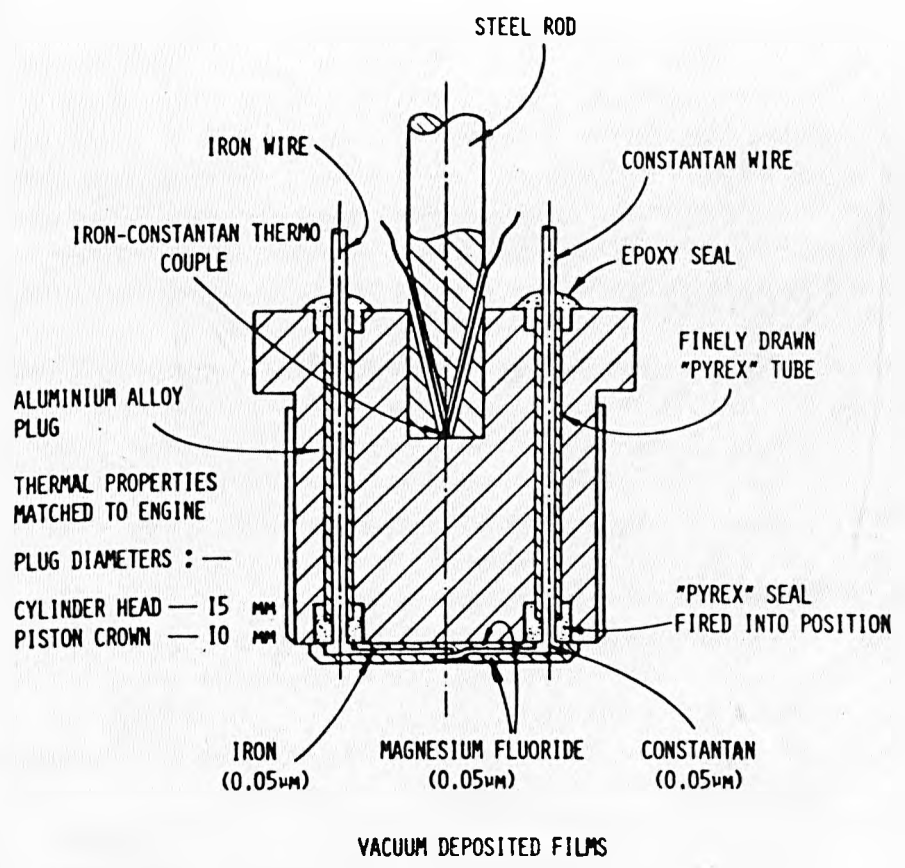
VARIOUS FRST DESIGNS



a) MATTAVI (92) 1974

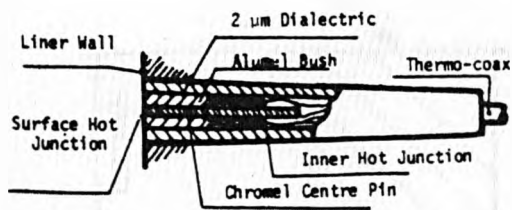


b) MATTAVI (92) 1974

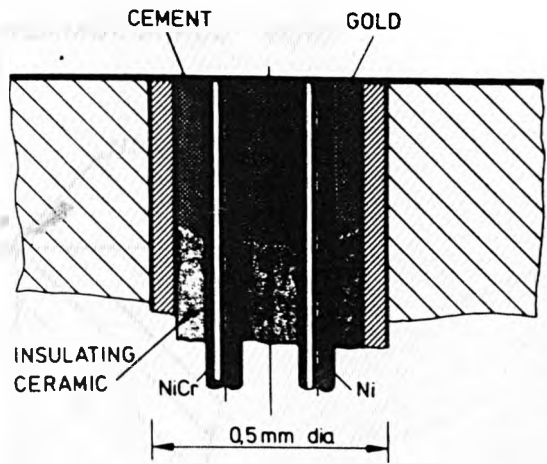


c) DENT (35) 1977

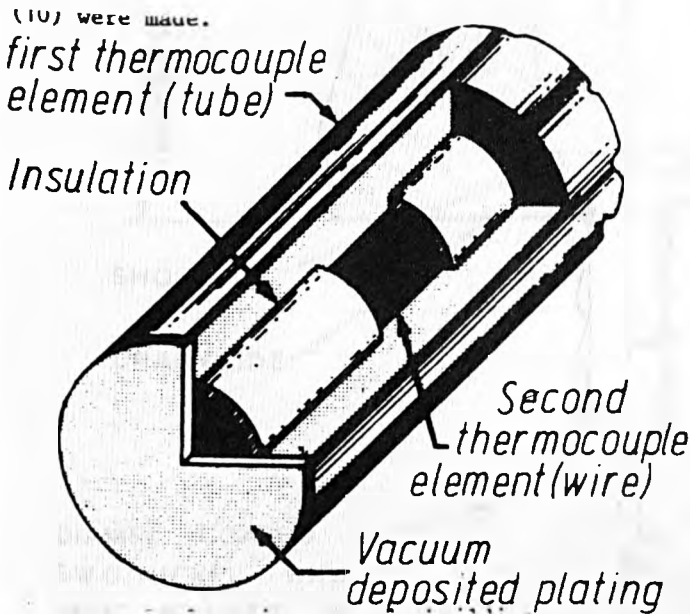
VARIOUS ERST DESIGNS



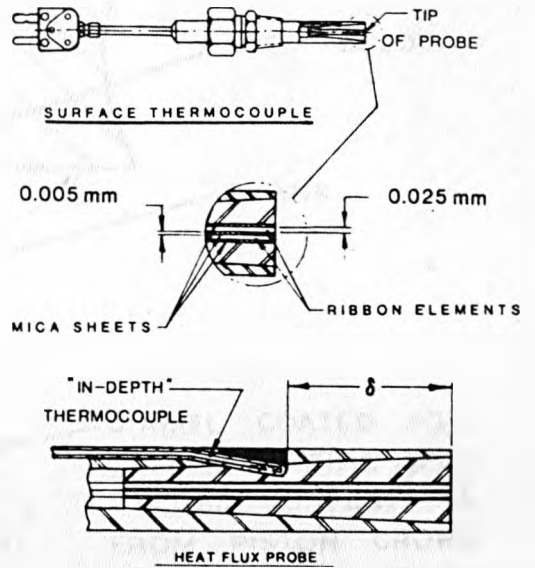
a) KAMEI (71) 1979



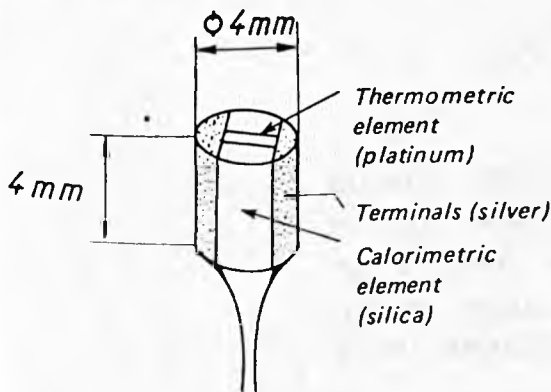
b) HOHEN (64) 1979



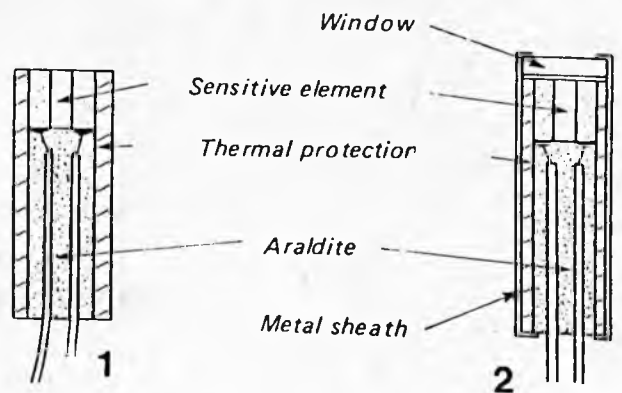
c) SIHLING (126) 1979



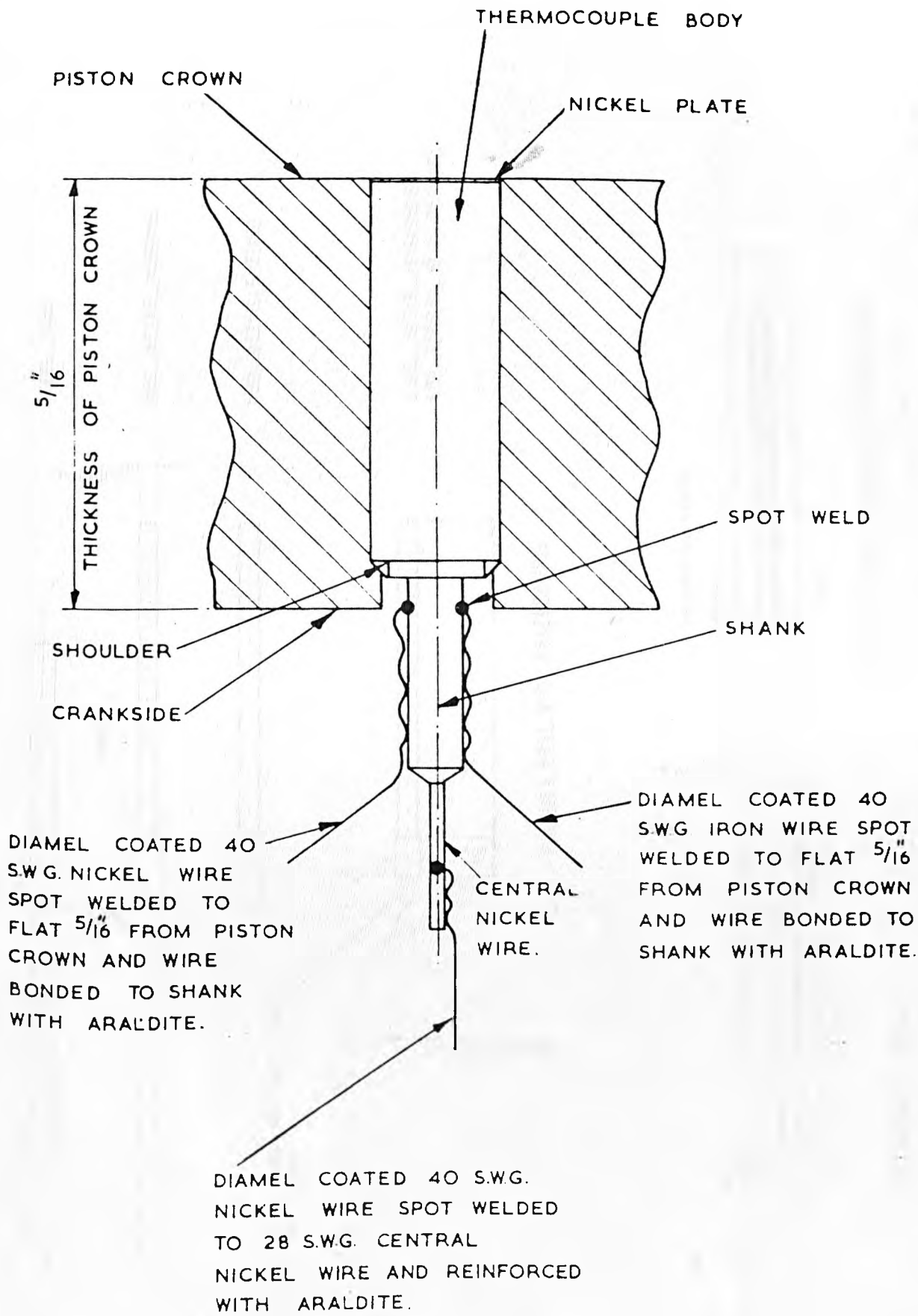
d) ALKIDAS (4) 1980



e) GUERNIGOU (55) 1980

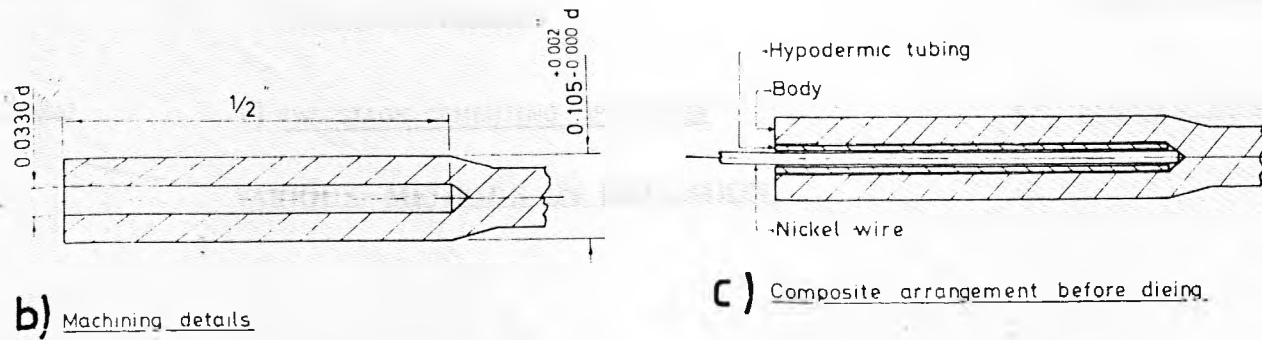
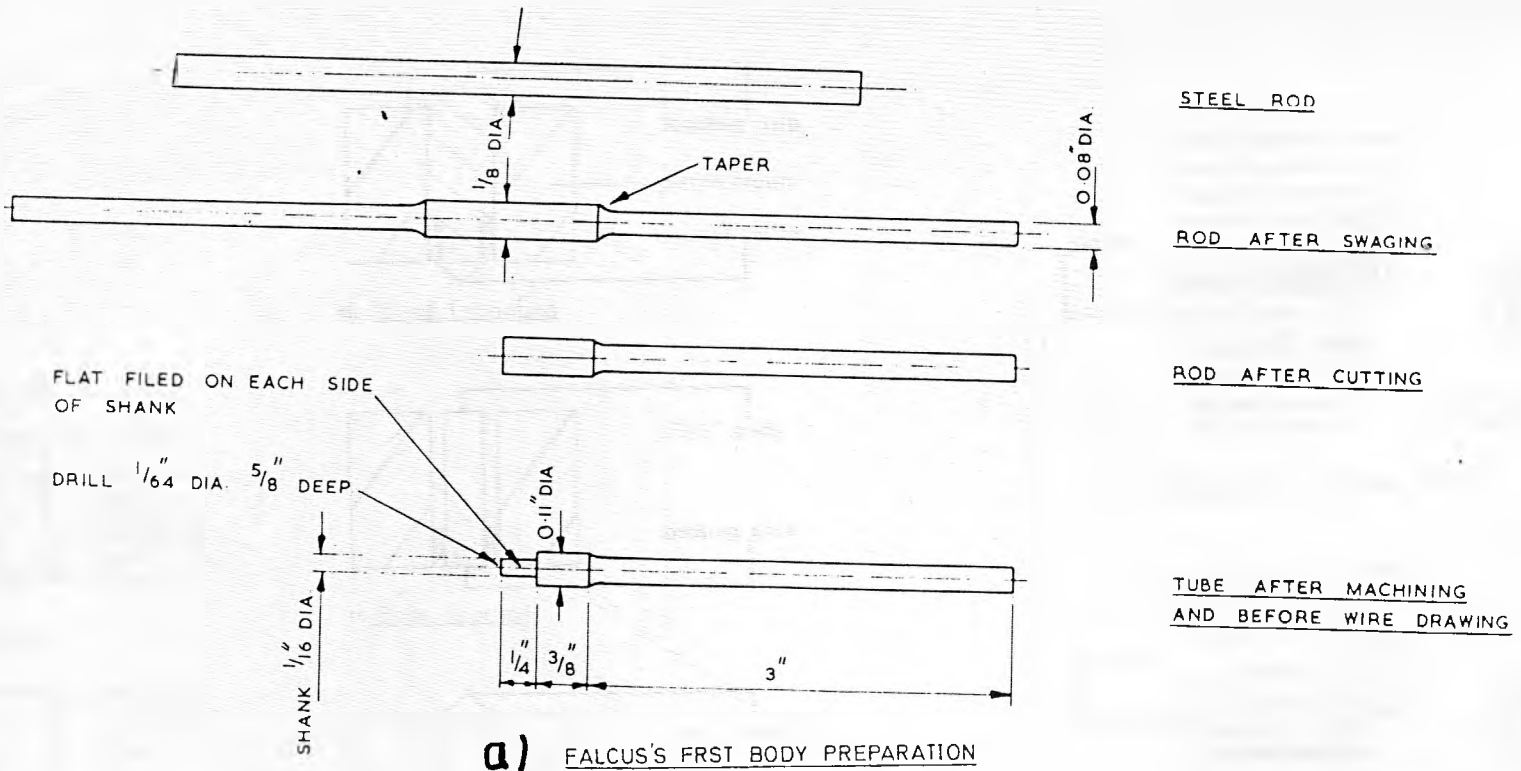


f) GUERNIGOU (55) 1980



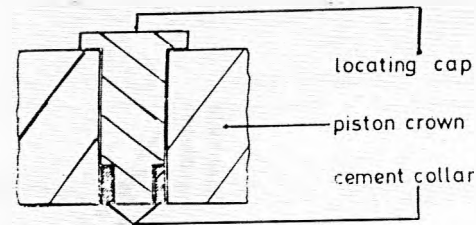
FALCUS'S FRST MOUNTING DETAILS

FIG-2-6

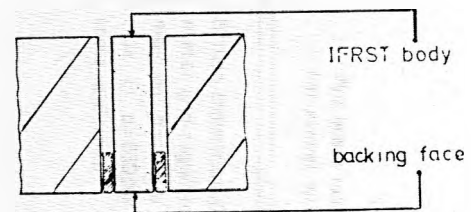


WAKEFIELD'S FRST BODY PREPARATION

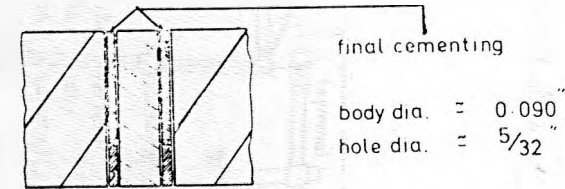
FIG. 2-7



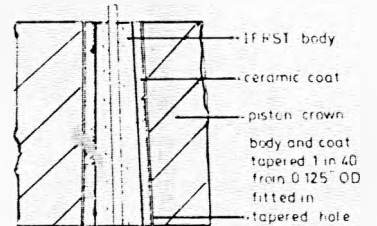
a) Collar formation



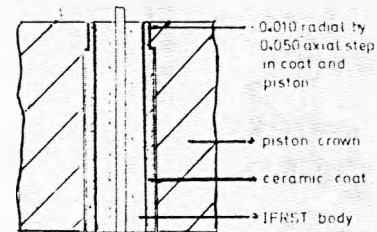
b) Body insertion



c) Final cement application



a) Tapered sprayed IFRST

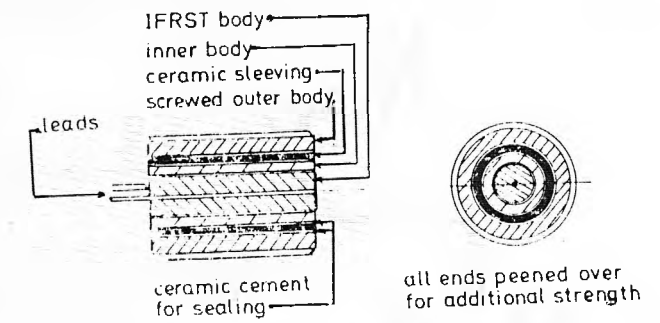


b) Stepped sprayed IFRST

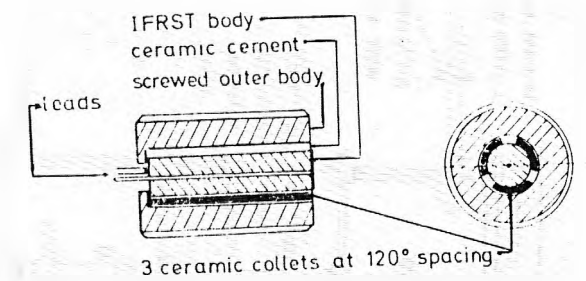
a) DIFFERENT SPRAYED IFRST DESIGNS

b) TWO STAGE CEMENTING OPERATION

VARIOUS METHODS OF INSULATION



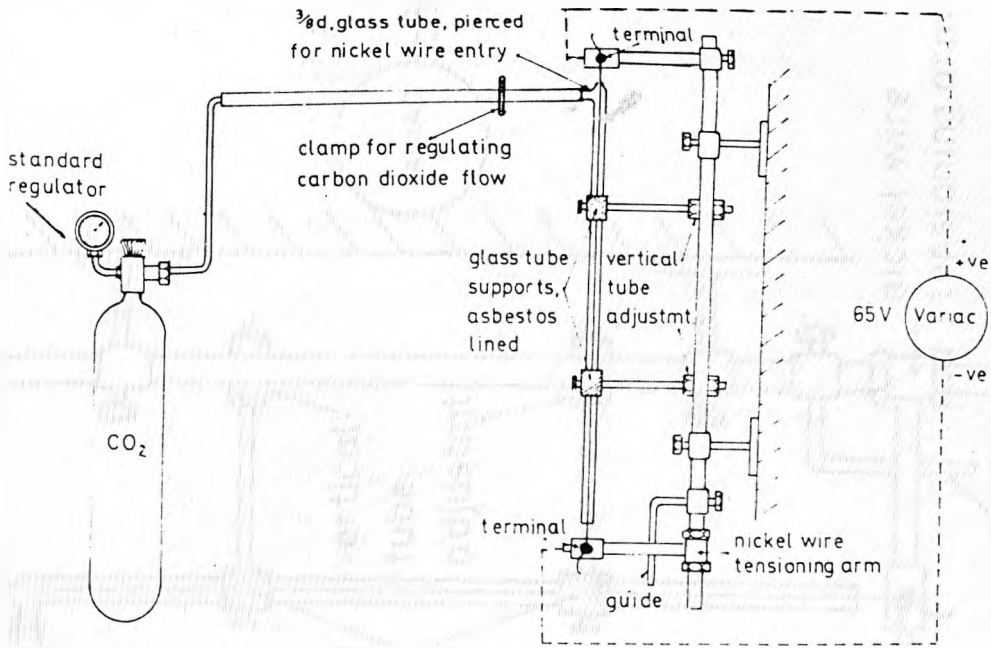
a) Composite sleeved IFRST



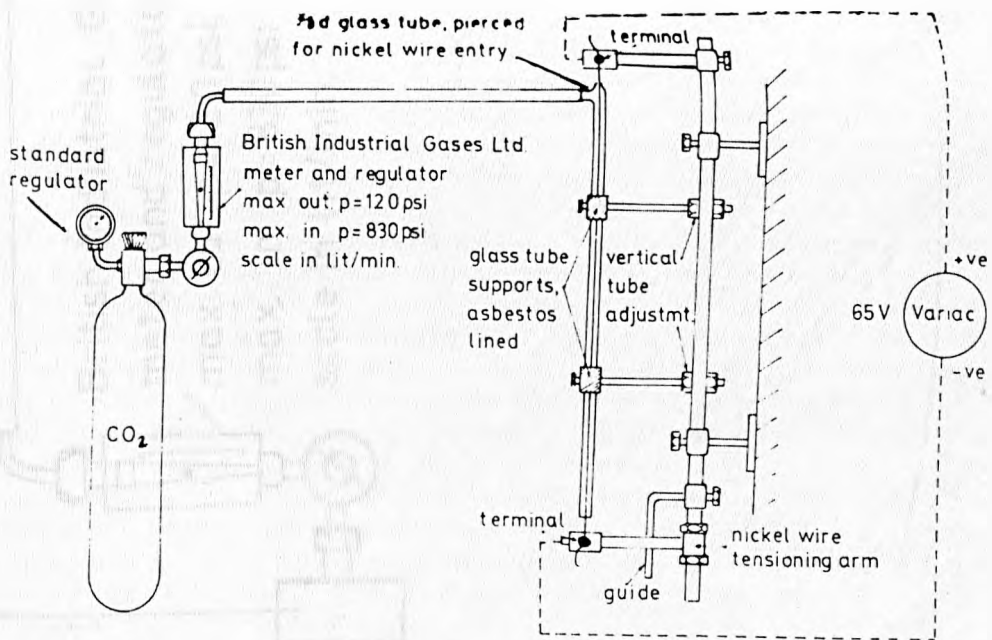
b) Collet sleeved IFRST

c) SLEEVED IFRST DESIGNS

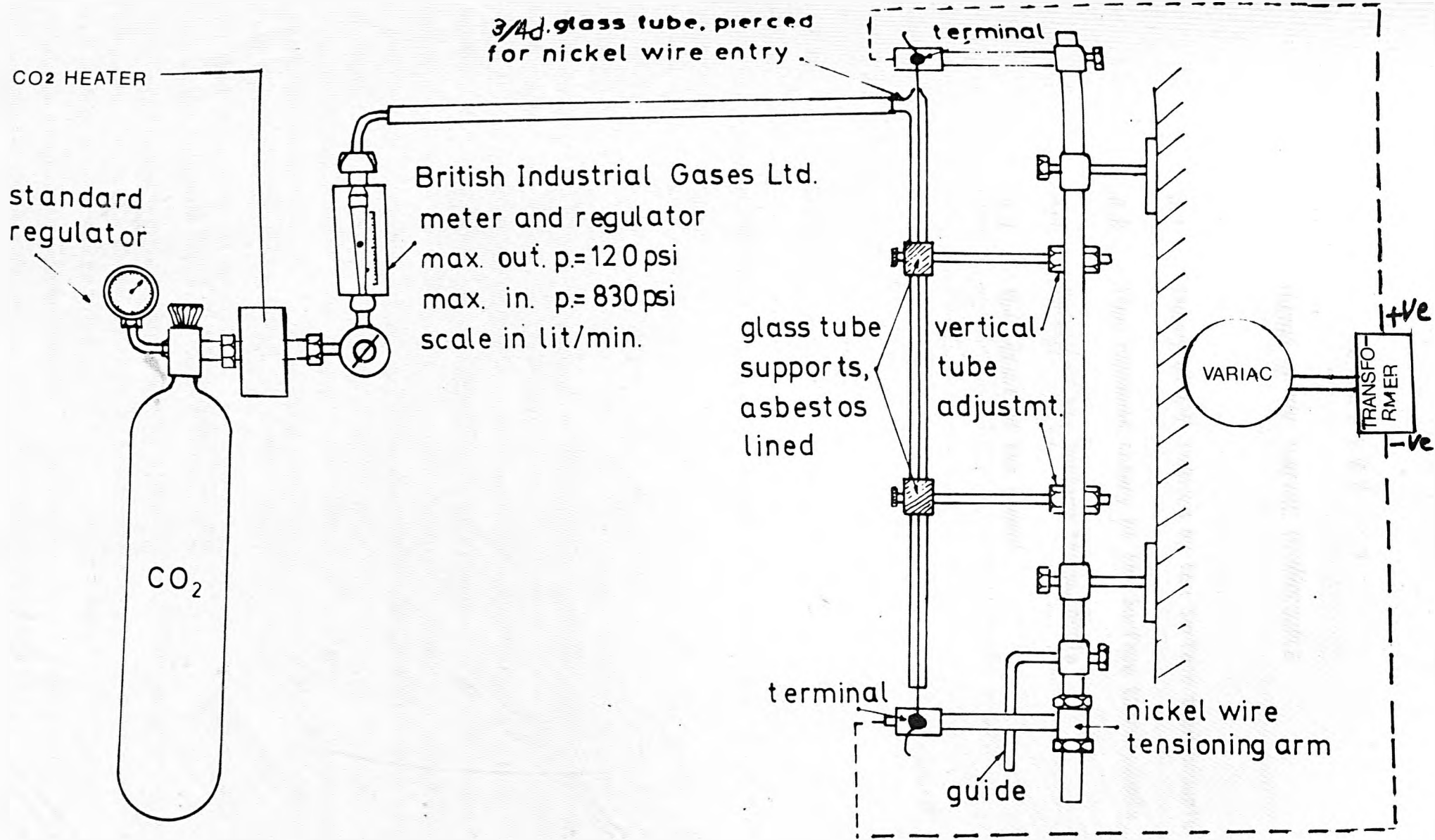
FIG-2-8



a) FALCUS'S NICKEL WIRE SURFACE OXIDATION RIG



b) WAKEFIELD'S NICKEL WIRE SURFACE OXIDATION RIG



REVISED NICKEL WIRE SURFACE OXIDATION RIG

FIG-2-10

CHAPTER 3

THEORY OF THE SURFACE THERMOCOUPLE

- 3.1 Theory of EMF induced by the Surface thermocouple
- 3.2 Time response theory of the Surface thermocouple
- 3.3 Theory of the Surface thermocouple
- 3.4 The effect of the cement

3.1 Theory of E.M.F. Induced by Surface Thermocouple

There will be five E.M.F.s generated, in a system such as shown in Figs. 3.1.a and 3.1.b, as follows:

1. A THOMSON E.M.F. which is produced in the Ni-wire AB itself and equal to:

$$(E.M.F)_{Ni} = E_B - E_A = S_{Ni}^* (T_B - T_A) \quad 3.1$$

where S_{Ni}^* is the seebeck coefficient for the Ni-wire.

2. PELTIER E.M.F which is produced at hot junction (Film) CB and equal to:

$$(E.M.F)_{Film} = E_C - E_B = S_{Film}^* (T_C - T_B) \quad 3.2$$

3. A THOMSON E.M.F which is produced in the Fe wire CD itself and equal to:

$$(E.M.F)_{Fe} = E_D - E_C = S_{Fe}^* (T_D - T_C) \quad 3.3$$

4. PELTIER E.M.F which is produced at cold junction ED and equal to:

$$(E.M.F)_{ED} = E_E - E_D = S_{Cold}^* (T_E - T_D) \quad 3.4$$

5. A THOMSON E.M.F which is produced in Ni-wire EF itself and equal to:

$$(E.M.F)_{Ni} = E_F - E_E = S_{Ni}^* (T_F - T_E) \quad 3.5$$

The total E.M.F induced from the circuit if no current flows are equal to the summation E.M.F. mentioned above,

$$\text{Let E.M.V} = V$$

$$V_{total} = V_{AB} + V_{BC} + V_{CD} + V_{DE} + V_{EF} \quad 3.6$$

$$V_{total} = S_{Ni}^* (T_B - T_A) + S_{Film}^* (T_C - T_B) + S_{Fe}^* (T_D - T_C) + S_{cold}^* (T_E - T_D) + S_{Ni}^* (T_F - T_E) \quad 3.7$$

If $T_E = T_D$ cold junction kept at the same temperature and if $T_F = T_A$ both points kept at room temperature.

Therefore the total E.M.F will be

$$V_{total} = S_{Ni}^* (T_B - T_E) + S_{Fe}^* (T_E - T_C) + S_{Film}^* (T_C - T_B) \quad 3.8$$

If the film is Nickel, then the total E.M.F will be:

$$V_{total} = S_{Ni}^* (T_C - T_E) + S_{Fe}^* (T_E - T_C) = (S_{Ni}^* - S_{Fe}^*) (T_C - T_E) \quad 3.9$$

since $T_C = T_B$

If the film is Copper, then the total E.M.F will be:

$$V_{total} = (S_{Ni}^* - S_{Fe}^*) (T_C - T_E) + (S_{Ni}^* - S_{Cu}^*) (T_B - T_C) \quad 3.10$$

Therefore if $T_B \neq T_C$ there is an error equal to $(S_{Ni}^* - S_{Cu}^*) (T_B - T_C)$. And if a test using Ni-film is compared with a test using CU-film the temperature difference $(T_B - T_C)$ may be determined.

3.2 Time Response Theory of the Surface Thermocouple:

The response time of a surface thermocouple is affected by the thickness of the film. As the film thickness increases, the time constant rapidly increases. The surface thermocouple measures a rapid temperature change, so the time response should be as short as possible, in order to respond to temperature changes at the exposed surface rapidly. The time constant is defined Ref. 14 as

the time required for the junction temperature to reach 62.3 per cent of the amplitude of a step-temperature change of the exposed surface. More information about the theory of time response reported in Refs. 24, 94.

For reponse rate of a heated homogeneous thin strip of uniform thickness and a semi-infinite medium, having thermal characteristics assumed to be constant Ref. 55. Following the procedures of Refs. 55, 93, the response time of the surface thermocouple was calculated for both Nickel and Copper film deposition of order of magnitude 0.5 and 0.38 ms respectively for 5 micron film thickness. For 1 micron film thickness, the time response will be for Nickel and Copper 20 μ sec and 15 μ s respectively.

The time response was adequate for the present purposes. Considering the highest engine test speed of 1500 r.p.m., if the output from the thermocouple was recorded every 5° interval, the time available will be 0.555 ms. The response time compares favourably with the results of Refs. 30, 55.

It is important to have the thermal junction as close to the surface as possible Refs. 14, 96. If the thermal junction thickness is so small so the film temperature can be taken as the surface temperature without making any considerable correction.

3.3 Theory of the Surface Thermocouple:

The principle assumption used to calculate the heat flux is that the heat flow through the walls of the combustion chamber is approximately one-dimensional.

In the present design the problem is in defining the junction temperature. Because of the cement core in the surface thermocouple there is a two dimensional temperature variation across the junction Nickel/Iron, although as proportion of the total surface area the ceramic is small.

An assessment assuming no heat flux between Iron and Cement and uniform heat flux at the cylinder surface, the problem can be represented by:

$$\frac{\partial^2 T}{\partial r^2} + \frac{1}{r} \frac{\partial T}{\partial r} + \frac{\partial^2 T}{\partial z^2} = \frac{1}{\alpha} \frac{\partial T}{\partial t} \quad 3.11$$

The solution will be complicated and difficult Refs. 24, 79, 108 since the available boundary conditions are not enough to satisfy equation 3.11. Therefore the effect of cement has been investigated experimentally as described in section 3.4 and the problem is considered to be one-dimensional.

Assuming one-dimensional unsteady temperature distribution in a solid wall, which is determined by the Fourier equation.

$$\frac{\partial T}{\partial t} = \alpha \frac{\partial^2 T}{\partial X^2} \quad 3.12$$

where α is the thermal diffusivity and is equal to $K/\rho c$ and X is the distance measured in the direction of heat flow. The equation is solved to give the temperature field in the wall depending on time and position normal to the surface.

The temperature variation on the gas-side of the wall is usually periodic, but is irregular during one period. It is necessary to replace the periodic fluctuation by using the Fourier analysis,

since this temperature variation is used as a boundary condition.

The equation for gas-side wall temperatures is:

$$(T_w)_{x=0} = (\bar{T}_w)_{x=0} + \sum_{k=1}^m A_k \cos kwt + B_k \sin kwt \quad 3.13$$

Equation 3.13 is one boundary condition for the solution of equation 3.12, the temperature on the coolant side of the wall is taken as the remaining boundary condition and is assumed to be a time averaged wall temperature, i.e.

$$(T_w)_{x=L} = \text{Constant} \quad 3.14$$

Before using the boundary conditions to solve the equation 3.12, it is necessary to determine the Fourier coefficients A_k and B_k .

The time mean of $(T_w)_{x=0}$ is:

$$\bar{T}_w = \frac{1}{2m} \sum_{i=0}^{2m-1} T_i \quad 3.15$$

By using the boundary condition and the value of the coefficients A_k and B_k , the solution of equation 3.12 becomes:

$$T = (\bar{T}_w)_{x=0} - \frac{x}{L} \left[(\bar{T}_w)_{x=0} - (\bar{T}_w)_{x=L} \right] + \sum_{k=1}^m e^{-xr} \left[A_k \cos (kwt-xr) + B_k \sin (kwt-xr) \right] \quad 3.16$$

where $r = \left[kw/2\alpha \right]^{\frac{1}{2}}$

Equation 3.16 completely defines the temperature field in the wall, therefore

$$T = f(x,t) \quad 3.17$$

since equation 3.16 and 3.17 gives the wall temperature as a function of x as well as t , the derivative of this equation, evaluated at $x=0$, because of the damping effect of the term e^{-xr} divergence during differentiation is not possible at $x \neq 0$.

The heat flux at gas-side of the wall is:

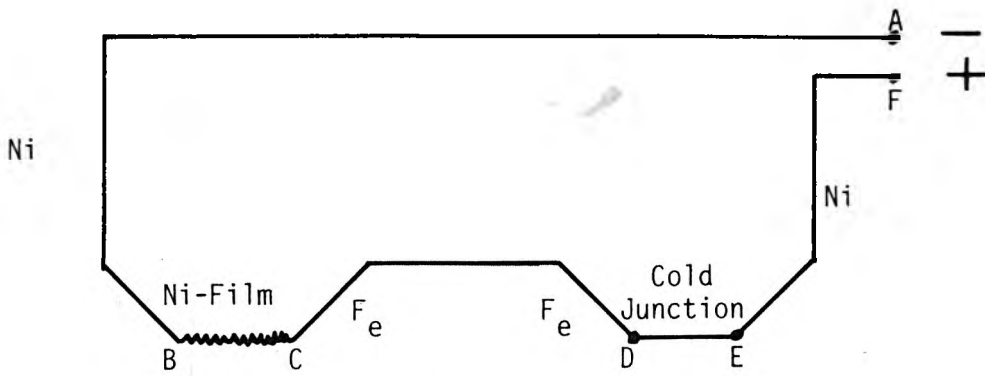
$$\frac{q}{A} = -k \left[\frac{\partial \bar{T}}{\partial x} \right]_{x=0} \quad 3.18$$

$$\frac{q}{A} = \frac{K}{L} \left[(\bar{T}_w)_{x=0} - (\bar{T}_w)_x \right] + K \sum_{k=1}^m r \left[(B_k - A_k) \sin kwt + (B_k + A_k) \cos kwt \right] \quad 3.19$$

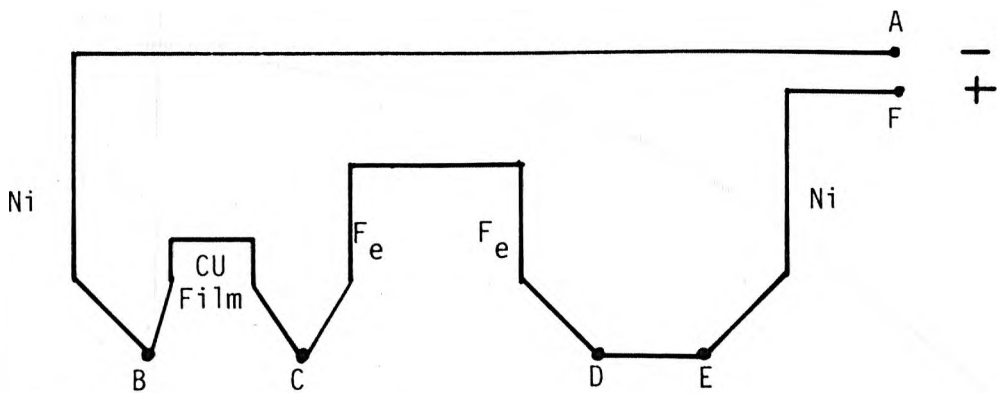
Equation 3.19 is used to calculate the heat flux from wall temperature measurements. (See Chapter 8).

3.3 The Effect of the Cement

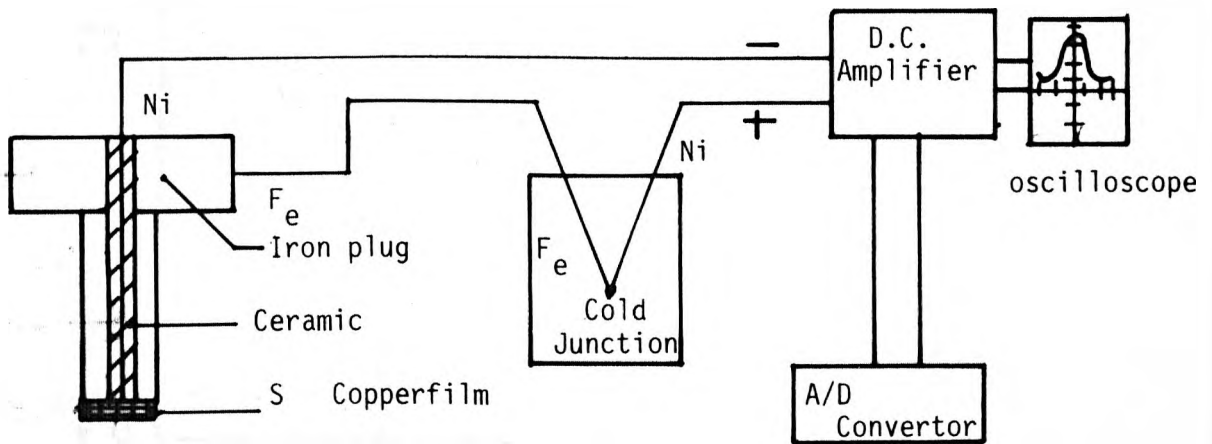
An investigation has been carried out experimentally to determine the effect of the cement on the surface thermocouple reading. Four surface thermocouples were made with different diameters of cement, 6.35 mm (0.25 in), 3.175 mm (0.125 in), 1.587 mm (0.0625 in) and 0.793 mm (0.03125 in). The four surface thermocouple plugs were coated with nickle film of order 5 micron thickness approximately. Each surface thermocouple was calibrated against mercury thermocouple in a control heater container of water at fixed temperature 100°C for all surface thermocouples. Fig. 3.2 shows the output reading at 100°C for each cement diameter of the surface thermocouple. It is assumed the curve to be extrapolated to zero diameter i.e. the surface thermocouple behaves as if there is no cement and a correction has been incorporated in the processing of the readings.



A) Ni-Film Circuit



B) CU-Film Circuit



C) Layout Connection for Surface Thermocouple

THE EFFECT OF CERAMIC DIAMETER ON THE OUTPUT VOLTAGE
OF SURFACE THERMOCOUPLE

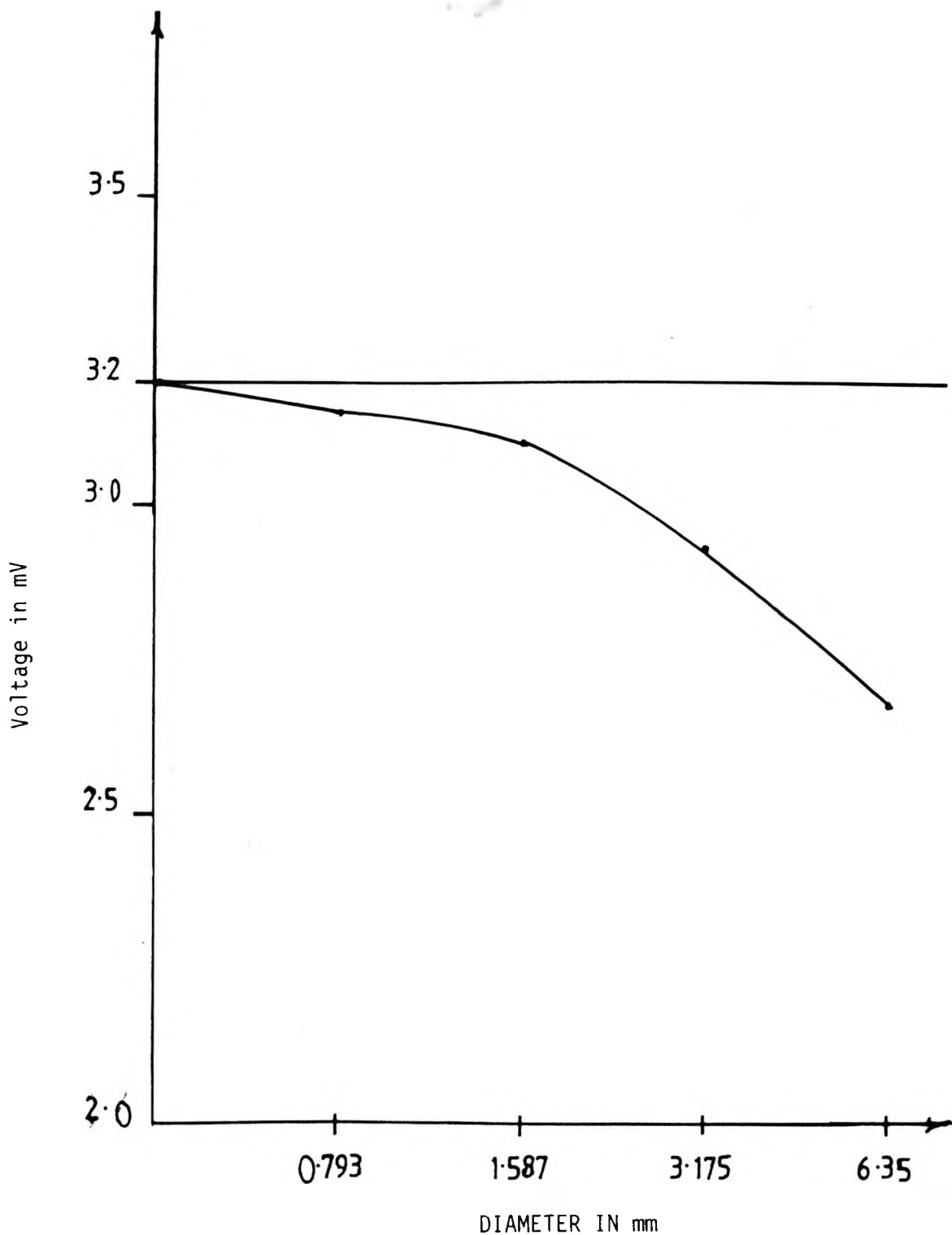


FIG. 3-2

CHAPTER 4

SURFACE THERMOCOUPLE DESIGN

- 4.1 Introduction
- 4.2 Manufacturing Process
- 4.3 Calibration

4.1 INTRODUCTION

A simple design to reduce the problems mentioned in Chapter 2 Section 4 was developed. The design shown in Fig. 4.1.a is basically the same as the Wakefield design, but chemical set cements have been used as both electrical insulator and a rigid holder for the Ni-wire.

4.2 MANUFACTURING PROCESSES

4.2.1 Body Preparation

Cast iron rod of 30 mm (1.18 inch) in diameter and 50 mm (1.96 inch) in length was used to produce the body of the surface thermocouple. The outside diameter is turned down to 23 mm (0.905 inch) and the length is cut to 33 mm (1.299 inch). A central hole of 1.587 mm (0.0625 inch) in diameter is drilled. The outside diameter is turned down and a 14 mm spark plug thread has been cut to suitable length. An 8 BA screw is inserted at the corner of the backing surface of the plug to connect the iron wire. The use of a screw avoids any junction e.m.f. that could occur with a soldered joint.

4.2.2 Cleaning Process

It is important to produce a good surface finish on the bore followed by cleaning in order to ensure that surfaces in contact with the cement are really clean and free from oil, grease, and rust. To obtain a good finish the hole was lapped.

The surface was then washed with a 1% solution of WSTR in hot water which should be allowed to dry before the cement is applied (as recommended by the manufacturer). This will not only clean the surface but will reduce the surface and interfacial tension of the adherends and will improve bonding of the cement.

4.2.3 Chemical Set Cement Filling Process

A chemical set cement type LQ/S6 was used (product of FORTAFIX co. Ltd.), which is resistant to water, oil, acid (except hydro flouric) and provides high dielectric strength, low thermal expansion and shrinkage, and high tensile and compressive strength. This cement is supplied in two parts, a powder filler and a liquid binder which are mixed together as 2:1 by weight respectively. They harden by an internal chemical action but remain soft and pliable long enough to permit ample time for handling (recommended time up to 7 minutes from practical experience). The surface thermocouple plug was held in a simple holder. The holder shown in Fig. 4.2 consists of three pieces, the middle one is drilled to fit the surface thermocouple plug and the other two located on both sides. Two fine holes are drilled one on each side to coincide with the centre of the surface thermocouple plug hole in order to insert the Ni-wire on the axis, the Ni-wire held on both sides by plastic screws to give the required tension. The powder filler and the liquid binder should be mixed well and then directly apply to fill the hole. The cement set initially in one hour and hardens completely in 48 to 60 hours at room temperature to allow the evaporation process. After the hardening process takes place, a central hole of 0.793 mm (0.03125 inch) in diameter is drilled into the cement, to form a thin layer of cement 0.3965 mm (0.006625 inch) in thickness inside the central hole of the plug for the wire.

4.2.4. Heat Treatment Process

Following the manufacturers instructions did not produce satisfactory results and the following modified procedure was followed. It is essential that the evaporation of the liquid solvent proceeds slowly to avoid porous bonding. Because the cement surface inside the plug hole is not fully exposed to air to allow natural evaporation, it must be heat treated to drive off surplus moisture, mechanical strength, dielectric and water resistance properties will also be improved. The following curing stages produced the desired properties:

1. Allow to air dry for 72 hours at room temperature.
2. Bake at 60°C for 24 hours, gradually raising the temperature from cold over a period of 2 to 3 hours.
3. Raise the temperature from 60°C to 100°C over 8 hours.
4. In very gradual increases raise the temperature to 150°C over 10 hours.
5. Increase the temperature to 250°C over 5 hours, allow to cool and then heat cure to the optimum working temperature 500°C. The actual working temperature for the cement used is 1000°C. To give good dielectric properties after curing, apply a coating of DIELECTRIC VARNISH SI/MS048. Allow to air dry at room temperature for 5 hours, then cure at 100°C for 3 hours and at 250°C for 4 hours.

4.2.5 Nickel Wire Insertion

The plug with a thin layer of cement and a central hole of 0.793 mm (0.03125 inch) in diameter was held in position in the holder mentioned in section 4.2.3 and then further cement was allowed to fill the hole under

gravity. Immediately a thermocouple quality 0.376 mm (0.0148 inch) diameter Nickel cut into 200 mm (7.874 inch) length, deinked by gentle stretching and cleaned with acetone, inserted carefully into the hole in the plug. After 72 hours the plug was removed from the holder and the Ni-wire at the thermocouple surface cut with care to avoid burring the ends. The wire on the back was left with an approximate length 90 mm (3.543 inch). The heat treatment procedure was then repeated as in Section 4.2.4.

4.2.6. Polishing Process

The filling cement should be raised approximately 2mm (0.0787 inch) above the surface to be polished. The support provided to the wire ensures that wire will finally be concentric with the surrounding cement and plug surface, and the cement will be flush with the metal surface and without flows. The initial finishing was done in a lathe using emery paper of reducing fineness.

The next process of grinding used a series of successively finer grit silicon-carbide paper 400, 600, 1200 under running water to remove the debris. In passing from one grade of paper to the next finer grade the surface was washed to remove grit and the surface turned through 90° to remove the previous set of scratches.

After grinding the surface is ready for polishing. It is thoroughly washed in water and dried, and then held against "Selvyt" (A cotton cloth with diamond insertions) covered rotating disc. The "Selvyt" cloth was moistened with a paraffin based lubricant and impregnated with polishing compounds consisting of small diamond particles in a wax carrier. The successive size grades are 6 micron, 1 micron and 0.25 micron, the surface

was washed with Genklene and Alcohol before progressing to the next fine grade. The final result should be highly polished, scratch free and the surface should be like a mirror. Continuity was tested by a vometer on the surface thermocouple.

4.2.7 Nickel Plating and Testing

The plating of the end of the plug was carried out in a N.G.N Vacuum coating machine chamber. The surface thermocouple holder was used to hold the plug tightly and perpendicular to the evaporation electrode. The layout of the system is shown in Fig. 4.3.

The initial development was carried out using a copper (Cu) film which was easier to deposit, but all later plugs had a nickel film.

The film thickness is approximately 3 to 5 micron. With nickel coating it is more difficult to obtain a uniform thickness due to the high melting point of Ni (1451°C), while the Cu melting point 1082°C makes the Cu coating process more reliable. In a motored engine a Cu film is adequate and is more easily manufactured.

A special meter was devised to test film coating, as the ordinary avometer induce a relatively high current which breaks down film. The meter shown in Fig. 4.1b induces a maximum current of 2.25 m Amper. Fig. 4.4. shows the flow chart of surface thermocouple manufacturing process.

4.3 CALIBRATION

It is necessary to calibrate the surface thermocouple against a standard. In order to calculate the E.M.F. induced by any pair of metals as a thermocouple, there are two ways to determine the E.M.F. induced Ref. (57). Either by a graphical method using Fig. 4.5 which represents the thermo-electric powers ($\frac{dE}{dT}$) of several metals compared with lead as standard metals, measured in micro-volts per 1°C, or by using Avenarius formula $E = bT + cT^2$, where b and c are constants and their values can be found in Ref. (57). Both methods of determining E.M.F. induced by iron-nickel thermocouple, give 3.2 mV at 100°C temperature difference above 0°C.

The standard iron-nickel thermocouple manufactured from commercial thermocouple wire was calibrated against a standard mercury thermometer, the output shows 3.198 mV and this shows high agreement with calculated value as shown in Fig. 4.6.

The surface thermocouple was calibrated against a standard mercury thermometer in a control-heating water container. The surface thermocouple with both nickel and copper film coating were tested in this way. The output of the surface thermocouple with copper film was less than the output of the surface thermocouple with nickel film even when left for along period in order to reach a uniform temperature. At 100°C temperature difference the copper film read 3.024 mV and the Nickel film 3.12 mV representing a difference of 2.687°C. This difference occurred with a number of different thermocouples and was always the same to experimental error. Since the outside end of the thermocouple was not immersed, temperature gradients in the plug were probably responsible. With a copper film the insulation

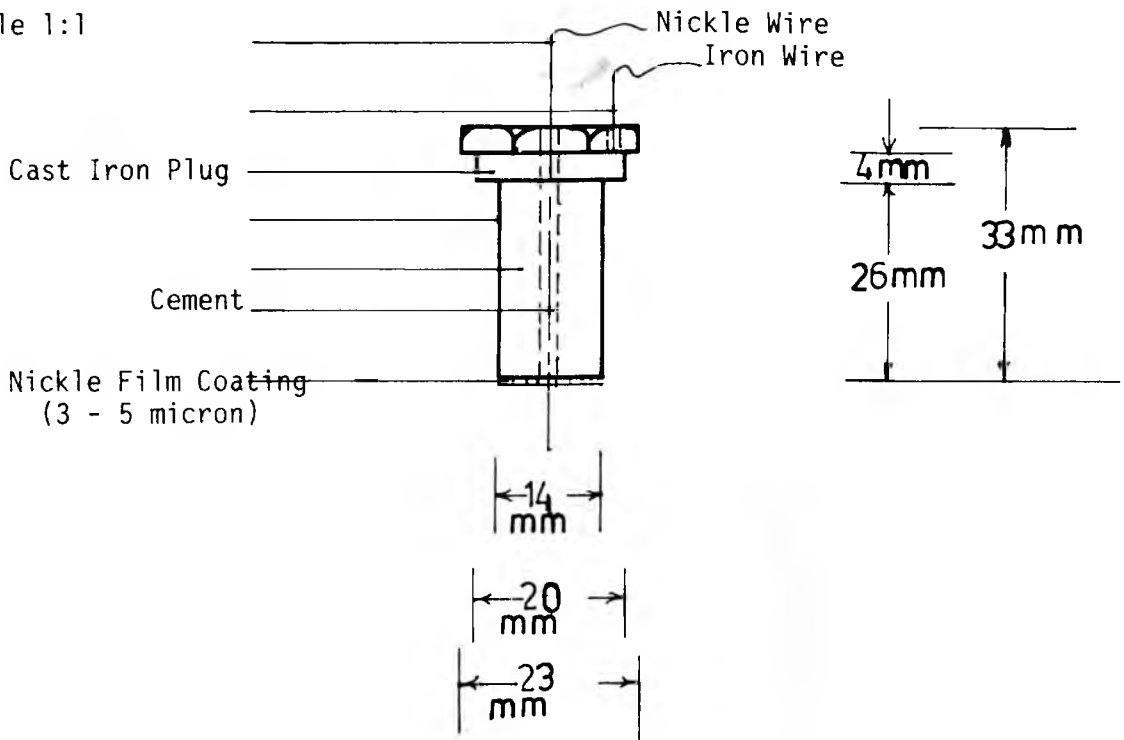
effect of the cement on the nickel wire would produce this effect. With a nickel film the Ni/Fe junction is at the cement/iron interface.

Both nickel and copper film thermocouples had output values less than the expected value of 3.2 mV at 100°C difference possibly due to the effect of the quality of the iron as shown in Fig. 4.7.

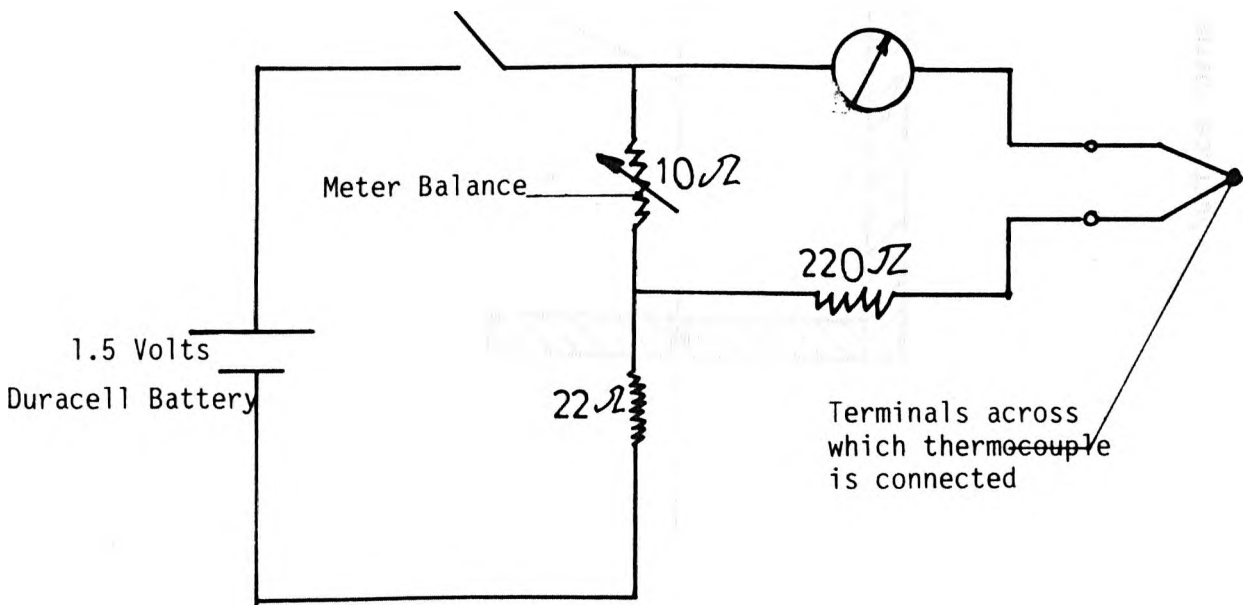
The surface thermocouple was calibrated before and after the test, the average value between the two calibrations has been used for processing the data the reason for a difference (less than 0.096 mV) is the oil contamination on the surface thermocouple during the test which reduced the output result. the calibration curves for both nickel and copper film surface thermocouple are shown in Fig. 4.8 and 4.9 respectively.

Fig. 4.1

Scale 1:1

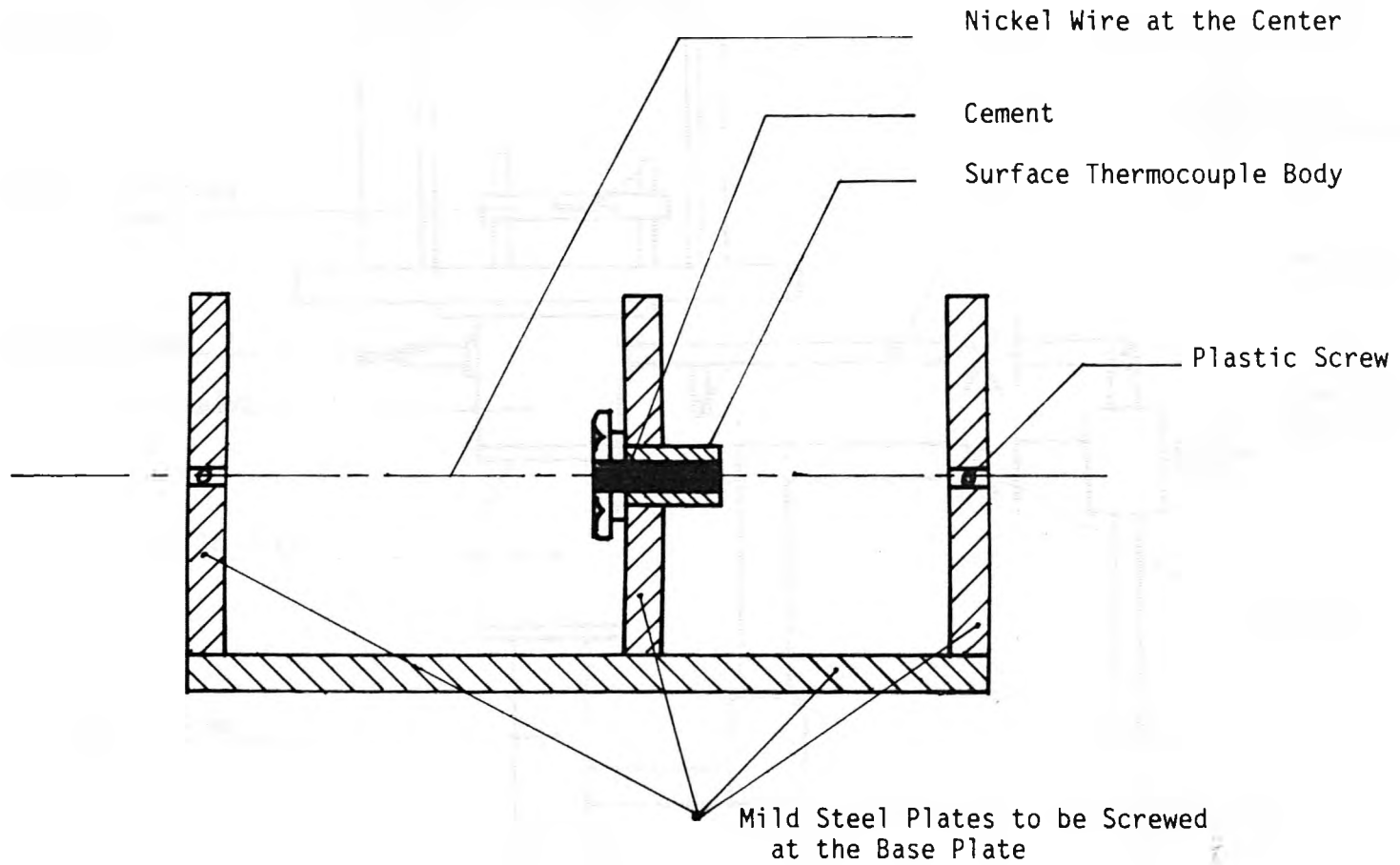


(a) Surface Thermocouple Design



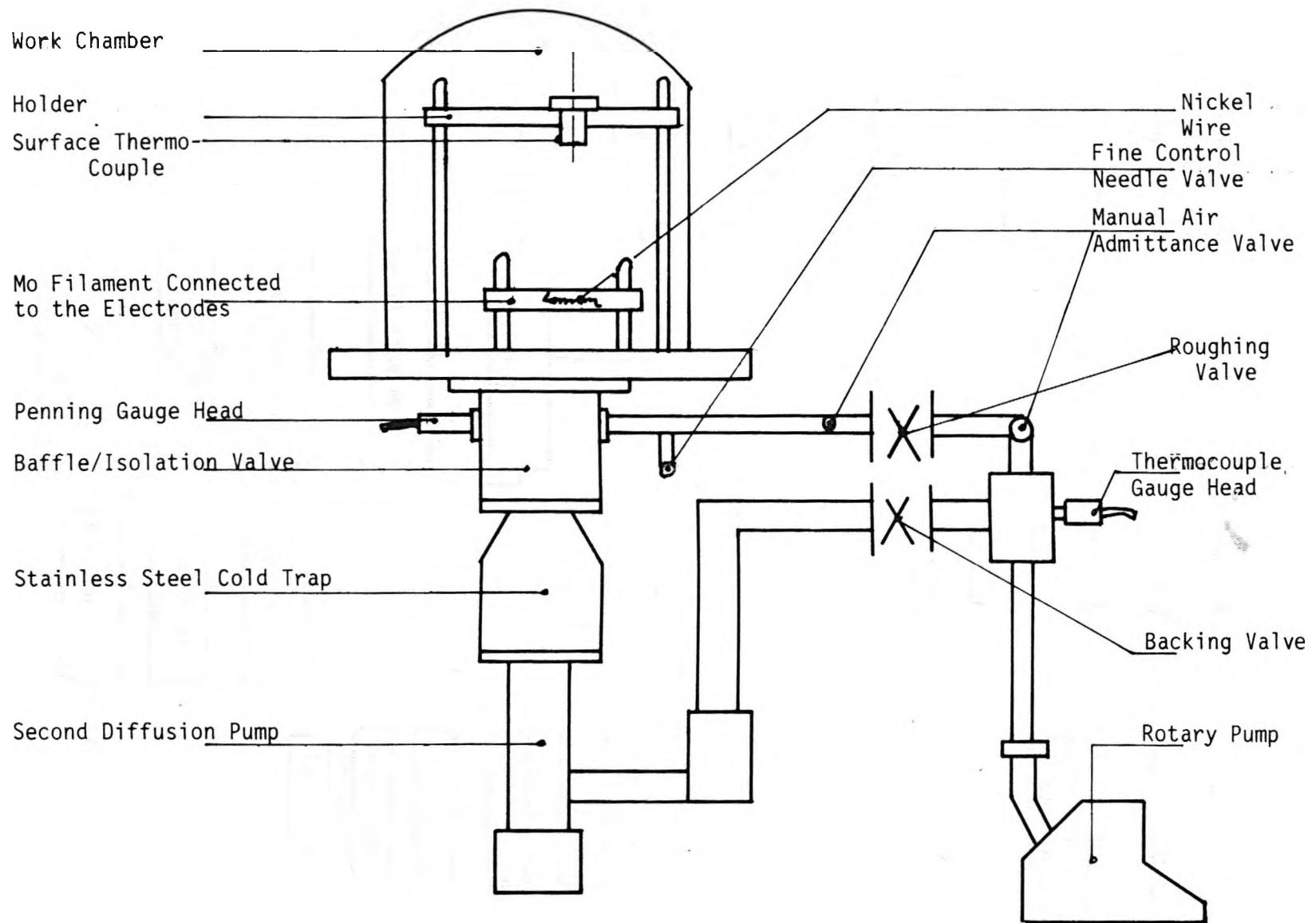
(b) Surface Thermocouple Electrical Test Meter

Scale 1:2



Surface Thermocouple Holder

Fig. 4.2



General Layout of the Coating Unit

Fig. 4.3

Surface Thermocouple Manufacturing Process

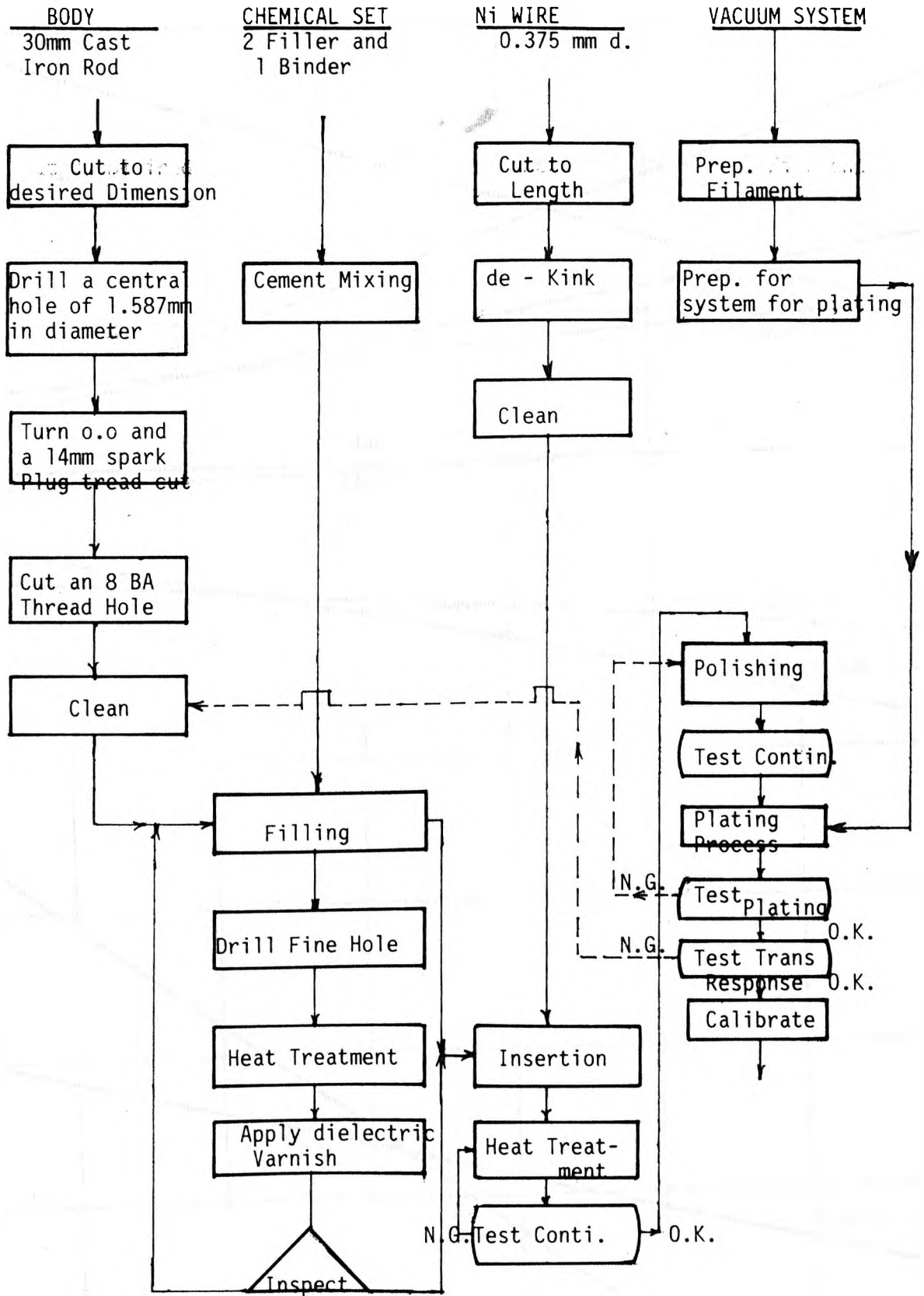


Fig. 4.4

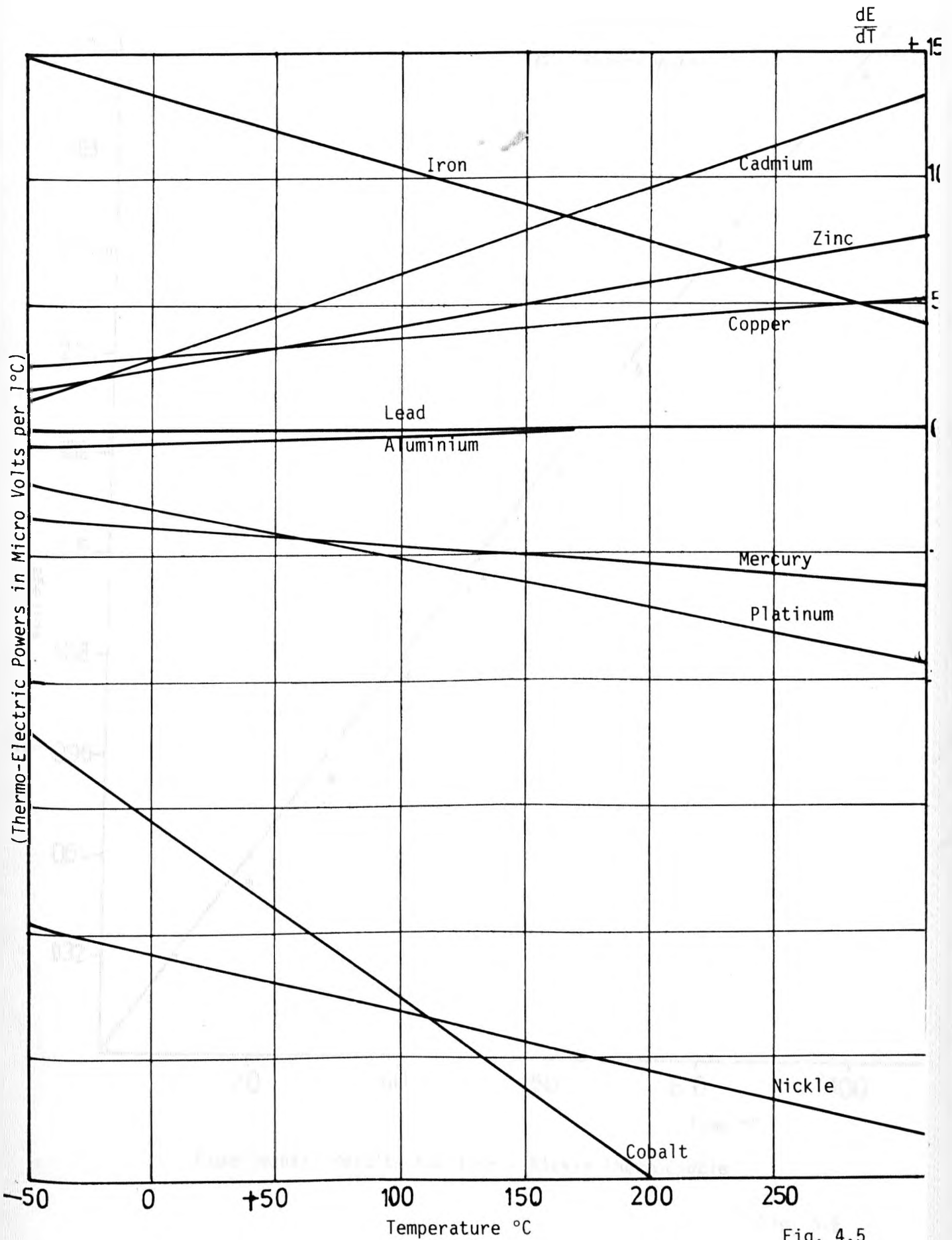
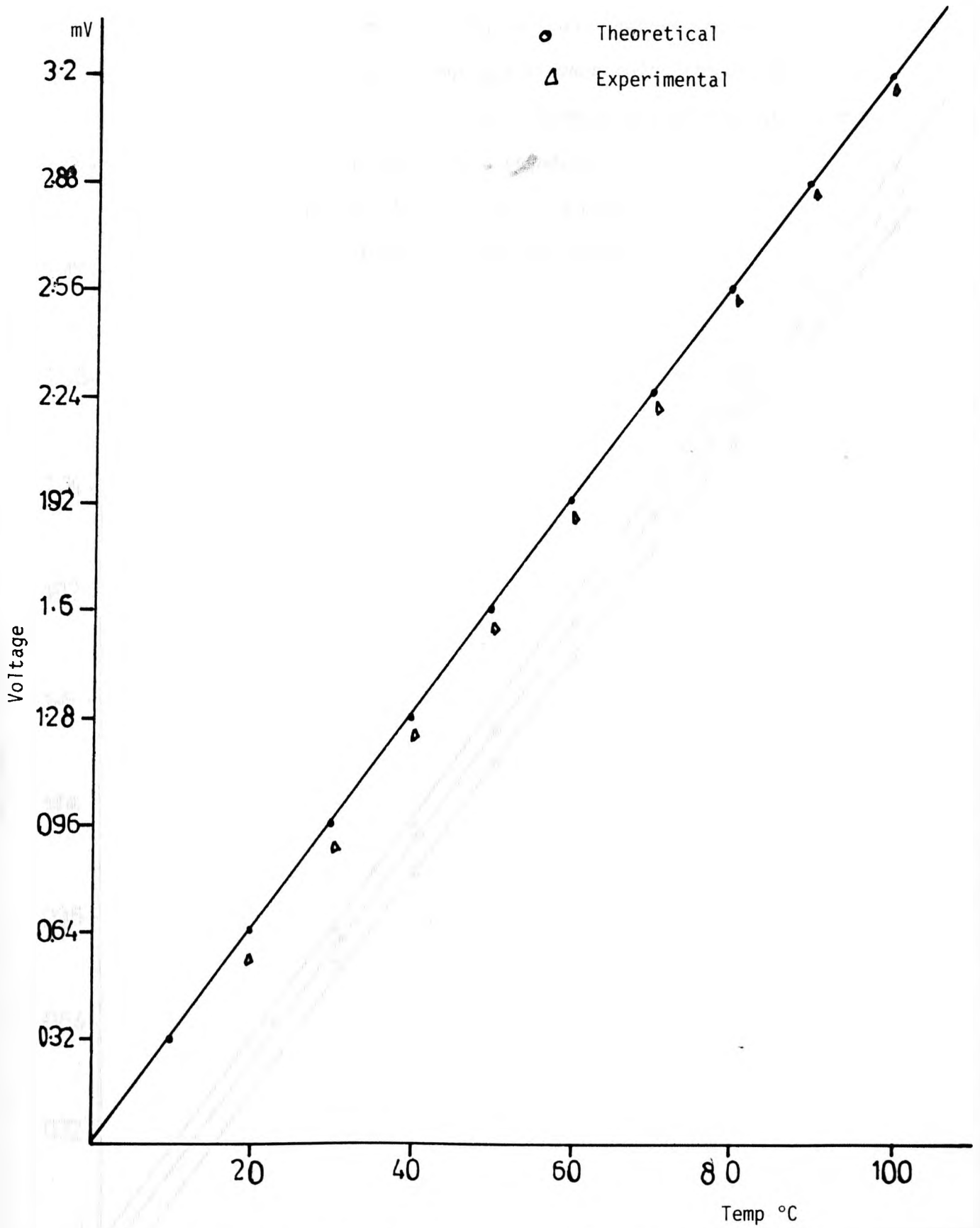


Fig. 4.5

The Thermo-Electric Powers of Several Metals Compared with Lead

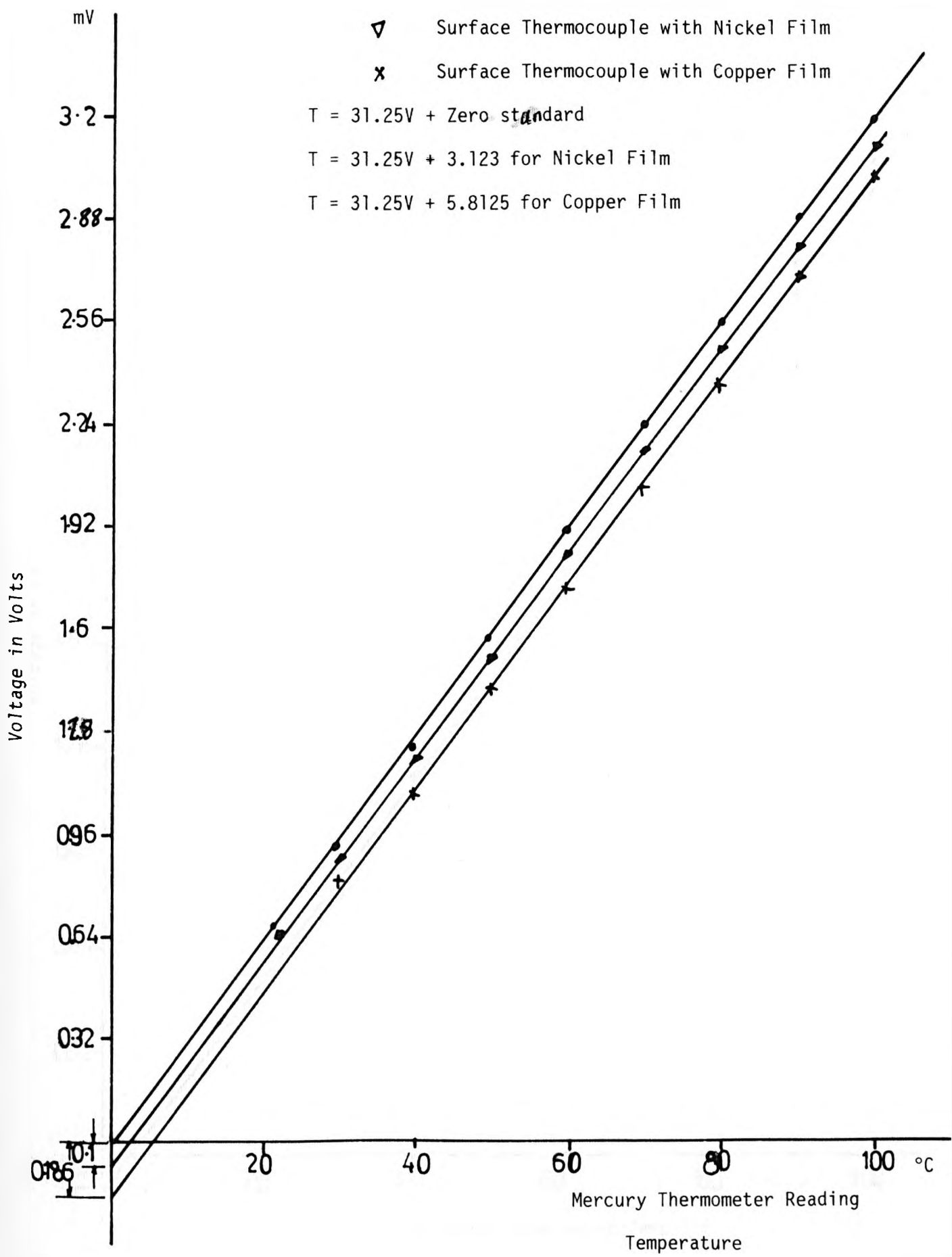


Experimental Results for Iron - Nickle Thermocouple

Fig. 4.6

- Standard Iron - Nickel Thermo
- ▽ Surface Thermocouple with Nickel Film
- × Surface Thermocouple with Copper Film

$T = 31.25V + \text{Zero standard}$
 $T = 31.25V + 3.123 \text{ for Nickel Film}$
 $T = 31.25V + 5.8125 \text{ for Copper Film}$



Calibration of Surface Thermocouple

Fig. 4.7

Calibration before and After the test

Nickle Film

○ Before test

△ After test

Mean Calibration is

$$T = 31.25 \times V + 3.25$$

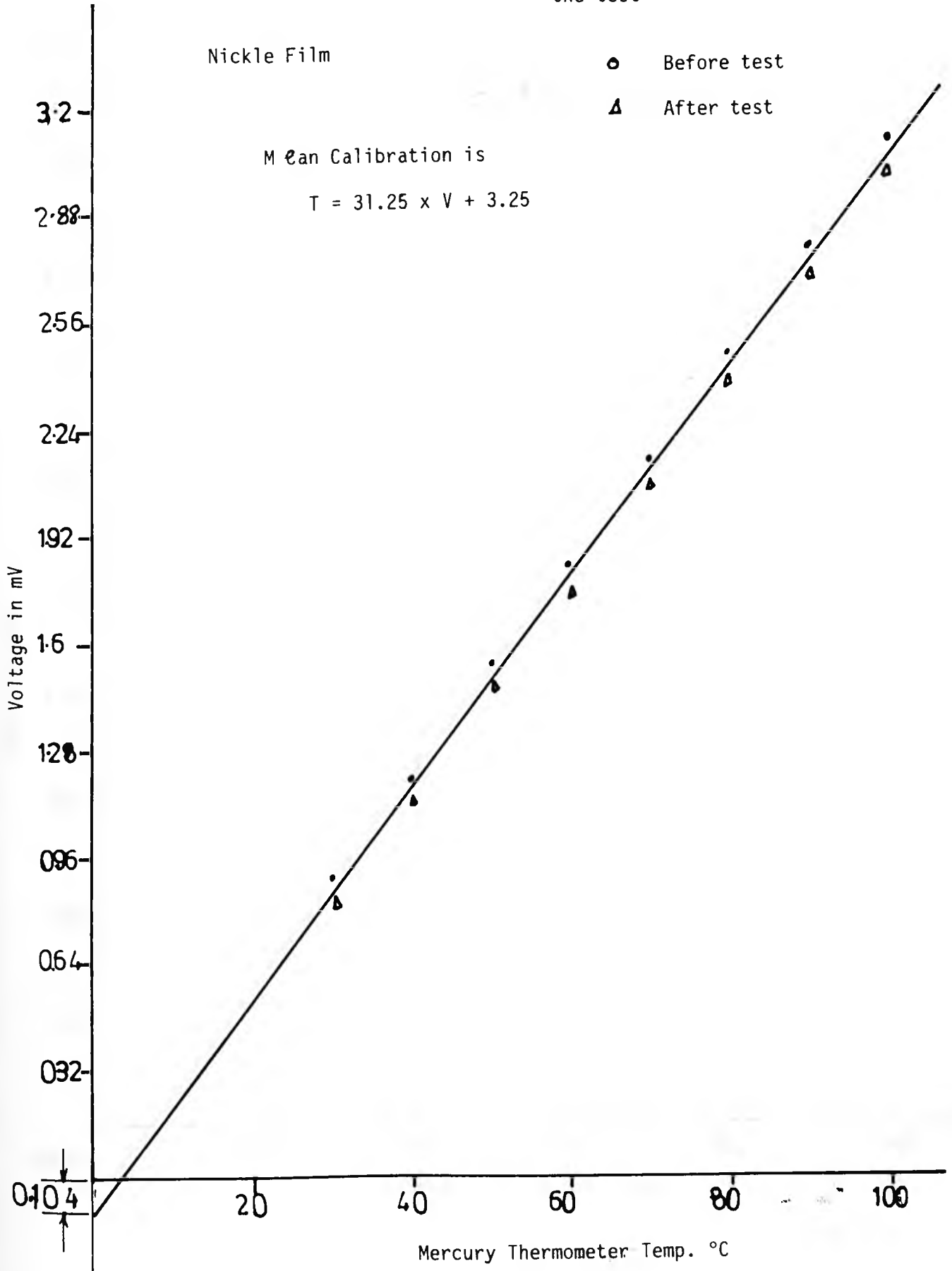


Fig. 4.8

Calibration of Surface Thermocouples before and After
the Test

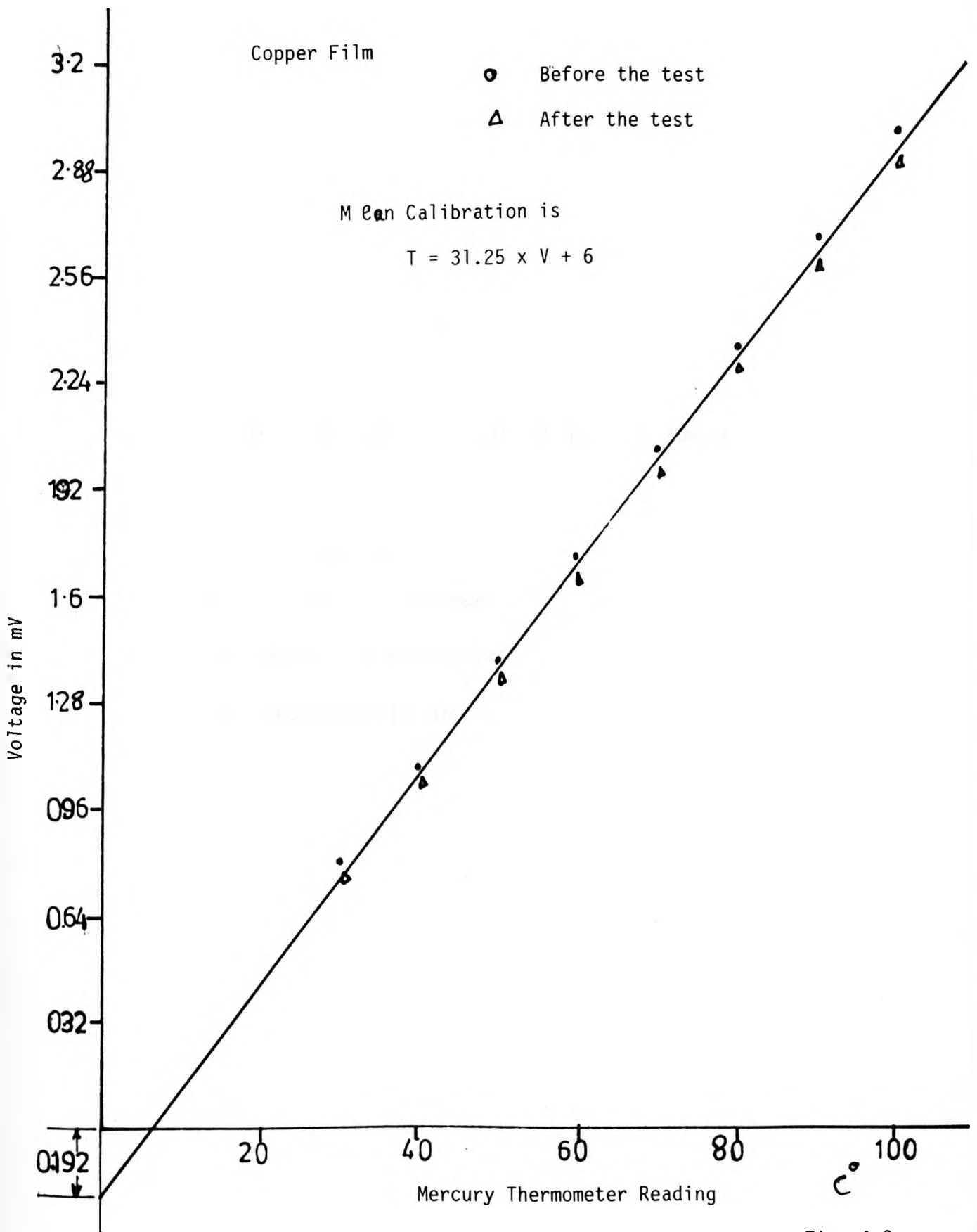


Fig. 4.9

CHAPTER 5

THEORY OF UNSTEADY HEAT TRANSFER IN I.C. ENGINE

- 5.1 Introduction
- 5.2 Theory of Turbulence
- 5.3 Methods of Predictions
- 5.4 Present Prediction

5.1 Introduction

The conclusion from what has been mentioned in chapter one related to the heat transfer predictions in the cylinder of an Internal Combustion engine for both spark-ignition and diesel engine, can be classified under four main categories based on the way of predictions and they are described in section 5.3. The theory of turbulence and its effect on heat transfer is described in section 5.2 and 5.4 respectively.

5.2 Theory of Turbulence

It is important to measure and describe the turbulence structure in an internal combustion engine. It affects power output, heat loss, exhaust emission and fuel consumption. The word turbulence has been used in different definitions in the literature on air motion in reciprocating engines. These differences come from the fact that not all cycle to cycle variations in instantaneous velocity are turbulence and there is difficulty in distinguishing what part of the variation is due to turbulence. Hinze Ref. 77 defines turbulence in the following way: "Turbulent fluid motion is an irregular condition of flow in which the various quantities show a random variation with time and space coordinates, so that statistically distinct average values can be discerned".

In steady flows the first important statistical parameter is the time average of the velocity, i.e. the mean flow velocity Ref. 82. In unsteady flows an ensemble average must be used instead of the time average of the velocity over a long time. This is defined by Bradshaw Ref. 23, "as a set of samples of a random process (eg. $U(x, y, z)$) for a set of different values of t or a set of repeats of an experiment." If the unsteady flow is cyclical and regular so that all the variation from cycle to cycle is according to turbulence, then turbulent intensity

could be defined in the same way as for steady flows with the ensemble average velocity instead of the mean flow velocity.

In engines cylinders, the gas flow is non-stationary and cyclically irregular Ref. 144. Therefore, any attempt to define the flow must take into account ensemble averaging, the cyclic fluctuations and the turbulent fluctuations. The instantaneous velocity at any point in the cycle is given by:-

$$U(t) = \bar{U} + U(CA) + U(CY) + U' \quad 5.1$$

where \bar{U} is the time average given by

$$\lim_{T \rightarrow \infty} \frac{1}{T} \int U(t) dt \quad 5.2$$

$\bar{U} + U(CA)$ is the ensemble average and

$U(CA)$ is a function of crank angle only.

$U(CY)$ is the cyclic fluctuation in velocity

U' is the turbulent fluctuation

$\bar{U} + U(CA)$ can be easily obtained by taking an average over many cycles at any point. However, $U(CY)$ is difficult to measure and the following formula is usually used:

$$U(CY) = \frac{1}{T} \int_0^T U(t) dt - \bar{U} - U(CA) \quad 5.3$$

where the time T over which the average is taken is less than the period of the cycle. The difficulty arises in choosing a suitable value for T . It must be large compared with the time scale of turbulent fluctuations (i.e. of U'). Semenov Ref. 123 used 24° CA for T , although this is arbitrary choose, and the errors are large when the directional velocity changes ($\bar{U} + U(CA) + U(CY)$) appreciably over the interval, giving false values for the turbulent fluctuations. Witze Ref. 149 disagreed with the model, saying that the definition of the cyclic variation was arbitrary as it represented a low frequency variation

in velocity depending on engine speed and crank angle interval used for the time average. He also considered that the use of a time average presumed local-stationarity in the flow. The model used by Witze consisted only of an ensemble average and a fluctuating component. The instantaneous velocity U for engine crank angle θ is defined as follows:

$$U(\theta) = \bar{U}(\theta) + U'(\theta) \quad 5.4$$

and

$$\bar{U}(\theta) = \frac{1}{N} \sum_{i=0}^{N-1} U(\theta + in\pi) \quad 5.5$$

where N is the number of revolutions at which the velocity measurement is taken

n is the number of strokes in each engine cycle.

The turbulence intensity U' is therefore defined by the expression

$$U'(\theta) = \sqrt{\overline{U^2(\theta)}} - \bar{U}(\theta) \quad 5.6$$

$$\text{where } \overline{U^2(\theta)} = \frac{1}{N} \sum_{i=0}^{N-1} U^2(\theta + in\pi) \quad 5.7$$

Equations 5.4 to 5.7 are used in the present work.

5.3 Methods of Predictions

5.3.1 Theory Predictions

This type of work is purely theoretical, utilising numerical computation of theoretical models Refs. 25, 37, 51, 52, 53, 54, 63, 113, 120, 130. Complete accurate solutions are not possible without empirical relationships obtained by experiments.

5.3.2 Empirical Predictions

The early empirical formula were established by Nusselt Ref. 103 and Eichelberg Ref. 39, 40, 41. The Nusselt formula is:

$$\frac{q}{A} = C_1 (1 + 0.38V_p) (P^2 T)^{\frac{1}{3}} (T_g - T_w) + C_2 (T_g^4 - T_w^4) \quad 5.8$$

This formula is not dimensionally correct because the constants have dimensions and can be written as

$$(NU) = (\alpha + \beta (Re)) ((Pr)/C_p) (T^4/p)^{\frac{1}{3}} \quad 5.9$$

The formula was based on simple experiment. The Eichelberg formula was carried in an operating engine and covers both radiant and convective heat transfer.

$$\frac{q}{A} = C(Vp)^{\frac{1}{3}} (PT)^{\frac{1}{2}} (T - T_w) \quad 5.10$$

Again the formula is not dimensionless and both mode of transfer are covered together.

Many other formula such as Overbye Ref. 107

$$\frac{qL}{3600 \cdot A K_i T_i} = \left(\frac{L V_p \rho_i C_{pi}}{K_i} \right) \left(\frac{0.26p}{rpi} - 0.035 \right) \times 10^{-4} + 0.1 \frac{P}{rpi} - 0.02 \quad 5.11$$

This formula is incomplete because the temperature difference doesn't appear, i.e. the same heat transfer can be predicted whatever the wall temperature is.

All the early empirical formula fails to satisfy the requirements.

5.3.3 Pipe Flow Heat Transfer Data Prediction

This approach is based on using the heat transfer theory of pipe flow (Nusselt equation) for turbulent convective steady heat transfer and applying it to the cylinder of an internal combustion engine (Knight Ref. 78 and Woschni Ref. 152). The Woschni's equation is

$$\frac{q}{A} = C_1 \frac{K}{D} (T_g - T_w) \left[\frac{(V_p + V_c)^D}{L} \right]^{0.8} \quad 5.12$$

$$\text{where } V_c = C_2 \frac{T_1 V}{P_1 V_1} (P - P_0) \quad 5.13$$

This velocity is added to cover the effect of the combustion and expansion stroke. Where P_1 and T_1 represent the known state of the working gas related to the instantaneous cylinder Volume V_1 . V is cylinder volume, and P_0 is gas pressure in the cylinder of the corresponding motored engine.

If the engine is motored equation (5.12) can be written as follows:

$$NU = 0.035 (Re)^{0.8} \quad 5.14$$

This approach gives a better understanding to heat transfer prediction in internal combustion engines by applying direct measurement of velocity and gas temperature unlike the empirical formula, but since there has been no direct attempt to verify the correctness it is difficult to say the prediction is satisfactory.

5.3.4 Annand's Method

This is an extension of the Woschni method including radiation. Using the methods of dimensional analysis for the convective component to steady the effects of various parameters upon the time-mean rate of heat transfer.

This has been done by many workers such as Elser Ref. 44 and Annand Refs. 8, 9. Annand re-examined most of the empirical formula then existing and put forward a new formula to predict the instantaneous heat transfer to cover both modes, convection and radiation

$$\frac{q}{A} = a \frac{K}{D} (Re)^b (T_g - T_w) + C (T_g^4 - T_w^4) \quad 5.15$$

where a , b and c are constants.

5.4 Present Work

In the present work the Annand's formula is re-examined and considered as a strong basis of the new correlation.

If the engine bore D is considered as a basic length dimension. The flow pattern will be characterized by an instantaneous velocity U and a set of velocity ratios. Assuming that mean values can be used, gas properties of importance will be the thermal conductivity K , the dynamic viscosity μ , the specific heat C_p and the density ρ , the temperature of both gas and surface. The rotational speed N to represent the oscillation frequency. The crank angle θ . The instantaneous cylinder pressure P , turbulence intensity and if there is combustion the rate of heat release q_c .

Therefore, the heat transfer coefficient for engines of similar geometry may be expressed as

$$\frac{q}{A(T_g - T_w)} = h = \text{Fn}(\bar{U}, \acute{U}, L, D, P, K, \mu, C_p, \rho, N, q_c, T_g, T_w) \quad 5.16$$

neglecting combustion if necessary, expressing time dependent parameters as functions of θ and rotational speed replaced by mean piston speed

$$V_p = 2LN/60 \quad 5.17$$

then the heat transfer coefficient

$$h = \text{Fn} \left[\bar{U}(\theta), P(\theta), T_g(\theta), T(\theta), V_p, \acute{U}(\theta), K(\theta), C_p(\theta), \rho(\theta), \mu(\theta), D \right] \quad 5.18$$

The main dimensional groups are Reynold Number, the ratios of mean velocity $\bar{U}(\theta)$ and turbulence $\acute{U}(\theta)$ to the mean piston velocity V_p , Prandtle Number, the ratio of turbulent transport of pressure forces to the conductive heat transfer $(P \acute{U} D / K T_g)$ (hereafter referred to as Energy Number) and temperature difference number $T_g / \Delta T$.

Therefore equation 5.18 can be reduced to the following form:

$$Nu = F_n \left[Re(\theta), Pr(\theta), \left(\frac{T_g}{\Delta T} \right), \left(\frac{\bar{U}(\theta) + U'(\theta)}{V_p} \right), \left(\frac{P U' D}{KT_g} \right) \right] \quad 5.19$$

The difficulty in most of the existing correlations is that all parameters which might affect the heat transfer are involved and the manner of combination between these parameters. As has been mentioned above the Re number will be the major parameter and this strongly supported by Annand Ref. 8,9, and Woschni Ref. 152.

Annand did not include turbulence as a variable and did not use group $T_g/\Delta T$ when choosing to ignore the minor groups. With introduction of turbulence the last two groups are thought to be significant. To check this it is necessary for direct measurement of charge motion (velocity and turbulence intensity) to be carried out.

To improve accuracy instantaneous measurement of Pressure, gas and wall temperature is desirable.

Assuming a functional relationship for equation 5.19 neglecting Pr number, equation 5.19 can be written as

$$Nu = f_n \left[Re(\theta), \left(\frac{T_g}{\Delta T} \right), \left(\frac{\bar{U}(\theta) + U'(\theta)}{V_p} \right), \left(\frac{P U' D}{KT_g} \right) \right] \quad 5.20$$

equation (5.20) states only that Nu number depends on the four parameters at the right side of the equation and no information is provided regarding the nature of the function. That is, equation 5.20 does not state how the Nu number depends on the other four parameters and the relation between them is unknown. However, if Nu number depends on the other parameters it most certainly can be combined by multiplication raised to any power, i.e. equation 5.20 can be written in the following form:-

$$Nu = a Re^{b1} \cdot \left(\frac{\bar{U} + U'}{V_p} \right)^{b2} \cdot \left(\frac{T_g}{\Delta T} \right)^{b3} \cdot \left(\frac{P U' D}{KT_g} \right)^{b4} \quad 5.21$$

where a, b1, b2, b3 and b4 are constants, where each exponent is equal to a constant which may be positive or negative.

The effect of radiation following Annand can be represented by

$$\frac{q}{A} = Q_{\text{radiation}} = C (T_g^4 - T_w^4) \quad 5.22$$

C is an average factor, applicable to both combustion - expansion stroke, and can be determined empirically Ref. 8.

Since the radiation term represents a small percent of the total heat transfer in a motored engine it is neglected in the present work.

Therefore equation 5.21 is represented by the process of combining the parameters and this is known as compounding method which is useful because dimensional analysis does not give the analyst much opportunity if any, to guide the analysis to a convenient solution.

Equation 5.21 is used in the present work to predict heat transfer in a motored engine. A computer programme is developed (Appendix 8.12) to obtain the best value of the exponents and the multiplying constant and with this achieved by including most of the tests which have been carried out. The solution of equation 5.21 is discussed in Chapter 8.5.4.

INSTRUMENTATION AND EXPERIMENTAL
EQUIPMENT

-
- 6.1 Introduction
 - 6.2 The Engines
 - 6.2.1 Austin-Ricardo Engine
 - 6.2.2 Ricardo E6 Engine
 - 6.3 Crank Angle Marker and Coupling Device Arrangement
 - 6.3.1 Existing Crank Angle Markers
 - 6.3.2 Crank Angle Marker System
 - 6.3.3 Coupling Device Arrangement
 - 6.4 Instrumentation Theory
 - 6.4.1 Analysis of the Hot-Wire Signal
 - 6.4.2 Analysis of Gas Temperature Resistance Thermometer
 - 6.4.3 Pressure Correction Method
 - 6.5 In Cylinder: Instrumentation
 - 6.5.1 Introduction
 - 6.5.2 Pressure
 - 6.5.3 Surface Wall Temperature
 - 6.5.4 Probes Construction
 - 6.5.5 Hot-Wire Anemometer
 - 6.5.6 Gas Thermometer Temperature
 - 6.5.7 Other Equipments
 - 6.6 In Cylinder: Calibration
 - 6.6.1 Pressure
 - 6.6.2 Gas Temperature
 - 6.6.3 Velocity

6.1 Introduction

Unsteady heat transfer in an internal combustion engine cylinder is complicated and of interest to many research workers. Many subjects are involved with heat transfer in internal combustion engine, so in order to have a better knowledge of studies, many parameters have to be measured over many cycles of the engine and at different crank angles. In this project an attempt was made to study the unsteady heat transfer in a motored internal combustion engine while measuring gas velocity, gas temperature, gas pressure and surface wall temperature. Hot-wire anemometer, wire resistance thermometer, kistler pressure transducer and surface thermocouple probe respectively were used for measuring purposes.

Two engines were used for the experiments, an Austin modified Ricardo E6 motored without inlet or exhaust valves this making the "combustion" chamber a closed cylinder in which air movements could only be set up by the motion of the piston. The second engine was a Ricardo E.6/T in the standard petrol engine configuration. The following sections describe the engines, in cylinder instrumentation theory, the probes construction used in the anemometry and the electronic equipments.

6.2 THE ENGINES

6.2.1 Austin-Ricardo Engine

This engine is an experimental two stroke engine based on a Ricardo E6 crank case. For the present tests the piston controlled ports are blocked and a flat plate used as a head. The engine may be motored by a 3.7 kw Dc motor up to a speed of 800 r.p.m. (600 r.p.m. in test).

Specification Bore : 81.756 mm (3.21875 inch)
 Stroke : 111.125 mm (4.375 inch)
 Compression Ratio : 8:1

The head was provided with four spark plug holes (14 mm in diameter). This made it possible to measure all the four parameters (gas velocity, gas temperature, gas pressure and wall temperature) at the same time as shown in Figure 6.1. The piston used has a flat-top piston. This engine was used to develop the instrumentation since it was easily stripped for replacing hot-wires etc.

6.2.2 Ricardo E6 Engine

This engine was a Ricardo E6 experimental engine with a petrol engine head.

Main specifications: Bore : 76.2 mm (3.0 ins)
 Stroke : 111.125 mm (4.375 ins)
 Motoring Speed : 500 - 3000rev/min
 Compression Ratio variable from 4.5 to 20
 Connecting Rod Length : 241.978 mm (9.5267 ins)
 Swept Volume : 507 ccs

The engine is of the single cylinder poppet-valve four-stroke type and it can be operated as diesel engine or petrol engine which is our interest as shown in Fig. 6.2.

The Salient features for present purposes are a cylindrical combustion chamber, a cast iron cylinder liner and head, the head having two 14 mm spark plug holes and one 10 mm hole not used because of its

inaccessability. A variable compression ratio 4.5 - 20:1, and a maximum motored speed of 3000 rpm. Fig. 6.3 shows the arrangement of the lubricating oil system and cooling system. A description of this engine appears in Ref. (115).

6.3 CRANK ANGLE MARKER AND COUPLING DEVICE ARRANGEMENT

6.3.1 Existing Crank Angle Markers

Both engines were already fitted with a similar crank angle marker on the fly wheel. Small rectangular grooves around its rim excited a small permanent magnet wound with a pickup coil. The grooves were spaced at 10 degree intervals except at T.D.C. and B.D.C. where the grooves were at 5 degree intervals. The output from the coil was fed to d.c. amplifier to give all the cycle crank angle marks point.

This crank angle marker has two main disadvantages:

1. It is difficult to obtain a sharp edge signal for T.D.C. and B.D.C. for accurate timing and computer triggering.
2. The programming of the data triggering system to read at a particular crank angle point would be difficult, especially when collecting large quantities of data at high speed over a large number of revolutions. This is necessary when trying to measure turbulence and other fluctuating quantities. A Ferranti optical Tachometer together with a special processing system was therefore used.

6.3.2 The Crank Angle Marker System

The system Fig. 6.4 was designed to collect data at any specified crank angle. To fit the Ferranti optical Tachometer (motor) to an engine, adaptors are required and for the present two engines these are described in section 6.3.3.

The FERRANTI optical incremental encoder type (23L 47/M 116) produces two outputs a 900 pulses/rev and a T.D.C. pulse. The 900 pulses/rev channel is processed by the electronic circuit as shown in Figs. 6.5, 6.6, 6.7, to give the following features:-

1. Divide the 900 pulses from optical TACHO by 15 to give 60 pulses/rev which is connected to a timer to obtain the engine speed.
2. Multiply the 900 pulses by 4 to give 3600 pulses/rev i.e. approximately $\frac{1}{10}$ of the degree can be measured. These pulses are used as a trigger for the data logging process and any desired crank angle point can be located by the select crank angle unit and data logged at that angle for a maximum of 1664 revolutions (limited by the computer storage).
3. The 3600 pulses/rev were divided into two channels. One of them is connected to an oscilloscope. On the oscilloscope the trace appears as 2 horizontal lines because of the high frequency produced by 3600 pulses /rev. The other channel is connected to the four digit number select crank angle unit.

The unit is then connected to a real time clock which produces the trigger pulse to the Analogue digital convertor of the Alpha-Computer.

4. A line from Ferranti optical Tacho gives a trigger for the T.D.C. and this may be used for triggering the oscilloscope during the period in which instrumentation is checked prior to computer logging to locate T.D.C. accurately, a light on the select crank angle system is illuminated at T.D.C. and the system may be adjusted statically.

6.3.3 Coupling Device Arrangement (TACHO-Motor Drive)

Although both engines have Ricardo crank shafts the detail differs and therefore two couplings were designed to fit the Austin-Ricardo engine as shown in Fig. 6.8a and to fit E6 - Ricardo engine as shown in Fig. 6.8b. The arrangement is designed to produce minimal torsional error.

The main part of coupling assembly is the Ferranti optical support (referred to as motor) which consists of a front flange connected to a cylinder with a locating flange at the end, four screws connect to the body of the engine around the drive shaft. The Austin-Ricardo engine has a small stub shaft on the end of the crank shaft, and a sleeve with a similar shaft was fitted to the E6, this enabling the same coupling to be used in both engines. All the parts were made from mild steel.

6.4 INSTRUMENTATION THEORY

6.4.1 Analysis of the Hot-Wire Signal

As the anemometer signal was a function of the temperature and pressure of the gas and since the anemometer was calibrated at room conditions only, it was necessary to obtain the relation satisfying the heat transfer from the wire. This is one of the problems to be considered in this section. Another problem concerns the thermometer wire temperature which lagged behind the gas temperature because of the wire's thermal inertia.

A method of calculating the true gas temperature from the wire temperature will be described in the next section, and follows that of Ref. (49).

The radiation effect has been neglected; the error due to this is less than 1% Refs. (15, 65). Also the effect of the heat conduction through the prongs is small and can be neglected if the length/diameter ratio of the wire is greater than 300 Refs. (43). The ratio for the hot wire used in the present work was 340 approximately so that end conduction effects were neglected. Many research workers have assumed that the hot-wire is at a uniform temperature equal to the mean wire temperature corresponding to the mean electrical resistance Refs. (11, 43, 61, 66, 67, 124). This gives a simple equation for the heat transfer from the wire:

$$I^2 R_{hw} = h \times \text{Area} \times (T_s - T_g) \quad 6.1$$

where, I is the electrical current through the wire

R_{hw} is the electrical resistance of the wire

h is the heat transfer coefficient

Area is the wire surface area

T_s is the sensor wire temperature, corresponds to R_{hw}

T_g is the temperature of the gas surrounding the wire

The output from the anemometer which was fed to the linearizer is the bridge voltage and this is proportional to the current through the sensor.

$$\text{Thus } V^2 = I^2 \times cc \quad 6.2$$

where cc is the conversion factor for the bridge. Equation 6.1 becomes:

$$V^2 R_{hw} = cc \times h \times \text{Area} \times (T_s - T_g) \quad 6.3$$

Most research workers use the expression for the heat transfer coefficient h , Ref. (43, 66, 67), in the form:-

$$Nu = C_1 + C_2 (Re)^n \quad 6.4$$

where Nu is the Nusselt number = $\frac{h \times d}{K_g}$

where d is the wire diameter and K_g the thermal conductivity of the gas.

Re is the Reynolds number = $\frac{\rho u d}{\mu}$

where ρ is the gas density

u is the gas velocity

μ is the coefficient of viscosity of the gas

C_1, C_2 and n are constants.

Equation 6.4 was used in this project. Substitution from Equation 6.4 into Equation 6.3 and after re-arrangement,

$$V^2 R_{hw} = (T_s - T_g) \times (A + B (\rho U)^n) \quad 6.5$$

where

$$A = \frac{cc \times Kg \times Area \times C_1}{d} = A_o \left(\frac{Kg}{Kg_o} \right) \quad 6.6$$

and

$$B = \frac{cc \times Kg \times Area \times C_2}{\mu^n \times d^{1-n}} = B_o \left(\frac{Kg}{Kg_o} \right) \left(\frac{\mu_o}{\mu} \right)^n \quad 6.7$$

(subscript_o refers to room condition). The values of A_o, B_o and n were obtained from the calibration curve of the hot-wire at room temperature. It was assumed that $Kg \propto (T)^{0.8}$ and $\mu \propto (T)^{0.76}$ Ref. (43), and therefore equation 6.6 becomes:

$$A = A_o \left(\frac{T}{T_o} \right)^{0.8} \quad 6.8$$

and the value of n = 0.48, from the calibrations, and equation 6.7 becomes:

$$B = B_o \left(\frac{T}{T_o} \right)^{0.8} \times \left[\left(\frac{T_o}{T} \right)^{0.76} \right]^{0.48} = B_o \left(\frac{T}{T_o} \right)^{0.435} \quad 6.9$$

The values of A and B were evaluated at the mean of the gas and wire temperatures. While the gas density was evaluated at the gas temperature to simplify the calculation Ref. (94)

6.4.2 Analysis of Gas Temperature Resistance Thermometer

The wire temperature lags behind the gas temperature because of the thermal inertia of the wire. Radiation from the wire to the surrounding and the conduction through the prongs were neglected as mentioned in section 6.4.1. The wire and prongs of the thermometer probe are at different

temperatures in non-steady condition of gas variation, and this is because of the difference in thermal inertia Ref. (15). In the hot-wire anemometer, there is a current flowing through the wire which makes the wire temperature higher than the prongs and the surroundings and prong effects are greater in the hot-wire than the resistance and were neglected in the hot-wire. Therefore the end conduction effects were considered to be negligible as in Ref. (15). On the other hand the effect of thermal inertia is significant.

By neglecting the heat effect caused by the very small current flowing through the wire, the energy balance across the wire is given by:

$$M\sigma \frac{dT_{tw}}{dt} = h \times A \times (T_g - T_{tw}) \quad 6.10$$

where M is the mass of the wire $= \frac{\pi d^2}{4} L \rho w$

A is the surface area of the wire $= \pi d L$

σ is the specific heat of the wire material

T_{tw} is the thermometer wire temperature.

After re-arranging equation 6.10

$$T_g = T_{tw} + \frac{d \rho w \sigma}{4h} \frac{dT_{tw}}{dt} \quad 6.11$$

where h provided the two wires are arranged in same position, is given by equation 6.4 i.e.

$$\frac{hd}{Kg} = C_1 + C_2 \left(\frac{\rho U d}{\mu} \right)^n \quad 6.4$$

and for the hot-wire, from equation 6.5

$$V^2 R_{hw} = (T_s - T_g) (A + B (\rho U)^n)$$

by combining equations 6.4, 6.5 and 6.11 to eliminate ρu and h to give an equation for T_g in terms of T_{tw} , $\frac{dT_{tw}}{dt}$, $V^2 R_{hw}$, which can be measured from the experiments, and the properties of the two wires.

In order to solve the equation to give T_g , it is necessary to determine the values of the constants C_1 , C_2 and n in equation 6.4. Ghirlando (Ref. (49)) used at the first attempt the values given by McAdams Ref. (94) who correlated the experimental data of numerous workers. The values were $C_1 = 0.32$, $C_2 = 0.43$ and $n = 0.5$ i.e.

$$Nu = 0.32 + 0.43 \sqrt{Re}$$

but Ghirlando found that the solution of the equation for T_g failed at a crank angle of 40° ATDC. However using the expression form Horvatin and Hussman Ref. (66), i.e. $Nu = 0.43 + 0.48 \sqrt{Re}$, a solution could be obtained at this crank angle.

In the present work these constants have been calculated from room temperature experiments using equations 6.6 and 6.7 for C_1 and C_2 respectively. The values of gas temperature by using the new constants were compared with those using the constants of Horvatin and Hussman Ref. (66). In order to calculate the constants C_1 and C_2 in equation 6.4, the following procedure is required:-

Equation 6.6 can be written as:

$$A = (CC) \times Kg \times \pi L \times C1 \quad 6.12$$

where (Area = $\pi d L$).

A: can be obtained from the calibration curve and equal to 0.654

CC: conversion vector for the bridge of the anemometer used which is (4206.0413) from DISA information.

K_g : Thermal conductivity of the gas at the room temperature and equal to:

$$K_g = K_{g_0} \left(\frac{T_g}{T_0} \right)^{0.8} \quad \text{From Ref. (43)}$$

$$K_{g_0} = 2.428 \times 10^{-2} \text{ w/m } k^\circ \quad \text{Ref. (117)}$$

$$T_g = 17.8 + 273 = 290.8^\circ K$$

$$T_0 = 275^\circ K$$

$$\therefore K_g = 2.428 \times 10^{-2} \left(\frac{290.8}{275} \right)^{0.8}$$

$\therefore K_g = 2.5389 \times 10^{-2} \text{ w/m } k^\circ$ and this value will be considered as K_g at room temperature.

L = The length of the hot-wire and equal to 3.4 mm (0.1338 inch)

Therefore the only unknown form equation 6.12 is C_1 which is equal to 0.573.

The same procedure was carried out to calculate C_2 by using equation 6.7.

$$B = \frac{cc \times K_g \times Area \times C_2}{\mu^n \times d^{1-n}}$$

$$C_2 = \frac{B \times \mu^n \times d^{1-n}}{cc \times K_g \times Area} \quad 6.13$$

$B = 0.26$ from the calibration curve.

$$\mu = \mu_0 \left(\frac{T}{T_0} \right)^{0.76}$$

where $\mu_0 = 1.708 \times 10^{-5} \text{ kg/m s}$ at $T_0 = 273^\circ K$ Ref. (58)

$$\therefore \mu = 1.7919 \times 10^{-5} \text{ kg/m s}$$

$n = 0.48$ from the calibration curve

Therefore $C_2 = 0.3$ and equation 6.4 becomes:

$$h = \frac{K_g}{d} \left(0.573 + 0.3 \left(\frac{\rho U d}{\mu} \right)^{0.48} \right) \quad 6.14$$

by substituting equation 6.14 into 6.11 gives:

$$T_g = T_{tw} + \frac{d \int_{tw}}{4} \frac{d}{K_g} \left[\frac{1}{0.573 + 0.3 \left(\frac{\rho U d}{\mu} \right)^{0.48}} \right] \frac{dT_{tw}}{dt}$$

OR

$$T_g = T_{tw} + \frac{1}{C \times T_g^{0.8} + D(\rho U)^{0.48} \times T_g^{0.435}} \quad 6.15$$

where $C = \frac{0.573}{\left[\rho t_w \frac{\sigma d^2}{4} \times \frac{T_o^{0.8}}{K_{g_o}} \times \frac{dT_{tw}}{dt} \right]}$

and $D = \left[\frac{0.30 \times d^{0.48} \times T_o^{0.365}}{\mu_o^{0.48}} \right] / \left[\int_{tw} \times \frac{\sigma d^2}{4} \times \frac{T_o^{0.8}}{K_{g_o}} \times \frac{dT_{tw}}{dt} \right]$

since $K_g = K_{g_o} \left[\frac{T_g}{T_o} \right]^{0.8}$ and $\mu = \mu_o \left[\frac{T_g}{T_o} \right]^{0.76}$

remembering that the gas properties for the thermometer wire were evaluated at the gas temperature, while for the hot-wire the properties were evaluated at the mean temperature. This is because for the hot-wire the difference between the gas and film temperature is much larger than for thermometer wire. In addition, this simplifies the above equation. The expression from Horvatin and Hussman is based on the gas temperature while the expression for McAdams is based on mean temperature as is the present value.

From equation 6.5,

$$(\text{PU})^n = \frac{1}{B} \left[\frac{V^2 R_{hw}}{(T_s - T_g)} - A \right] \quad 6.16$$

and from equation 6.8

$$A = A_o \left[\frac{T_s + T_g}{2} \times \frac{2}{T_a + T_s} \right]^{0.8}$$

with $T_o = T_a$, the atmospheric temperature.

$$\text{Hence } A = \left[\frac{A_o^{1.25} \times T_s}{T_a + T_s} + \frac{A_o^{1.25} \times T_g}{T_a + T_s} \right]^{0.8} = (J + k \times T_g)^{0.8}$$

where

$$J = \frac{A_o^{1.25} \times T_s}{T_a + T_s}$$

and

$$K = \frac{A_o^{1.25}}{T_a + T_s}$$

From equation 6.9

$$B = B_o \left[\frac{T_s + T_g}{2} \times \frac{2}{T_a + T_s} \right]^{0.435} = (L + M \times T_g)^{0.435}$$

where

$$L = \frac{B_o^{2.3} \times T_s}{T_a + T_s}$$

and

$$M = \frac{B_o^{2.3}}{T_a + T_s}$$

and assume also $R = T_s / (V^2 \times R_{hw})$ and $S = 1 / (V^2 \times R_{hw})$

Therefore equation 6.16 can be written as:

$$(\text{PU})^n = (L + M \times T_g)^{-0.435} \left[(R - S \times T_g)^{-1} - (J + k \times T_g)^{0.8} \right] \quad (6.17)$$

by combining equation 6.17 and 6.15 to eliminate ρu and by re-arranging:

$$T_{tw} = T_g - \frac{(L + M \times T_g)^{0.208/n}}{C \times T_g^{0.8} \times (L + M \times T_g)^{0.208/n} + D \times T_g^{0.435} \times [(R - S \times T_g)^{-1} - (J + k \times T_g)^{0.8}]^{0.48/n}} \quad (6.18)$$

The only unknown in equation 6.18 is T_g only. The equation can be solved by using a simple Newton iteration method, i.e. if the first assumption is T^* , then a more accurate solution will be obtained at T , where $T = T^* - f(T^*)/f'(T^*)$. The first value of T^* considered was the thermometer wire temperature T_{tw} . Equation 6.18 is different from the equation 6.18a obtained by Ghirlando Ref. 49. There is an error in calculating T_g from equation 6.18a and this is due to incorrect terms found in evaluating D.

$$T_{tw} = T_g - \frac{(L + M \times T_g)^{\frac{1}{4}n}}{L \times T_g^{0.8} \times (L + M \times T_g)^{\frac{1}{4}n} + D \times T_g^{0.42} \times (R - S \times T_g)^{-1} - (J + K \times T_g)^{0.8 \frac{1}{2}n}} \quad 6.18f$$

where $D = \left[\frac{0.48 \times d^{0.5} \times T_o^{0.76}}{\mu_o} \right] / \left[\rho_{tw} \frac{\pi d^2}{4} \times \frac{T_o^{0.8}}{Kg_o} \times \frac{\partial T_{tw}}{\partial t} \right]$

6.4.3 Pressure Correction Method

The accuracy in cylinder pressure measurement in an internal combustion engine is important Refs. (16, 90) since this parameter has an effect on the heat transfer calculation.

The pressure measured by a quartz-crystal transducer is a differential pressure and it is necessary to determine the true pressure. The method reported by Ghirlando Ref. (49) was employed here. Assuming the gas pressure in the cylinder to be $P + E$, then E will be constant for any particular test, where P is the pressure measured from an arbitrary datum and E is the difference between this datum and zero absolute pressure.

From equation 6.10, if $\frac{dT_{tw}}{dt} = 0$ i.e. at the peak wire temperature,

then $T_g = T_{tw}$ the gas temperature is equal to the wire temperature. The crank angle at which the wire temperature is a maximum varied from one test to another, approximately 4° ATDC to 7° ATDC at 600 r.p.m. and 1500 r.p.m. respectively. The variables referred by subscript m at this crank angle.

Since there is no great variation in gas temperature near B.D.C., it can be assumed that $T_g = T_{tw}$ at B.D.C. and during the valve closed period the mass of gas in the cylinder at the maximum wire temperature (i.e. near T.D.C.) equal the mass of gas at B.D.C. and the reasons for this are:

1. Since the pressure diagram is symmetrical about T.D.C. which is near enough the crank angle for the peak wire temperature T_m , the gas is halfway through leaking out at T_m , while at B.D.C. the gas is half through leaking in.
2. These leakages are only of the order of a few per cent of the mass in the cylinder.

Since the mass of gas is the same at B.D.C. and at the maximum wire temperature, from the gas laws the following equation can be obtained:

$$\frac{(P + E)_m \times V_m}{T_m} = \frac{(P + E)_{\text{bdc}} \times V_{\text{bdc}}}{T_{\text{bdc}}} \quad 6.19$$

where the subscript m refers to conditions at maximum wire temperature and the subscript bdc to conditions at bottom dead center. It should be pointed out that P_m is not the maximum pressure but the pressure at the same crank angle as T_m . Similarly V_m is the volume at this crank angle.

The pressure P_m and P_{bdc} are read directly from the data disc to the Alpha-computer. So are the temperatures T_m and T_{bdc} since, from the above explanation, the gas temperature is equal to the wire temperature at these two points. The volume V_{bdc} is known, while V_m can be calculated if the crank angle at which T_m occurs is measured. The E is only the unknown and can be obtained from equation 6.19

6.5 IN CYLINDER INSTRUMENTATION

6.5.1 Introduction

The hot-wire anemometer is sensitive to its own temperature and the mass flow rate ($\rho \times U$) and gas temperature in which it is placed. Therefore to measure the velocity of the gas, the temperature and pressure of the gas must also be known in a rapidly changing situation.

This section describes only the instrumentation used to measure and record the anemometer signals, pressure and temperature of the gas, and the surface temperature of the cylinder wall. It also describes the anemometer probes and how they were made. The theory of processing the signals is described in section 6.4, and the computerised logging and subsequent calculation in Chapter 8.

6.5.2 Pressure

The pressure was measured with a Kistler 601A pressure transducer. This is of the piezo-electric type and must be operated with a high impedance amplifier to prevent rapid charge leakage. A Kistler charge amplifier type S66M5 was used. The output from the charge amplifier was then fed to the analogue to digital convertor (A/D) on the Alpha-computer terminal unit. The charge decay with the piezo-electric system meant that the absolute pressure level of the pressure diagrams was not known. A semi-theoretical method of fixing this absolute level is referred by

Two sewing needles were inserted in the two holes and secured with the high temperature chemical cement mentioned in Chapter 4 as shown in Fig. 6.9.c. Before the cement hardened, the needles were set to the desired depth. The assembly was then inserted into the spark plug hole and secured with the cement, allowing 72 hours for complete hardening.

After the cement was set, the eyes of the two needles at the outer end were soldered to a pair of lead-wire. A 10-micron (3.937×10^{-4} in) diameter platinum - Iridium wire was then spot welded across the inside tips of the needle under a microscope, figure 6.10 shows the arrangement of the probe and its holder. The resistance thermometer was constructed in a similar manner to the hot-wire. The same dimensions were used for both in order that the thermometer would read the temperature at a similar location to the hot-wire anemometer (2mm below the head surface).

The probes were welded using an existing welding generator. It consisted of a bank of capacitors and d.c. power supply. Discharging the capacitors provided the current pulses for the spot-welding. The technique used for welding the probes differed from the usual one, and was developed in the department. After placing the wire over the prongs, one pole of the bank of charged capacitors was connected to one of the prongs, while the other pole was connected to a copper-electrode. The electrode was then carefully moved towards the prong connected to the capacitor, until a spark was produced which welded the wire. Where necessary, repeated sparking was used to build up a satisfactory weld. The wire was welded to the other prong in a similar way. In the more usual technique, the electrode is connected to the capacitors via an open switch. After putting the wire on the prongs, the electrode is placed over one of the prongs such that the wire is sandwiched between this prong and the electrode and is in contact with both of them. The prong is connected

Ghirlando Ref.(49). In order to minimize charge decay, the cables and connectors between the transducer and charge amplifier, besides the transducer components, were washed in pure alcohol regularly.

6.5.3. Surface Wall Temperature

The surface wall temperature was measured by surface thermocouple described in chapter. 4. The E.M.F. is generated between the two junctions, the hot junction at the surface thermocouple which is represented by the Ni-film-iron interface and the cold junction which is kept at zero °C.

The output signal from the surface thermocouple was fed to a d.c. amplifier, CEC type 1-165 with high gain, frequency response, accuracy and low noise. The amplifier was calibrated with and without thermocouple (refer to the manual).

The output from the amplifier is fed to the Analogue to digital convertor (A/D) on the Alpha-computer, and another output from the amplifier is connected to the oscilloscope to ensure the signal fed to the A/D convertor is correct.

6.5.4 Probes Construction

The two probes, one for the hot-wire anemometry and the other for the thermometry, were designed in similar ways. The probe was made by using a spark plug body. The spark plug was drilled all the way through with a hole 8 mm (0.3149 inch) in diameter, a bigger hole was made 16 mm (0.6299 inch) in diameter and 15 mm (0.59 inch) in depth at the top of the spark plug body as shown in figure 6.9.a. A nylon 66 rod was shaped to fit the spark plug hole, and two holes 0.45 mm (1.77×10^{-2} in) in diameter and 3 mm (0.118 in) a part drilled in the nylon rod as shown in Figure. 6.9.b.

to the other pole of capacitors. When the switch is closed, the capacitors discharge and the heat generated welds the wire to the prong. This method breaking the wire which does not occur with the spark method. The procedure is repeated for the other prong. The size of the probe is such, of course, that the welding must be done under a microscope.

6.5.5. Hot-Wire Anemometer

The hot-wire probe was connected to a DISA 55M10 constant temperature anemometer box (1.4 x cold resistance). The output from the box could not be taken directly to the A/D convertor, as it consists of relatively large voltage fluctuations superimposed on a large D.C. bridge voltage (output varied from 5 - 8 volts) and the output voltage from the anemometer is a nonlinear function of the flow velocity. This nonlinearity has little influence in measurements of small degrees of turbulence; in this case a small portion of the calibration curve may be considered sufficiently linear. At higher turbulence intensities, however, distortion caused by the curvature of the calibration curve becomes significant; also measurements at varying velocities are made difficult by sensitivity variations. In most cases, mathematical treatment of such outputs is unsatisfactory; automatic electronic linearization was used. The output from anemometer was connected to a DISA 55M25 linearizer, and the output from linearizer which also reduces the D.C. bridge voltage was connected to the A/D convertor and the oscilloscope. The linearizer was calibrated for different input voltage before being used.

6.5.6 Gas Thermometer Temperature

The gas temperature was measured with a fine wire resistance thermometer. The sensing element was similar to the hot-wire probe. The thermometer wire was operated in an a.c. bridge network, whose power supply and bridge balance were supplied by a Tektronix Type Q-Unit, which in turn was supplied by a Tektronix 133 power supply. The bridge voltage was 5 v r.m.s. and the carrier frequency was 25 KHZ. Resistance and capacitance balances were incorporated and two arms of the bridge were contained in the unit. The other two arms consisted of the fine-wire in series with a decade resistance box and a fixed 1 k resistor. The decade box was set at 1 k except when calibrating the system. The bridge must be balanced before measuring the gas temperature. The output from the Q-unit is connected to two terminal, one connection is to the A/D convertor and the Alpha-computer and the other to an oscilloscope to ensure the signal fed to the computer is correct.

6.5.7 Other Equipment

Fig. 6.11 shows the arrangement of all instrumentation. A four channel oscilloscope type storage was included in the set up, so that during a test run a check could be kept on the proper working of all the instruments and particularly on whether the fine-wire probes were still intact. A "poloroid" camera was attached to the oscilloscope and "Poloroid" film type 47 used to obtain a picture which was then compared with the one logged by the computer.

During the experimental work or during calibration, a SOLARTRON 7045 digital voltmeter was used as a reference. A copper-constantan thermocouple on the back surface of the surface thermocouple plug was connected to a cu-constantan Comark. electronic thermometer.

6.6 IN CYLINDER CALIBRATIONS

6.6.1 Pressure

The pressure measuring system was calibrated on a Budenburg dead weight tester. This calibration, of which figure 6.12 is typical, gave a direct relationship between the voltage output and the applied pressure. Before each reading, the pressure in the dead weight tester was reduced to atmospheric and the charge amplifier grounded. The pressure was then rapidly raised to the desired level and the reading have been taken by an oscilloscope and digital voltmeter. The pressure was then reduced to atmospheric in readiness for the next reading. This procedure overcame the build-up of drift during calibration. In the experiments, the pressure was below atmospheric for part of the engine cycle, and to evaluate the pressure for this part of the cycle, the above calibration was extrapolated. A check of validity of using and extrapolated calibration have been done by Ghirlando Ref. 49. From the check the transducer has the same sensitivity below and above atmospheric pressure. It was therefore valid to extrapolate the main calibration to calculate the pressure below atmospheric.

6.6.2 Gas Temperature

The bridge used for measuring the gas temperature was calibrated to give the relationship between the voltage and probe resistance. This was done by varying the decade box in series with the probe in steps of 1 ohm and recording the voltage, figure 6.13. The temperature coefficient of resistance for a sample of the wire was taken from the DISA information catalogue. Before each test the resistance of the temperature probe was measured at room temperature using the bridge of the DISA anemometer box. Hence, knowing the relationship between the voltage and probe resistance,

the temperature coefficient of resistance of the wire and the probe resistance at room temperature, it was possible to reduce the experimental measurements to values of wire temperatures.

This indirect calibration of the thermometer is similar to that used by Benson and Brundrett Ref. (15), who considered it impractical to calibrate the thermometer directly because of the difficulty of constructing a simple furnace without incurring temperature gradients. In the present work it would have been more impractical to calibrate in steady state to the maximum temperature reached in the tests (150 - 450°C) since nylon softens at about 264°C Ref. (23). In the actual tests, the nylon inside the probe holder is exposed to these relatively high temperatures only for very brief intervals of time.

The method used to calculate gas temperature from wire temperatures is discussed in section 6.4.2. The two are different because of the thermal inertia of the wire.

6.6.3 Velocity

The anemometer was calibrated at room temperature and pressure only, and a semi-empirical relation was used to calculate velocities from the experimental records. The calibration served to determine certain constants in the relation, whose derivation is discussed in section 6.4.1.

To calibrate the probe, the probe and its holder was placed at the center of a duct of the departmental calibration wind tunnel. A pitot-tube was placed at the same level and corresponding position as the hot-wire but avoiding interference between them. Inclined manometers, with methylated spirit of specific gravity of 0.825, were used to measure the pressure from the pitot tubes.

The calibration curves, of which figure 6.14 is typical, were plotted on logarithmic scales to give the constants B_0 and n ; see (section 6.4.1). The hot-wire was re-calibrated after the test, because of the oil deposits on the wire which tend to increase the heat transfer, and the mean values of A_0 , B_0 and n for these tests are the mean of the two calibration, before and after the test, as shown in figure 6.14. Test with wires which broke before the procedure was completed were rejected, once experience was gained the failure rate was relatively low.

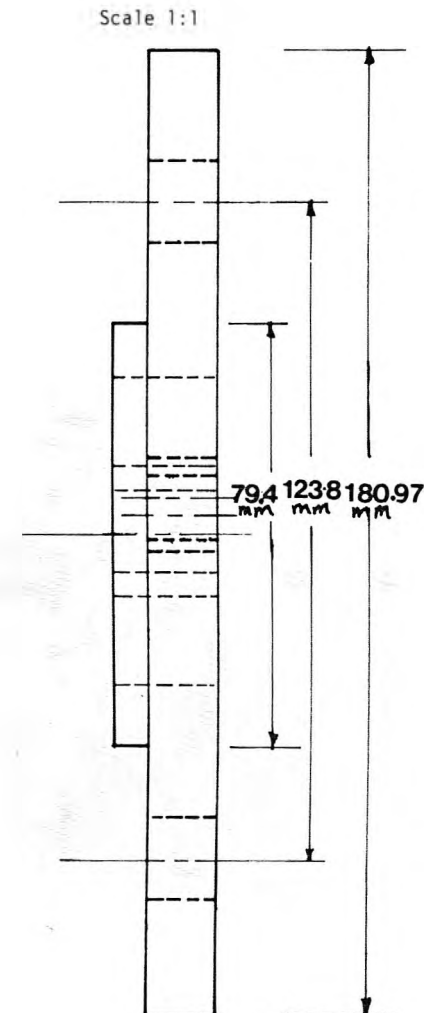
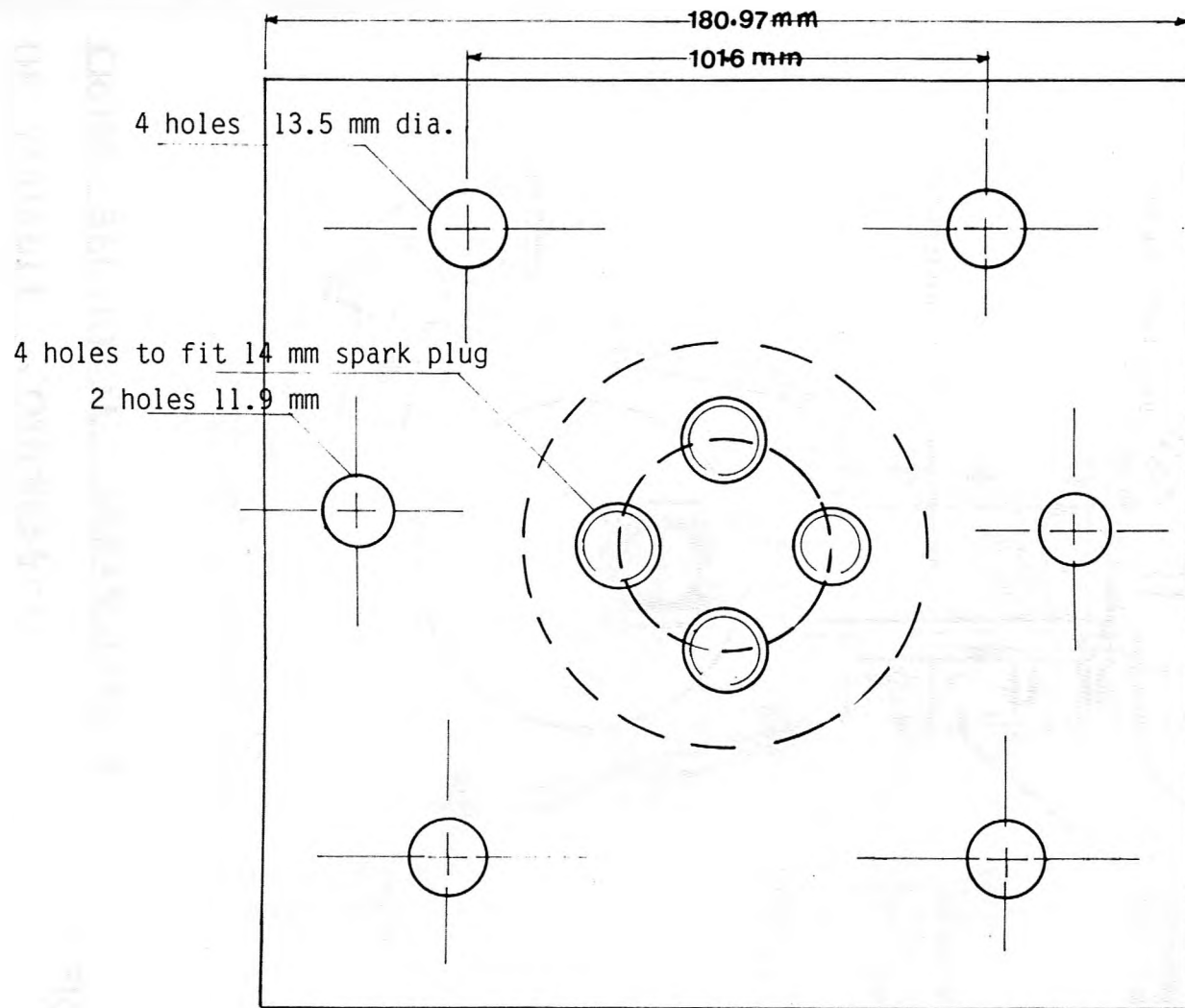
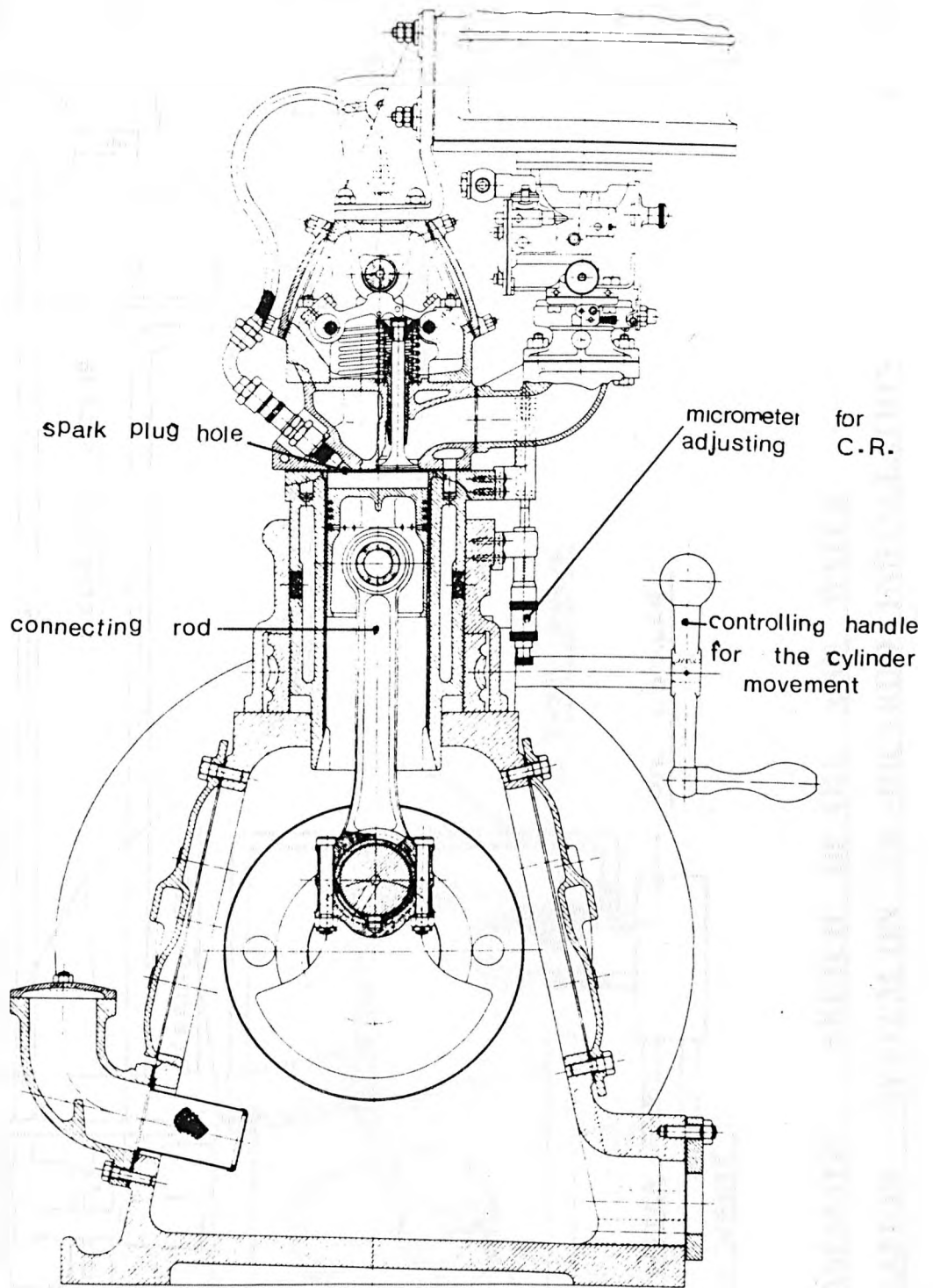


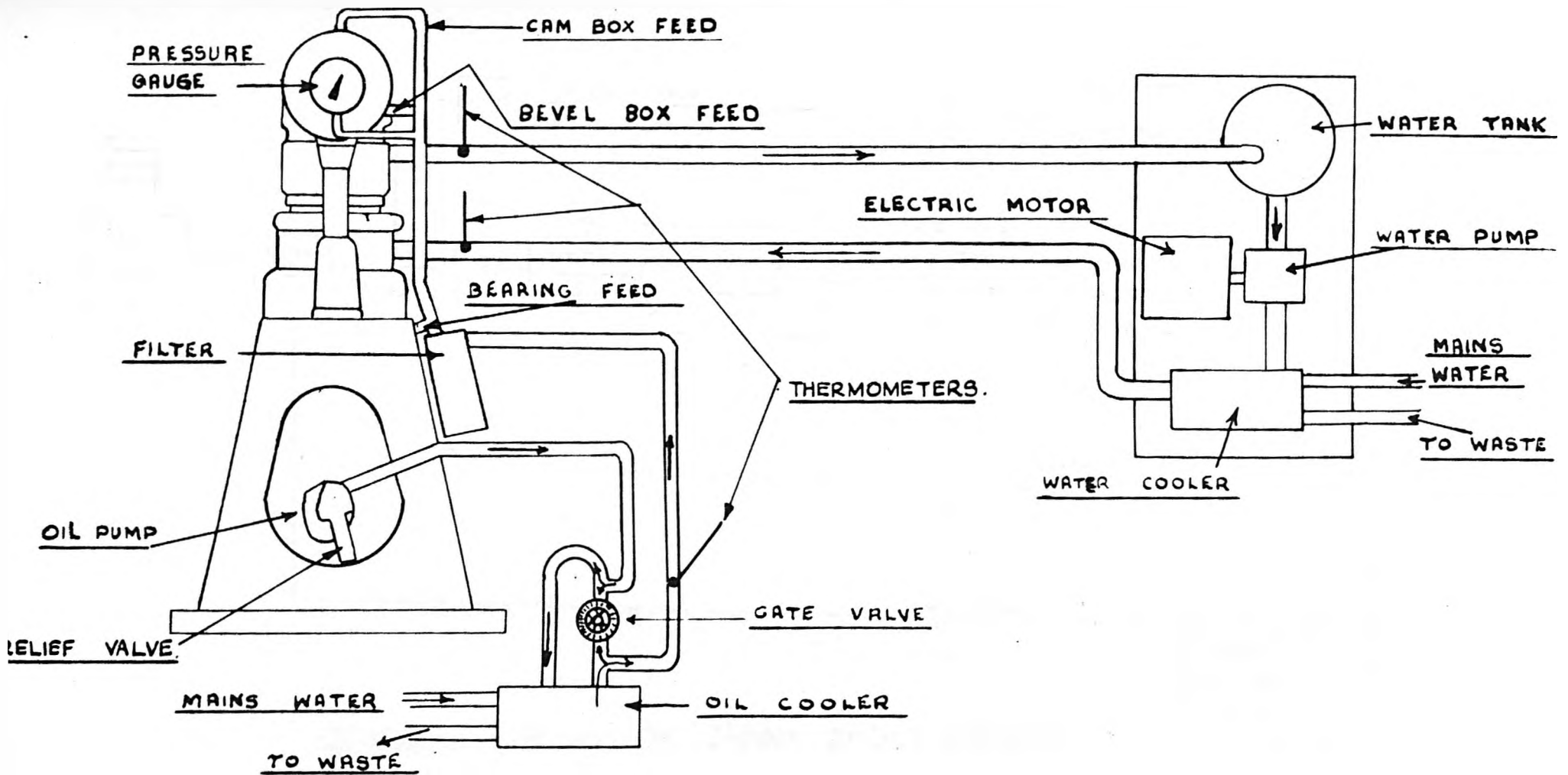
FIG. 6.1

CYLINDER HEAD FOR AUSTIN-RICARDO ENGINE



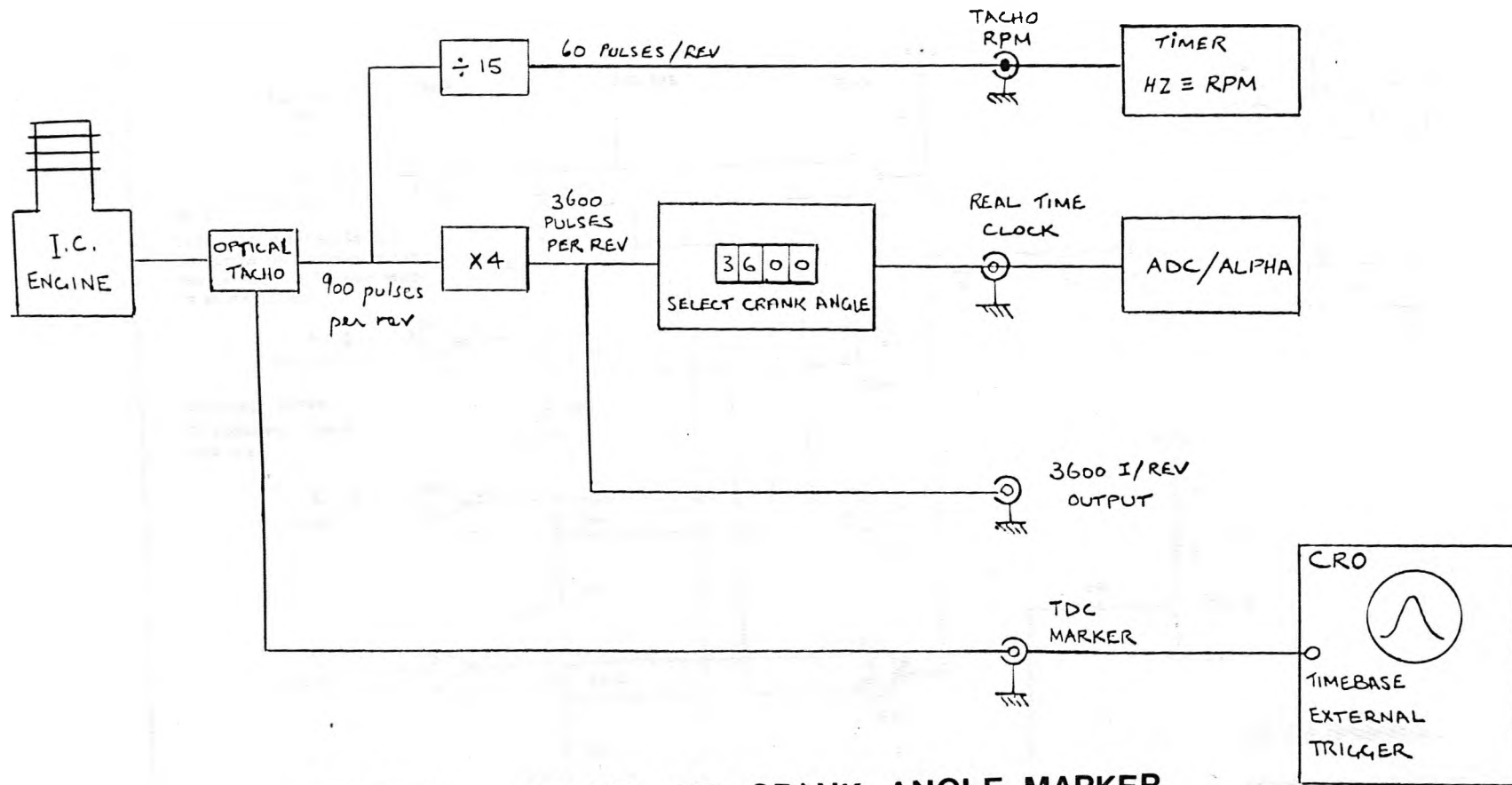
CROSS SECTIONAL ARRANGEMENT
OF VARIABLE COMPRESSION
E6-RICARDO ENGINE

FIG-6-2



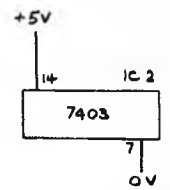
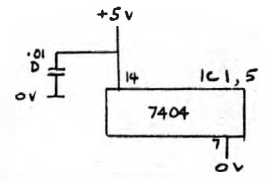
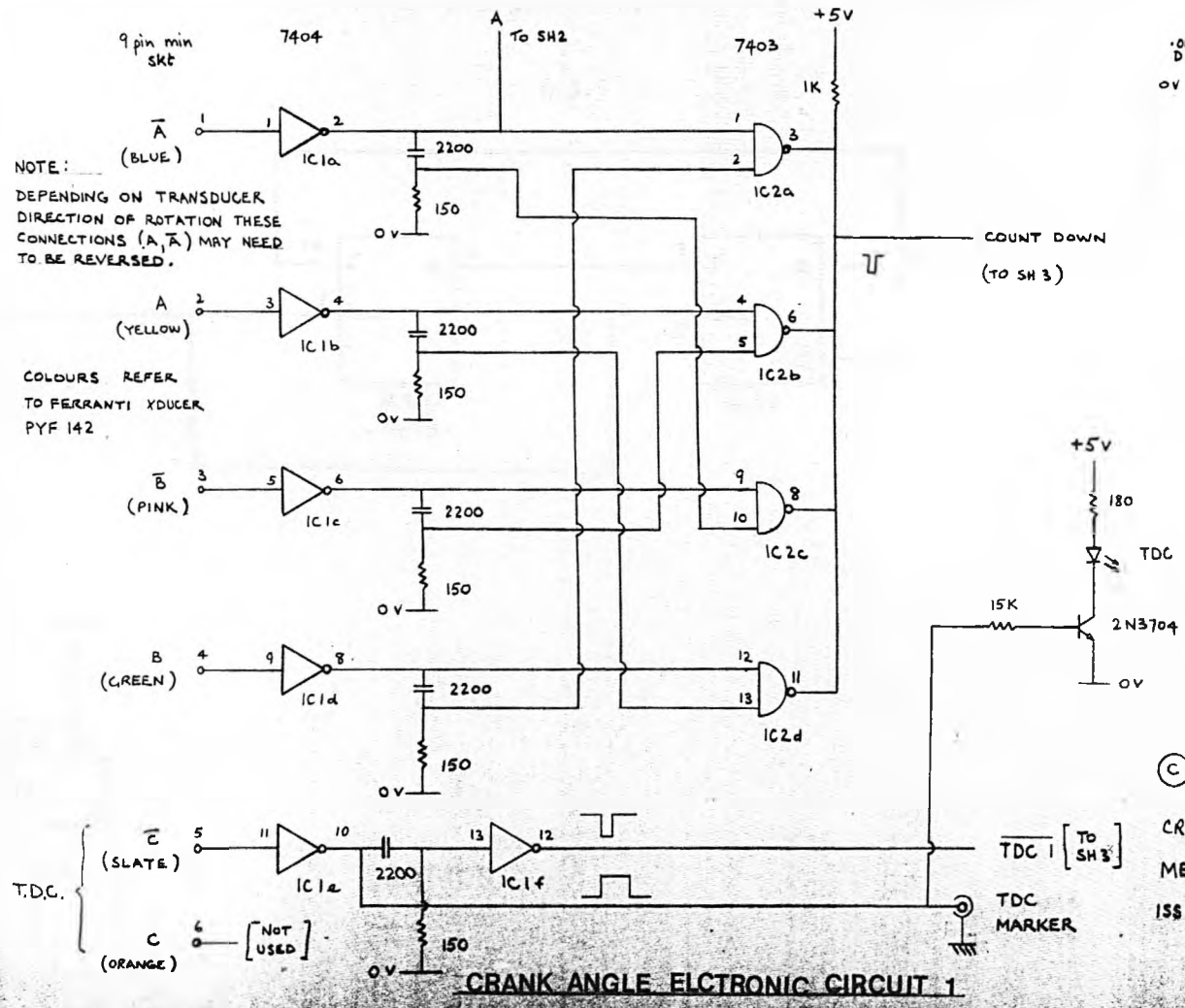
DIAGRAMMATIC SKETCH OF OIL AND WATER CIRCULATION SYSTEM ON E6-RICARDO INSTALLATION

FIG . 6.3



GENERAL LAYOUT OF CRANK ANGLE MARKER

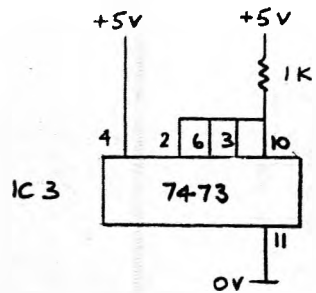
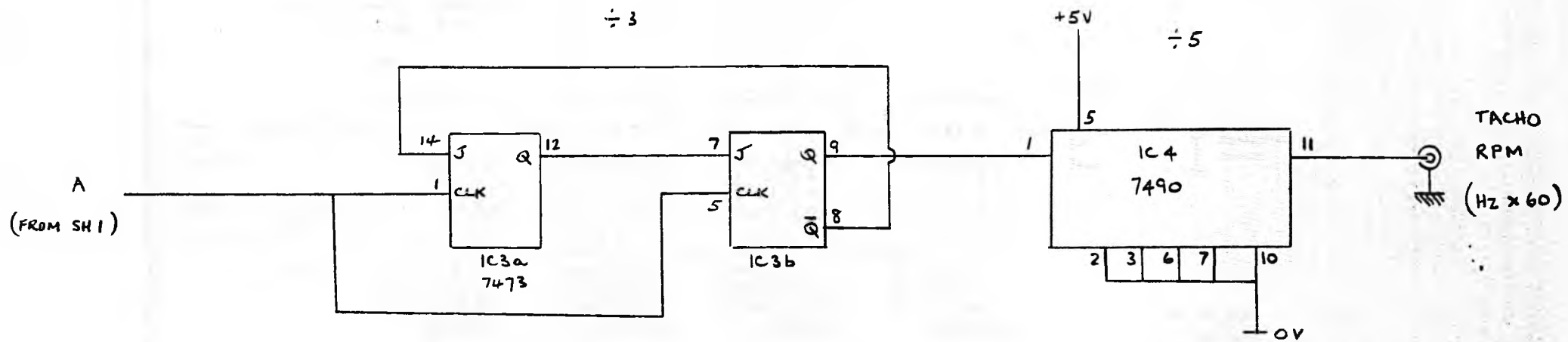
FIG-6.4



© J. A. HARDCASTLE

CRANK ANGLE MARKER
MEE 13003 SH 1
ISS 1 28.1.92

FIG-6-5

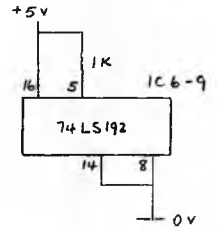
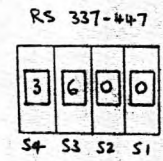
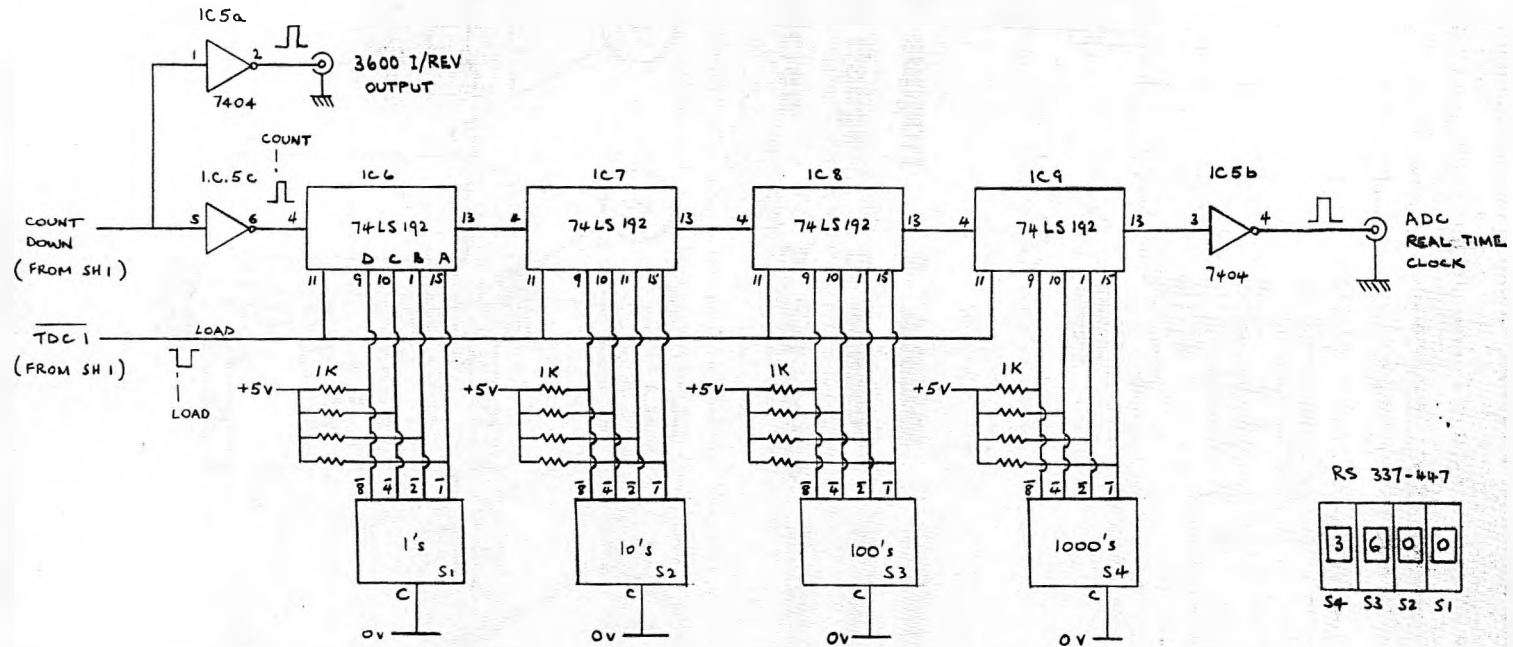


C·A ELECTRONIC CIRCUIT 2

© J. A. HARDCASTLE

CRANK ANGLE MARKER

MEE 13003 SH 2



C·A ELECTRONIC CIRCUIT 3

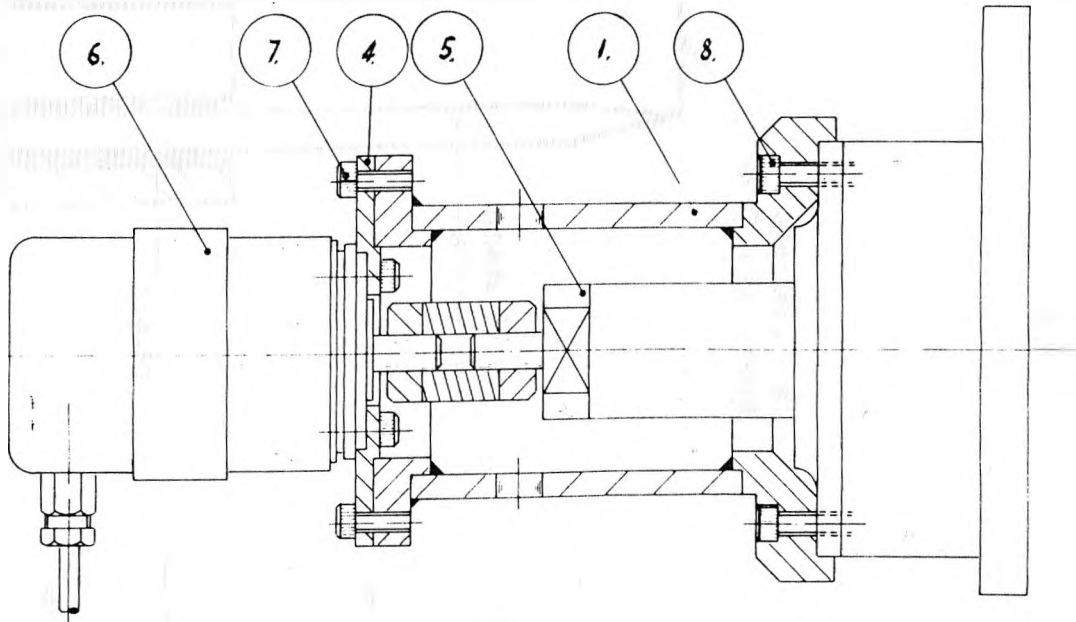
© J. A. HARDCASTLE

CRANK ANGLE MARKER

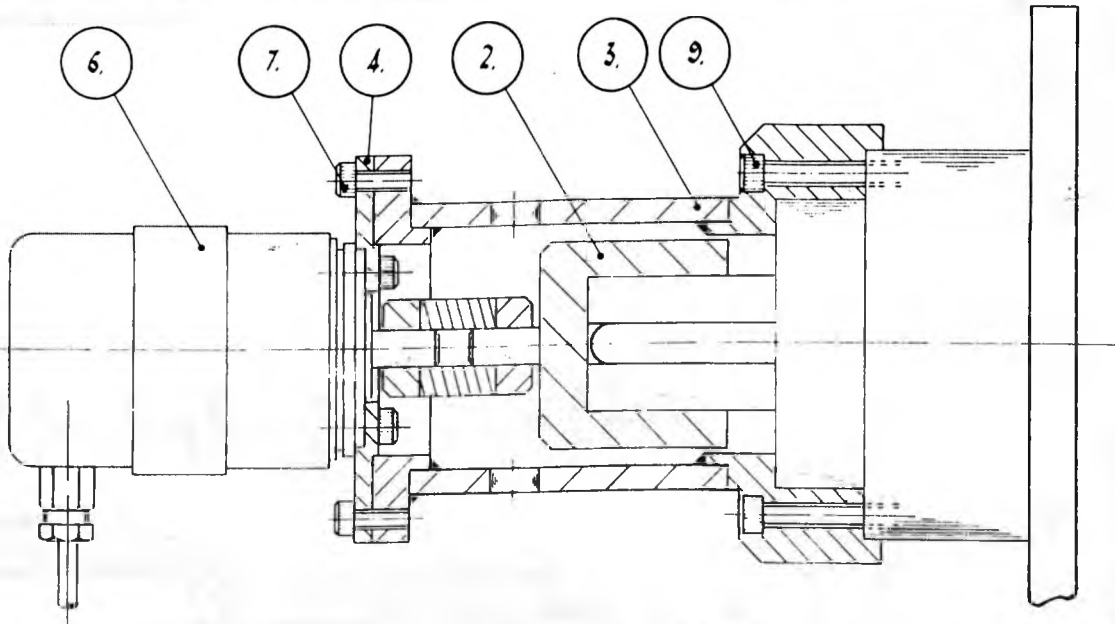
MEE 13003 SH3

ISS 2 16.2.82 FIG-6-7

A) ARRANGEMENT OF TACHO-MOTOR ON
AUSTIN-RICARDO ENGINE



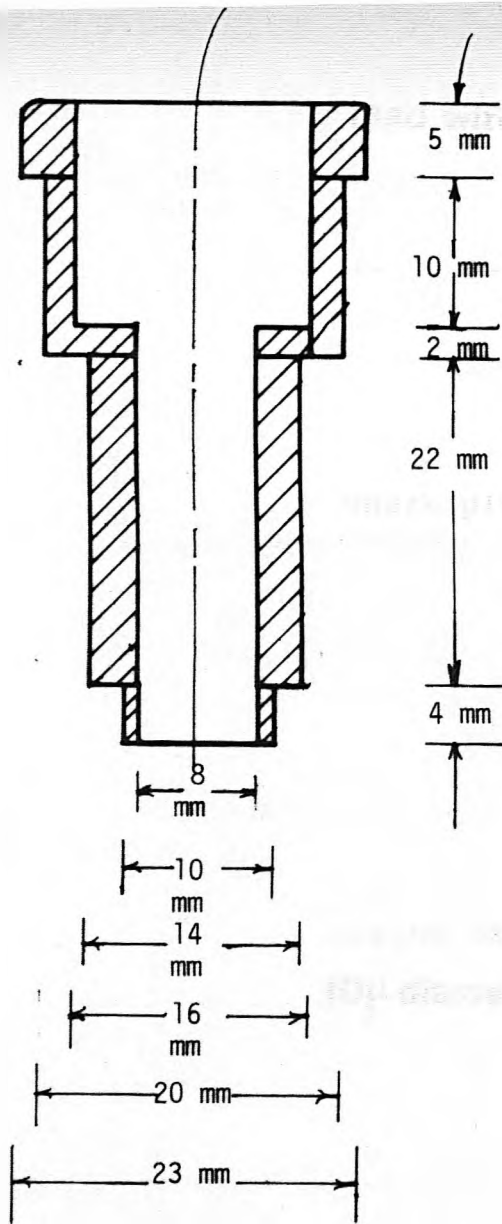
- | | | |
|------------------|--------------|------------------|
| 1. Motor support | 2. Adaptor | 3. Motor support |
| 4. Motor flange | 5. Adaptor | 6. Tacho-motor |
| 7. Set-screw | 8. Set-screw | 9. Set-screw |



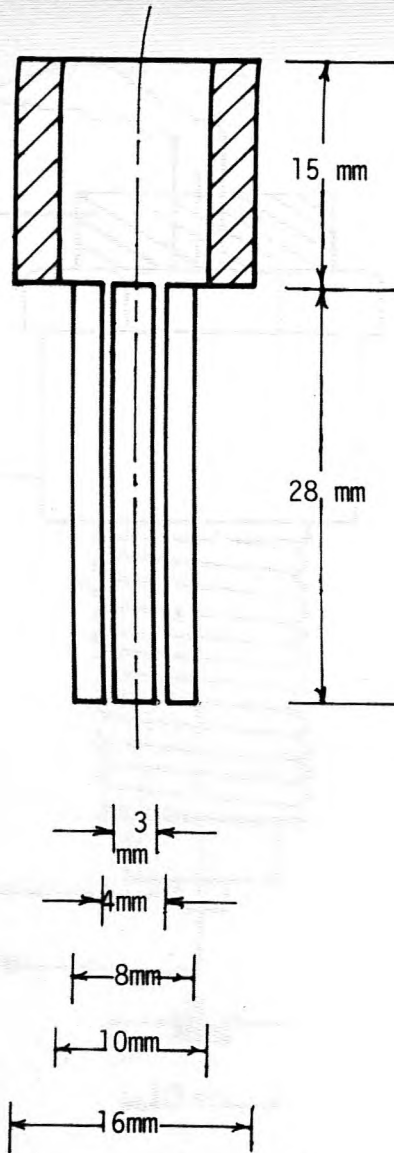
B) ARRANGEMENT OF TACHO-MOTOR ON
CELL E-6 RICARDO ENGINE

FIG 6.8

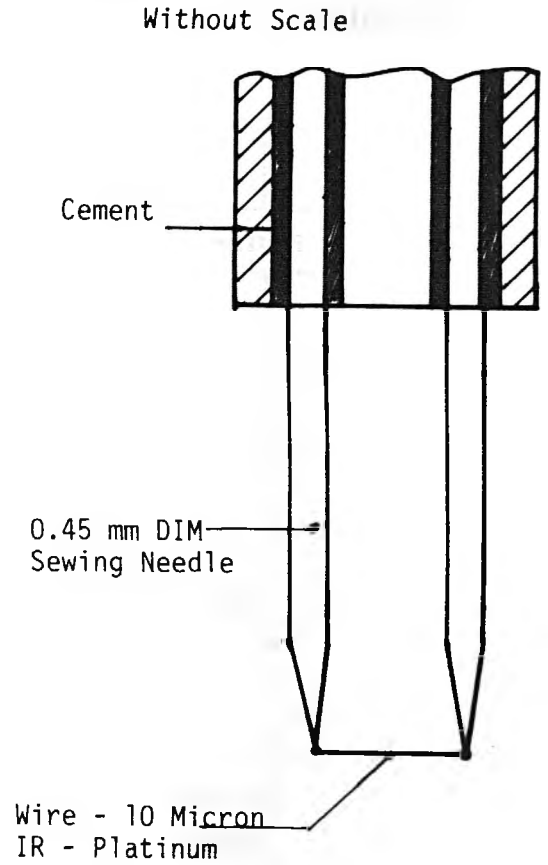
Scale 2:1



(a) HOT-WIRE HOLDER



(b) NYLON ROD



(c) SEWING NEEDLE ARRANGEMENT

FIG. 6.9

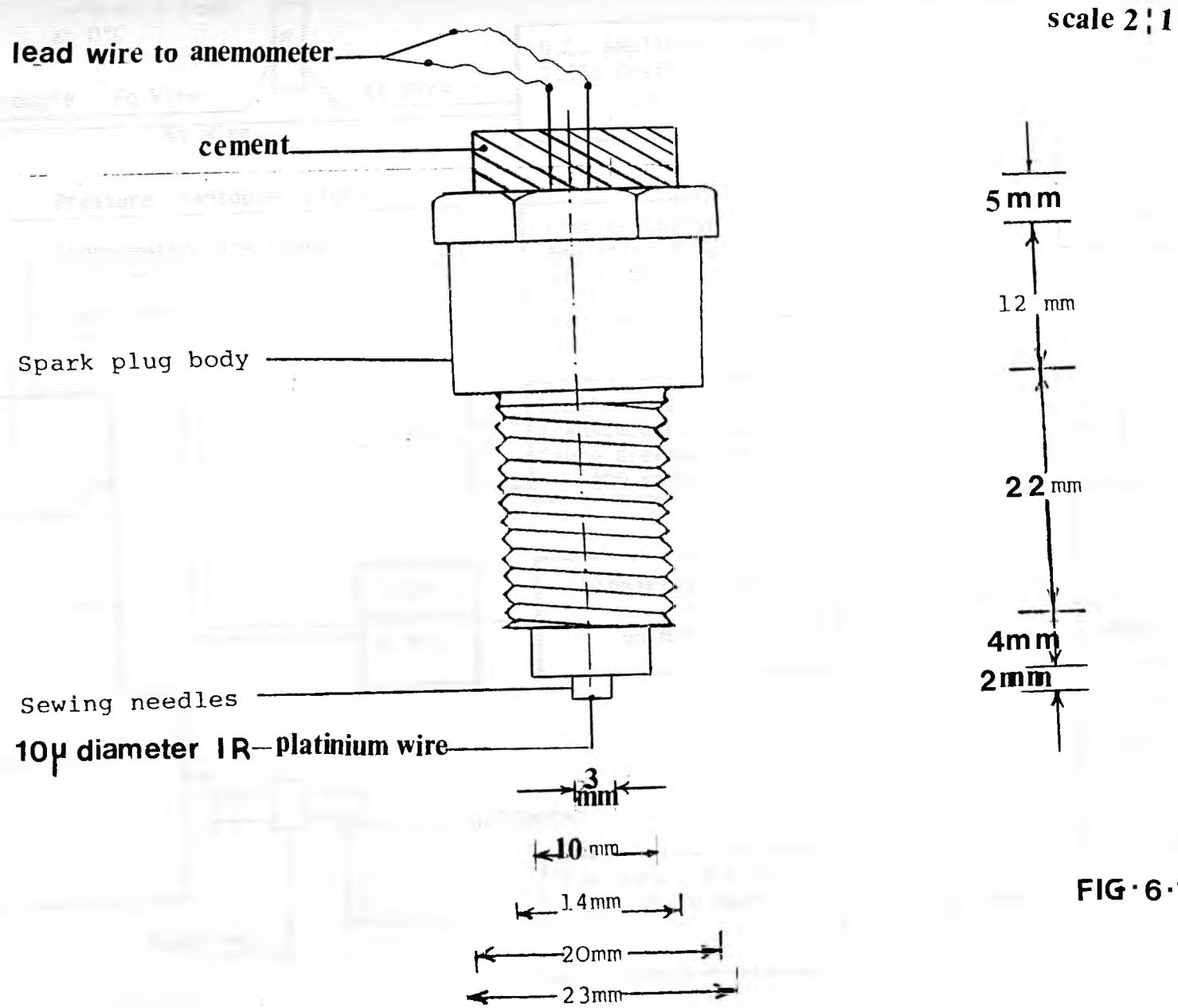
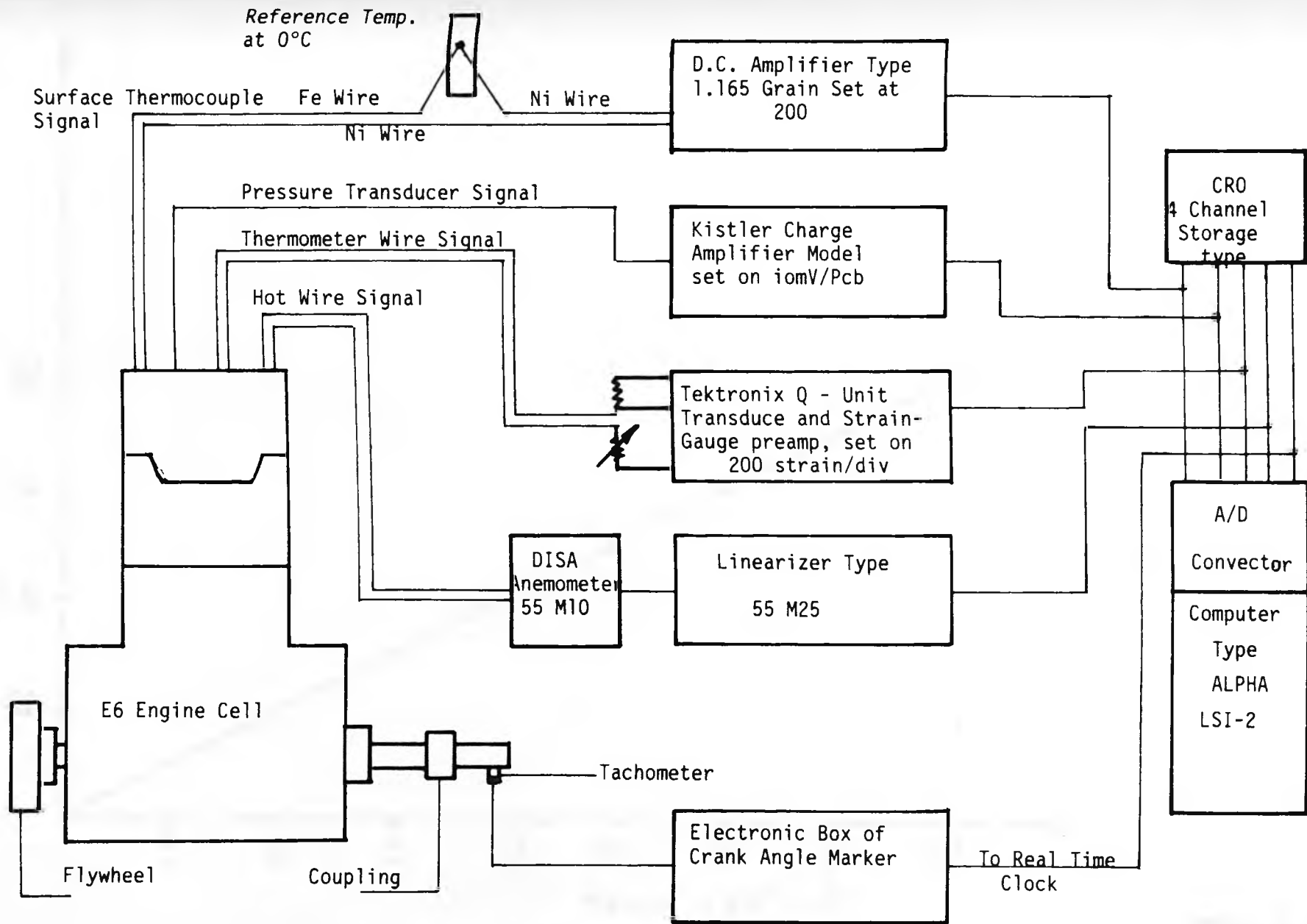


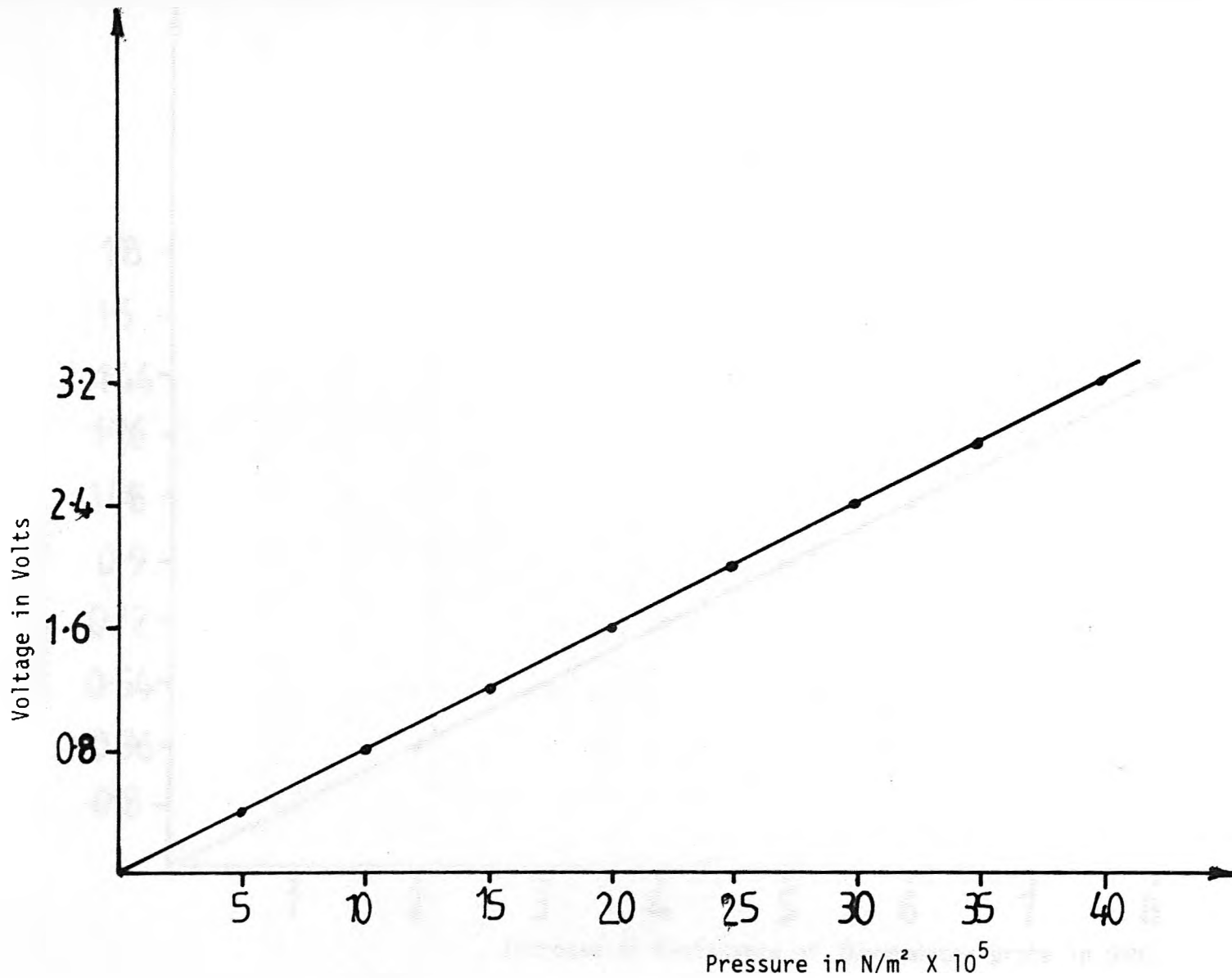
FIG. 6-10

HOT-WIRE HOLDER ASSEMBLY



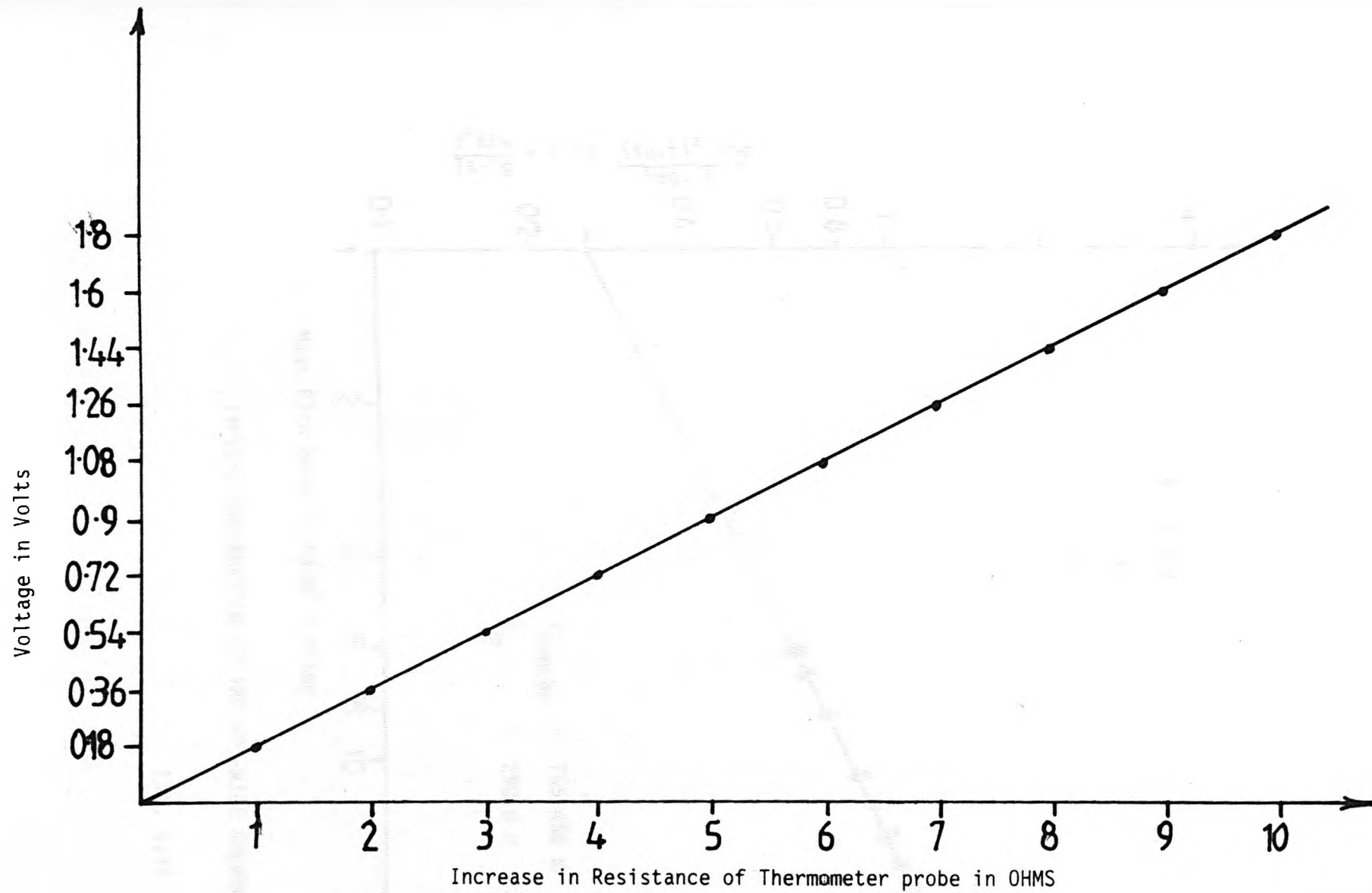
BLOCK DIAGRAM OF THE INSTRUMENTATION

FIG-6-11



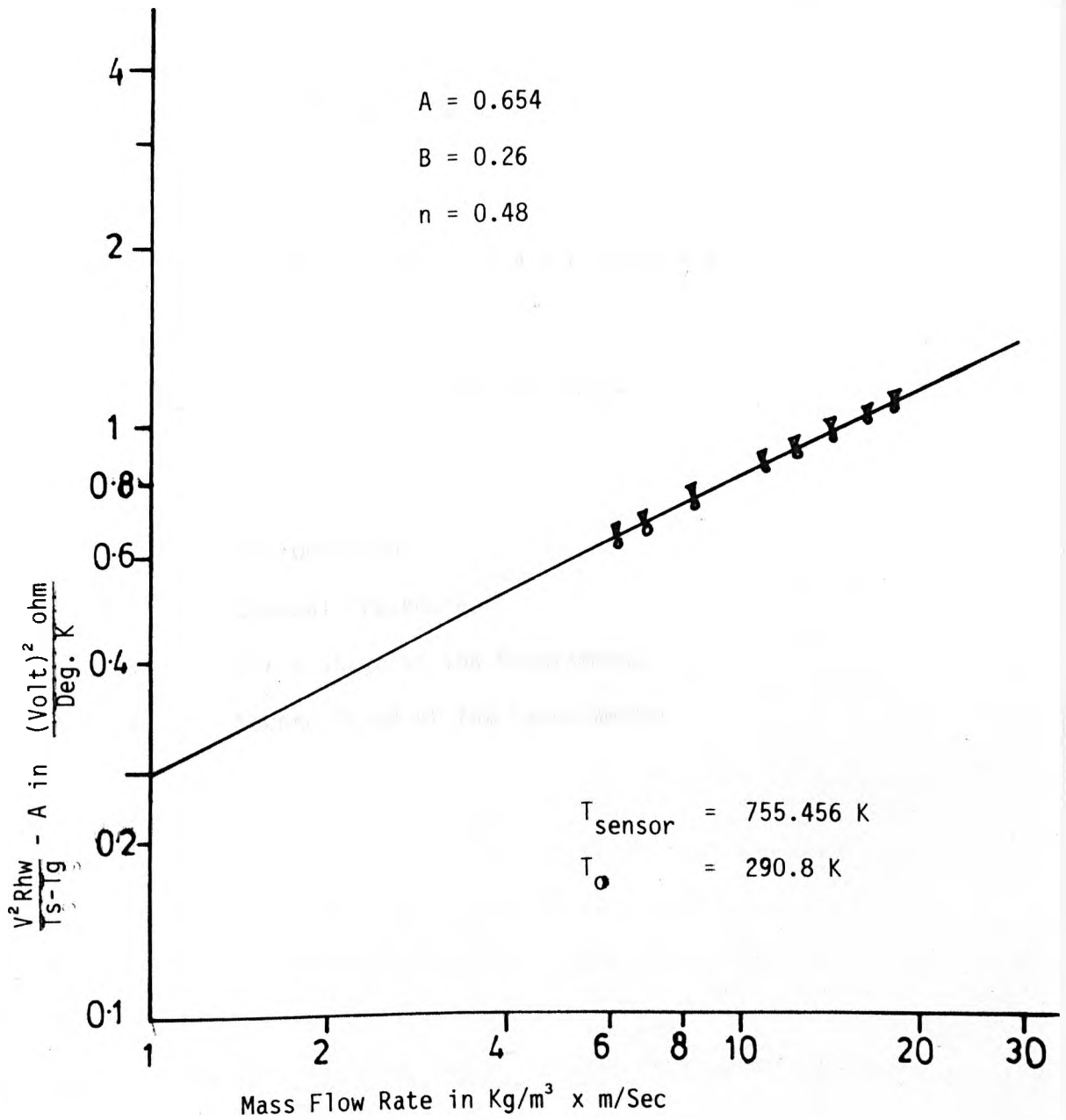
TYPICAL PRESSURE CALIBRATION

FIG. 6-12



TYPICAL CALIBRATION OF THE "TEMPERATURE" BRIDGE

FIG-6-13



TYPICAL CALIBRATION OF THE HOT-WIRE ANEMOMETER

Fig. 6.14

CHAPTER 7

EXPERIMENTAL PROCEDURE

- 7.1 Introduction
- 7.2 General Procedure
- 7.3 First Stage of the Experiments
- 7.4 Second Stage of the Experiments

7.1 Introduction

The condition in the cylinder of the internal combustion engine is complex, so the experimental procedure and the method of measuring the parameter is of interest.. Most of the workers in this field used the same method of measuring the parameters i.e. recording the whole cycle at a time for gas pressure and temperature, gas velocity and surface wall temperatures, Refs. (3, 4, 8, 31, 35, 59, 78, 81, 107). This procedure has been criticised because one cycle cannot represent the time averaged measurements inside the cylinder, and turbulence can only be determined over a large number of cycles in a non-steady situation.

Annand and Ma Ref. (9) and Alkidas and Myers Ref. (6) concluded that there is cycle to cycle variation of measurements in the surface wall temperature as well as the other properties of the cylinder, so their work was based on the measurements averaged over a large number of cycles.

In the present work a different procedure was used to obtain as accurate result as possible. The procedure is to average the measuring parameter at one particular crank angle over many revolutions up to 1664 (a computer storage limitation), and the number of the revolutions taken depends on the parameter e.g. turbulence requires the maximum number, pressure requires less.

At any particular crank angle, the parameter measured, will be for this angle after Top Dead Centre (TDC) and this is achieved by the special crank angle marker developed in the department as mentioned in Chapter 6 Section 3.2, i.e. if the measuring parameter occurs at 30° crank angle the output result gives two readings one at 30° crank angle and the other

at 390° crank angle over the required number of revolutions.

7.2 General Procedure

To establish the experimental procedure, first of all the variables to be considered were chosen. These were compression ratio, the engine speed and the location of the probe. Three engine speeds were selected, i.e. 600, 1000, and 1500 rev/min and for each particular speed the experiment was carried out for three different compression ratios, i.e. 8, 10, and 12. The location of the probes was limited because the cylinder head had two plug holes only, i.e. two measurement positions have been used in the combustion chamber for each particular speed and compression ratio.

During equipment development one set of experiments were carried out for fixed speed and compression ratio, i.e. 800 rev/min and 8 respectively, for the Austin-Ricardo engine these being the most convenient conditions. Four holes were available in the cylinder head and it was possible to measure the four parameters at the same time.

In the E6 tests two parameters were measured at a time. All the wire experiments were carried out at one depth from the surface which is 2 mm (0.787×10^{-3} inch). The distance is arbitrary since in the rapidly fluctuating in cylinder situation it is difficult to define an edge to the boundary effects.

The number of measurements for each of the experiments using the E6 engine were (3 speed x 3 Compression Ratio x 2 Locations x 4 Parameters x 1 Depth), 72. The test porcedure was:

- (i) Measure the electrical resistance of both wire probe before starting the engine, then calculate and set operating resistance of the hot-wire probe ($1.4 \times \text{Cold Resistance}$).
- (ii) Balance the gas temperature bridge.
- (iii) Set the amplifier of the surface thermocouple to the desirable magnification (usually at 200).
- (iv) Calibrate all the instruments as described in Chapter 6.
- (v) Set the Compression Ratio.
- (vi) Run at the first speed.
- (vii) Re-calibrate the hot-wire probe and the surface thermocouple at the end of the run.
- (viii) Run at the second speed.
- (ix) Re-calibrate the hot-wire probe and the surface thermocouple at the end of the run.
- (x) Run at the third speed.
- (xi) Re-calibrate the hot-wire probe and the surface thermocouple at the end of the run.

(xii) Alter the compression ratio.

(xiii) Repeat the procedure for the 3 speeds.

(xiv) Change the location and repeat the procedure.

This procedure was difficult because the hot-wire or gas thermometer wire were fragile and easily broken. In the case of breakage new probes were made and a new calibration carried out before continuing. The pressure and gas temperature systems were calibrated as described in Chapter 6. Little change was detected and re-calibration was not as frequently as the hot-wire and surface thermocouple probe. In the case of the surface thermocouple plug and the hot-wire probes, each new plug and probe needed regular calibration (including the linearizer for the hot wire). In the case of the pressure and gas temperature systems, they were more reliable and consistent but checks were carried out regularly.

7.3 First Stage of the Experiment - Wall Temperature and Cylinder Pressure

In the first stage of the experiment the surface wall temperature and pressure were measured. The experiment at each crank angle was carried out for 3 speeds, 600, 1000 and 1500 rev/min and for each speed 3 different compression ratios and two different positions at one fixed depth. The total number of tests were 36 (3 speed x 3 compression ratio x 2 positions x 2 parameter x 1 depth). The crank angle marker was set manually for a particular crank angle degree. Then after finishing the data collection for that crank angle the crank angle marker was reset to another point of the cycle to start another collection. When all angles

were completed the probes were reversed in position usually. The tests were carried out at 30° degree intervals, tests were also carried out at 10° and 5° degree interval (tests of 10° and 5° intervals were compared with the test of 30° intervals at the same conditions). The engine was allowed to reach steady state and then all signals were logged.

7.4 Second Stage of the Experiment - Gas Temperature and Hot-Wire Anemometer

In this stage the hot-wire and thermometer wire signals were measured. The engine was operated at the same 36 conditions as in section 7.3. The software and the method of collecting data will be described in detail in Chapter 8.

CHAPTER 8

DATA LOGGING AND CALCULATION

- 8.1 Introduction
- 8.2 Instrumentation
- 8.3 DATA Collection Procedure
- 8.4 DATA Processing Method
- 8.5 Calculation

8.1 Introduction

DATA logging systems have been used in most recent engineering applications, but in the internal combustion engine field the development of monitoring signals from various engine transducers and logging data progressed by the late 60's to the minicomputer Ref.(121.)

Until recently in most of the work published on experimental methods great difficulty was reported in retrieving the experimental data which is necessary to the mathematical analysis. Semi-automatic data retrieval system such as analogue - to digital convertors with output connected to a paper punch or typewriter have been used as a first stage to improve the instrumentation of the data collection system, but if the processes are very rapid, the mechanical limitations of paper-tape punches or typewriters make it very difficult to retrieve the output of the analogue-to-digital convertors.

Several schemes have been used in which high-speed magnetic tape units have been employed both as storage for digital information from the analogue-to-digital convertor and as a method of storing the original analogue signals, the tape unit being replayed at a greatly reduced speed for the analogue-to-digital conversion. On this system there is a limitation to the number of channels to be accommodated because of the high cost of each unit used.

Recent developments in readily available relatively cheap computer memory have changed the situation. In 1968 Smyth Ref. (127) used a high speed digital computer as the device for accepting the analogue-to-digital conversion of the original signals. His methods basically consisted of installing various types of sensors which gave a d.c. voltage proportional to the variable being measured. This was transmitted to

an on-line control computer installation which sampled the signals, converted them to digital form, and stored the results in a core memory before transmission to a high-speed digital processing computer for the final heat transfer analysis.

Recently, several research workers have used on-line data acquisition and control in internal combustion engine research. The work of Ref. (16) has been in continuous development over 12 years, in particular the automated test bed in its final form. Their system enables any faults to be identified at an early stage and the setting-up time has been reduced to minimum.

Sarstem Ref. (121), Larsen and his group Ref. (84) and Shiling and Woschni Ref. (126) have been involved in using different types of computers and components. Now there is quite a large amount of University and Industrial activity in the area of on-line data acquisition and control with most of the projects.

The conclusion from what has been said above, of introducing the on-line computer and control for internal combustion engine research, are;

- (1) Computerised data logging systems provide an excellent and accurate recording for rapidly changing signals.
- (2) Greatly reduce the error caused by handling the data from various sensors, which are recorded by UV recorder or any other recording instrument, and process them by another data-processing machine.

- (3) Many signals can be recorded at the same time and the number of the signals to be recorded depend upon the type of the system which has been used, sometimes up to 64 signals.
- (4) The sampling rate of data is fast, it is variable and it depends on the type and the number of the signals to be recorded, and matches the requirements of measuring a signal in a response time of the order of a micro second.
- (5) Efficiency in labour and time, and is easy to control the collecting and processing of data.

In the present work the ALPHA L SI-2 mini computer was used for logging and processing the data. Many necessary devices have been interfaced with the computer to give an efficient logging and processing method, as shown in Fig. 8.1. These will be explained in the next sections.

Two machine language programs (ML) were developed and used to control the logging and conversion process and to store the data on a data diskette, these programs were run from a second diskette. The software needed to initially process the data (averaging and conversion from digital to required units of P, T etc) was written in Basic Language (CAI Basic). These results were then stored on disk and for the processing took place on a PDP11/34 computer. The interfacing of the ALPHA disk format to the PDP11 format is described in Appendix 8.8.

8.2 Instrumentation

8.2.1 The Computer

An ALPHA LSI-2 mini computer of core memory size 48K bytes was used. This unit has four interfaces, A/D convertor interface, teley type interface, high speed tape reader and Disk drive unit. A basic language (CAI) and machine language programs (ML) can be used. Also it is possible to link the ML programs to Basic, and a special method used to create an extended version of Basic which can contain up to 20 ML subroutines Ref. (7, 21).

8.2.2. Floppy Disk Operating System (ALPHA LSI-2)

The drive disk type PERIFLEX 6550-01 is used to operate the diskette (or floppy disk) which is 198.12 mm (7.8 inch) in diameter, single sided and the capacity storage is up to $\frac{1}{4}$ mega bytes of information. The disk is divided into 77 cylinders or tracks which are numbered 0 to 76. Each cylinder is sub-divided into 26 sectors numbered 1 to 26 which means that there are 2002 sectors on a diskette. Data is recorded in blocks of up to 64 16-bit words (128 bytes) per sector therefore a disk will hold 128K 16-bit words.

There are three types of diskette configuration:-

- (A) System diskette:- The operating system itself resides on this diskette with parts of it being brought into the machine memory as required. It also contains permanent programs such as BASIC and the various utility programs available under the ALPHA Disk operating systems (DOS). The system diskette must be initiallised and given a directory before it can be used.

(B) File Diskette:- This type can be used to store the programs user files and also for storing the data. The file diskette must be initialised and given a directory before it can be used.

(C) Data Diskette:- This type can be used directly without any initialisation to store binary data not basic floating point or text data.

It should be pointed out that the light on the front panel of the disk drive (i.e. the unit write light) will be on most of the time except when collecting data or material is being entered from the keyboard.

8.2.3 Analogue-To Digital Convertor (A/D)

The 12-bit resolution A/D convertor is accessed via an 8-channel analogue multiplexer. The range of the A/D convertor is +5 volts to -5 Volts. Any number of channels between one and eight may be used and they may be accessed in any required grouping simultaneously and the results held in a buffer until read by the computer. Channel numbers must be in the range 0 to 7.

To control the A/D convertor and multiplexer the OTA or OTX:12,2 instruction was used. The effect of the A or X register however will depend upon whether 'mode' or 'channel' has been selected.

The 'Mode' used to control the A/D convertor was a single sequential scan (channels are read in parallel by the convertor and the 12-bit converted result read sequentially by the computer) which allows the user to select "Start" and "Finish" channels. When the A/D convertor is started the selected channels will be digitized sequentially and then

the A/D convertor will halt. The instruction for single sequential scan is:-

SEL	:	12,7	(select Mode)
LXP	:	2	(Load X-registered for single sequential scan)
OTX	:	12,2	(control the A/D convertor)
SEL	:	12,6	(prepare for channel)

For each channel the computer must use an RDA or RDX : 12,6 instruction to take the data as it comes from the digitizer. All the instructions in the ML programs are explained in Appendix 8.2.

8.2.4 Real-Time Clock Generator

The conversion process can be started by a pulse applied to the "real-time clock input". A variable crystal clock is provided so that conversions or conversion sequences can be accurately timed. There are many different ranges of pulse rate at the crystal clock (10 μ second to 9 seconds), the selected pulse rate depends on the type of experiment carried out, the rate data collection matching the experiment.

In the present work the crank angle marker produced a pulse at T.D.C. and the selected angle which was connected directly to the real-time clock to control the starting of the conversion process.

8.2.5 Teletype Writer

A DATA dynamics Teletype Writer type 390 was used. The main function is the basic communication medium between the user and the operating system. It is considered as a keyboard and through it, the user communicates with the system executive routines, user programs

operating under the system, and system utilities. This is not the only such interface, other devices such as a card reader or line printer may be used.

8.3 The Procedure of Collection Data Process

The first step was to switch on the system. After a short time a greater-than sign (>) should be printed on the Teletype. If this fails to appear the system should be bootstrapped using the directions in Appendix 8.1. The system disk and data disk were loaded in the disk drive and the drive numbers must be F0 and F1 respectively.

Two machine programs have been developed, WS1 and WS2 as in Appendix 8.3 and 8.4 respectively, which controlled the conversion process. The program WS1 controls the start cylinder and finish cylinder, start channel and finish channel required. The maximum number of data samples is 1664 samples per cylinder (computer storage limitation). The program WS2 is modified from WS1 in order to control the number of data samples required which depended on the type of the signal to be loaded, e.g. if the signal is pressure the number of data samples required is less than the number of data samples required for hot-wire signal.

The data was logged as described in Appendix 8.5. Each set of readings was specified via the teletype (i.e. crank angle for reading, number of cylinder to be read, number of channels to be read, and total number of times the readings should be taken) as in Appendix 8.6.

The number of channels to be collected at particular crank angle were varied from (1 to 8) in each cycle and the logging process could be carried out over many cycles in order to obtain the average value of these samples. Collecting data at a particular crank angle on consecutive revolutions rather than incrementing the crank angle during a revolution should give a turbulence result less subjected to experimental drift (e.g. hot-wire readings are obtained in a few seconds rather than minutes).

It should be pointed out that the A/D convertor loads all channel signals at the same time and therefore no allowance is needed for crank angle travel during the data logging of the channels.

The approximate time per channel for conversion was ($2.5\mu\text{s}$) for the A/D convertor and about $10\mu\text{s}$ for the computer to read it. The times available to load 1 degree crank angle at speeds of 600 r.p.m. and 3600 r.p.m. are $277\mu\text{s}$ and $46\mu\text{s}$ respectively. Therefore there is sufficient time to complete the conversion log the data and prepare for the next revolution to repeat the same procedure. Appendix 8.7 shows the flow chart of the logging process which is controlled by a machine language program.

8.4 DATA Process Method

The data stored on the data disk are in the form of digital numbers. These numbers need to be processed to volts and then to the corresponding experimental unit by knowing the relation between the voltage and the unit from the calibration curve.

The processing software was written in Basic language on the system disk and the process was carried out on the α -computer itself at the early stage of the project. A machine language subroutine was used in order to read data from the disk and make it available to the Basic program which called it.

As an alternative a program was developed Ref. (21) in order to process the data on the departmental computer (type PDP 11/34). This program called "ALPHA" could be called to read data from a diskette which had been written on the ALPHA computer and write the data into an INTEGER VIRTUAL ARRAY FILE. This file can then be very easily accessed from BASIC as in Appendix 8.8. It is possible to read the disk in four files, but this will use up 500 memory blocks on the PDP-11 disk. With time sharing in operation it is usually necessary to read less than four files.

8.5 Calculation

8.5.1 Calculating Gas Temperature from Gas Pressure:-

From equation 6.10, the energy balance is given by:

$$M_{\sigma} \frac{\partial T_{tw}}{\partial t} = h \times A \times (T_g - T_{tw}) \quad 8.1$$

so when

$$\frac{\partial T_{tw}}{\partial t} = 0, T_g = T_{tw}$$

i.e. at the peak wire temperature, the gas temperature is equal to the wire temperature, Ref. 49. As has been mentioned in Chapter 6.4.3 the following equation can be used.

$$\frac{P_m \times V_m}{T_m} = \frac{P_{B.D.C} \times V_{B.D.C}}{T_{B.D.C.}} \quad 8.2$$

volumes at various crank angles were calculated from the following equations given by Ref. 15.

$$V = V_c + \left(\frac{\pi}{4} D^2\right) \left(\frac{L}{2}\right) [1 + n - (n^2 - \sin^2 \alpha)^{\frac{1}{2}} - \cos \alpha] \quad 8.3$$

- where V is the cylinder volume
- V_c is the clearance volume
- n is the connecting rod length
- α is the crank angle
- L is the stroke
- D is the cylinder bore.

Since $T_{B.D.C.} = T_{tw}$ from what has been said in Chapter 6.4.3 so the calculation for gas temperature was carried out only for the closed period by using the values of pressure and volume at different crank angles. A computer programme was developed to calculate the gas temperature (Appendix 8.9). Another computer programme was developed to solve equation 6.18 to obtain the gas temperature from the thermometer wire temperature, Appendix 8.10.

8.5.2 Calculating heat flux from surface temperature:-

The heat flux at various crank angles was calculated using equation 3.18.

$$\frac{q}{A} = -K \left[\frac{\partial T_w}{\partial X} \right]_{x=0} \quad 8.4$$

and

$$(\bar{T}_w)_{x=0} = (\bar{T}_w)_{x=L} - \frac{X}{L} [(\bar{T}_w)_{x=0} - (\bar{T}_w)_{x=L}] + \sum_{k=1}^m \frac{-xr}{e}$$

$$[Ak \cos (kwt-xr) + Bk \sin (kwt-xr)] \quad 8.5$$

The derivative of equation 8.5 with respect to X was carried out at x=0 as mentioned in Chapter 3.3. Equation 8.4 becomes

$$\frac{q}{A} = \frac{K}{L} [(\bar{T}_w)_{x=0} - (\bar{T}_w)_{x=L}] + K \sum_{k=1}^m r[(B_k - A_k) \sin kwt + (B_k + A_k) \cos kwt]$$

8.6

To solve equation 8.6 a computer programme was developed in Appendix 8.11.

8.5.3 Calculation of Re and Nu numbers:

$$Re = \frac{\rho \bar{U} D}{\mu}$$

where ρ = gas density in kg/m³ and equal $\rho = P/R T_g$

where p = gas pressure in N/m²

R = gas constant = 287 J/Kg K°

T_g = gas temperature in K°

\bar{U} = Ensembled average instantaneous velocity in m/sec

D = cylinder bore diameter in meter

μ = dynamic viscosity in kg/m.sec

$$\mu = \mu_0 T^m = 3.16 \times 10^{-7} \times T_g^{0.645} \quad (\text{Ref. 8})$$

$$Nu = \frac{hD}{K}$$

h = heat transfer coefficient in w/m².k°

k = gas thermal conductivity in w/m.k°

$$k = \mu \cdot Cp / 0.7 \quad (\text{Ref. 8})$$

where Cp = specific heat J/Kg.k°

$$Cp = 0.224 + (0.471 \times T_g / 10000) \quad (\text{Ref. 8})$$

8.5.4 Correlation

A computer programme was developed to solve the equation (Appendix 8.12)

$$Nu = a (Re)^{b1} \cdot \left(\frac{\bar{U} + \acute{U}}{V_p}\right)^{b2} \cdot \left(\frac{T_g}{\Delta T}\right)^{b3} \cdot \left(\frac{P \acute{U} D}{KT_g}\right)^{b4}$$

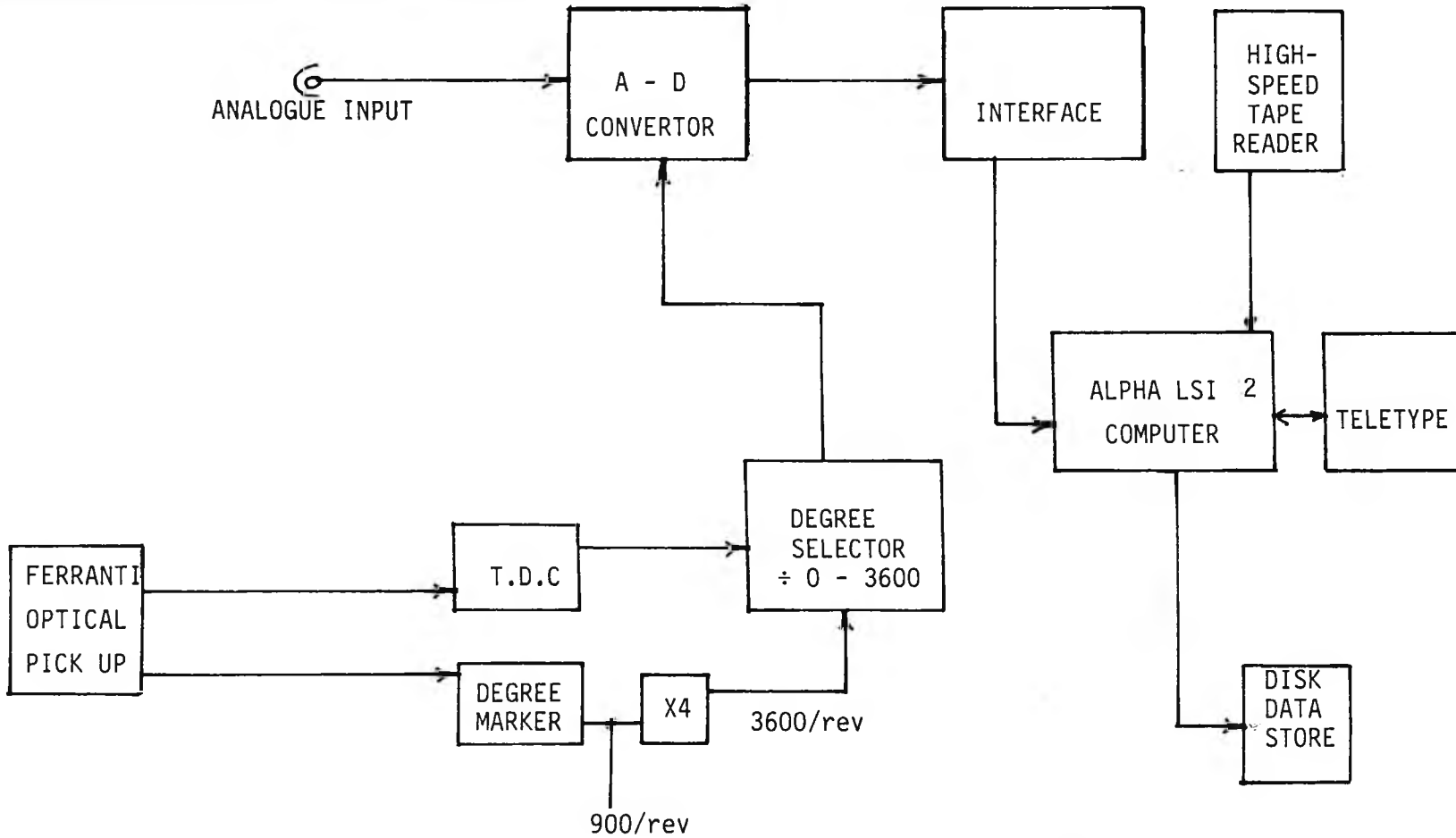
The values of constants obtained with induction - exhaust stroke are

$$\begin{aligned} a &= 0.561 \\ b1 &= 0.694 \\ b2 &= -0.818 \\ b3 &= 0.964 \\ b4 &= 0.078 \end{aligned}$$

and the values with compression - expansion stroke are

$$\begin{aligned} a &= 1.9861 \\ b1 &= 0.706 \\ b2 &= -0.321 \\ b3 &= 0.883 \\ b4 &= -0.1 \end{aligned}$$

A sample of data and results are represented in Appendix 8.13.



DATA LOGGING SYSTEM BLOCK DIAGRAM

Fig. 8.1.

CHAPTER 9

DISCUSSION OF RESULTS

9.1 Introduction

9.2 Primary Results

9.3 Derived Results

9.4 Correlation

9.1 INTRODUCTION

In this chapter the results are divided into three different categories. The first category represents the primary (measured) results including the surface wall and gas temperature, gas pressure, mean velocity and turbulence. These parameters are discussed in section 9.2. The second category is the derived results calculated from the primary results and these are (heat flux, Reynold number and Nusselt number) represented in section 9.3. The third category problem in combining the measured and derived parameters, to give a satisfactory prediction for heat flux in a cylinder of an internal combustion engine, is difficult since it cannot involve all the complex mechanisms. The introduction of turbulence in the present work has significant effect on the heat flux. These arguments are discussed in section 9.4.

The effects of compression ratio, speed position, crank angle interval and the number of cycles over which the average of parameters is taken are discussed in the following section as well as the efficiency of using the data logging systems.

9.2 PRIMARY RESULTS

9.2.1 Surface Wall Temperature:-

Plate 1 shows a typical oscillogram record of the output of the surface temperature measuring themocouple. As can be seen the a.c. component of the signal has a very small amplitutde compared with the d.c. component and this makes it necessary that the noise level of the system should be as low as possible. Therefore the amplifier used must be adequate to obtain the required magnification of the output of the surface thermocouple. In addition, the uniform coating of the Ni-film and the calibration of the surface thermocouple before and

after the test is essential for the high accuracy. The high accuracy is important since the surface thermocouple signal is used as a boundary condition for the solution of the partial differential equation governing transient heat flow described in Chapter 3.3.

The effect of the oil contamination on the output of the surface thermocouple is shown in Plate 1. a, b. In Figure A the amplitude of the signal output is reduced, after seven hours of using the surface thermocouple, when it is compared with the amplitude of Figure b which represents the use of a new surface thermocouple, both Figures a and b are under the same test conditions. Refer to Refs. 96, 107 for more information about the effect of the oil contamination on surface thermocouple.

Because of the high melting temperature of the Ni-film, it is difficult to obtain a uniform coating surface while with the Cu-film it is obtainable. This explains why the output signal from the surface thermocouple with Ni-film deposition is noisy while with the Cu-film there is less noise as shown in Plate 1. g, h respectively.

The output of the surface thermocouple fed to the computer is approximately the same as the one fed to the oscilloscope which is shown in Plate 1.

In order to investigate the effects of varying the compression ratios for a fixed speed, measurements were made at compression ratios of 8, 10 and 12:1. These tests are shown in Figures 9.1 - 9.3 representing nine tests. The scatter in results is indicated in Figures 9.13 - 9.14. As can be seen from the figures, if the compression ratio is increased the Wall Temperature is increased. The increment in temperature with compression ratio is uniform at 600 and 1000 rpm but is significantly different to that at 1500 rpm. In the later test the

cooling water mean temperature increase is greater between 10 and 12:1 compression as is the surface thermocouple back temperature (The values of both temperature are mentioned on the graphs).

The influence of varying the engine speed on the wall temperature readings for a fixed compression ratio are shown in Figures 9.4 - 9.6. The Wall Temperature is strongly affected by varying the speed, as the speed increased the Wall Temperature is also increased. While the compression ratio has slight effect. The measurements were made at speeds of 600, 1000 and 1500 rpm. It is difficult to extend the range of studies, because as the speed is increased the vibration is increased and consequently the level of noise is increased which leads to incorrect output of the surface thermocouple especially when the engine is motored.

The effect of selecting the interval of crank angle at which the measurements are taken are shown in figures 9.7 - 9.9. The measurements were taken at three different intervals 5, 10 and 30 degrees under the same test conditions. In figure 9.7 reproductibility for test to test is good, the better discrimination of 5, 10 degree intervals only showing a slight dip ATDC. Increasing compression ratio Figures 9.8, 9.9 shows that test results are less reproducible.

The effect of the locations, at which the surface thermocouple is placed, on the surface Wall Temperature are shown in Figures 9.10 - 9.12. Although the measurements values are different from position to another, but they have the same behaviour especially near TDC, and these results compared favourably with those of Refs. 4, 6, 107, 146. This explains why the surface Wall Temperature is different from one point to another in the combustion chambers, this is shown in Plate 2. Figures A and B.

The selection of the correct number of cycles at which the average values are taken depend on the type of parameter to be considered. In case of Wall Temperature the number of cycles chosen are 100, these were adequate for the present investigation since the difference in average value is slightly affected by increasing the number of cycles to the double. Figures 9.13 and 9.14 show instantaneous values of Wall Temperature and its average for a particular crank angle position.

From all figures 9.1 - 9.12 the surface Wall Temperature is increased suddenly after the crank angle 270 degrees, and this is due to the compression stroke, and reaching the maximum value at 4 to 9 degree ATDC.

9.2.2 Pressure:-

As with all the components of the system, it is desirable to have accurate measurements of the gas pressure since the gas temperature, as estimated from the pressure readings, would be compared with those resulting from the gas thermometer. In addition the pressure affects all the parameters to be measured as well as the heat flux. The output received by the computer has been compared with the oscilloscope, this checked the reliability of the computerised data logging as shown in Plate 1 and Plate 2 figures A, B, C, D.

After a certain time, the pressure signal begins to drift due to the effect of temperature on the pressure transducer. To avoid this drift, a cooling system must be used to cooldown the pressure transducer and this is especially used in case of running engine. In the present work the engine is motoring therefore the cooling system was not used, but the average value of the pressure was taken over 100 cycles to make sure the drift as low as possible and the maximum error due to the drift and noise was approximately 10 per cent. Using the average value of the pressure readings with the correction Factor mentioned in Chapter 6.4.3, the error reduce to 4.5 percent. Figures 9.25 and 9.26

show the variation of the pressure reading and its average over 100 cycles for two particular crank angles (360 and zero degrees) respectively. The drift is significant at induction and exhaust stroke due to the low pressure measurement, the pressure is negative at certain crank angle points of the cycle.

The effect of the compression ratio on the pressure reading is shown in Figures 9.15 to 9.17. As the compression ratio increased the pressure value is increased.

The effect of varying the speed on the pressure reading is shown in figures 9.18 to 9.20.

There is no significant effect of the position on the pressure reading since the pressure is approximately uniform in the combustion chamber and this is shown in Figure 9.21. There is little effect of crank angle intervals (30, 10, 5 degrees) on the pressure measurements as shown in Figures 9.22 to 9.24 and this is due to the reliable signal of the pressure transducer.

From all the figures 9.15 to 9.26, it can be seen that the pressure is approximately symmetrical about TDC. The maximum value of the gas pressure is achieved at TDC. Although if a much finer angle step was used the peak would probably be slightly ATDC. For the present purposes the error is acceptable.

9.2.3 Gas Temperature

The gas temperature is one of the most difficult parameters to be measured accurately, since the measuring wire must be robust and have a reasonable response and this was achieved by using 10 micron platinum Iridium alloy. Plate 2 Figure C and Plate 3 show the signal output of the thermometer temperature (checks were made to compare this signal with the one monitored by the computer).

As has been mentioned in Chapter 6.4.2 the thermometer temperature lags behind the true gas temperature because of the thermal inertia of the wire.

At the first attempt, the method by Ghirlando Ref. 49 was used, and some obvious errors occurred, as they did points in Ghirlando's work. The method is based on constants taken from Ref. 94 and Ref. 66. The equations used by Ghirlando were checked and an error found and corrected, and the constants modified. A new formula (Chapter 6.4.2. equation no. 6.18) and the corrected Ghirlando formula (equation no. 6.18a) are compared in Figure 9.27. As it can be seen from the figure there is no significant difference in corrected gas temperature between the two solutions.

The calculated gas temperature from gas pressure for closed periods were carried out for all the tests ($PV = MRT$). Figures 9.28 to 9.30 represent samples of one test at three different crank angle intervals (30, 10, 5 degrees) respectively. As it can be seen from the figures the calculated value is higher than both uncorrected and corrected temperature. As the compression stroke is started the temperature difference (between calculated, corrected and thermometer temperatures) is small and it increases towards the TDC.

The measurements of gas temperature were made for three different compressions and the results are shown in figures 9.31 to 9.33. As it can be seen from the figures the correction to the thermometer temperature is significant for both compression and expansion stroke.

The effects of varying the speed on both gas and thermometer temperature were shown through figures 9.34 to 9.36. The measurements, as it can be observed from the figures, have less discrepancy at both induction and exhaust strokes than both compression and expansion strokes. This is because the temperature is only changing slowly and the thermal inertia has less effect. The gas temperature is higher than the thermometer

temperature at both induction and compression strokes while at both expansion and exhaust strokes is lower, this is due to the sign of the thermometer temperature slope $\frac{\partial T_{tw}}{\partial t}$. These are shown through all figures 9.28 to 9.36.

The effect of the position on the thermometer wire temperature is shown through the figures 9.37 to 9.39, which show that the value of thermometer temperature is depend on the position of measurement at which the thermometer wire is placed, and consequently the corrected gas temperature will have the same behaviour. This explains some of the discrepancy with $T = PV/MR$ which is a mean temperature of whole cylinder rather than a local temperature close to wall.

The crank angle intervals (30, 10 and 5 degrees), at which the thermometer temperature measurements were made, have little effect as can be seen through figures 9.40 to 9.42.

All the thermometer wire temperature measurements were made at each particular crank angle the values used represent average values taken over many cycles. After certain numbers of cycles the average value is slightly affected and this number is considered adequate (100 cycles in the present work). Figures 9.43 and 9.44 show an average value of thermometer temperature over 250 cycles for two particular crank angles 360 and 0 degrees respectively. After 100 cycles the temperature starting to drift and this is clearly shown in figure 9.44. Therefore, the selected number of cycles is determined between two limits. The first is at which the average value is slightly affected and the second is the beginning of the drift. All instrumentation recorded a drift indicating the drift to be a change in the engine state.

9.2.4 Hot Wire Signal

The hot-wire results are presented in the form of graphs of ensemble average velocity \bar{U} and turbulence intensity u' against crank angle for the various experimental conditions (compression ratio, engine speed, position and crank angle interval).

The hot wire operating temperature had to be kept greater than the gas temperature surrounding the wire for sensitivity reasons. This means that at higher gas temperature (i.e. near TDC) the temperature difference between the wire and the gas becomes small, and the hot wire results become more sensitive to errors in the measurement of the gas temperature. It was considered reasonable to assume that measurements at temperature differences of over 100°C would be quite reliable. An assumption made by Ref. 49 was that measurements at temperature differences of over 75°C would be reliable. Most of the tests were at temperature differences over 100°C.

Plate 3 shows typical records obtained from the anemometer with and without the linerizer. These as usual were compared with the results obtained by the computer and show insignificant differences thus proving the reliability of the data logging.

For the hot wire results, the direction of the gas velocity is not known, as the results represent the component of gas velocity that lies in the plane perpendicular to the wire axis.

Figures 9.45 to 9.65 represent all the measurements made for mean velocity and turbulence across the head as measured by the hot wire. At all speeds and compression ratios similar variations may be observed. Explanations of the curves can only be tentative but a possible interpretation could be as follows.

In figure 9.45 velocity variations are the result of

1. The jet velocity through the IV and EV
2. The direction taken by the jet, whether across the head or down the cylinder.
3. The movement of vortices in the cylinder Ref. 83.

The magnitude of the velocity will be related to the piston speed and the opening and closing of the valves.

During the induction stroke a maximum is reached with IVO at maximum piston speed and a deceleration occurs as it returns with IVC and minor oscillations are jet deflection and vortex motion effects. During expansion little motion occurs due to the cylindrical E6 combustion chamber until at EVO and the exhaust stroke occurs. The exhausting flow producing a second major peak.

The turbulent intensity, as shown in Figure 9.45, shows a strong correlation with the mean velocity during most of the engine cycle except a part of the cycle after IVC, the turbulent intensity has dropped with the termination of jet flow through the IV, but the mean velocity remains high due to swirl.

Three different compression ratios were considered to study the effect of compression ratio on the mean velocity and turbulence intensity as shown in Figures 9.46 to 9.48. As can be seen from the figures there is no significant effect to observe.

The effect of engine speed on the mean velocity and turbulence intensity is shown through the figures 9.49 to 9.51. As the engine speed increases the mean velocity increases, the magnitude of this increase is not constant throughout the cycle.

Semenov Ref. 124, reported a dependency of mean velocity during compression on engine speed raised to the 2.1 power. His results were based on time averages over 24 degree crank angle. The results here by

show a more linear relationship of mean velocity to engine speed during most of the engine cycle and this favourably agreed with those obtained by Ref. 83 and 149.

The changes of turbulent intensity with changes in engine speed are similar to those in the mean velocity and are illustrated in figures 9.49 to 9.51.

The effect of position on mean velocity and turbulence intensity is shown through figures 9.52 to 9.60. There is significant effect on mean velocity and turbulence intensity by the location of the hot wire sensor and this explains the fact that measurements taken with a hot-wire sensor give the magnitude of the velocity component normal to the sensor at one location in the combustion chamber. It would be very difficult for a probe to be in a location in the direct path of the incoming jet Ref. 149.

Only between 200° and 320° C.A. is a slight difference in mean velocity as smaller intervals are taken. There is little effect on turbulence Figures 9.61 to 9.63.

The number of cycles at which the instantaneous measured is of importance to obtain a reliable turbulence level and accurate mean velocity. Most of the tests were made at 500 cycles. Figures 9.64 and 9.65 show the instantaneous velocity over 250 cycles for two particular crank angle 360 and zero degrees respectively.

In Figure 9.64 in which velocities are low and flow is reversed some errors are apparent. The processing of the hot wire, and thermometer wire and pressure signals have produced a few negative results indicating experimental error and possible errors in the calculation method. Since (-Ve) velocities exist there is also some error in the mean and turbulent velocities calculations, 360° crank angle is the worst case of these errors.

9.3 Derived Results

9.3.1 Heat Flux:-

Instantaneous heat transfer results through the gas-wall interface as computed from the surface temperature variation are presented through figures 9.66 to 9.77. In the calculations of the results, as explained in Chapter 3.3, a one dimensional model is assumed and some error in the heat flux is to be expected due to three dimensional effects as well as experimental errors in surface temperature measurements. As can be seen from the figures, highest heat transfer rates occur during the compression and expansion strokes near TDC. This major portion of unsteady heat transfer takes place between the interval 80 degrees BTDC (compression) and 70 degrees ATDC (expansion). This is of the same order as the respective values obtained by Overbye Ref. 107 (80 degrees BTDC to 80 degrees ATDC) and Knight Ref. 78 (60 degrees BTDC to 60 degrees ATDC). This is the region of most interest in heat transfer studies. Furthermore, in this region the heat flux measurement is more accurate because of the larger temperature differences.

During the intake and exhaust strokes the level of heat flux is comparatively very low and large errors may occur in the calculation of heat flux from experimental surface temperature measurements. There is both positive and negative heat transfer as the gas-wall temperature difference changes sign. Figures 9.66 to 9.77 for heat flux may be compared to temperature difference figures 9.78 to 9.84.

Figures 9.66 to 9.68 represent the effect of compression ratio on the instantaneous heat transfer. Little effect is observed over most of the cycle except near TDC where the gas-wall temperature difference effect becomes more significant.

Since most workers have used mean engine speed in their correlations, observed heat flux values have been plotted at different engine speeds in figures 9.69 to 9.71. As can be seen from the figures as the engine speed is increased, there is an increase in negative heat flux especially during the exhaust stroke. This is due to the increase in surface temperature since the gas temperature is only slightly affected at this part of the cycle Figures 9.78 to 9.84. The peak heat flux is retarded slightly as the speed increases and is probably due to the thermal inertia of the wall but is generally close to TDC.

The heat flux at two different locations are presented through figures 9.72 to 9.74. The heat flux, as can be observed, is different from one position to another depending on the local conditions at the point where the sensor is placed. Although measurements were carried out at only two locations, adequate information is available.

Other workers have taken measurements at 2-6 locations Refs. 3-6, 31, 60, 146, which show the heat flux is different from one point to another in the combustion chamber. It was pointed out by Ref. 31 that due to the circular symmetry of the flat piston top and the flat head surface as in E6 the heat flux would be the same in a motored engine at the same distance from the cylinder center in a motored engine; thus, the heat flux measured at one position on the circle of radius r inches would represent the heat fluxes at any other position on the same circle.

Little effect of crank angle interval on heat flux measurement is observed. Figures 9.75 to 9.77 represent the effect for three different intervals (5, 10, 30 degrees).

The heat flux is calculated from the surface temperature records and this is averaged over hundred cycles because the measured value of surface temperature varies from cycle to cycle Figures 9.13 and 9.14.

A considerable cycle-to-cycle variation in heat flux was also observed by Ref. 6, this variation is at the time of the initial high rate of increase of the heat flux. The cycle-to-cycle variation of the peak heat flux is relatively small.

The definition used for the heat transfer coefficient h ($h = \frac{Q}{T_g - T_w}$) is taken from steady heat transfer methods. In the case of unsteady heat transfer in internal combustion engines, the denominator can have a zero value with finite Q as shown through figures 9.78 and 9.84, thus giving infinite values for heat transfer coefficient. This is due to the thermal inertia of the boundary layer and the definition of h using the bulk temperature of the gas. The concept of infinite heat transfer coefficient is physically unrealistic, but fortunately for the part of cycle which in a large proportion of unsteady heat transfer takes place, around TDC for both the compression and expansion stroke (which is the area of most interest), the heat transfer coefficient has finite values. Annand Ref. 8 argues that flux during these short periods of indeterminate h is negligible.

The heat flux peak for most tests are at the same point of the cycle. Also there is no significant phase difference between the peak gas and surface temperatures, which is contrary to the results obtained with the theoretical model used by Elser Ref. 44 but does agree with the result obtained by Hassan Ref. 59. In general the peak flux values coincide with the peak temperature difference values as can be seen in figures 9.80 and 9.84. At other crank angles that peak flux angle, some phase difference is apparent.

9.3.2 Reynold Number

This parameter is the most important parameter to the description of the structure of the flow and an effective parameters to the heat transfer rate. It has been the usual practice in heat transfer work in involving internal combustion engines to take the piston diameter as

the characteristic length in the calculation of Reynolds number for the cylinder heat transfer. In the present study the cycle-cycle ensemble averaged local velocity is used for Reynolds number calculations instead of mean piston speed which has been used by many workers Refs. 8, 9, 39-41, 103.

Local Reynolds numbers as a function of crank angle for three different compression ratios and three engine speeds are presented in Figures 9.85 and 9.86. The effect of engine speed is significant while at higher compressions little change is observed figures 9.85 and 9.86. As has been mentioned before section 9.3.1, that the area of interest is 80 degrees before and after TDC. The Reynolds number is increased BTDC in case of the compression stroke and decreases ATDC in the case of expansion stroke. Although peak occurs slightly BTDC. This is mainly because of increasing and decreasing the density, in the case of compression and expansion stroke respectively, rather than velocity that is slowly decaying. The decay of velocities at TDC where density change is small produces the peak slightly BTDC. In the other part of the cycle the Reynolds number is fluctuating, having values depending on the mean velocity value at any particular crank angle. Later, the local Reynolds number will be considered as a major function in the correlation of unsteady heat transfer in the internal combustion engine.

9.3.3 Energy Number ($P\dot{U}D/KT_g$)

The introduction of this parameter in the present work is of interest. This parameter has an effect on the heat transfer rate in an internal combustion engine. Since it involves the pressure and turbulence intensity and the last two parameters have a direct effect on heat transfer rate. This energy number as has been mentioned in chapter 5.4 represents the ratio of turbulent transport of pressure forces to the conductive heat transfer, this affecting the energy

balance of the boundary region. This number will be high when the turbulence or the pressure or both have significant effect. As can be seen from Figures 9.87 and 9.88 the energy number has significant value at 30, 90 and 540 degrees crank angle. This is because the turbulence is high at these points, while the other high values occur during both compression and expansion strokes and are due to the pressure effect. The maximum value of this number is about TDC where pressure is highest although turbulence is low.

The effect of speed and compression ratio can be observed through Figures 9.82 and 9.83 respectively. As the speed and compression ratio increase the energy number is increased.

9.3.4 Nusselt Number

This number is derived from the experimental heat flux results, and will be the most important parameters to be investigated. The Nusselt number is usually taken as hD/K , where D is the cylinder bore and K the thermal conductivity of the gas. Most recent investigators propose their correlations in terms of Nusselt number.

Figure 9.89 represents the Nusselt number, over whole cycles, against crank angle. As has been mentioned before the area of least experimental error and the most important in the cycle is 80 degrees BTDC and ATDC. In other parts of the cycle either the Nusselt number is insignificant or has an infinite value and with a smaller temperature difference the error is increased. Initially therefore the obtaining of a correlation has concentrated on this region.

The Nusselt number is increased during the compression stroke and decreases in the expansion stroke.

The effect of variations in the speed and compression ratio on the Nusselt number can be observed through Figures 9.90 and 9.91. The maximum value of Nusselt number is slightly ATDC.

9.3.5 Gas Temperature Ratio, $(T_g/\Delta T)$

This parameter is a dimensionless number representing the effect of both gas temperature and gas-wall temperature difference. This number is thought to be significant as a direct variable affecting the heat flux in the cylinder of an internal combustion engine. Most existing formula do not involve the gas temperature as a direct variable, its effect only appearing in the gas properties.

The number is significantly affected during compression and expansion stroke, decreasing through compression and reaching a minimum value before TDC (approximately 10 degrees BTDC). Then starting to increase through the expansion stroke Figures 9.87 and 9.88. At some points in the cycle the gas ratio will be very large having infinite values as does the heat transfer coefficient. As before initial concentration is made in regions around TDC.

The effect of variations of engine speed and compression ratio can be observed through Figures 9.92 and 9.93. It is quite clear that the effect of the engine speed is fairly significant while the compression ratio has less effect.

9.3.6 Total Velocity Ratio $(\bar{U} + \bar{U}')/V_p$

It is clear there is a significant effect of the speed on the heat transfer rate in the cylinder of an internal combustion engine. Ref. 149 for example assumes the mean velocity and turbulence intensity to be approximately linearly proportional to engine speed, except during the exhaust stroke (540° Crank angle).

Therefore it is desirable to include a parameter in the correlation representing this effect. The mean velocity and turbulence intensity have been normalized by the average piston speed ($V_p = \frac{2 L N}{60}$) to form a dimensionless number.

The effect of the compression ratio and speed were illustrated in figures 9.89 and 9.90 respectively. Little effect of the compression ratio on the total velocity ratio is observed. During exhaust the number falls with increasing speed as found by Ref. 149. During induction and compression strokes less effect is seen. The effect of this number and the other numbers on heat transfer rate are discussed in section 9.4.

9.4 CORRELATION

It is difficult to find one formula for the whole cycle in the spark ignition engine. It is suggested that division of the cycle into parts according to whether the valves are open or closed is appropriate since the flow in the cylinder will be different.

Two correlations for instantaneous heat flux have been developed, one for compression - Expansion strokes and the other for induction - Exhaust strokes. The correlations show that the experimental results for a motored engine at three different compression ratios and three different speeds can be represented by equation 5.21 where the constants and the power index of the dimensionless parameters are different in the two correlations (see Chapter 8.5.4) Although the correlations show an agreement with the experimental results and include the effect of turbulence, it is probable that other variables are not completely represented. In engines of other geometries or when combustion is taking place further terms may be needed.

Figure 9.96 represents the correlation between measured and predicted Nusselt number for induction - exhaust stroke. This correlation shows ± 25 percent discrepancy with experimental results. Figure 9.97 represents the correlation for compression - expansion stroke, and this shows ± 12 per cent of discrepancy with the experimental results. These large errors only occur at a few points where an experimental error in the measured parameters occur at these points. Neglecting these, the errors are reduced approximately to ∓ 11 per cent in the case of induction - exhaust stroke and ∓ 5 in the case of compression - expansion stroke.

Experimental and correlated Nusselt numbers are plotted against the crank angle Figure 9.98. It shows an agreement with each other for the compression - expansion stroke. The effect of both compression ratio and speed on correlated and experimental Nusselt number are shown in Figures 9.99 and 9.100 respectively. The best results are obtained at mean compression and speed of the tests (10:1, 1000 r.p.m). For the compression - expansion revolution different correlation constants are required.

Figures 9.101 to 9.105 represents the correlated and experimental Nusselt number against crank angle for whole cycle under different engines conditions. Agreement of the correlation with the experimental result is shown through the induction stroke but there is less agreement in the case of exhaust stroke. The parts of the cycle between 240° - 300° crank angle and between 420° - 480° crank angle, are regions in which $(T_g - T_w)$ are small and experimental errors are exaggerated. These intervals are omitted on the figures.

The local Nusselt number is different from point to point in the cylinder and a proper evaluation of this number at any point depends on the accurate measurements of the gas velocity, turbulence, gas and wall temperature at the same point. The predicted heat flux can be obtained

from the correlation.

Samples of results are plotted through figures 9.106 to 9.110. The predicted heat flux shows an agreement with the experimental heat flux as calculated from surface wall temperature. The predicted heat transfer at expansion stroke is much enclosed to the experimental values than any other part of the cycle.

The effect of the compression ratio and engine speed on both predicted and experimental heat flux is shown through figures 9.111 and 9.112. The compression ratio has less effect on predicted heat flux than the speed. As can be observed from all the figures that the predicted heat flux around TDC is lower than the experimental values in all cases except at high speed and compression ratio figures 9.110 and 9.108 respectively.

A comparison between the present correlation and existing formula is desirable. The present correlation and experimental heat flux were compared with the early correlations, figure 9.113. The greatest discrepancy between the predicted and experimental values exist in the case of Nusselt formula Ref. 103. This formula was based on hot bomb test, therefore the heat transfer due to forced convection would be small, because of low gas velocities obtained in the bomb compared with an engine cylinder. This supports the argument of Annand Ref. 8 in his review of the early existing formula. Brillings formula gives the same approach as Nusselt formula. Eichelbergs formula Ref. 40 gives a higher value for predicted heat transfer than those obtained by Nusselt and Brillings, because the investigation was made in real engines, but there is still a high discrepancy between the present correlation and Eichelberg's correlation.

Annand's correlation principally based on Overbye data Ref. 107 shows a large discrepancy with Woschni Ref. 154 figure 9.114. The present experiments agree more closely with Woschni but are still lower at the peak figure 9.115, and show more reversed heat transfer during exhaust and induction strokes than any of the other correlations. Adjustment of the constants in Annand's equation (Chapter 5.3.4) reproduce the effect observed in the present work.

In the present work the wall temperatures were low and the reversed transfer was therefore more significant. The actual discrepancy in cycle integrated heat flux between the present and Overbye work will be less since the negative flux cancels the excess positive flux.

Incorporating as it does the effects of local velocity and turbulence the present correlation should be better but this needs to be checked in engines of different geometries and the E6 engine with aerodynamic modifications.

CR = 10, N = 1500 rpm

1. $T_w = 1$ Volt/Div

2. $P = 1$ Volt/Div

Time base 20 m s

FIGURE A

CR = 10, N = 1500 rpm

1. $T_w = 1$ Volt/Div

2. $P = 1$ Volt/Div

Time base 20 m s

FIGURE B

CR = 10, N = 1000 rpm

1. $T_w = 1$ Volt/Div

2. $P = 1$ Volt/Div

Time base 20 m s

Copper film

FIGURE C

CR = 10, N = 600 rpm

1. $T_w = 1$ Volt/Div

2. $P = 1$ Volt/Div

Time base 20 m s

Nickel film

FIGURE D

CR = 8, N = 1000 rpm

1. $T_w = 1$ Volt/Div

2. $P = 1$ Volt/Div

Time base 20 m s

FIGURE E

CR = 8, N = 600 rpm

1. $T_w = 1$ Volt/Div

2. $P = 1$ Volt/Div

Time base 50 m s

FIGURE F

CR = 10, N = 1000 rpm

1. $T_w = 1$ Volt/Div

2. $P = 1$ Volt/Div

Time base 20 m s

Nickel film

FIGURE G

CR = 10, N = 1000 rpm

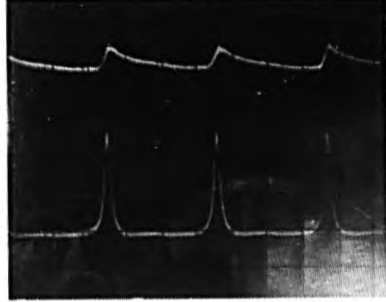
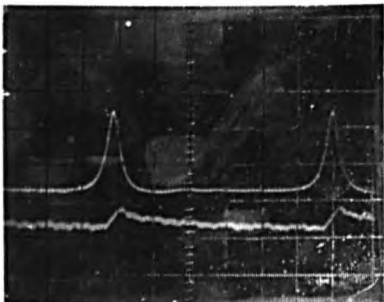
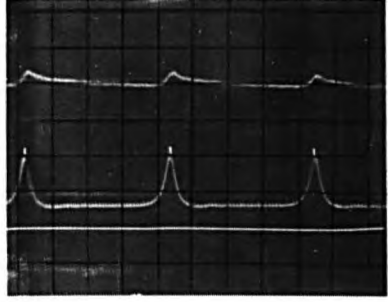
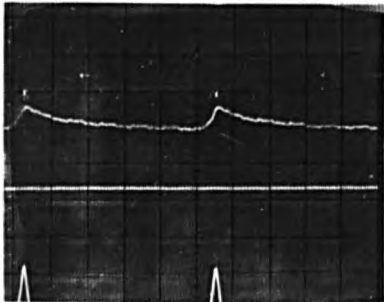
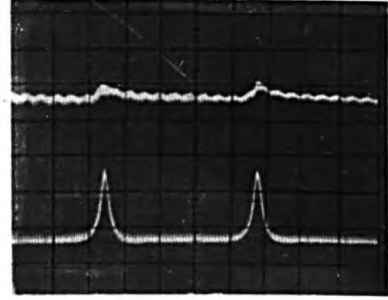
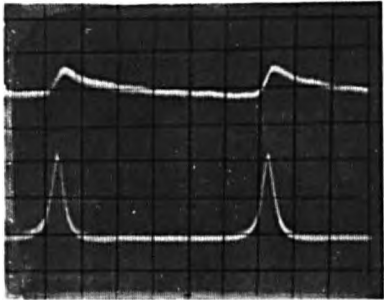
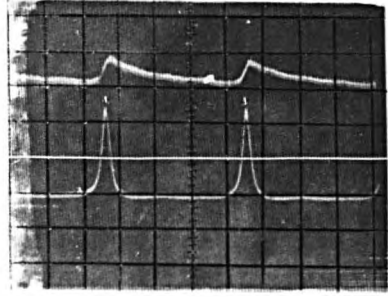
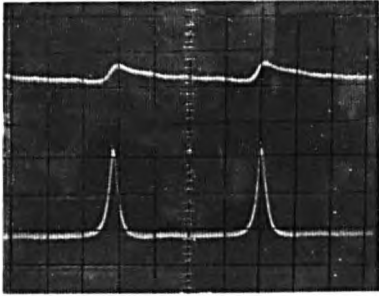
1. $T_w = 1$ Volt/Div

2. $P = 1$ Volt/Div

Time base 50 m s

Copper film

FIGURE H



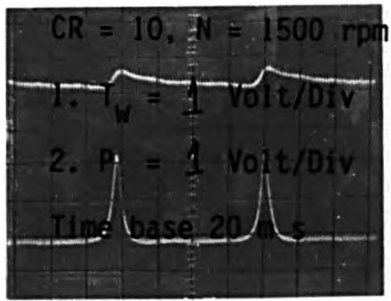


FIGURE A

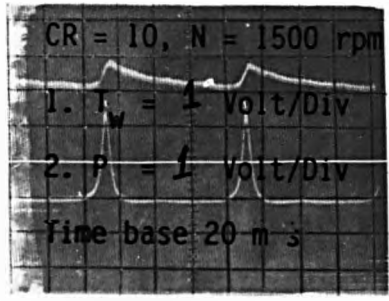


FIGURE B

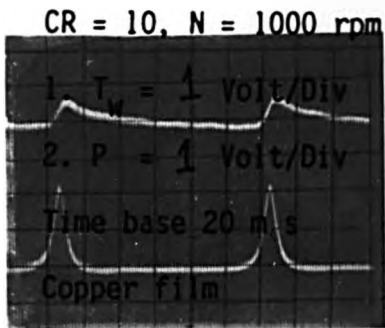


FIGURE C

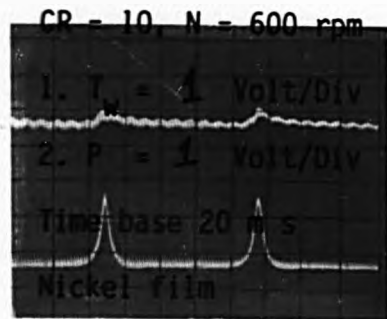


FIGURE D

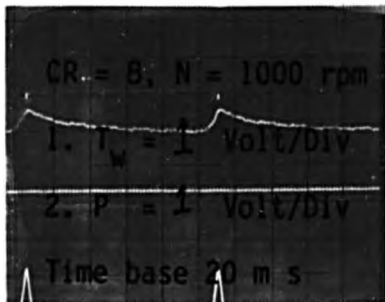


FIGURE E

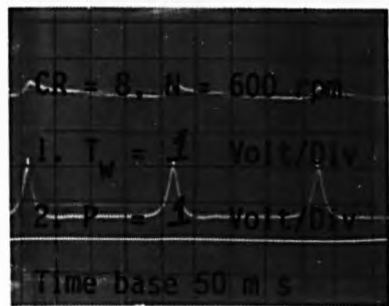


FIGURE F

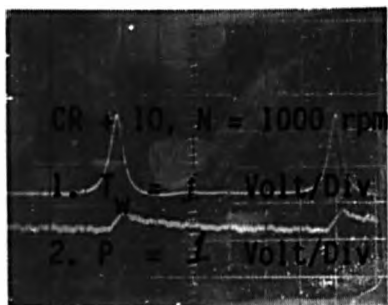


FIGURE G

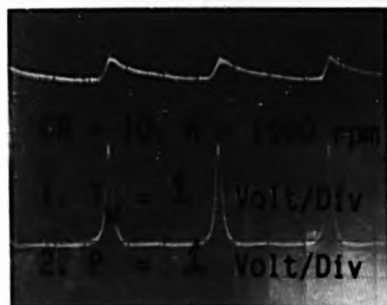


FIGURE H

CR = 10, N = 1000 rpm

1. $T_w = 1$ Volt/Div

2. $P = 0.5$ Volt/Div

Time base 20 m s

Position 1

FIGURE A

CR = 10, N = 1000 rpm

1. $T_w = 1$ Volt/Div

2. $P = 0.5$ Volt/Div

Time base 20 m s

Position 2

FIGURE B

CR = 8, N = 600 rpm

1. $T_g = 0.2$ Volt/Div

2. $P = 0.5$ Volt/Div

Time base 50 m s

FIGURE C

CR = 10, N = 1000 rpm

1. $T_w = 1$ Volt/Div

2. $P = 1$ Volt/Div

Time base 20 m s

FIGURE D

CR = 10, N = 600 rpm

1. Hot-wire = 2 Volt/Div

2. Lineariser = 1 Volt/Div

3. $P = 0.5$ Volt/Div

Time base 50 m s

FIGURE E

CR = 8, N = 600 rpm

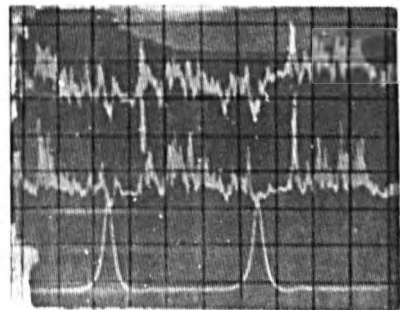
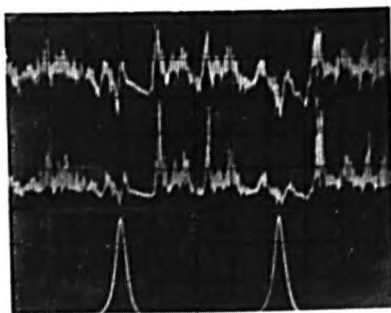
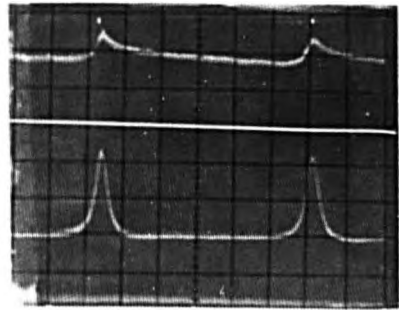
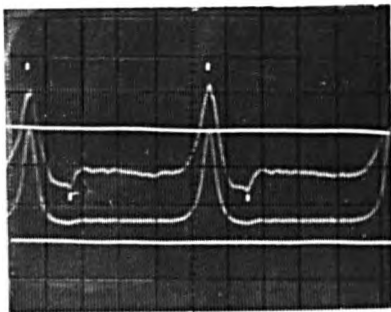
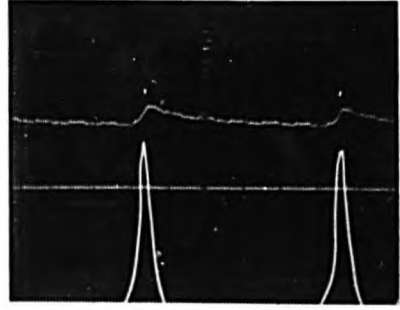
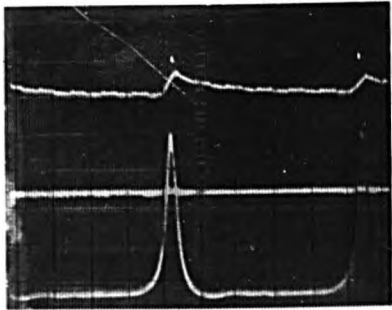
1. Hot-wire = 2 Volt/Div

2. Lineariser = 1 Volt/Div

3. $P = 0.5$ Volt/Div

Time base 50 m s

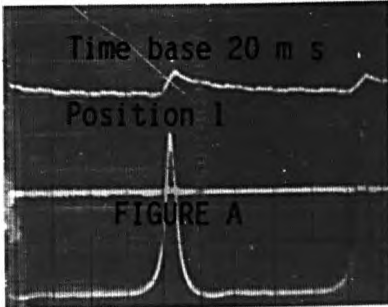
FIGURE F



CR = 10, N = 1000 rpm

1. $T_w = 1$ Volt/Div

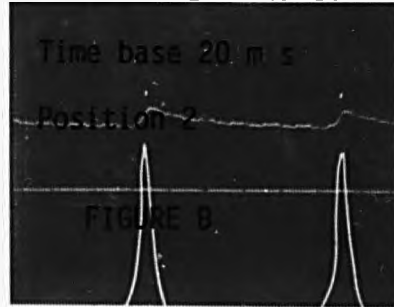
2. $P = 0.5$ Volt/Div



CR = 10, N = 1000 rpm

1. $T_w = 1$ Volt/Div

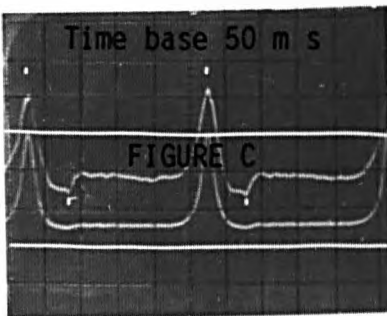
2. $P = 0.5$ Volt/Div



CR + 8, N = 600 rpm

1. $T_g = 0.2$ Volt/Div

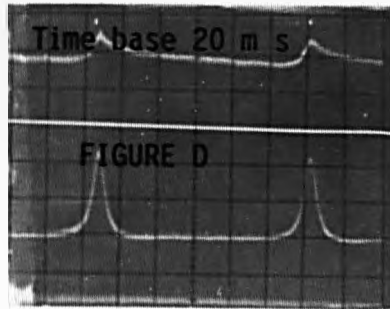
2. $P = 0.5$ Volt/Div



CR + 10, N = 1000 rpm

1. $T_w = 1$ Volt/Div

2. $P = 1$ Volt/Div

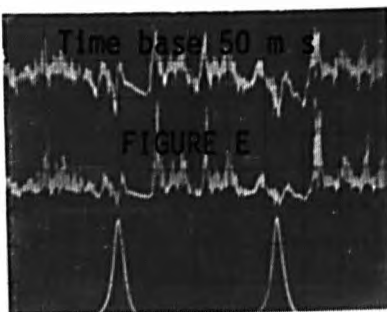


CR = 10, N = 600 rpm

1. Hot-wire = 2 Volt/Div

2. Lineariser = 1 Volt/Div

3. $P = 0.5$ Volt/Div

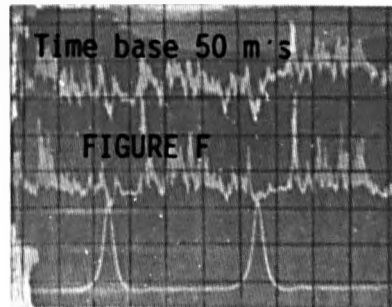


CR = 8, N = 600 rpm

1. Hot-wire = 2 Volt/Div

2. Lineariser = 1 Volt/Div

3. $P = 0.5$ Volt/Div



CR = 8, N = 1500 rpm

1. Hot-wire = 2 Volt/Div
2. Lineariser = 1 Volt/Div
3. $T_g = 0.2$ Volt/Div

Time base 20 m s

FIGURE A

CR = 8, N = 1000 rpm

1. Hot-wire = 2 Volt/Div
2. Lineariser = 1 Volt/Div
3. $T_g = 0.2$ Volt/Div

Time base 50 m s

FIGURE B

CR = 10, n = 1500 rpm

1. Hot-wire = 2 Volt/Div
2. Lineariser = 1 Volt/Div
3. $T_g = 0.2$ Volt/Div

Time base 20 m s

FIGURE C

CR = 10, N = 1000 rpm

1. Hot-wire = 2 Volt/Div
2. Lineariser = 1 Volt/Div
3. $T_g = 0.2$ Volt/Div

Time base 20 m s

FIGURE D

CR = 12, N = 1500 rpm

1. Hot-wire = 2 Volt/Div
2. Lineariser = 1 Volt/Div
3. $T_g = 0.2$ Volt/Div

Time base 20 m s

FIGURE E

CR = 12, N = 1000 rpm

1. Hot-wire = 2 Volt/Div
2. Lineariser = 1 Volt/Div
3. $T_g = 0.2$ Volt/Div

Time base 50 m s

FIGURE F

CR = 10, N = 1500 rpm

1. Hot-wire = 2 Volt/Div
2. Lineariser = 1 Volt/Div
3. $T_g = 0.2$ Volt/Div

Time base 20 m s

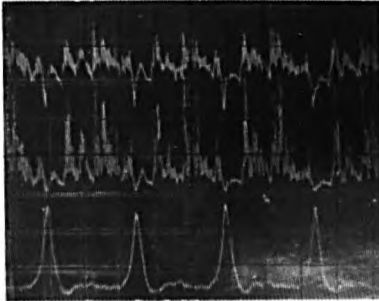
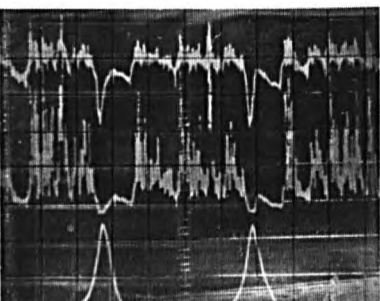
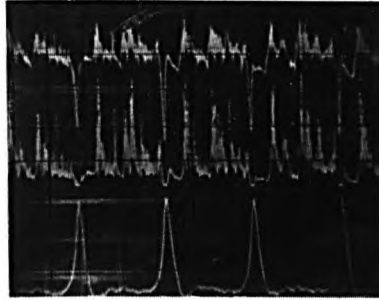
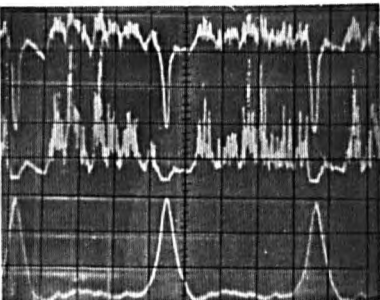
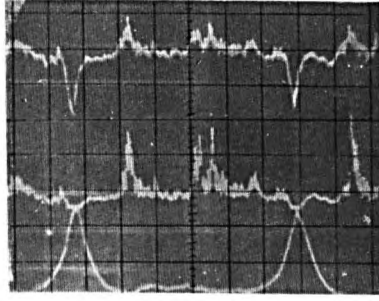
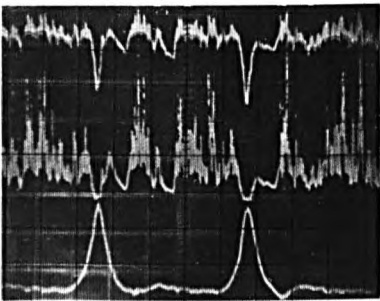
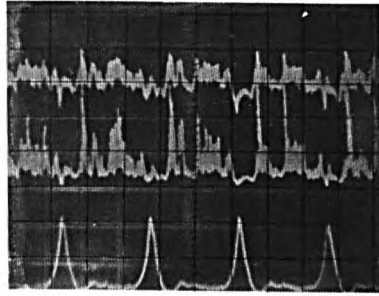
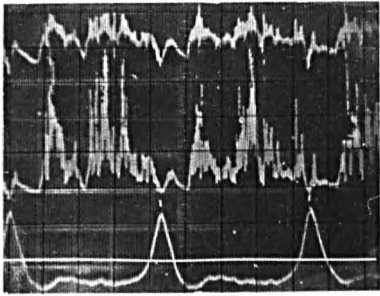
FIGURE G

CR = 10, N = 1000 rpm

1. Hot-wire = 2 Volt/Div
2. Lineariser = 1 Volt/Div
3. $T_g = 0.2$ Volt/Div

Time base 50 m s

FIGURE H



CR = 8, N = 1500 rpm

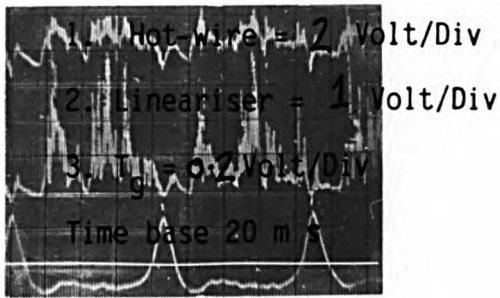


FIGURE A

CR = 8, N = 1000 rpm

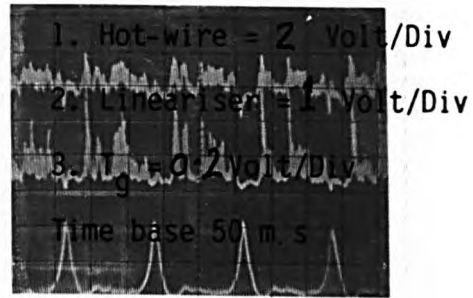


FIGURE B

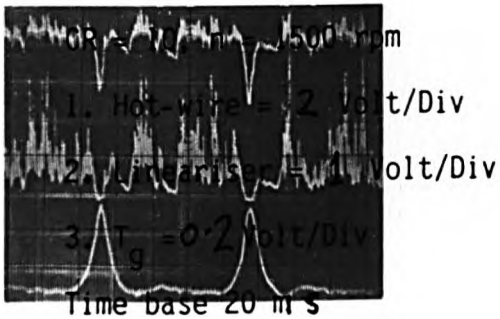


FIGURE C

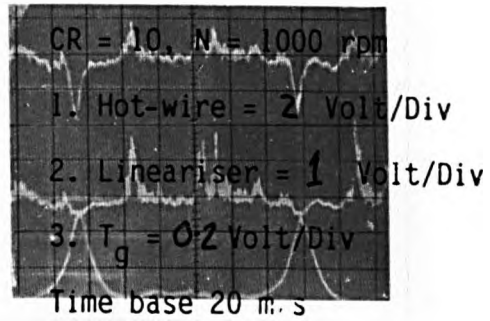


FIGURE D

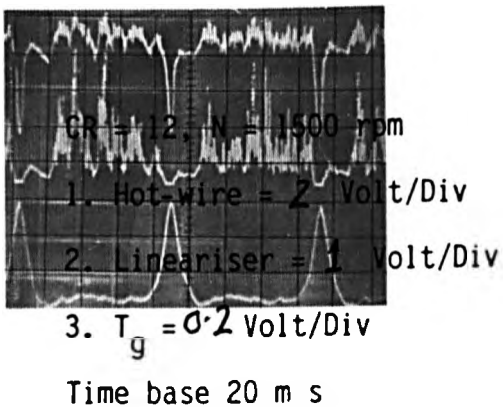


FIGURE E

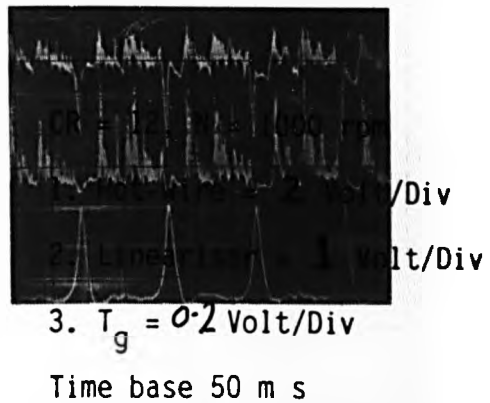


FIGURE F

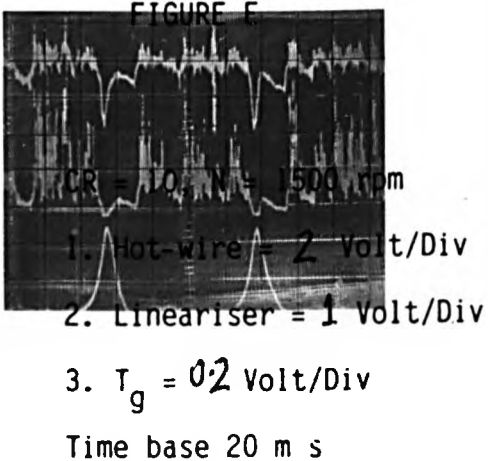


FIGURE G

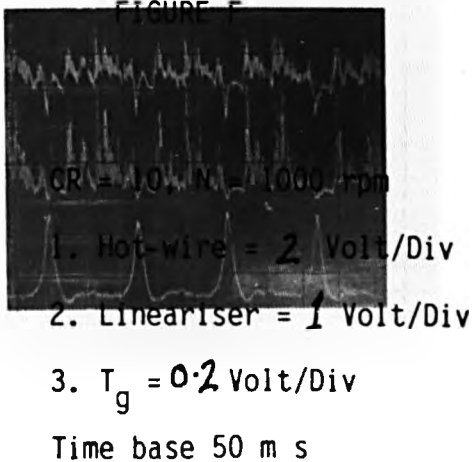


FIGURE H

FIG. 9.1

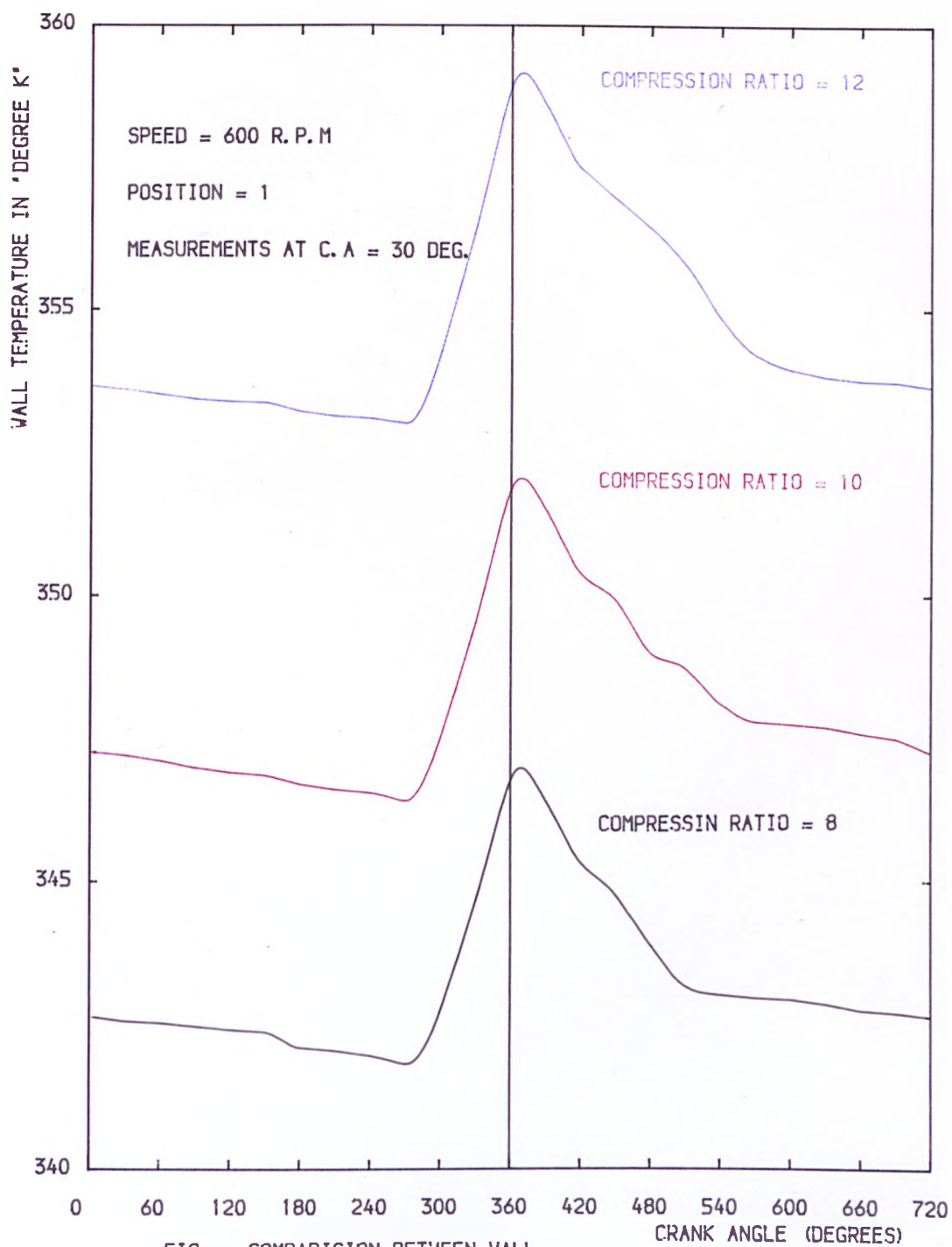


FIG. COMPARISON BETWEEN WALL TEMP. AT DIFFERENT COMPRESSION RATIO

FIG. 9.2

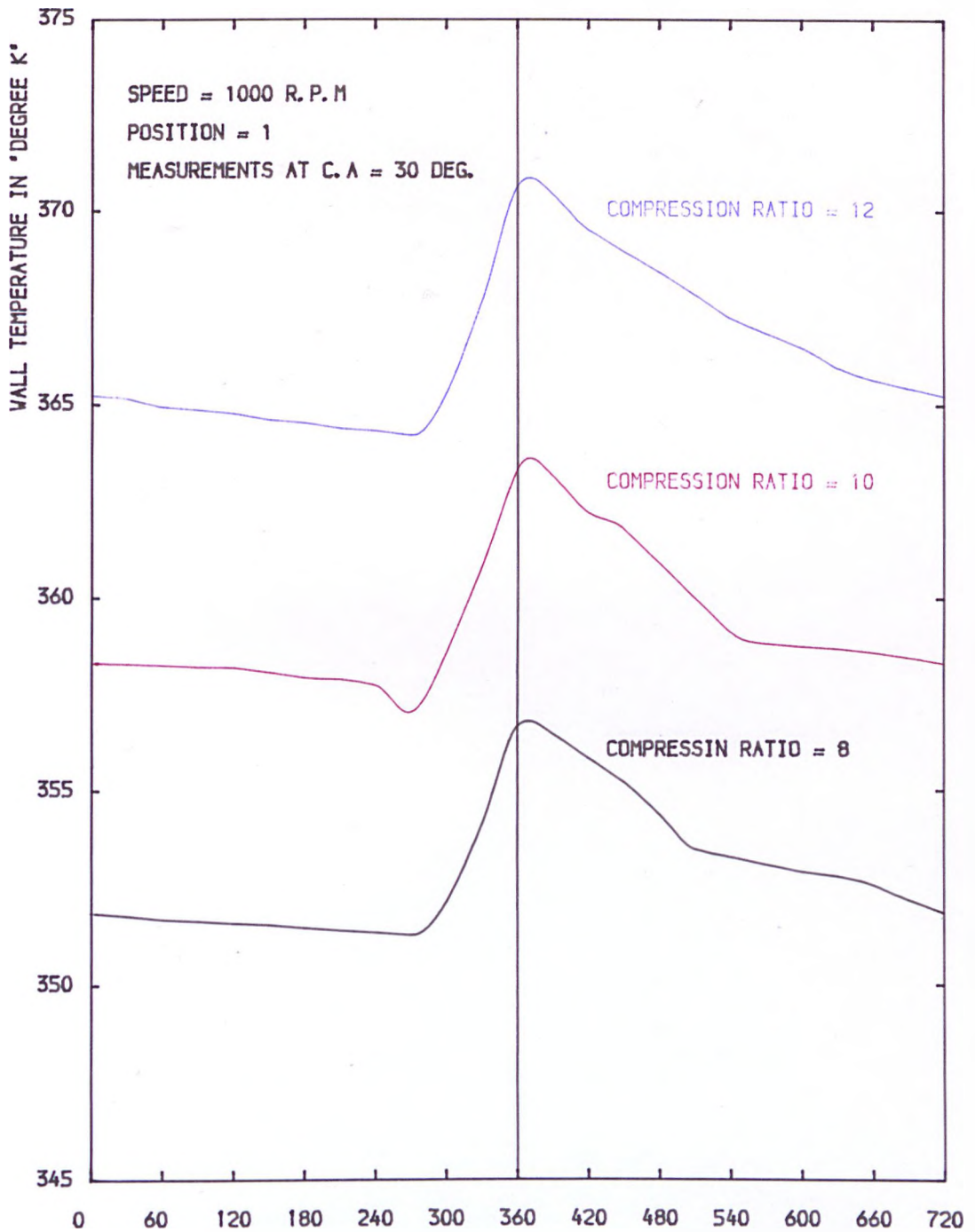


FIG. COMPARISON BETWEEN WALL
TEMP. AT DIFFERENT COMPRESSION RATIO

FIG. 9.3

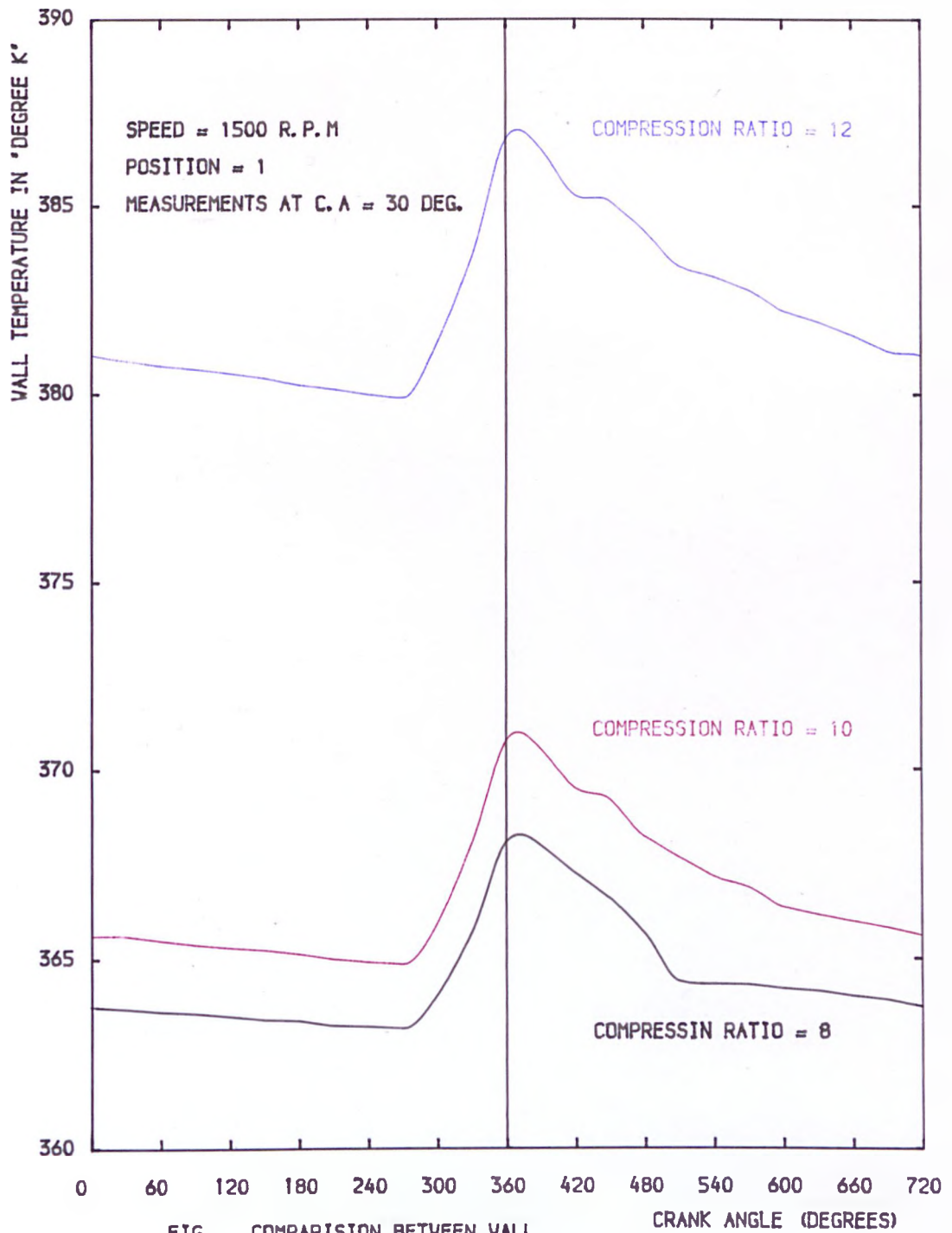


FIG. COMPARISON BETWEEN WALL
TEMP. AT DIFFERENT COMPRESSION RATIO

FIG. 9.4

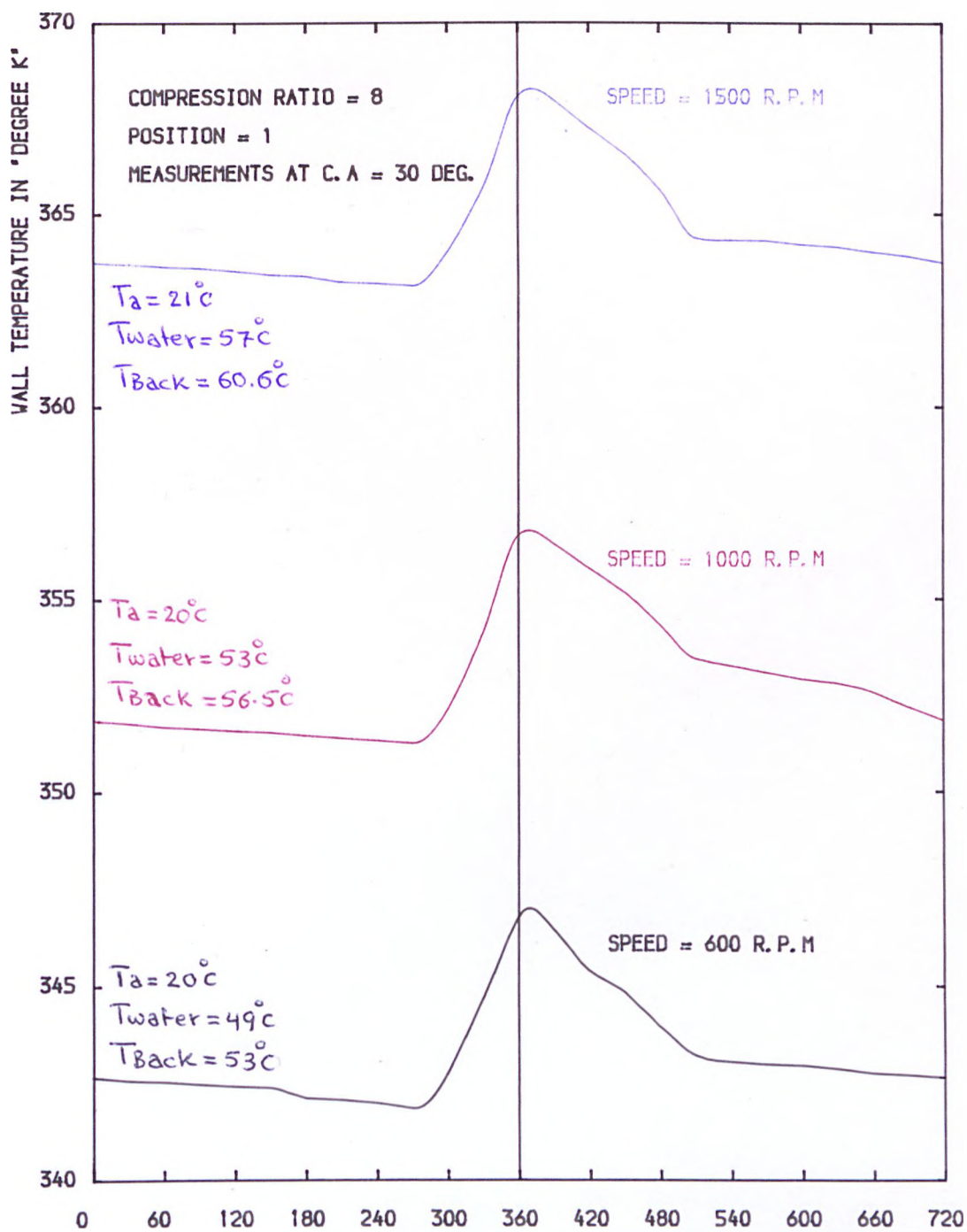


FIG. COMPARISON BETWEEN WALL
TEMP. AT DIFFERENT SPEED

FIG. 9.5

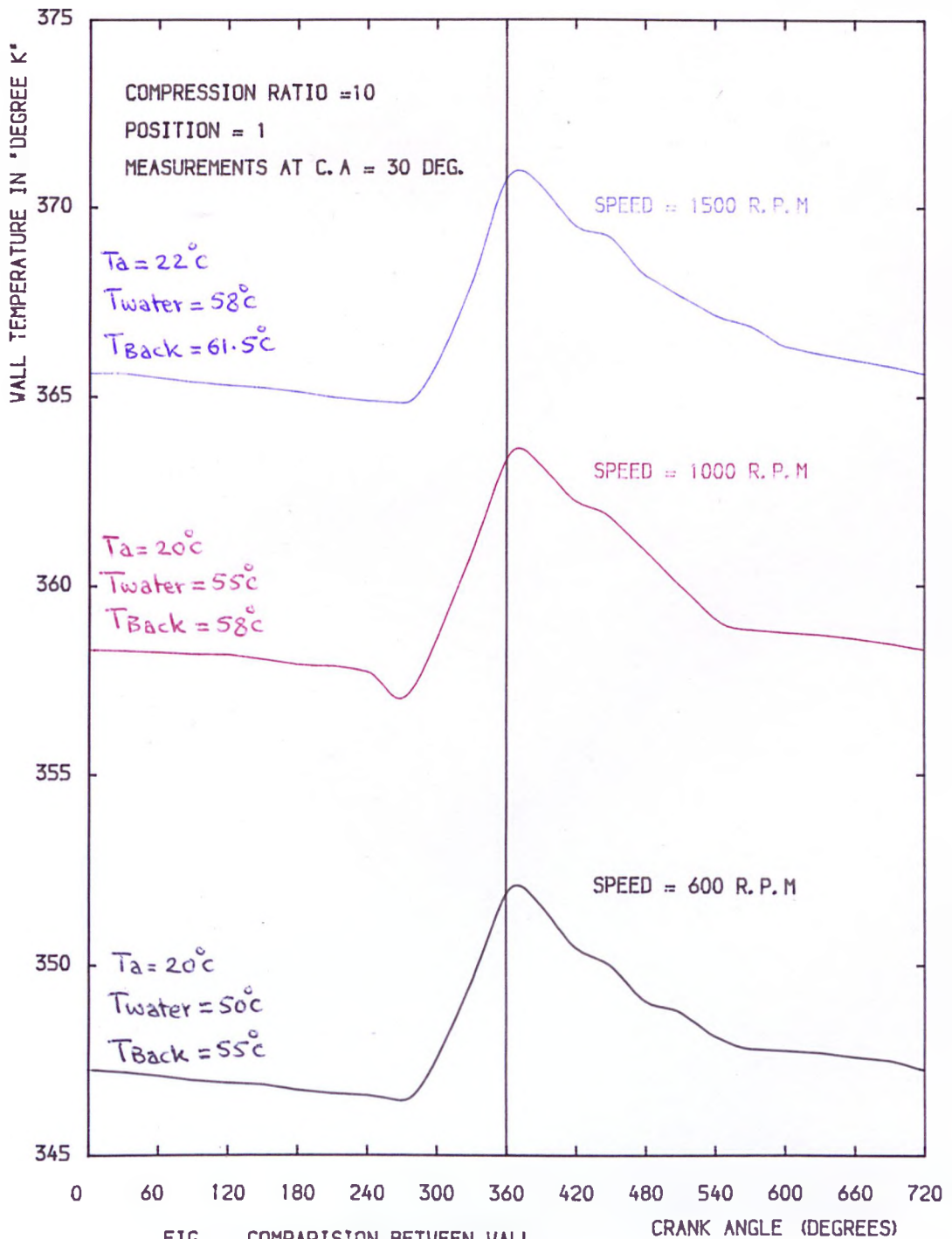


FIG. COMPARISON BETWEEN WALL
TEMP. AT DIFFERENT SPEED

FIG. 9.6

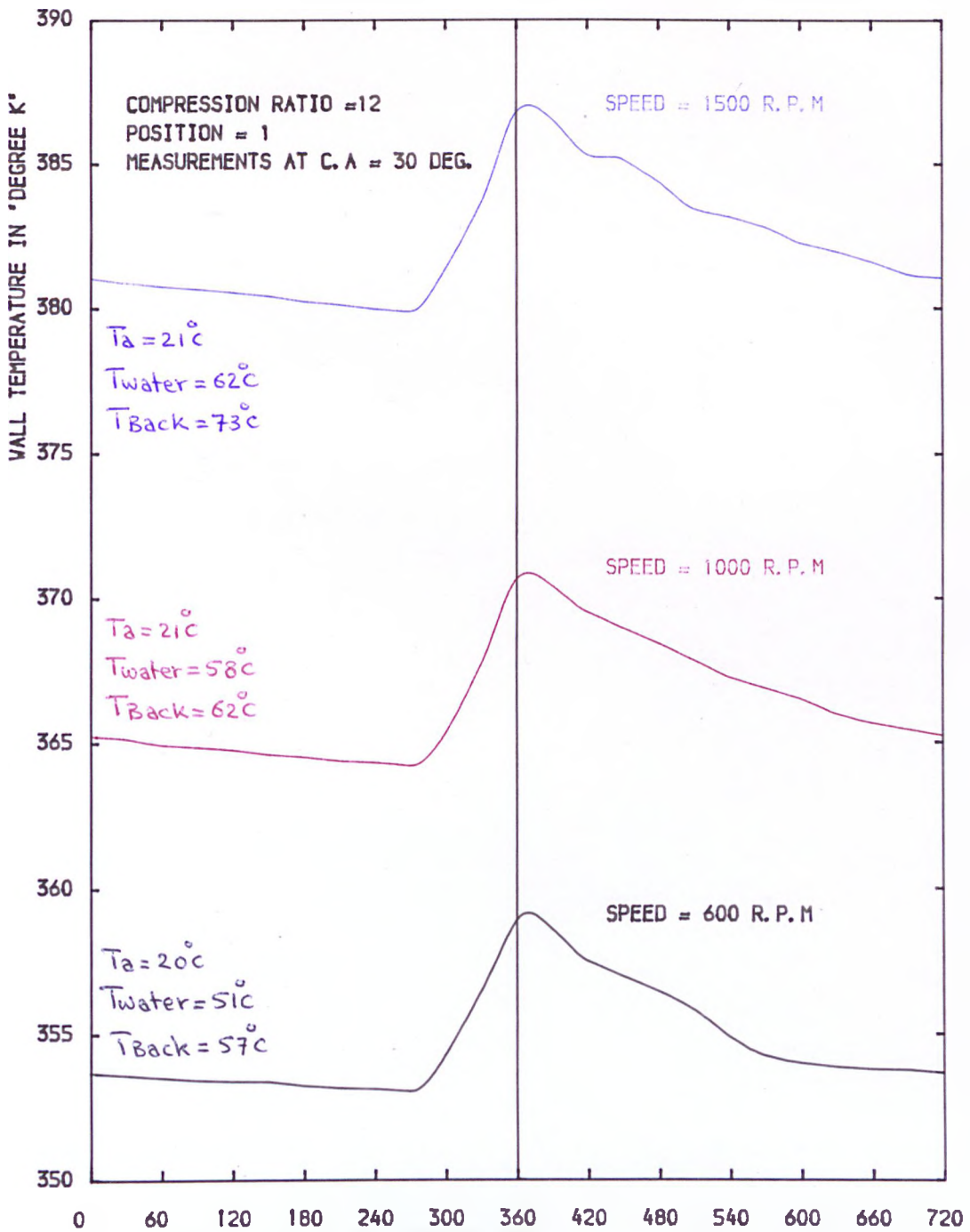


FIG. COMPARISON BETWEEN WALL TEMP. AT DIFFERENT SPEED

FIG. 9.7

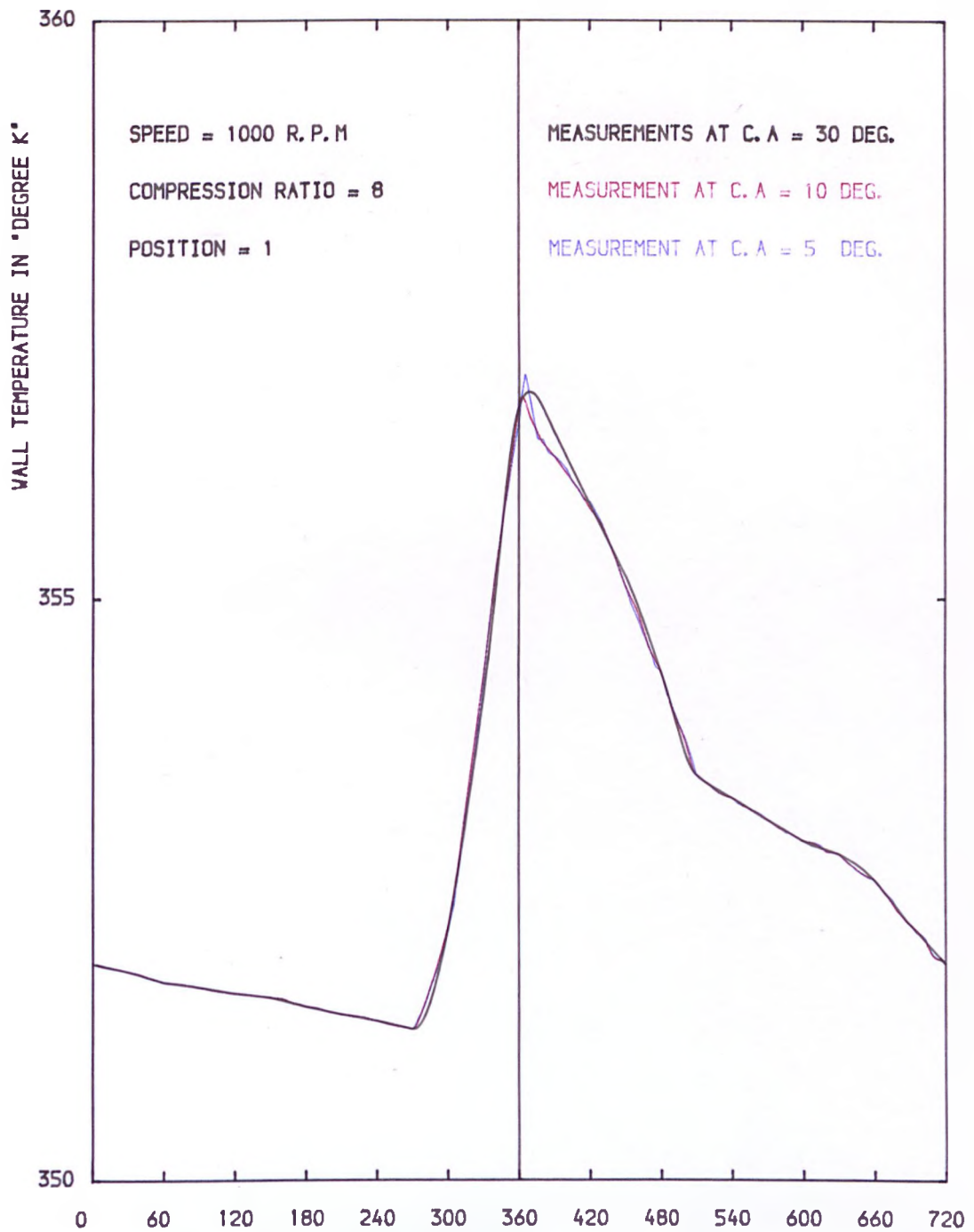


FIG. COMPARISON BETWEEN WALL
TEMP. AT DIFFERENT C. A MEASUREMENT

FIG. 9.8

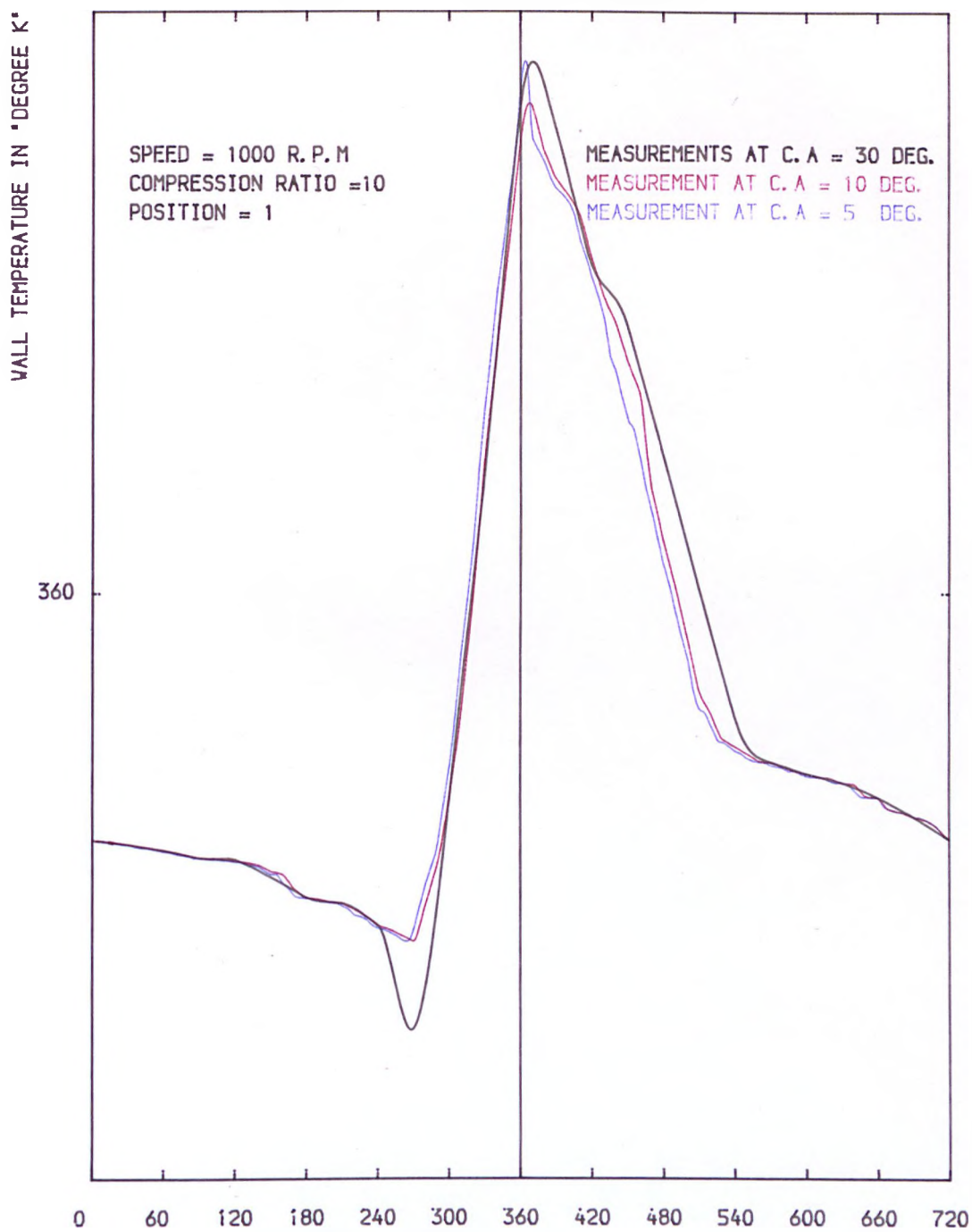


FIG. COMPARISON BETWEEN WALL
TEMP. AT DIFFERENT C. A MEASUREMENT

FIG. 9.9

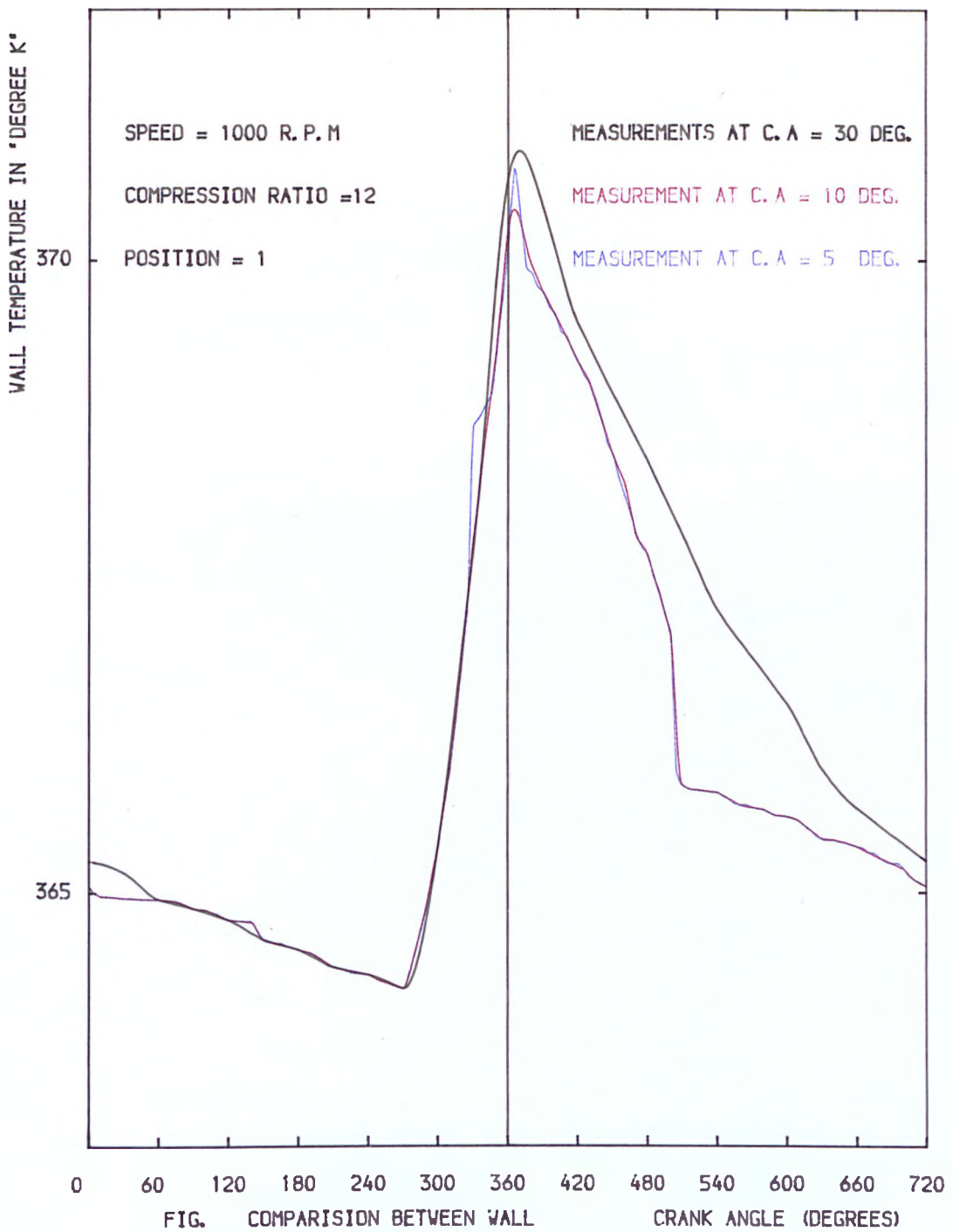


FIG. COMPARISON BETWEEN WALL TEMP. AT DIFFERENT C. A MEASUREMENT

FIG. 9.10

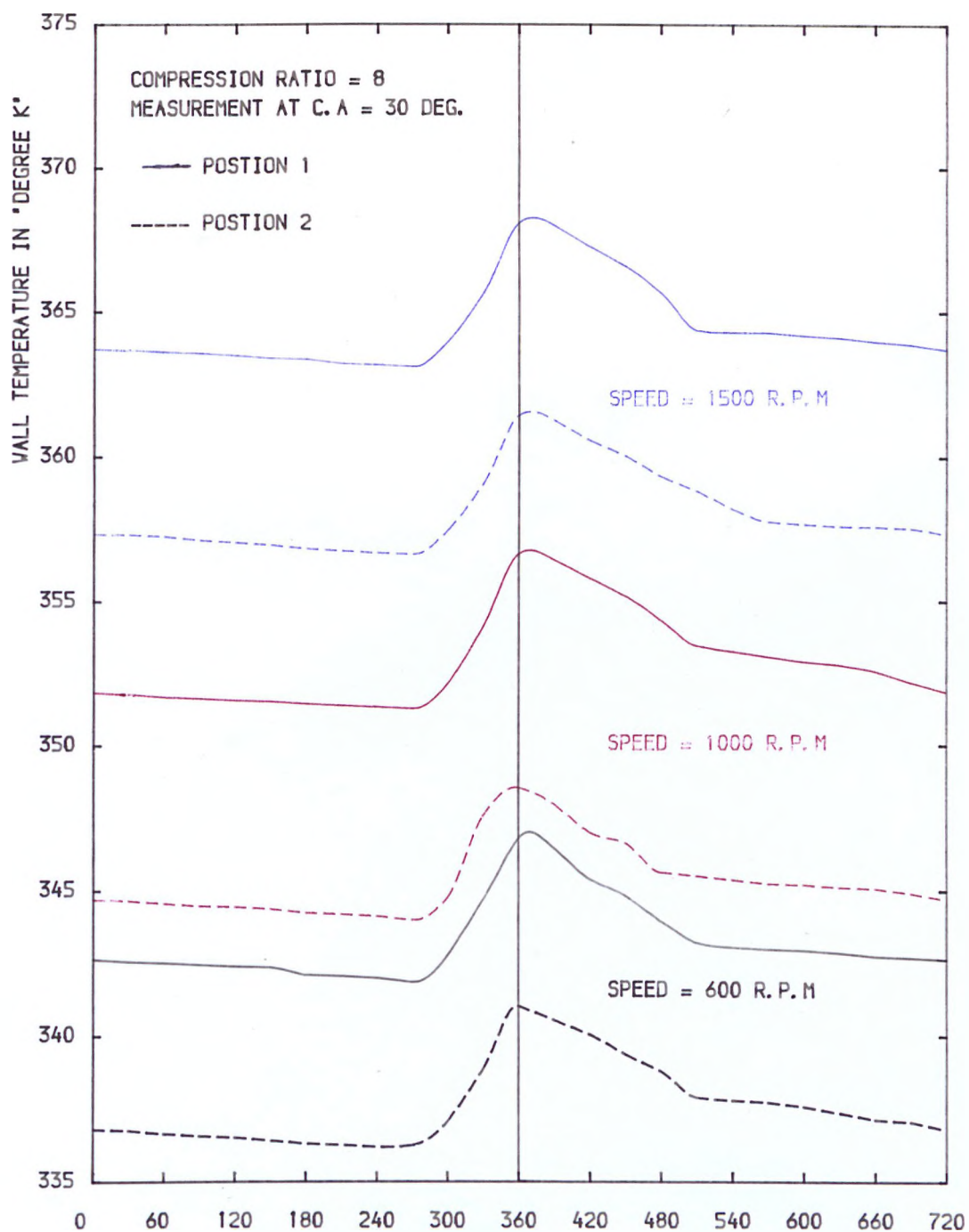


FIG. COMPARISON BETWEEN WALL
TEMP. AT DIFFERENT POSTION

FIG. 9.11

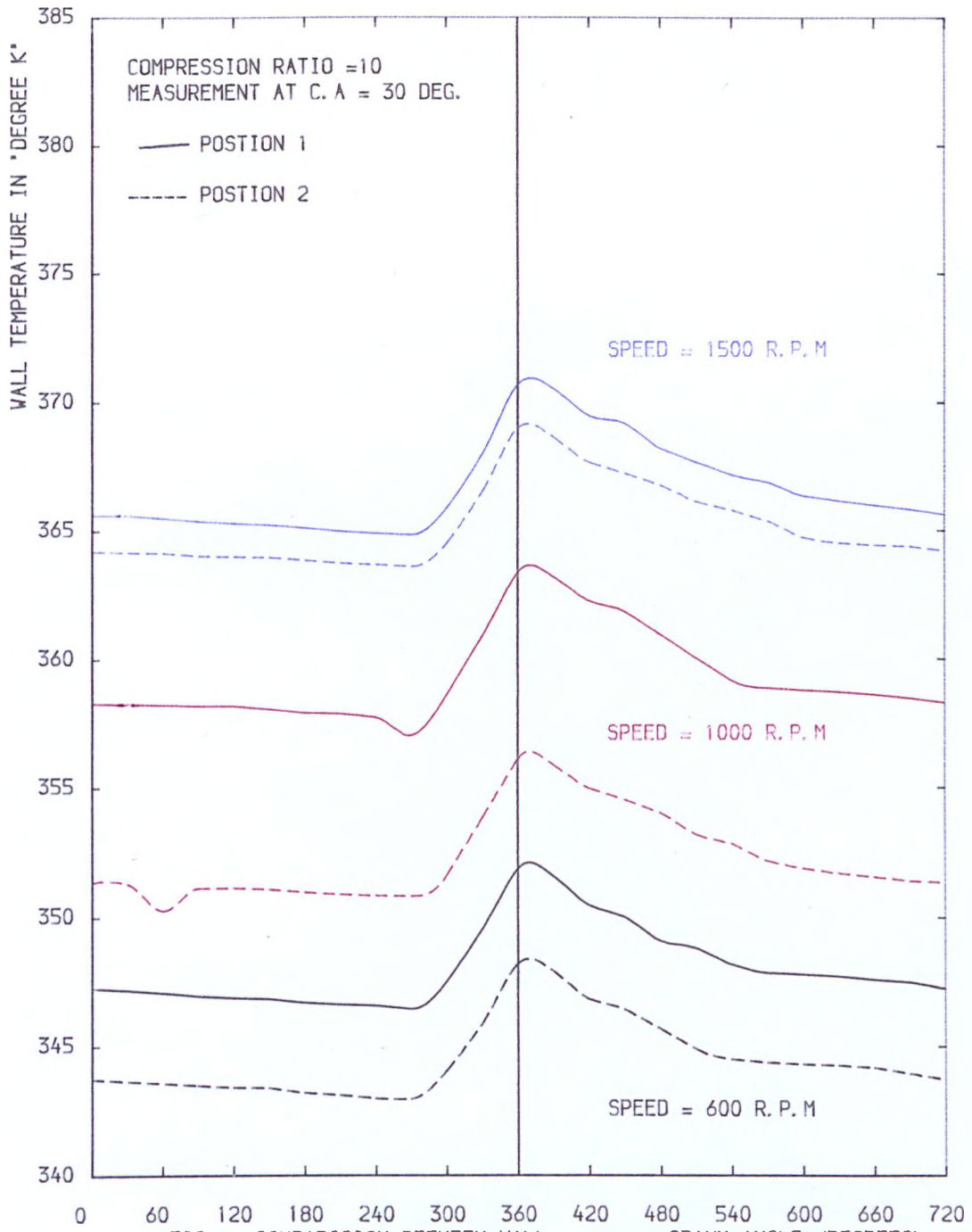


FIG. COMPARISION BETWEEN WALL
TEMP. AT DIFFERENT POSTION

FIG. 9.12

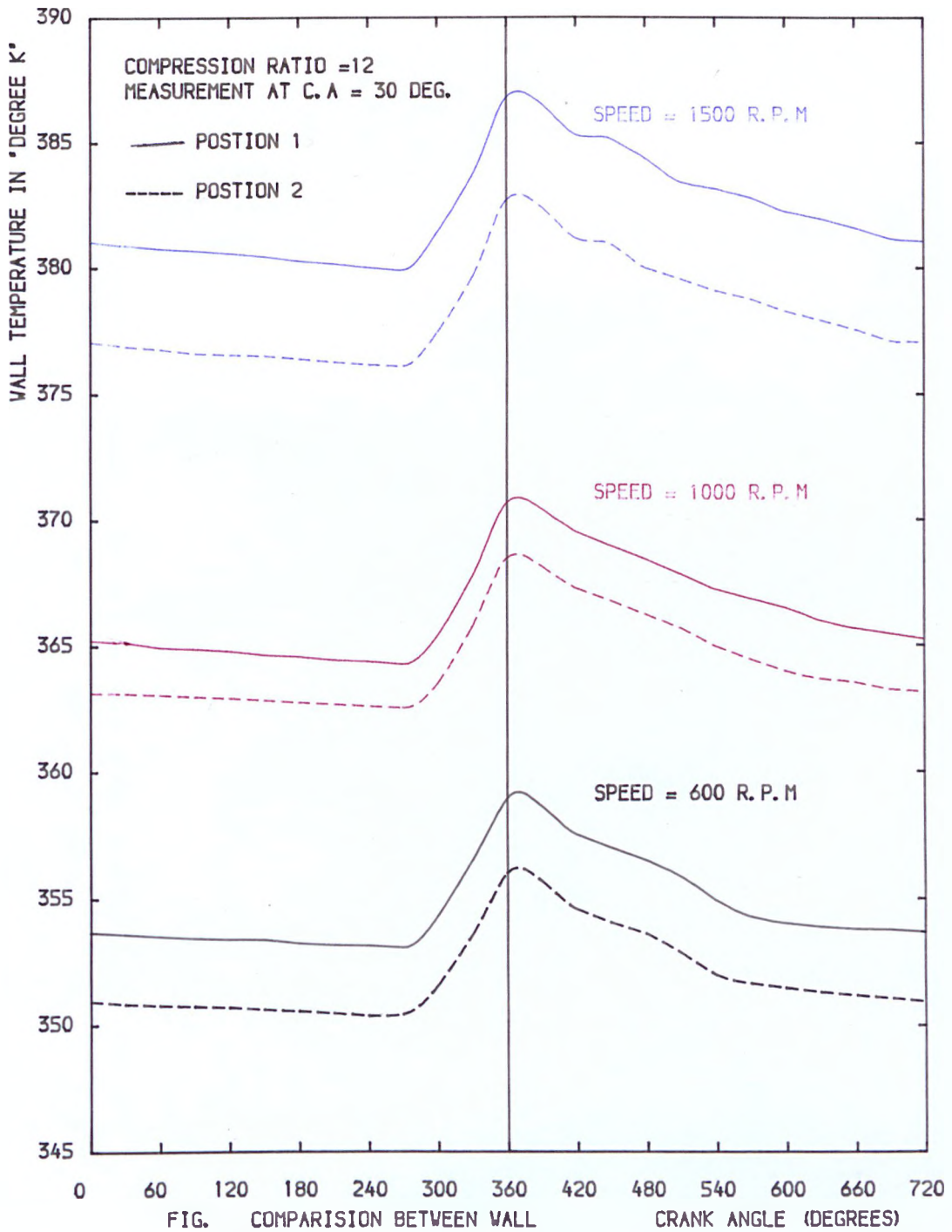


FIG. COMPARISON BETWEEN WALL
TEMP. AT DIFFERENT POSTION

FIG. 9.13

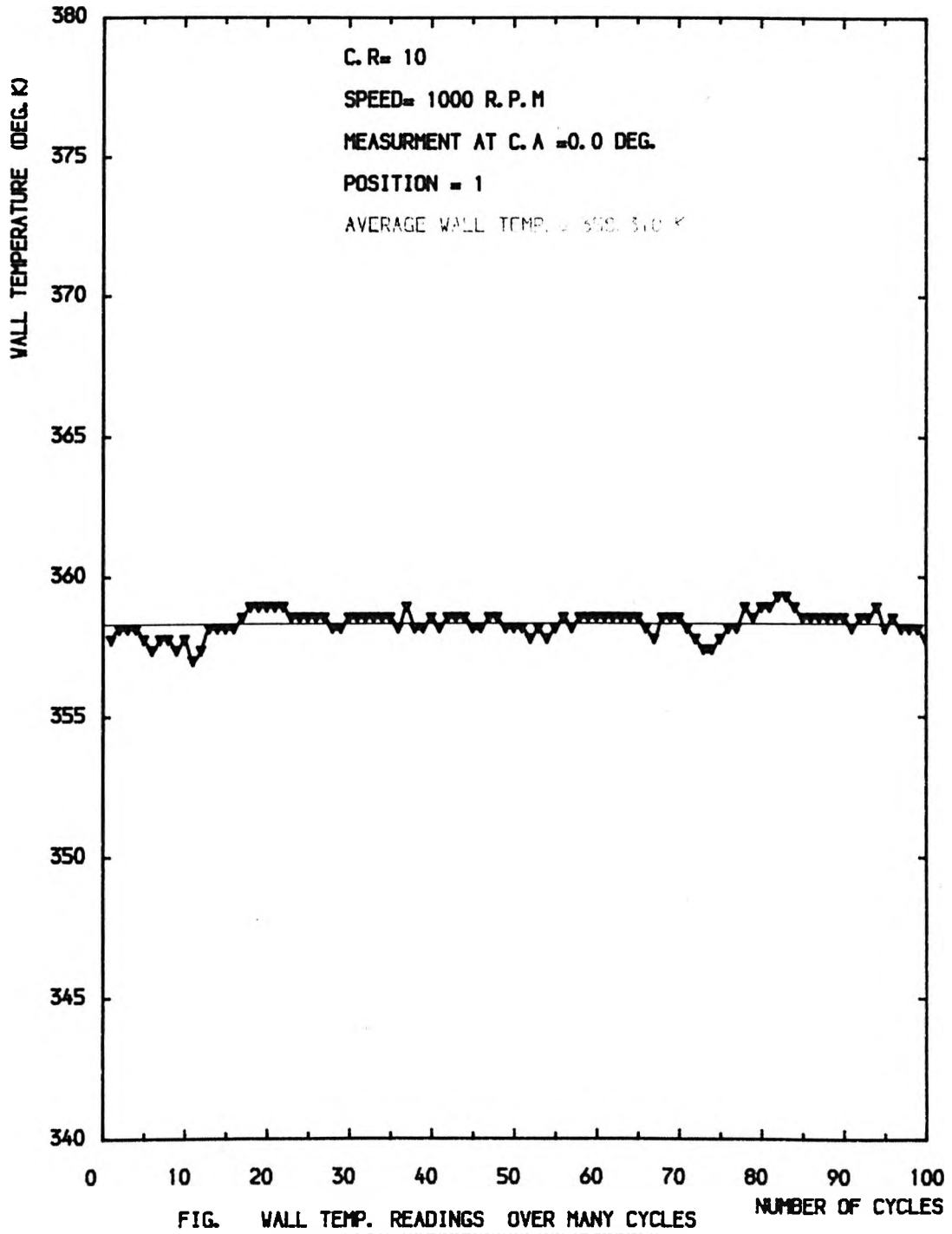


FIG. 9.14

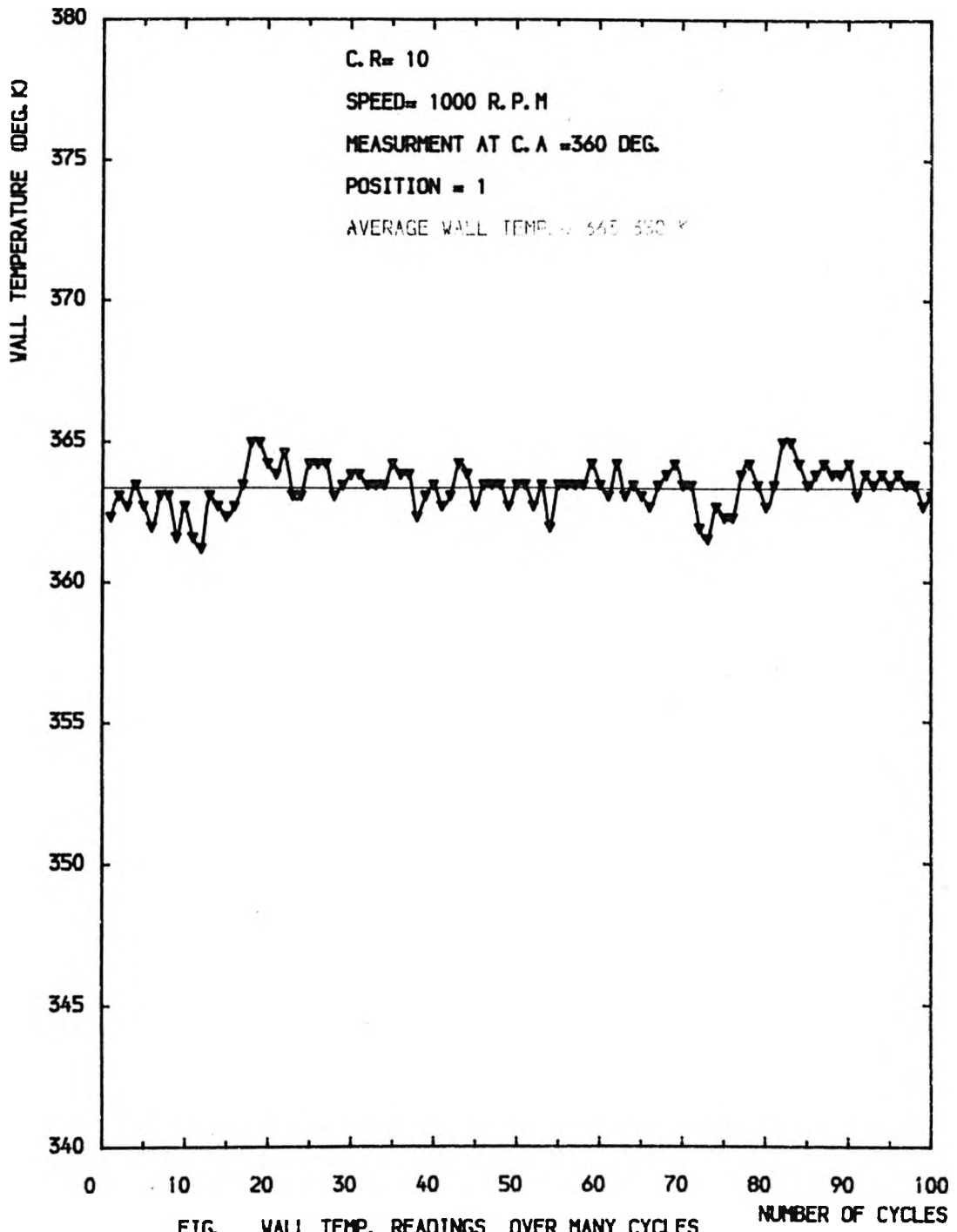


FIG. 9.15

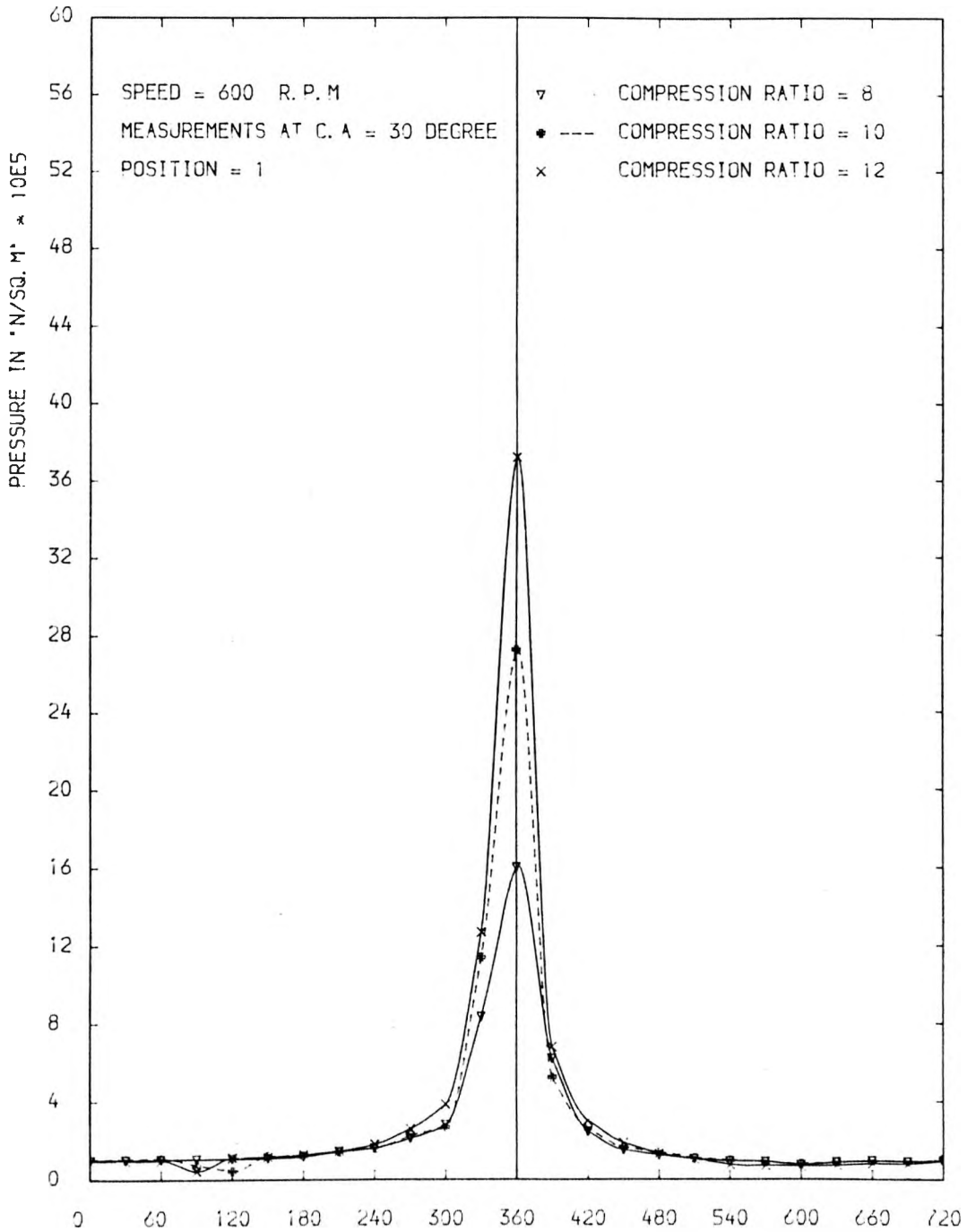


FIG. 9.15 COMPARISON BETWEEN PRESSURE AT DIFFERENT C.R

FIG. 9.16

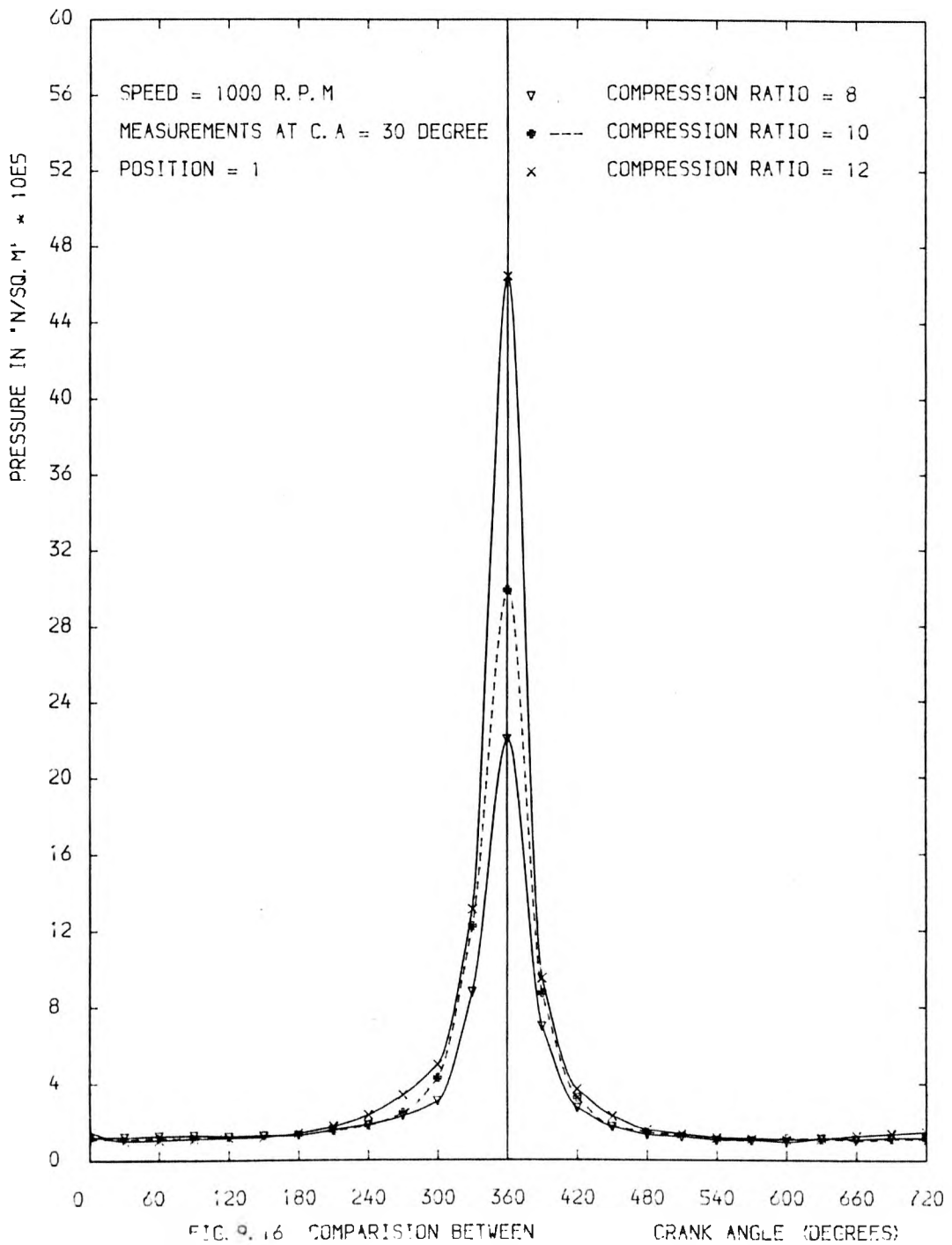


FIG. 9.16 COMPARISON BETWEEN
PRESSURE AT DIFFERENT C. R.

FIG. 9.17

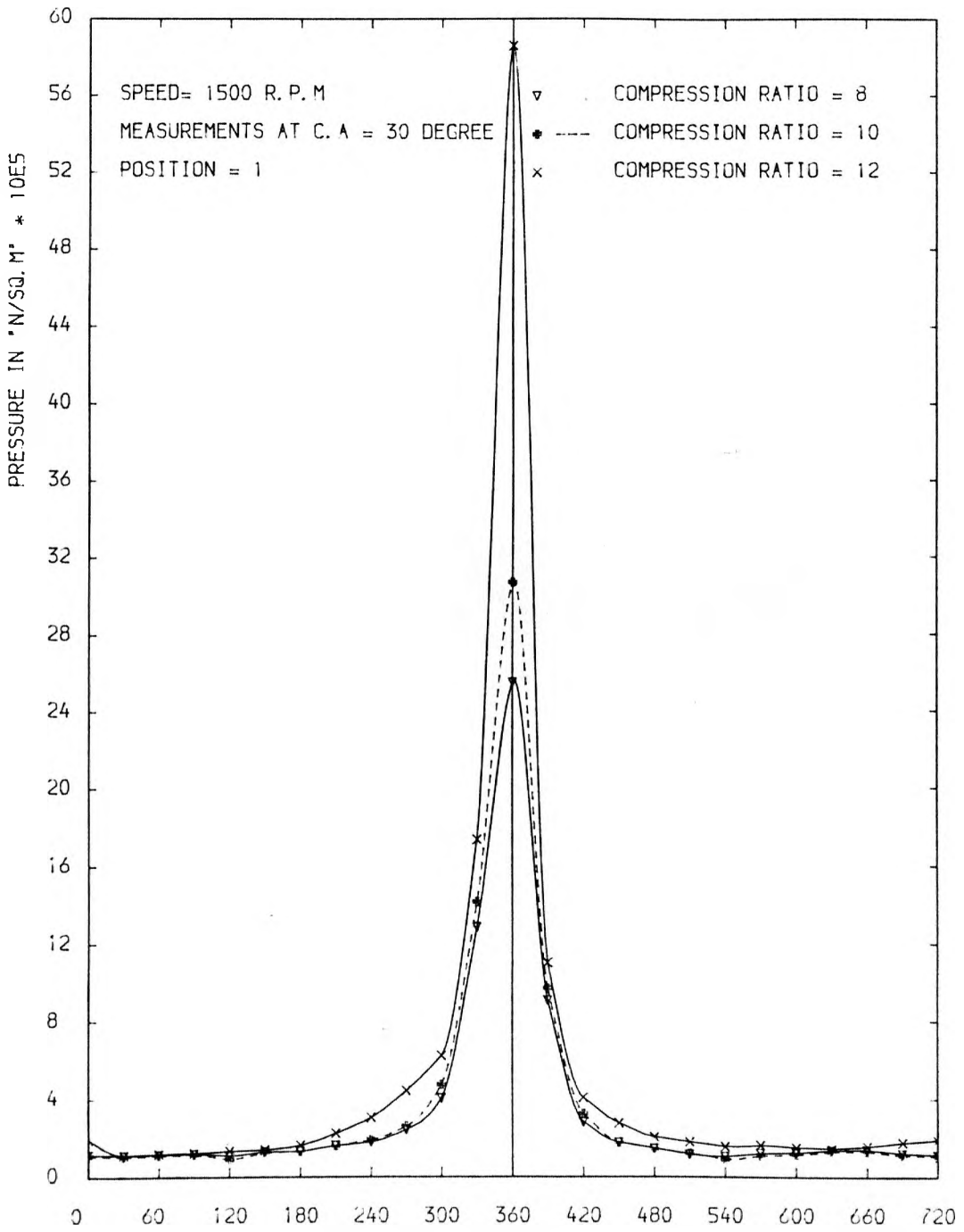


FIG. 9.17 COMPARISON BETWEEN PRESSURE AT DIFFERENT C. R.

FIG. 9.18

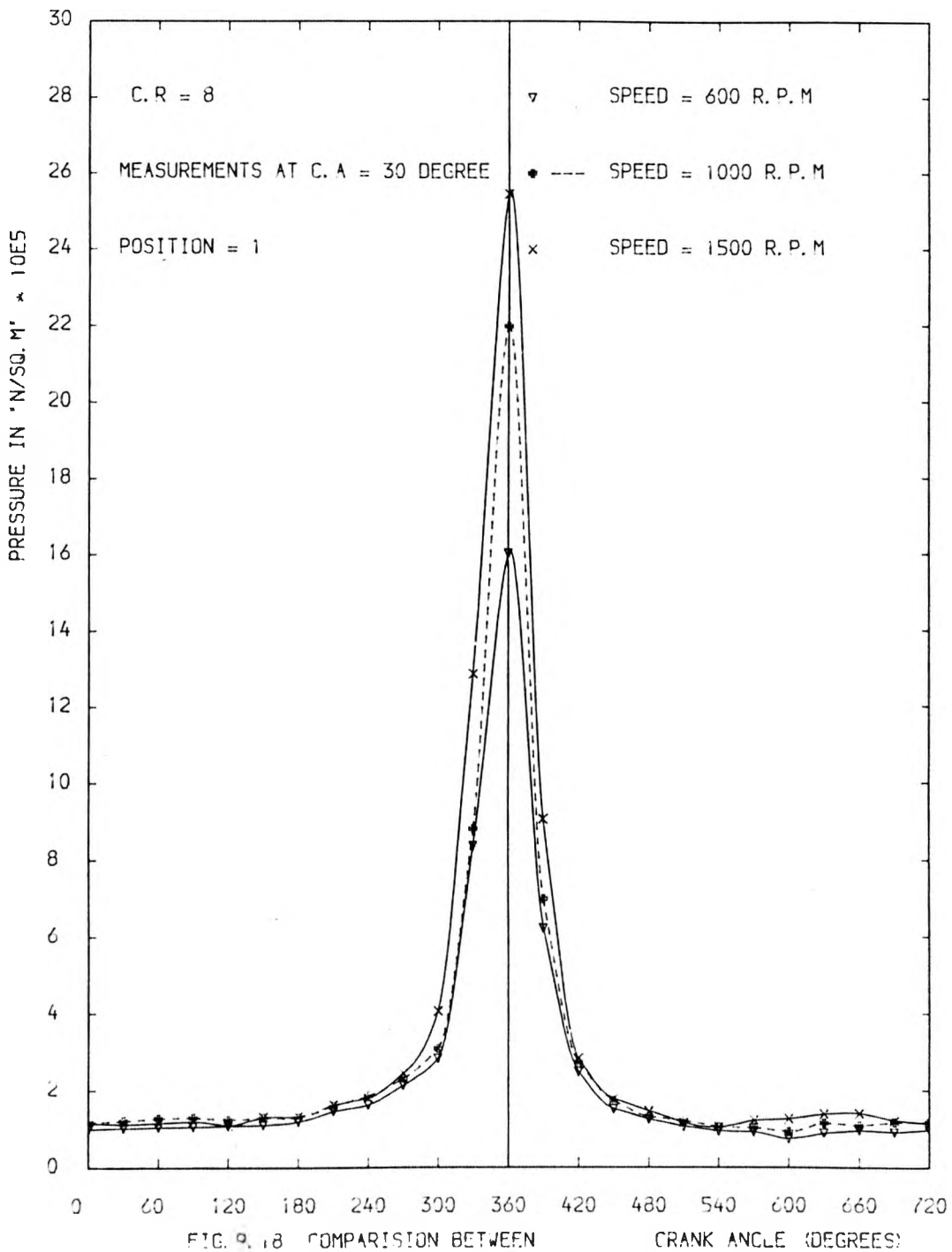


FIG. 9.18 COMPARISON BETWEEN PRESSURE AT DIFFERENT SPEEDS

CRANK ANGLE (DEGREES)

FIG. 9.19

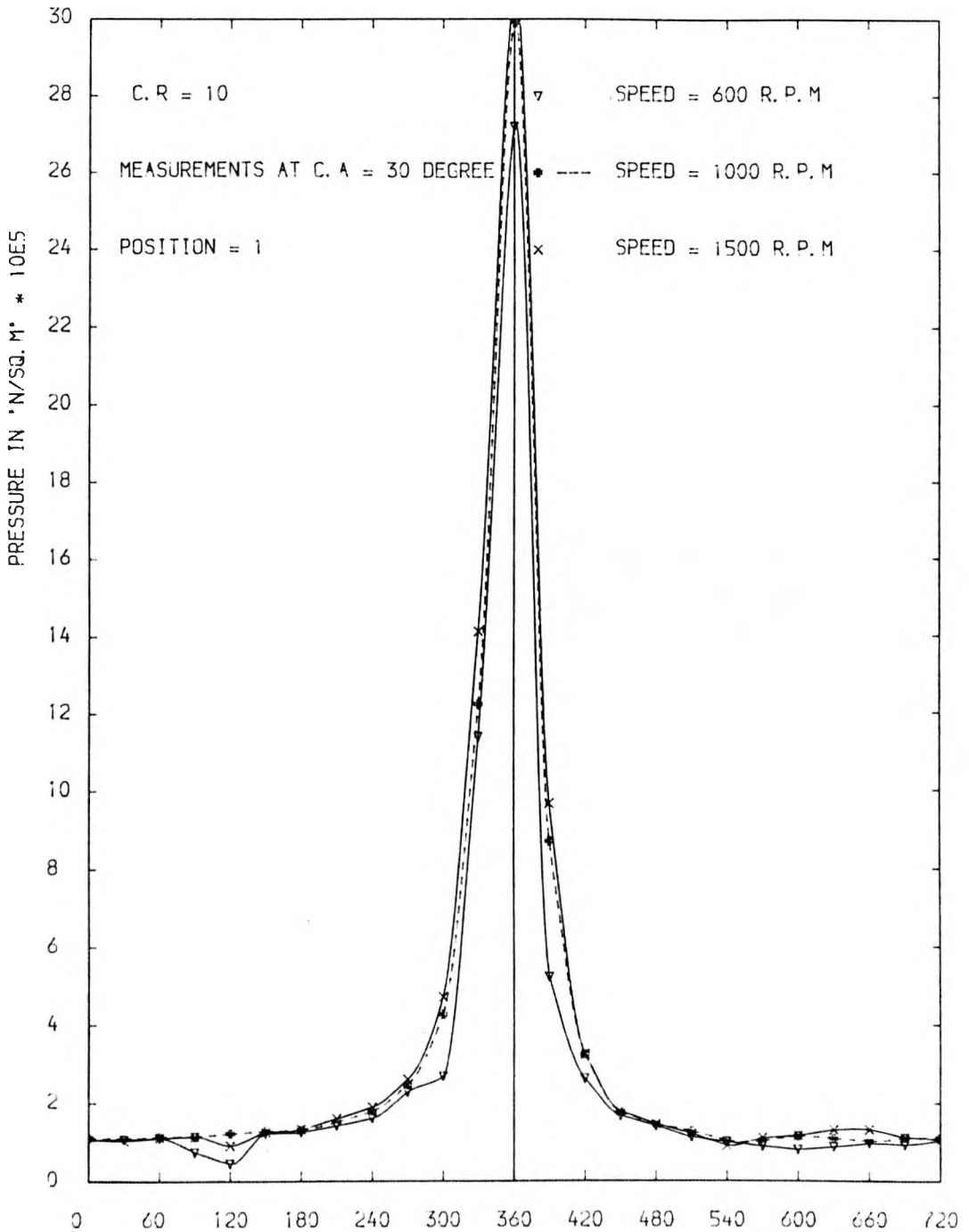


FIG. 9.19 COMPARISON BETWEEN PRESSURE AT DIFFERENT SPEEDS

FIG. 9.20

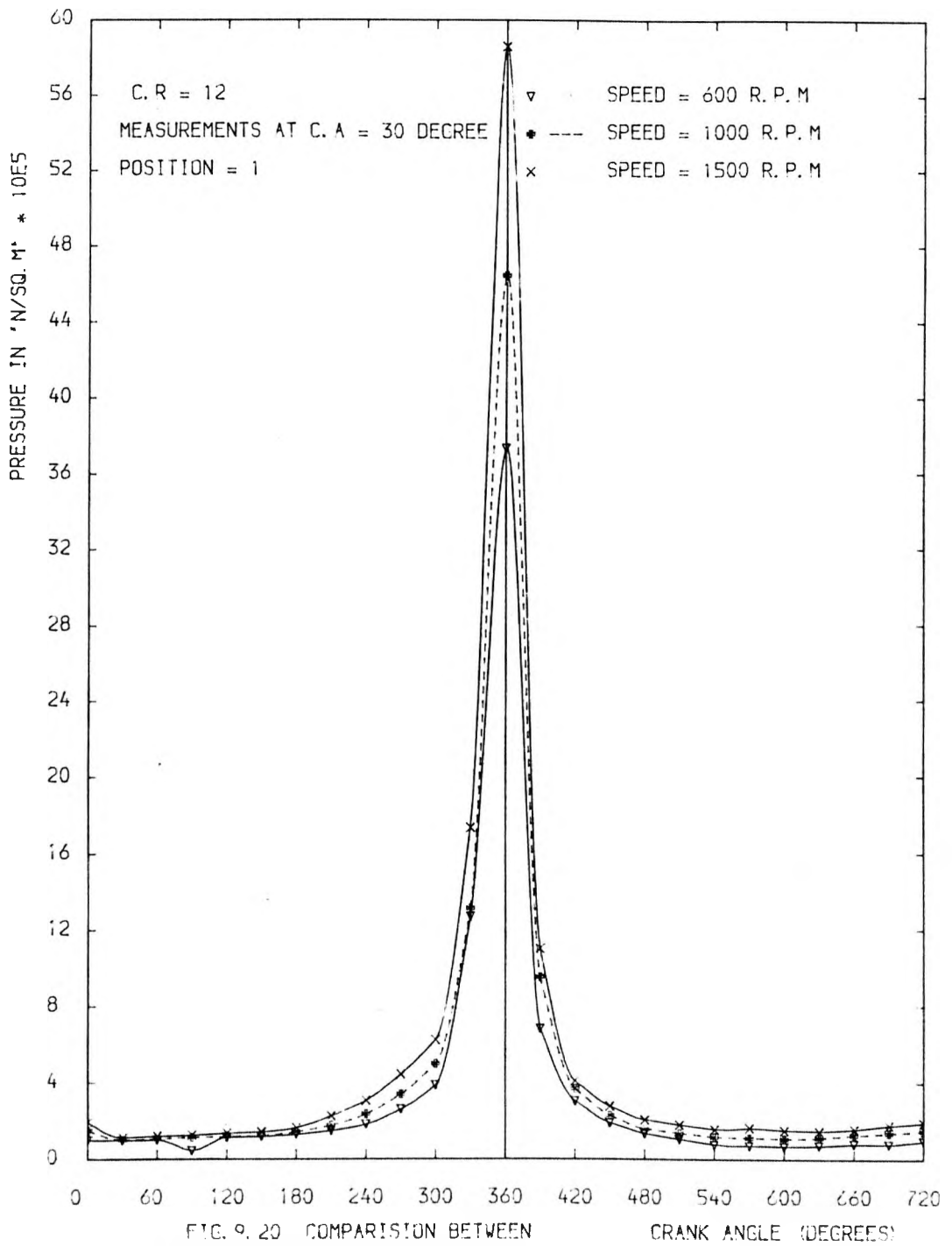


FIG. 9.21

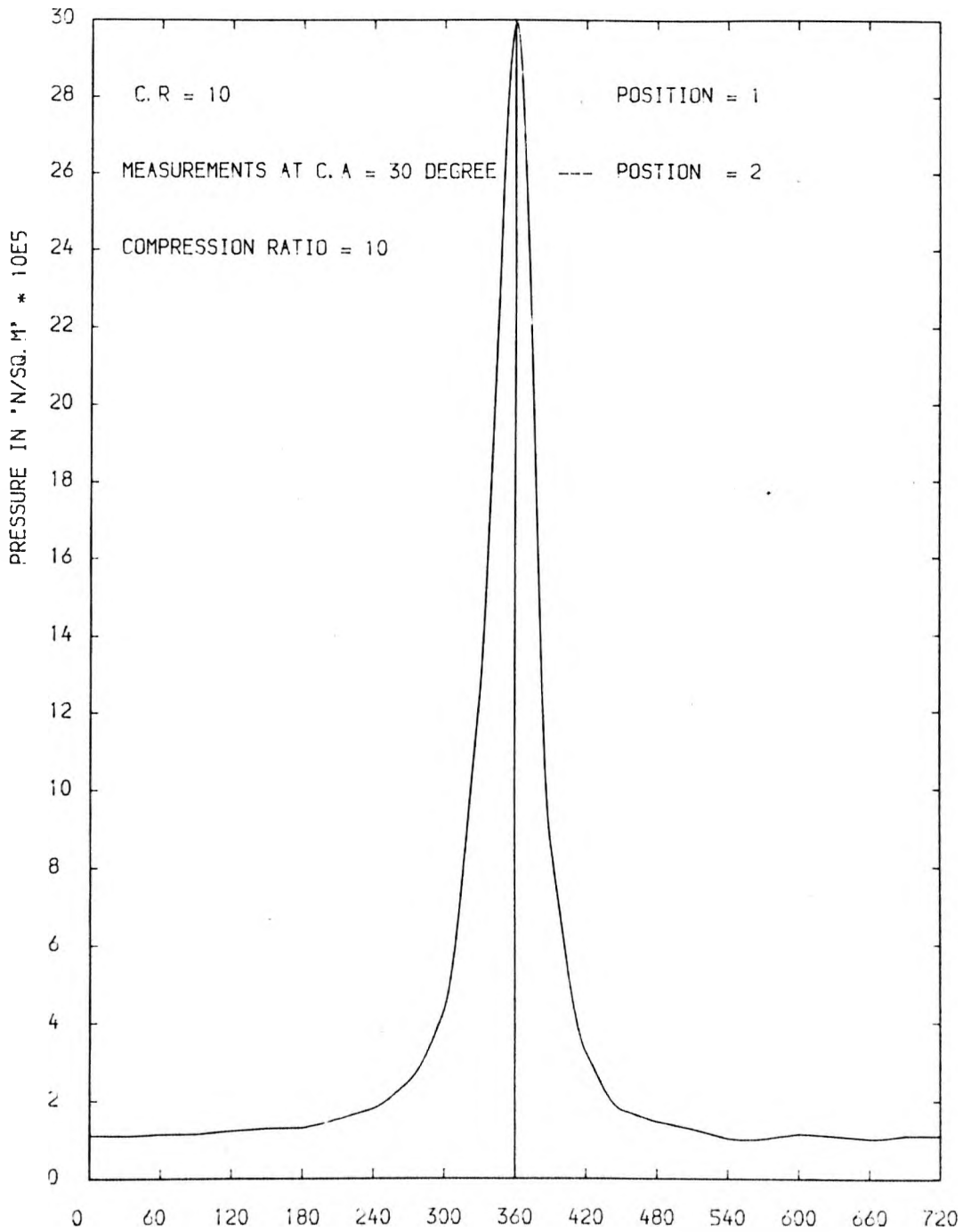


FIG. 9.21 COMPARISON BETWEEN
PRESSURE AT DIFFERENT POSITION

FIG. 9.22

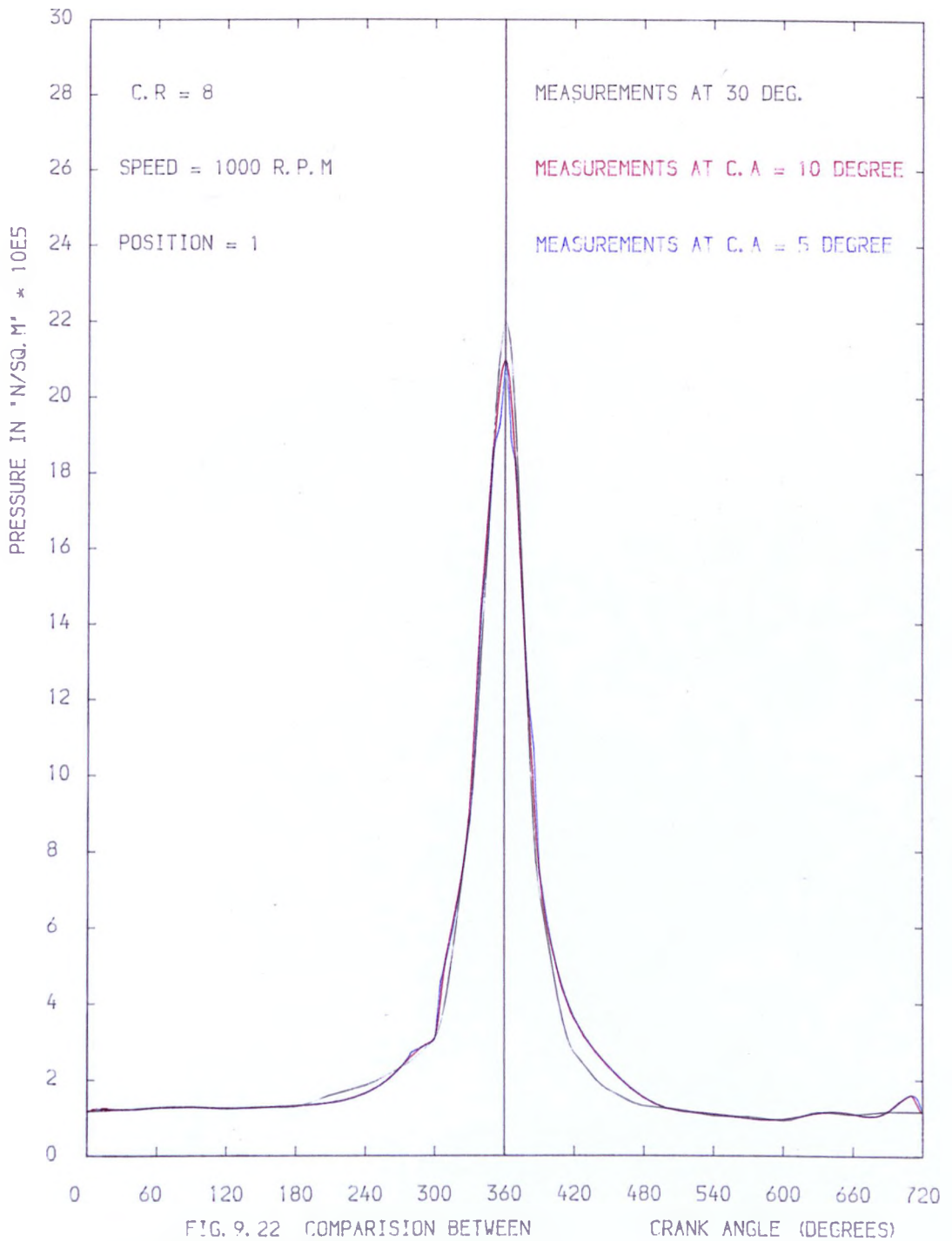


FIG. 9.23

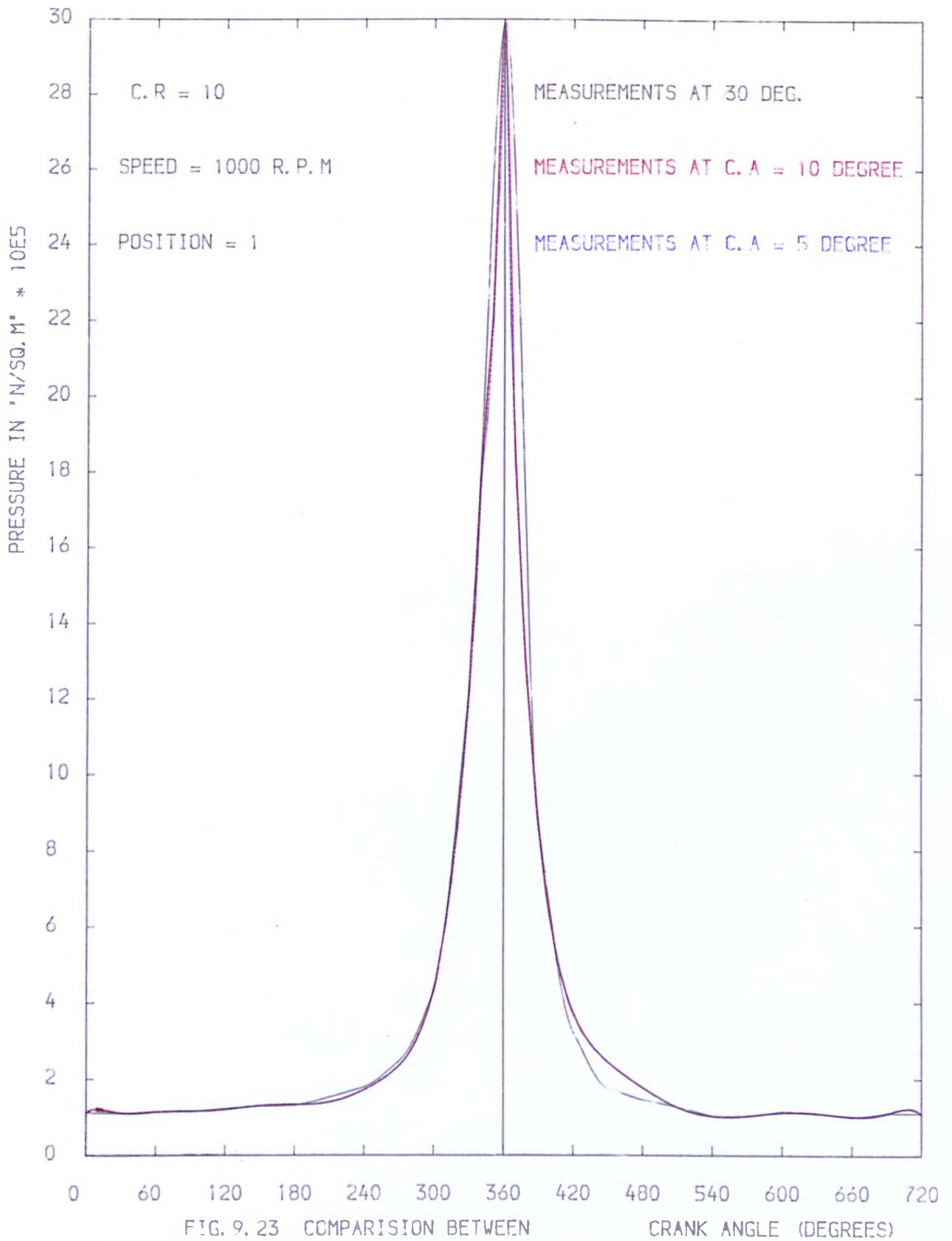


FIG. 9.23 COMPARISON BETWEEN
PRESSURE AT DIFFERENT C. A MEASUREMENTS

CRANK ANGLE (DEGREES)

FIG. 9.24

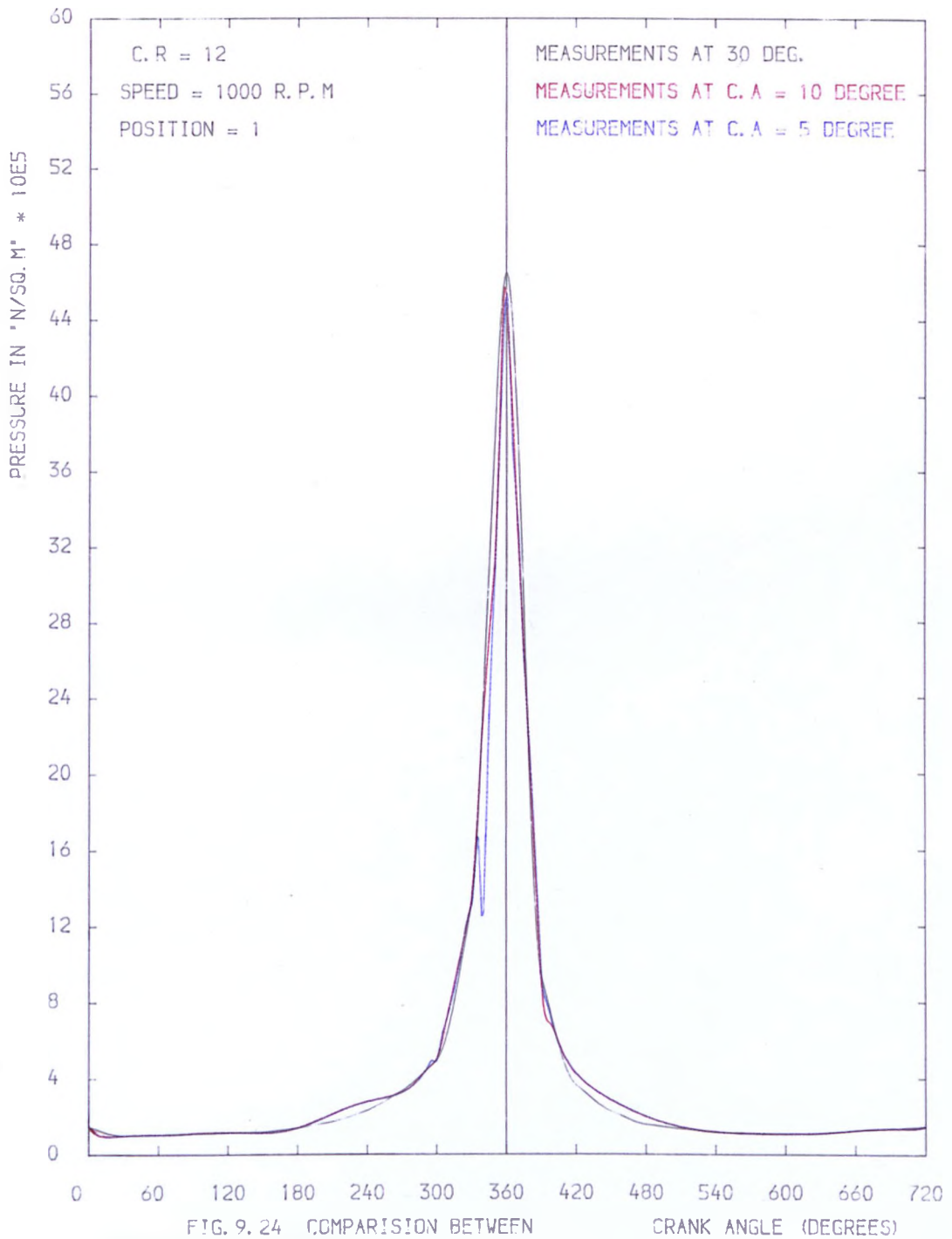


FIG. 9.25

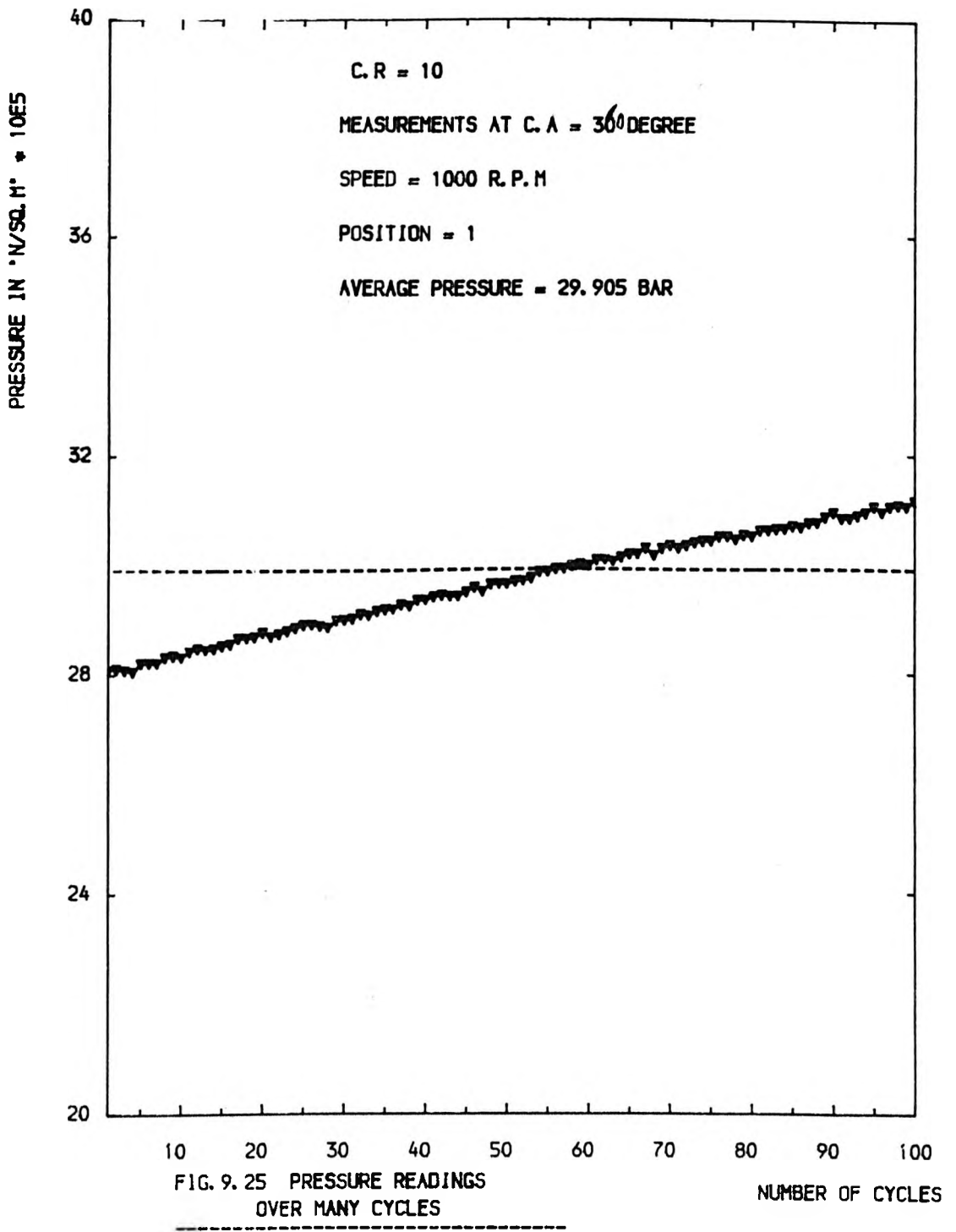


FIG. 9.26

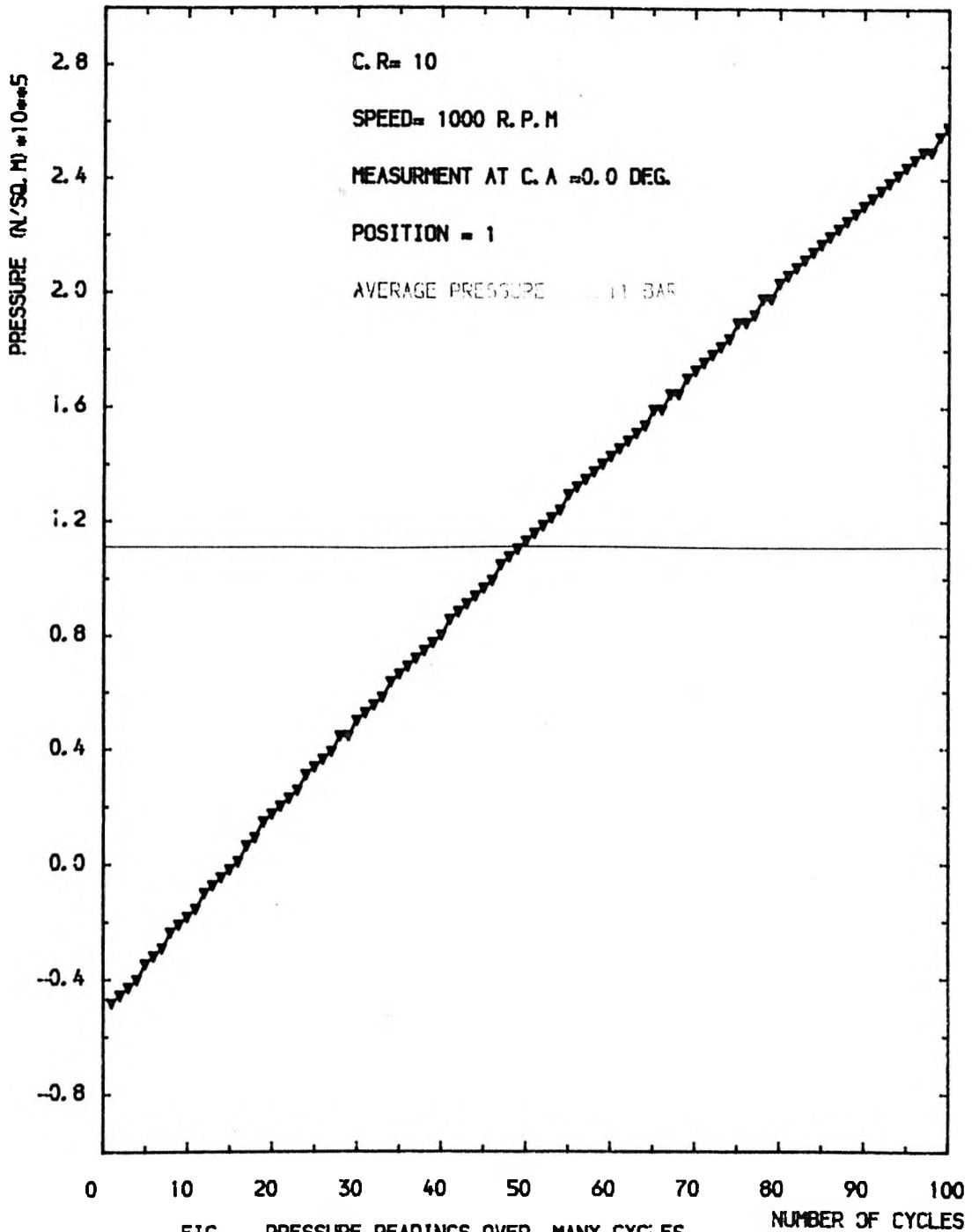


FIG. 9.27

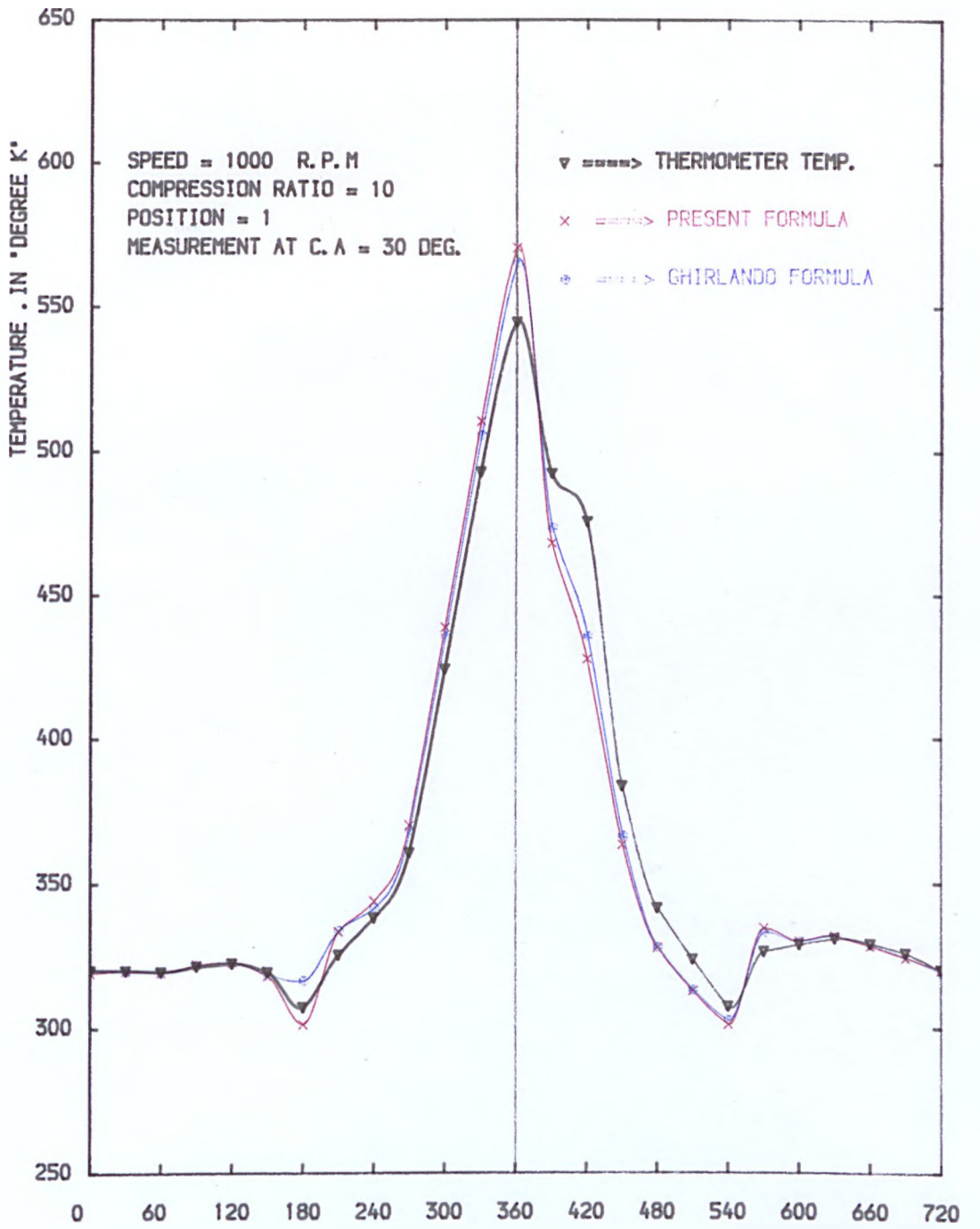


FIG. 9.27 COMPARISON BETWEEN GHIRLANDO, & PRESENT FORMULA FOR CORRECTED GAS TEMP.

FIG. 9.28

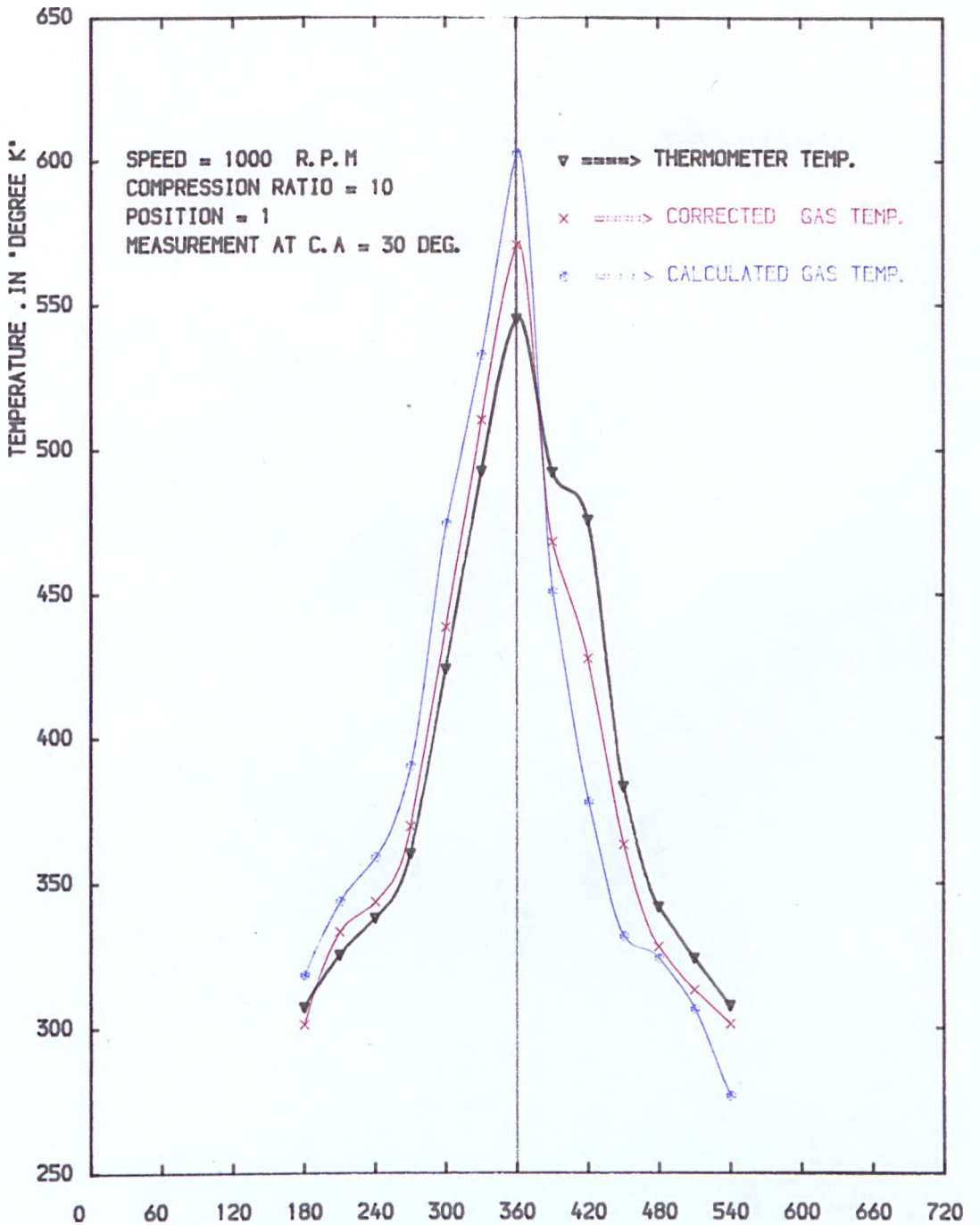


FIG. 9.28 COMPARISON BETWEEN CORRECTED, CALCULATED GAS & THERMOMETER TEMP. FOR CLOSED PERIOD

FIG. 9.29

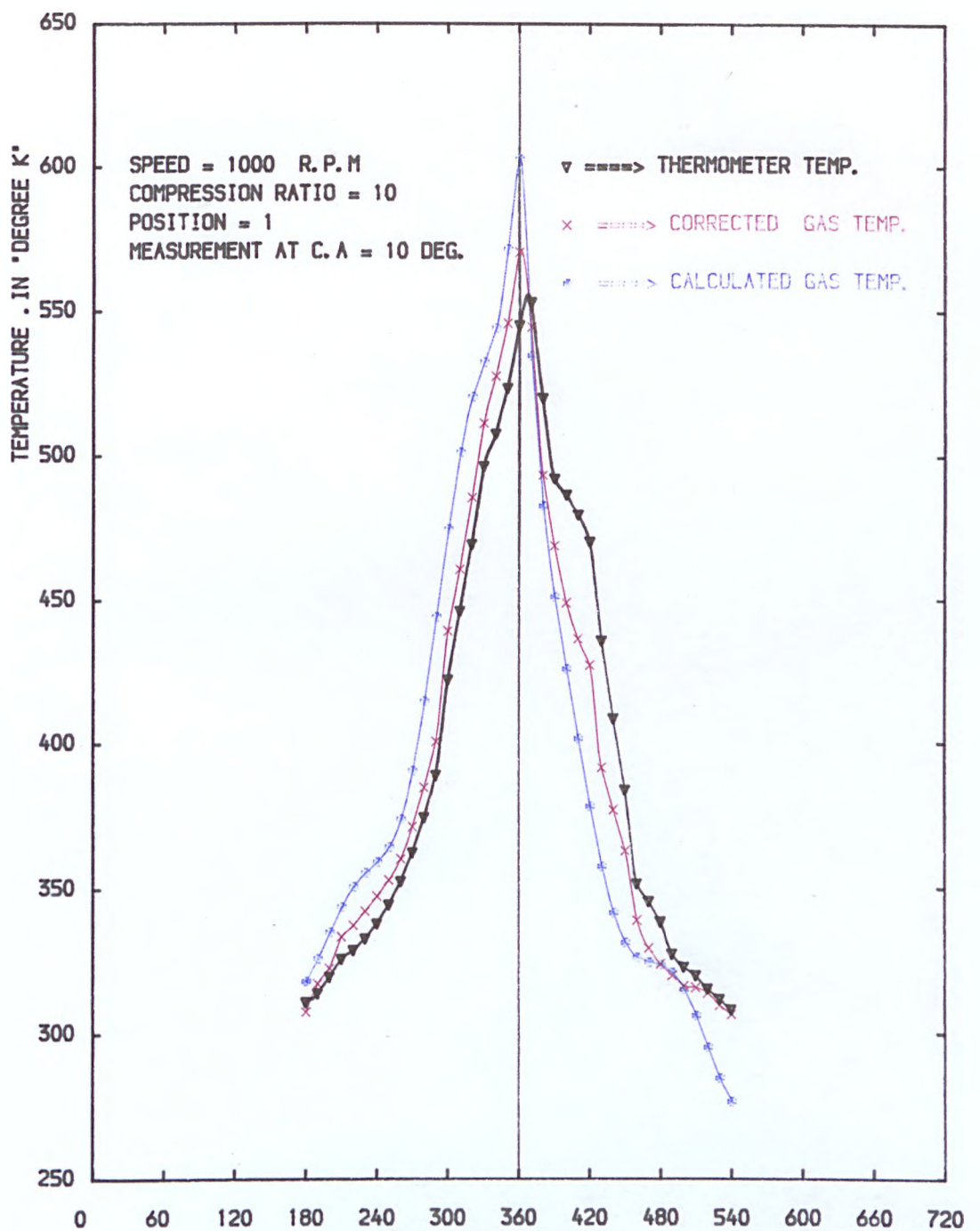


FIG. 9.29 COMPARISON BETWEEN CORRECTED, CALCULATED GAS & THERMOMETER TEMP. FOR CLOSED PERIOD

FIG. 9.30

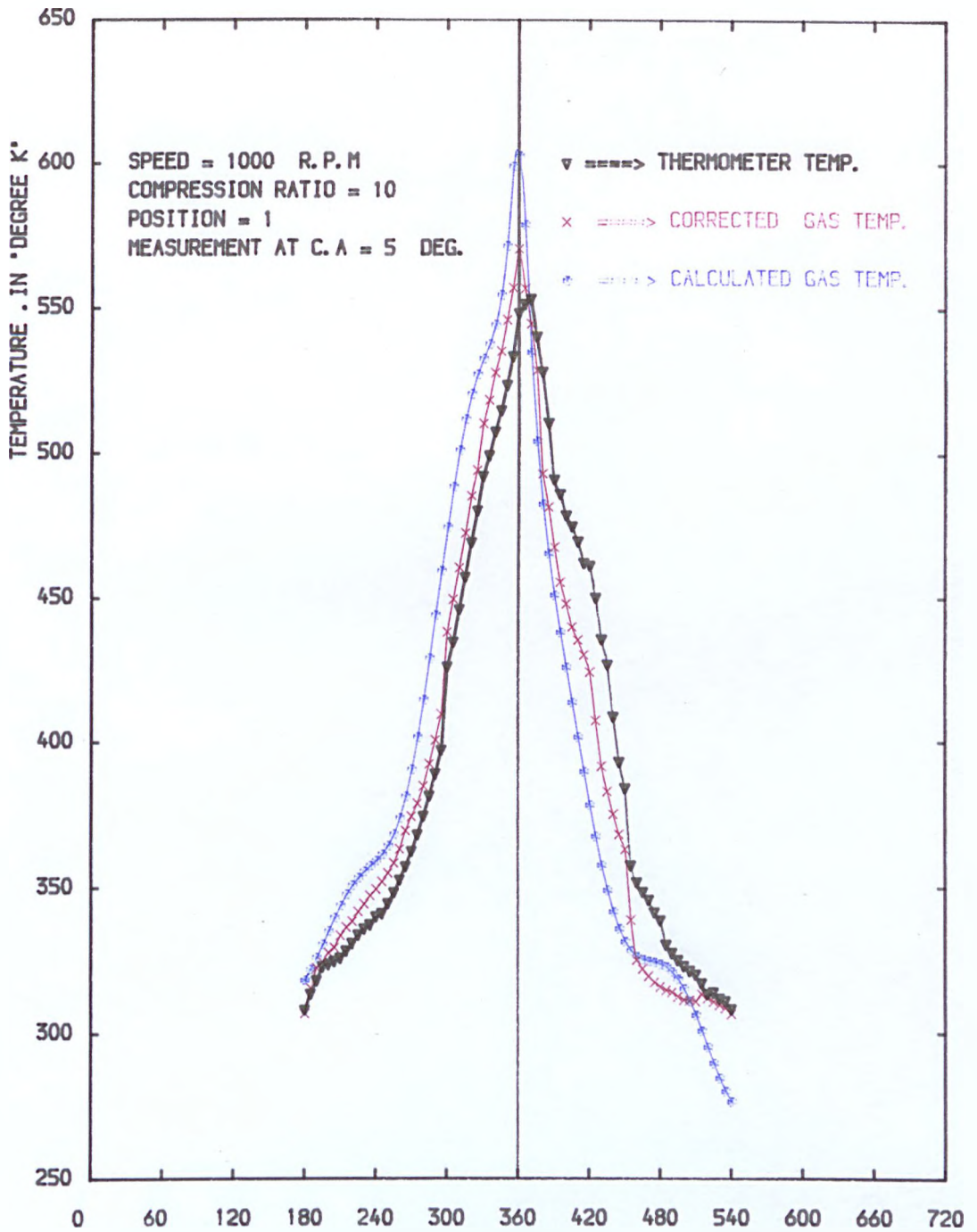


FIG. 9.30 COMPARISON BETWEEN CORRECTED, CALCULATED GAS & THERMOMETER TEMP. FOR CLOSED PERIOD

FIG. 9.31

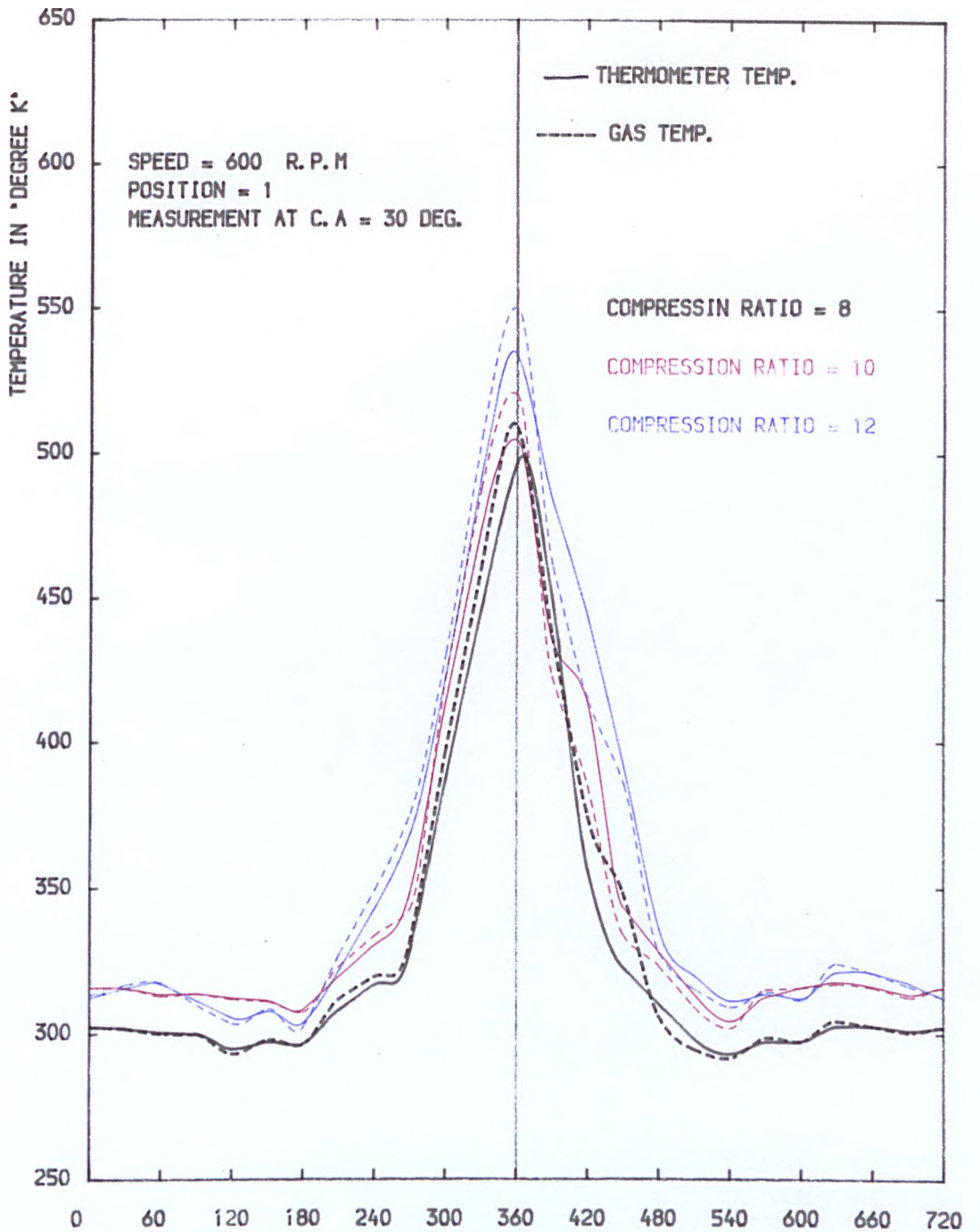


FIG. 9.31 COMPARISON BETWEEN CORRECTED GAS & THERMOMETER TEMP. AT DIFFERENT COMPRESSION RATIOS

FIG. 9.32

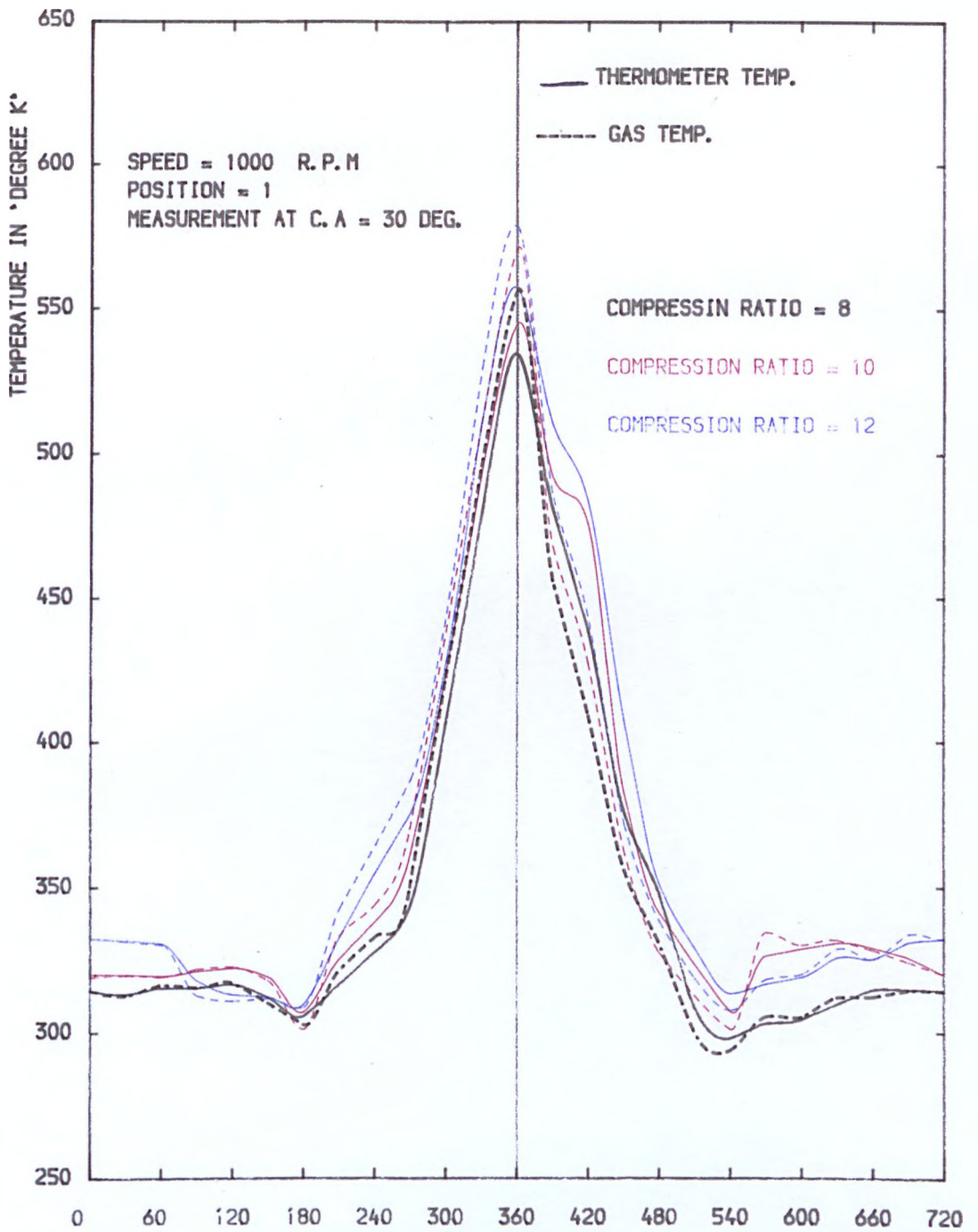


FIG. 9.32 COMPARISON BETWEEN CORRECTED GAS & THERMOMETER TEMP. AT DIFFERENT COMPRESSION RATIOS

FIG. 9.33

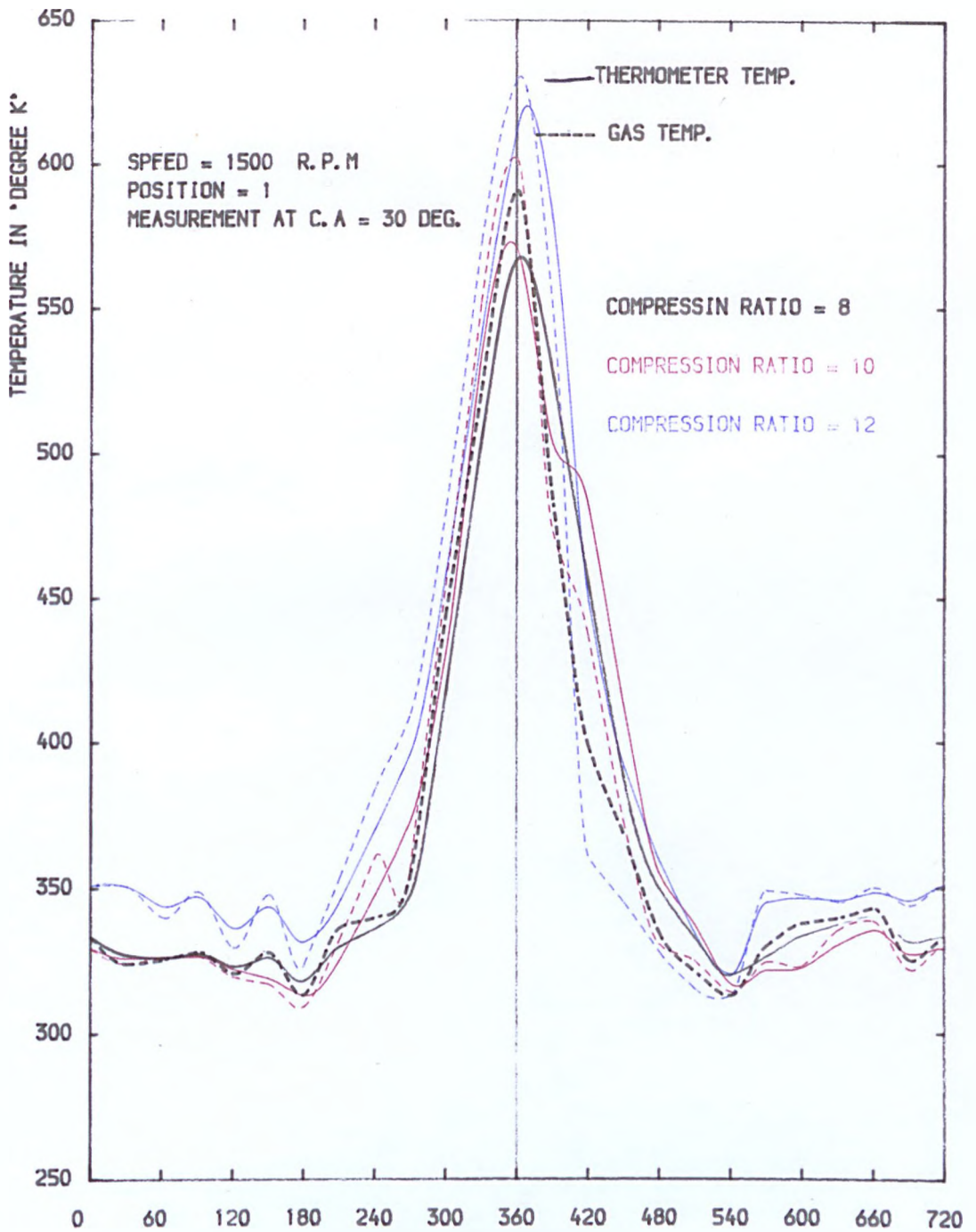


FIG. 9.33 COMPARISON BETWEEN CORRECTED GAS & THERMOMETER TEMP. AT DIFFERENT COMPRESSION RATIOS

FIG. 9.34

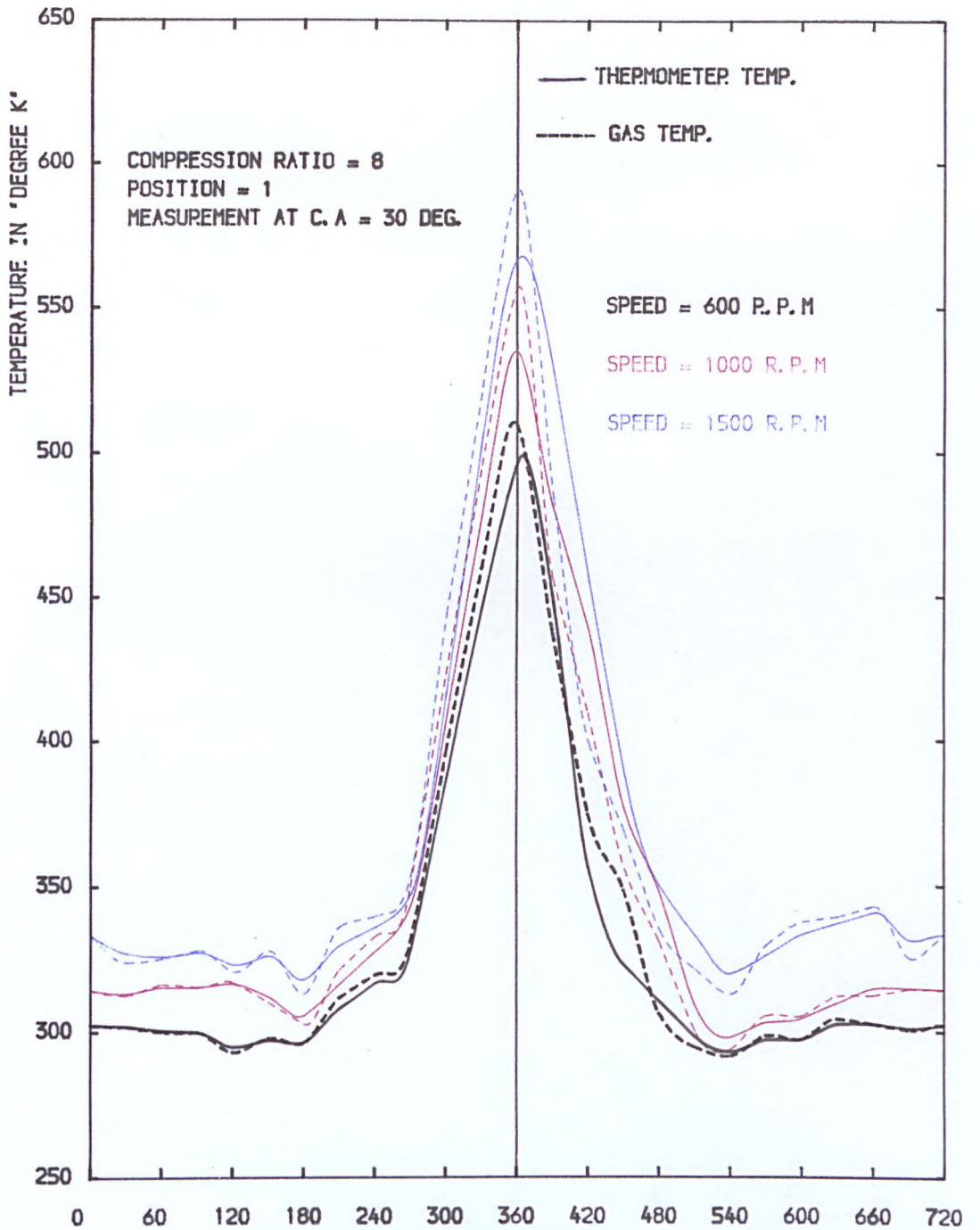


FIG. 9.34 COMPARISON BETWEEN CORRECTED GAS & THERMOMETER TEMP. AT DIFFERENT SPEEDS

FIG. 9.35

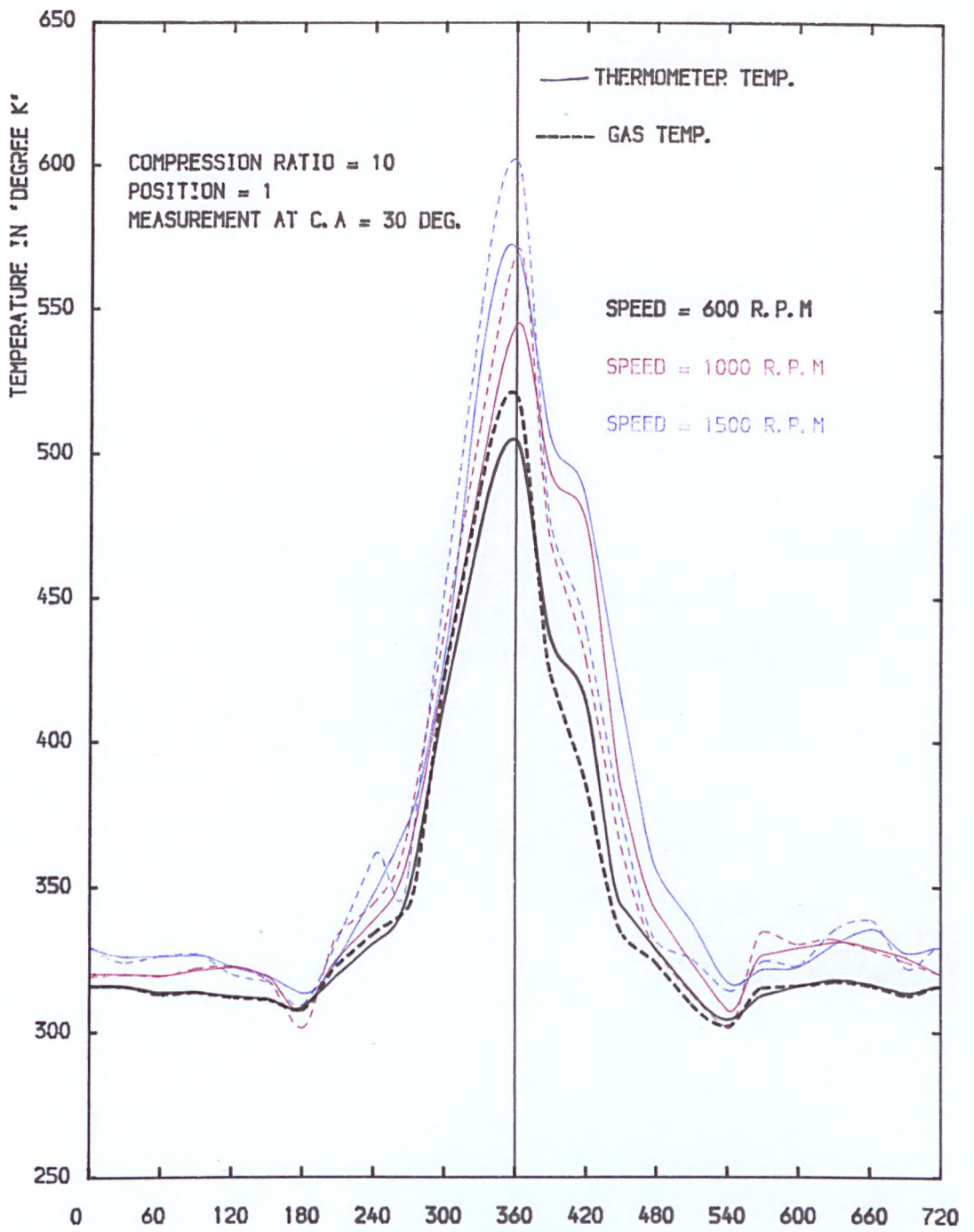


FIG. 9.35 COMPARISON BETWEEN CORRECTED GAS & THERMOMETER TEMP. AT DIFFERENT SPEEDS

FIG. 9.36

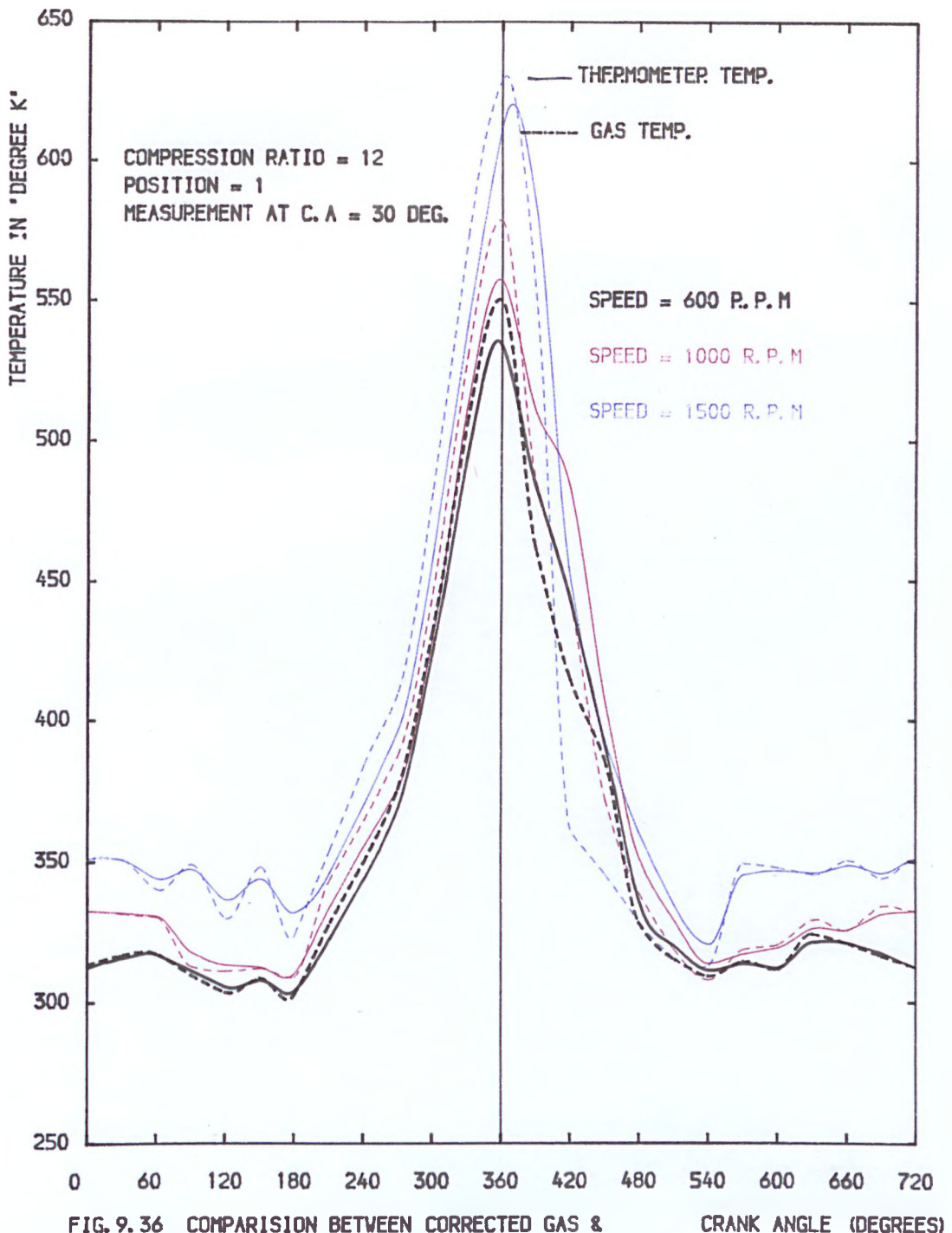


FIG. 9.36 COMPARISON BETWEEN CORRECTED GAS & THERMOMETER TEMP. AT DIFFERENT SPEEDS

FIG. 9.37

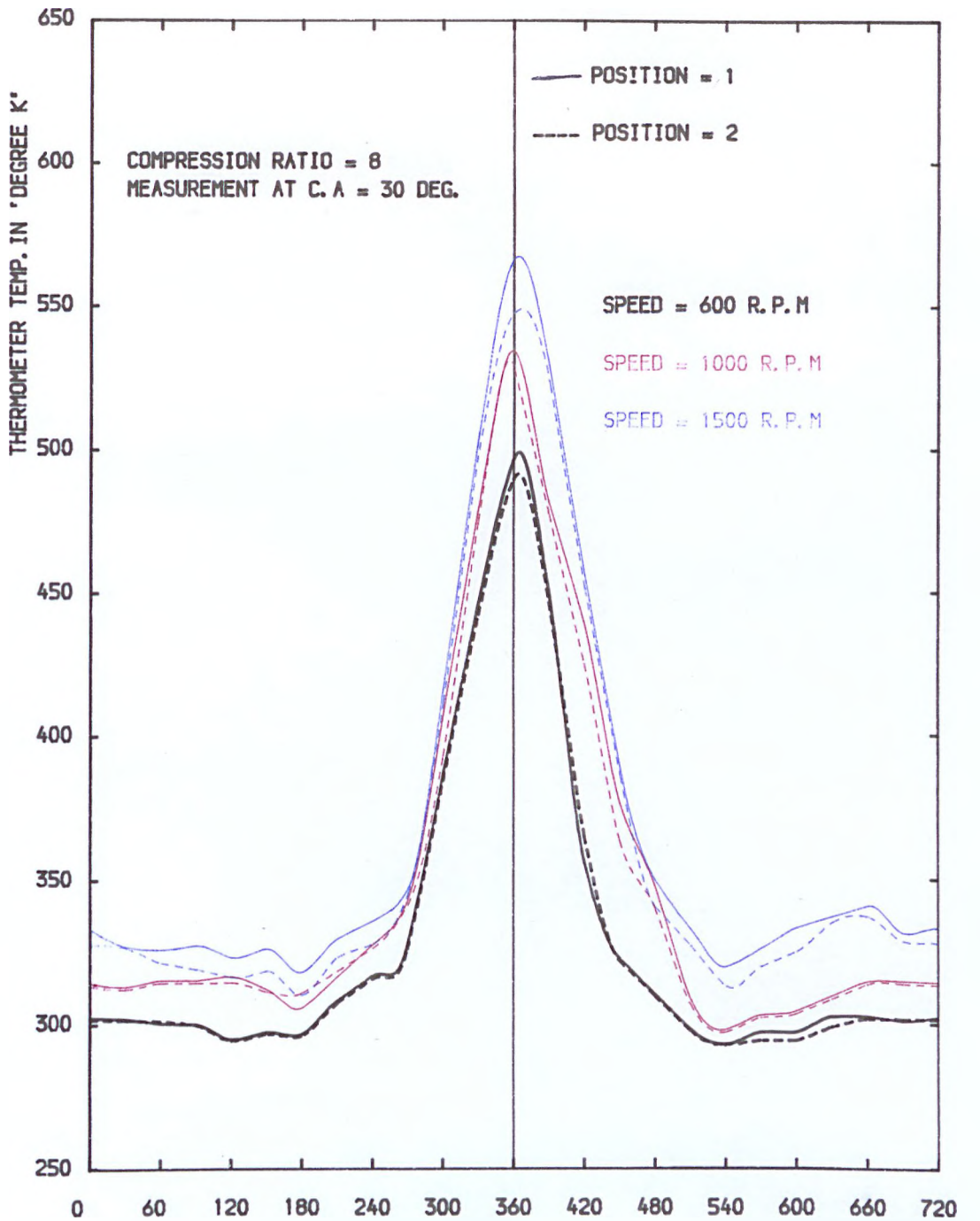


FIG. 9.37 COMPARISON BETWEEN
THERMOMETER TEMP. AT DIFFERENT POSITION

CRANK ANGLE (DEGREES)

FIG. 9.38

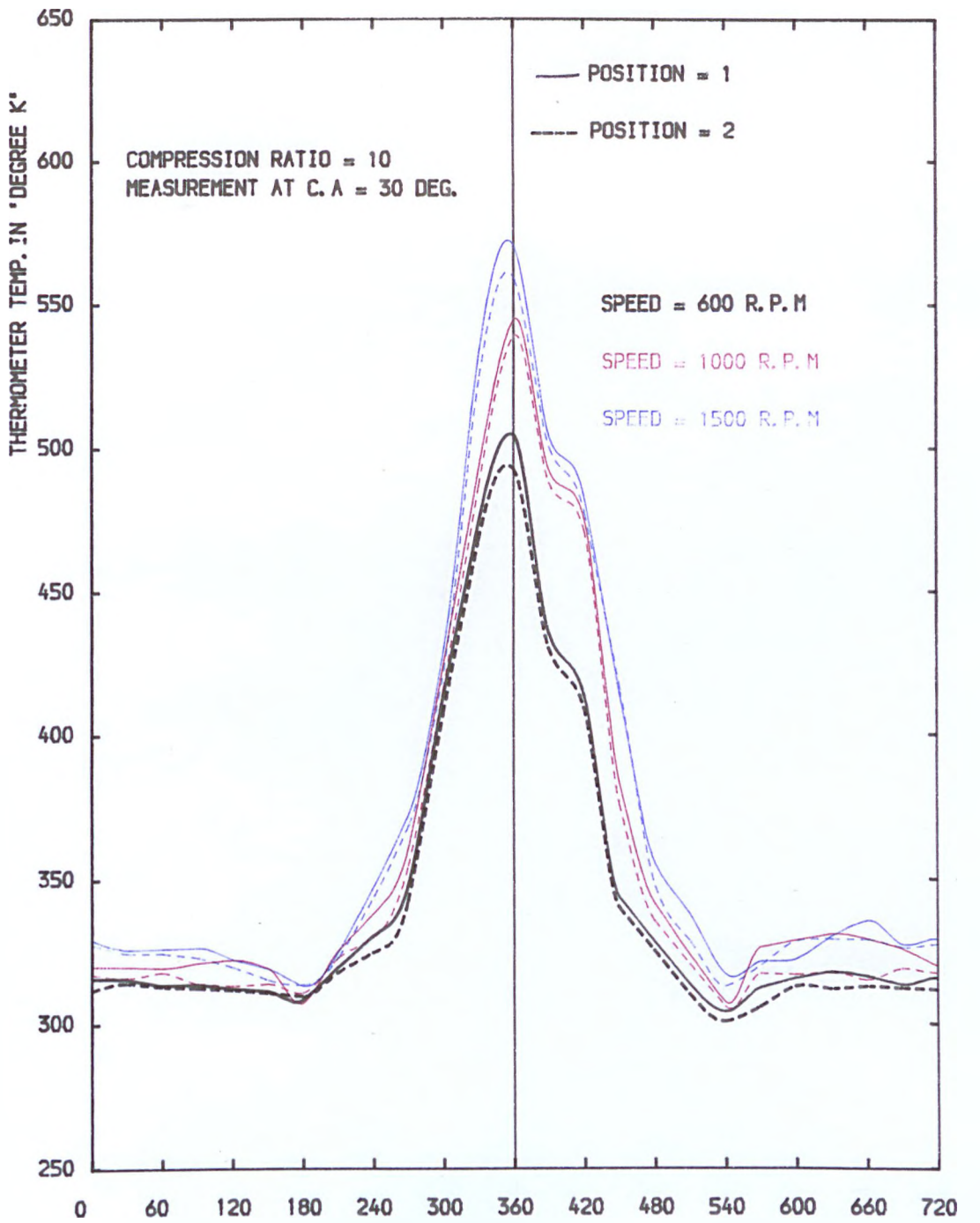


FIG. 9.38 COMPARISON BETWEEN THERMOMETER TEMP. AT DIFFERENT POSITION

FIG. 9.39

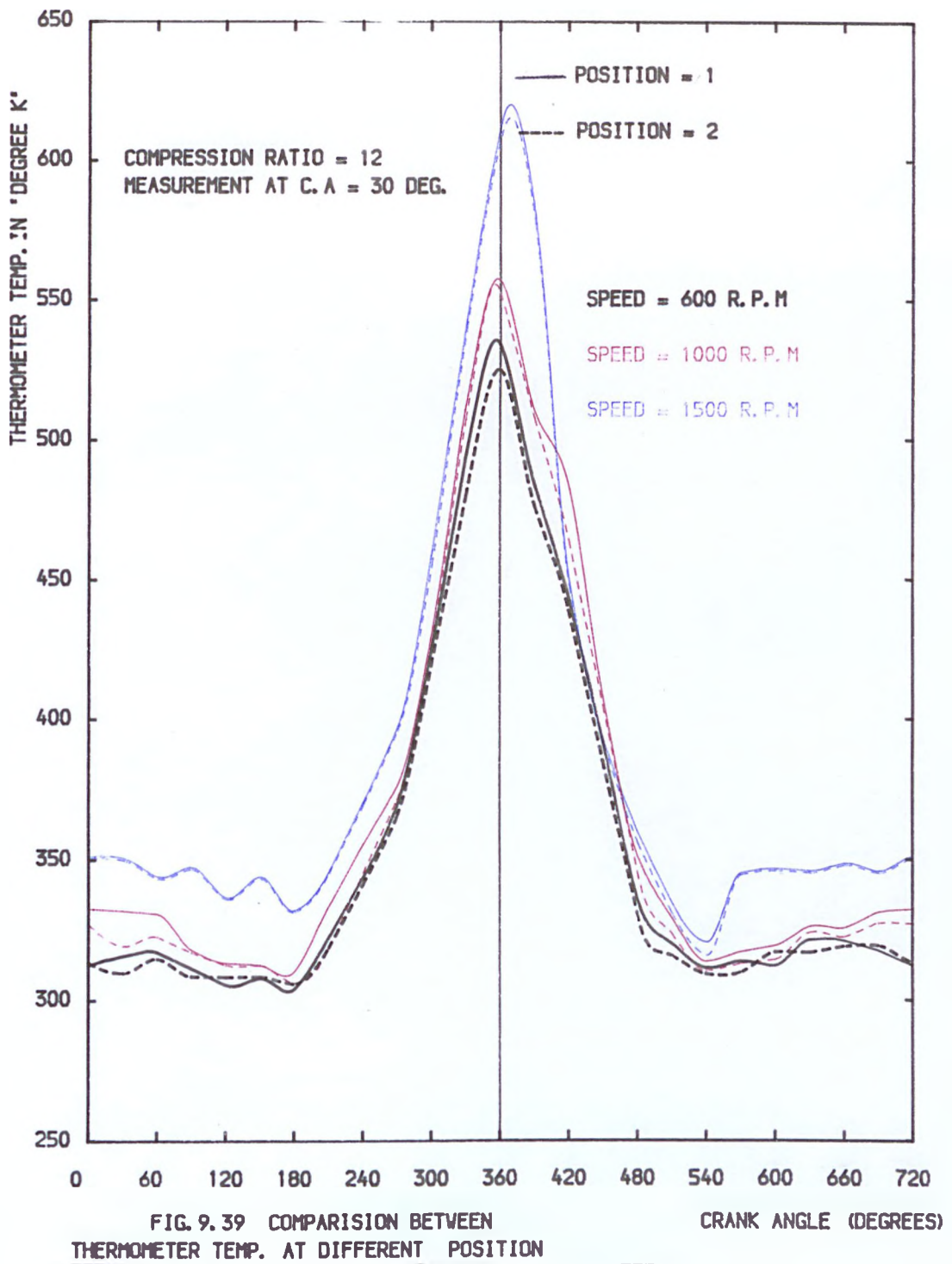


FIG. 9.40

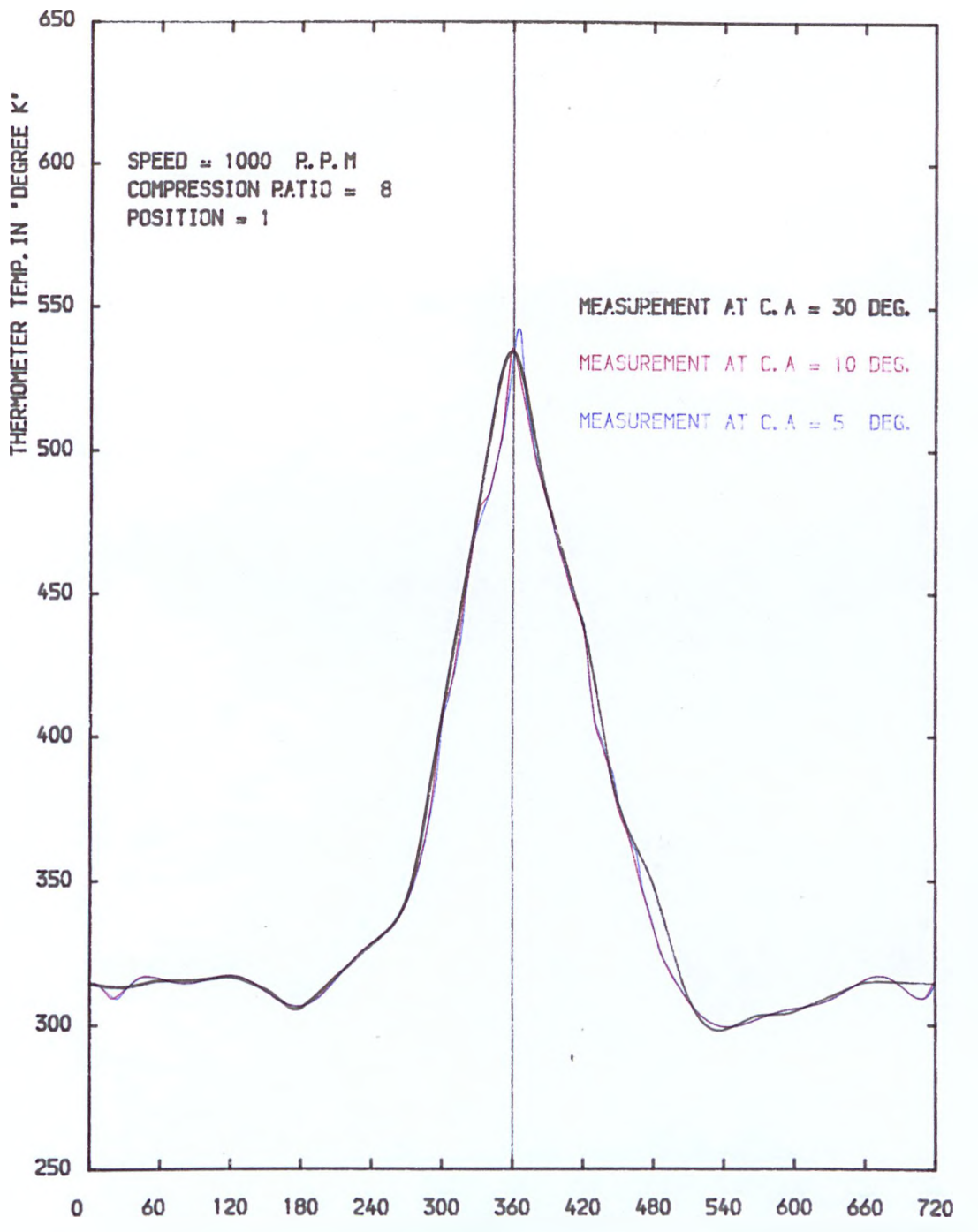


FIG. 9.40 COMPARISON BETWEEN THERMOMETER TEMP. AT DIFFERENT C. A MEASUREMENTS

FIG. 9.41

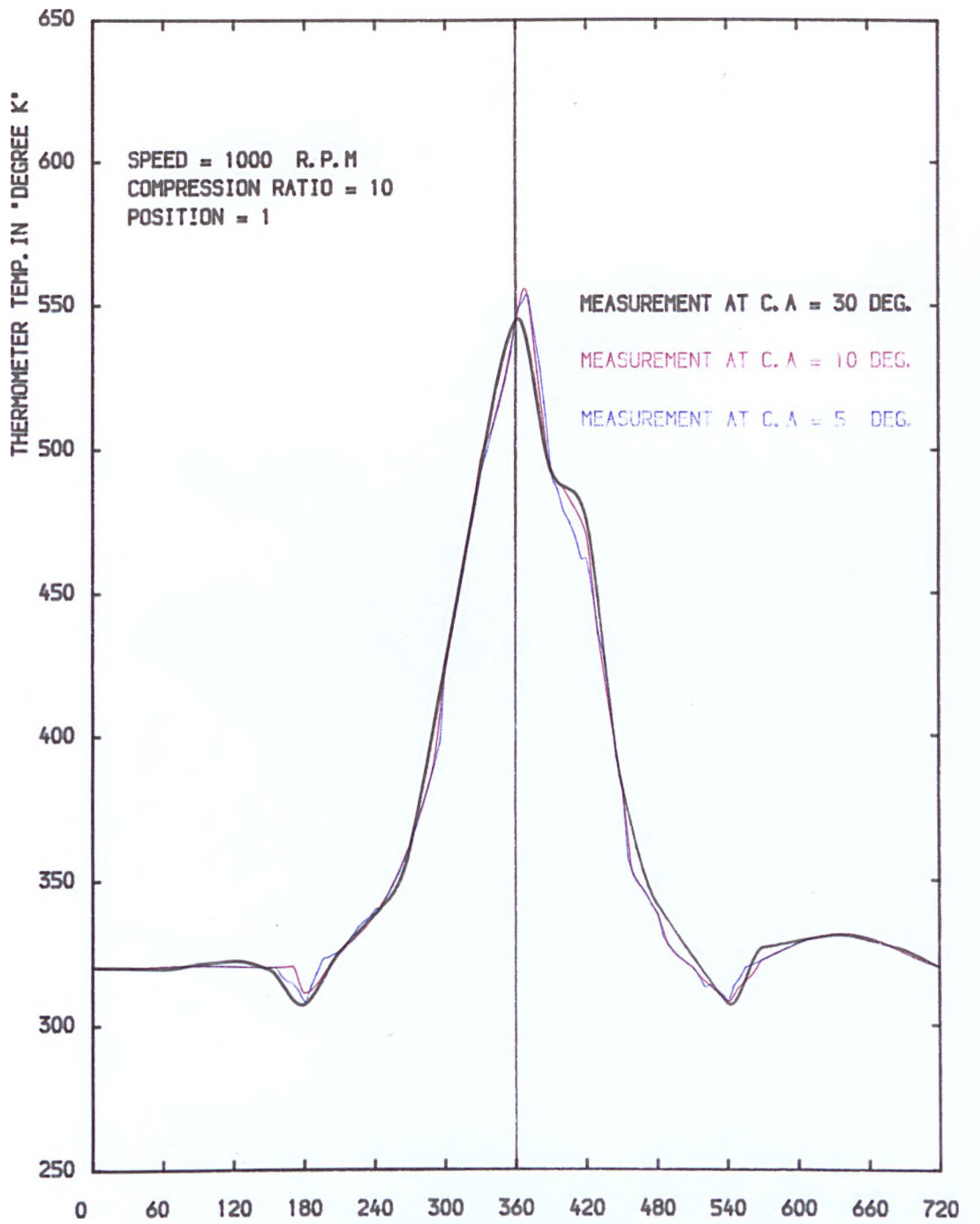


FIG. 9.41 COMPARISON BETWEEN THERMOMETER TEMP. AT DIFFERENT C. A MEASUREMENTS

FIG. 9.42

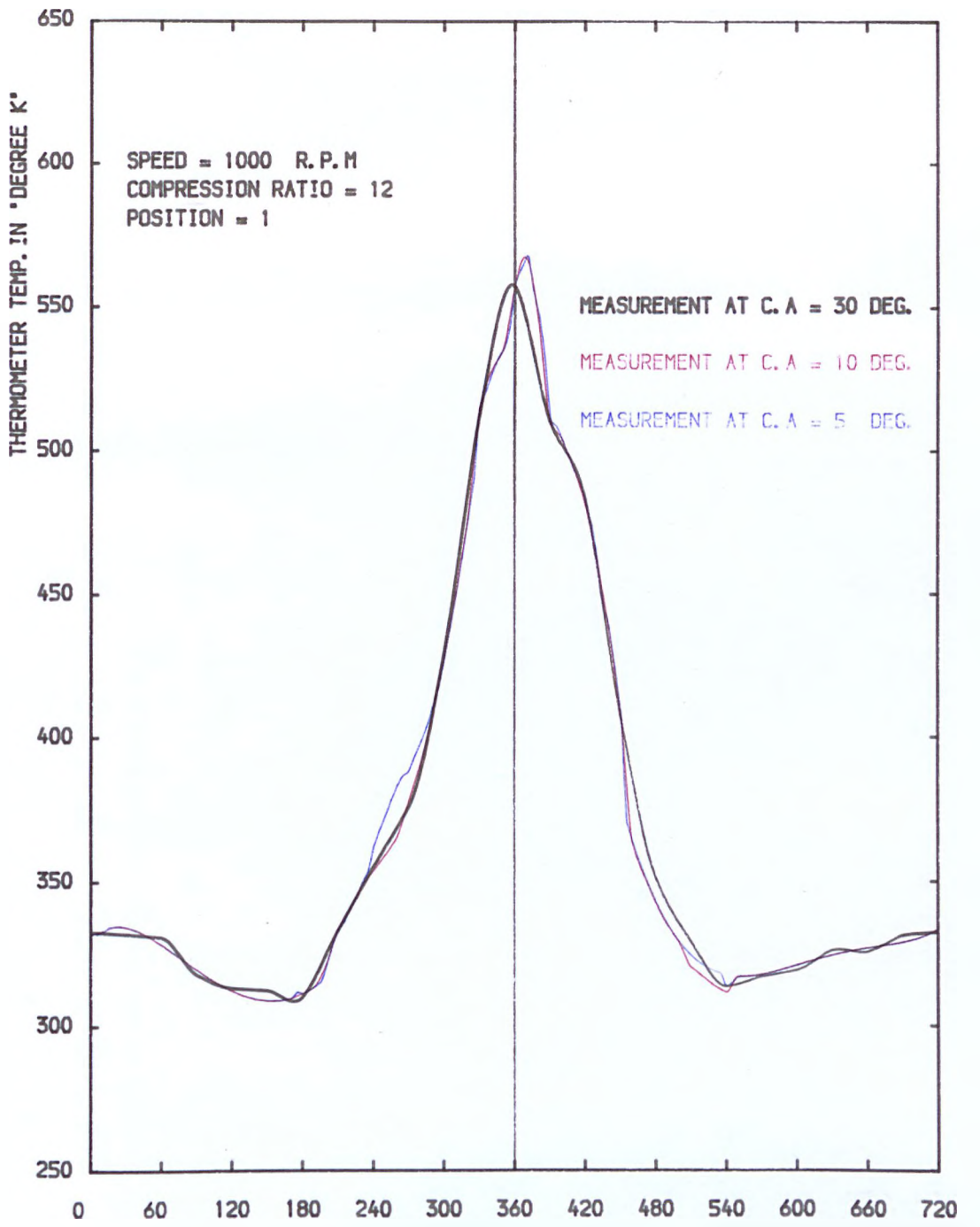


FIG. 9.42 COMPARISON BETWEEN THERMOMETER TEMP. AT DIFFERENT C. A MEASUREMENTS

FIG. 9.43

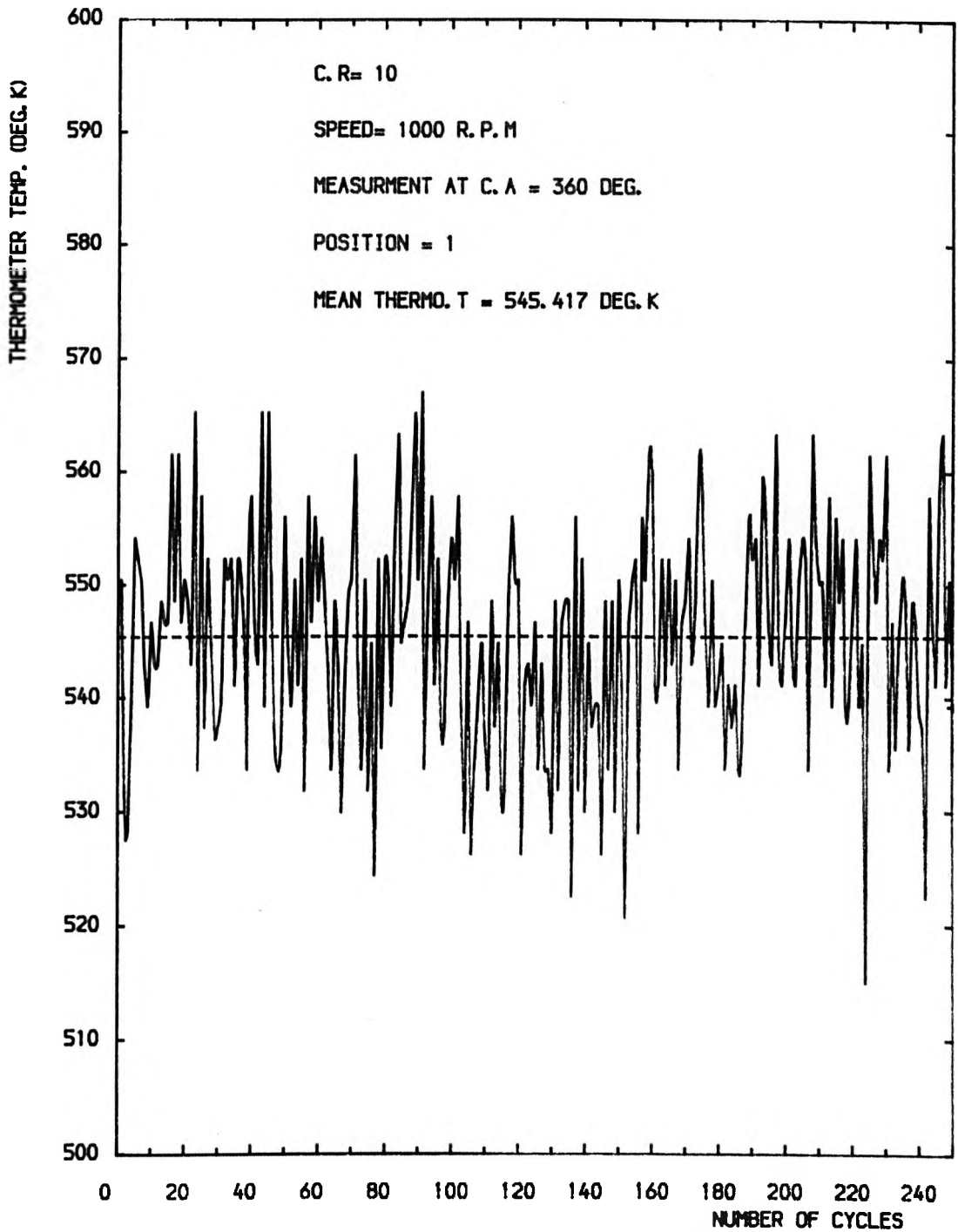


FIG. 9.43 THERMOMETER TEMPERATURE OVER MANY CYCLES

FIG. 9.44

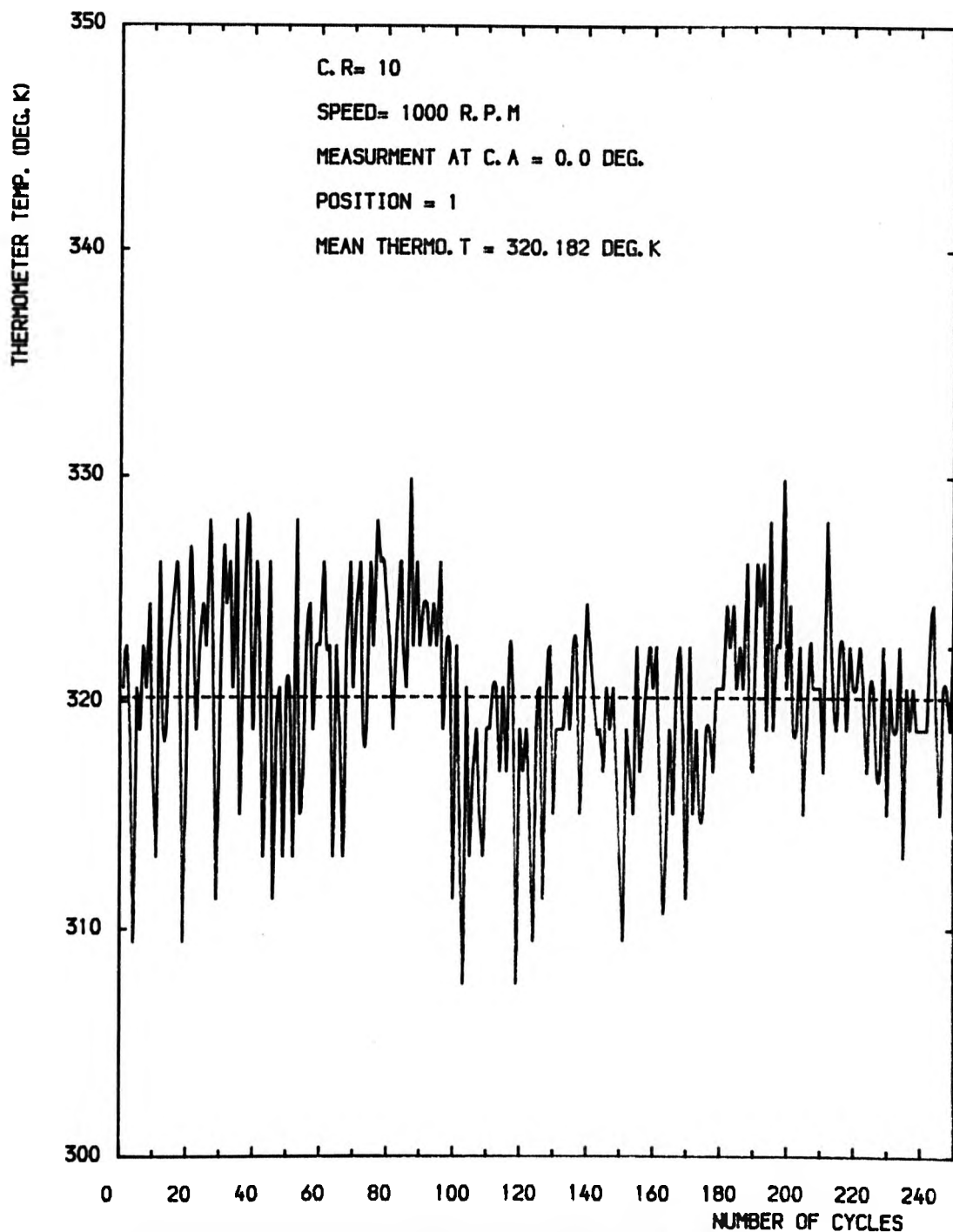


FIG. 9.44 THERMOMETER TEMPERATURE OVER MANY CYCLES

FIG. 9.45

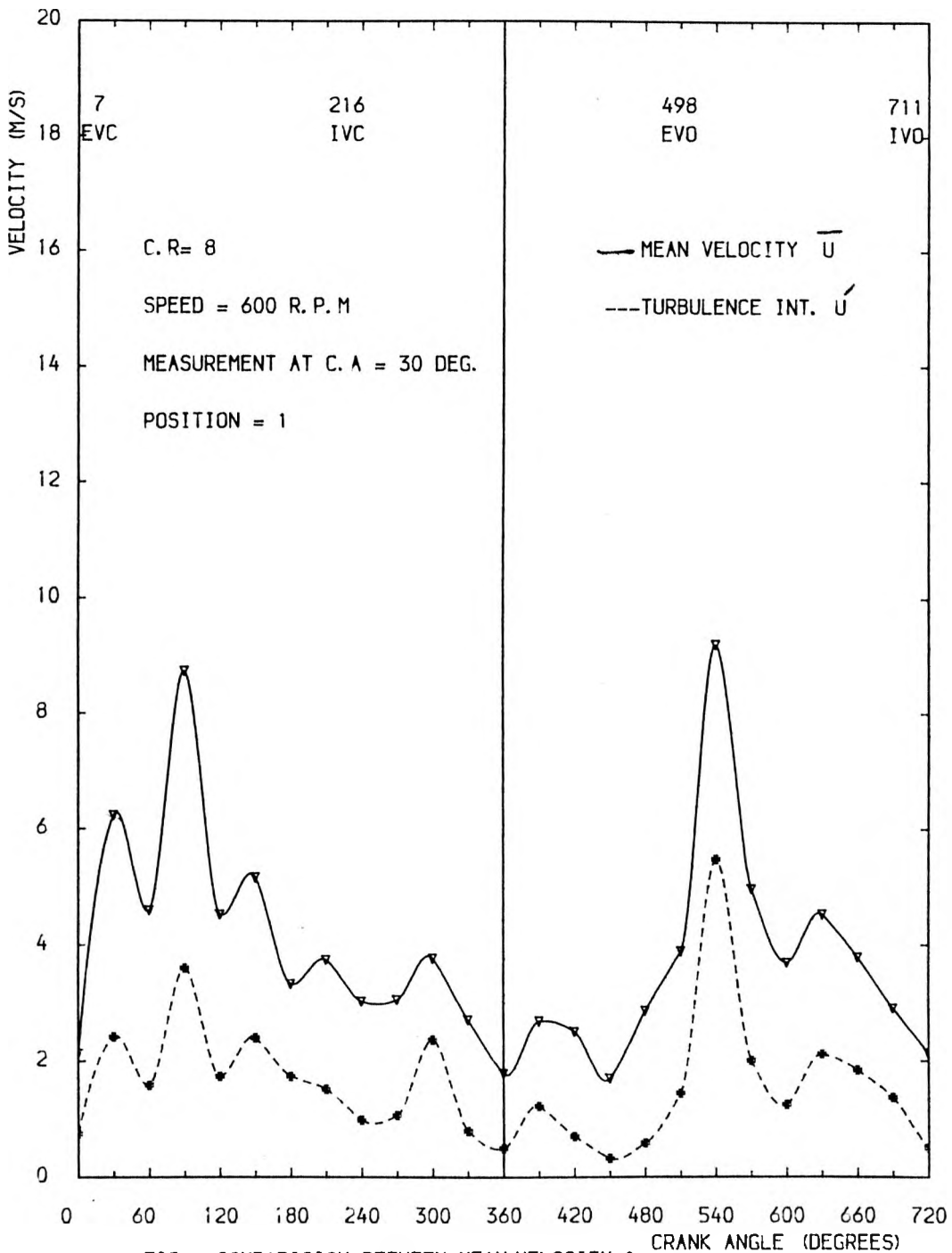


FIG. COMPARISON BETWEEN MEAN VELOCITY & TURBULENCE INT. WITH C. A

FIG. 9.46

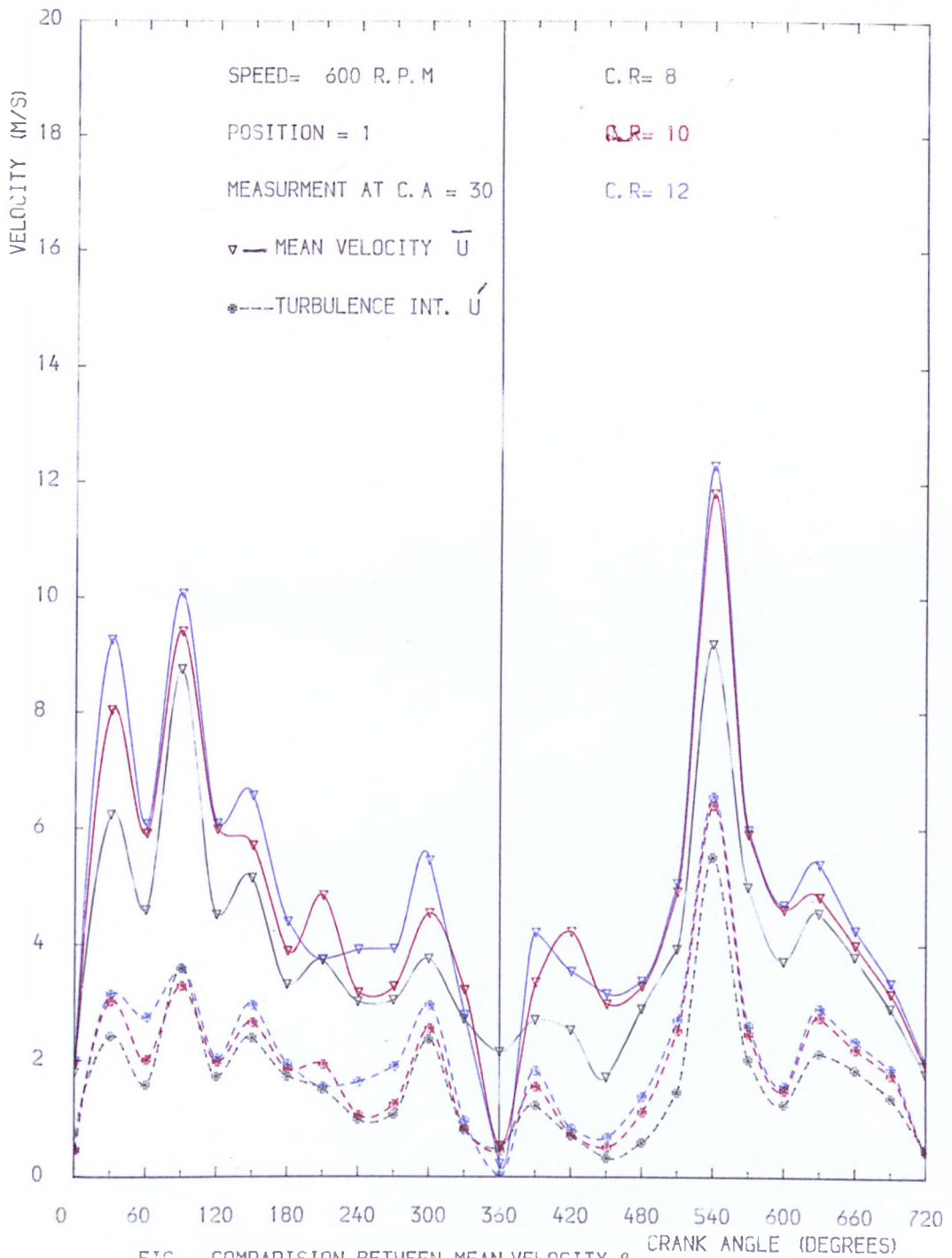


FIG. COMPARISON BETWEEN MEAN VELOCITY & TURBULENCE INT. AT DIFFERENT C.R.

FIG. 9.47

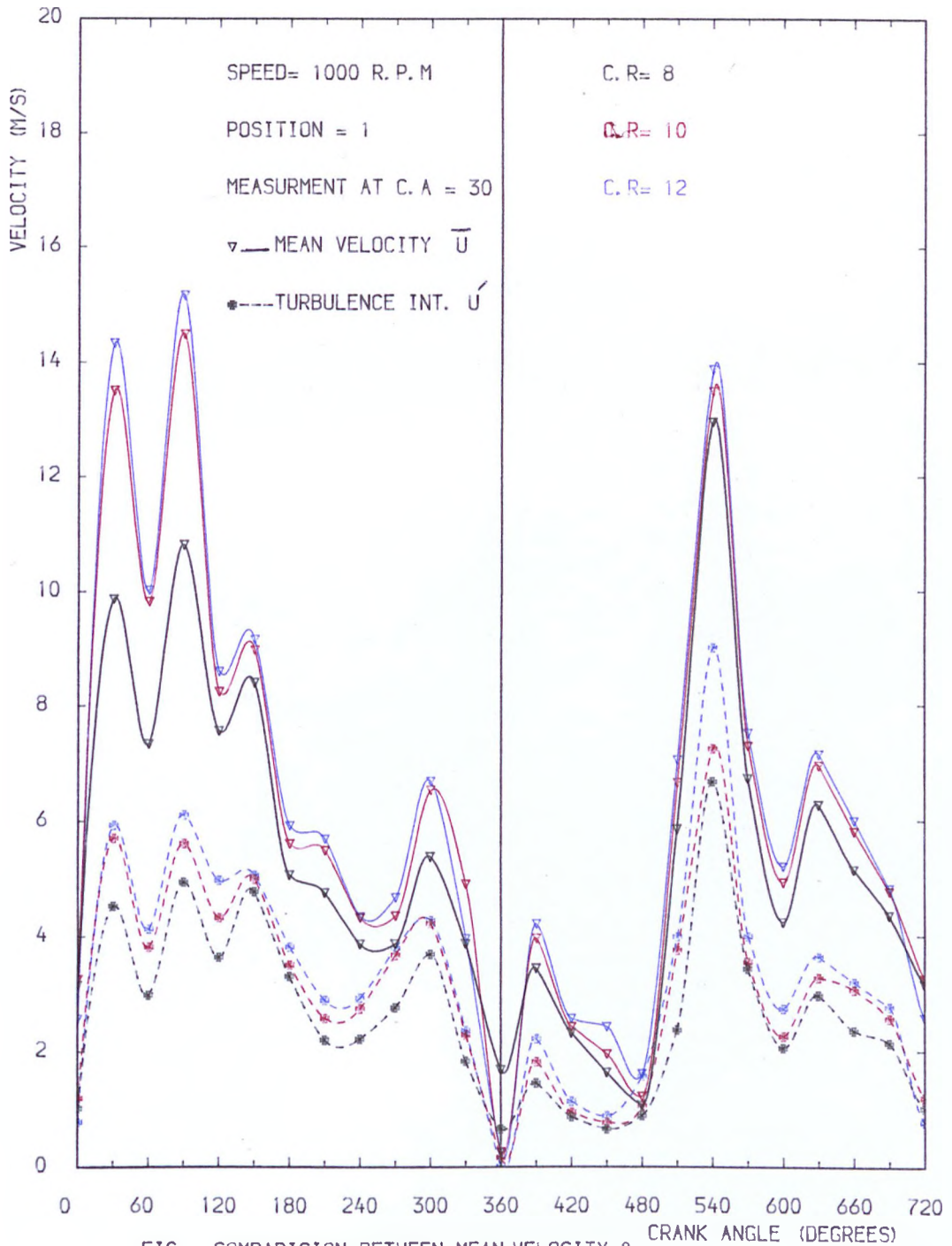


FIG. COMPARISON BETWEEN MEAN VELOCITY & TURBULENCE INT. AT DIFFERENT C. R

FIG. 9.48

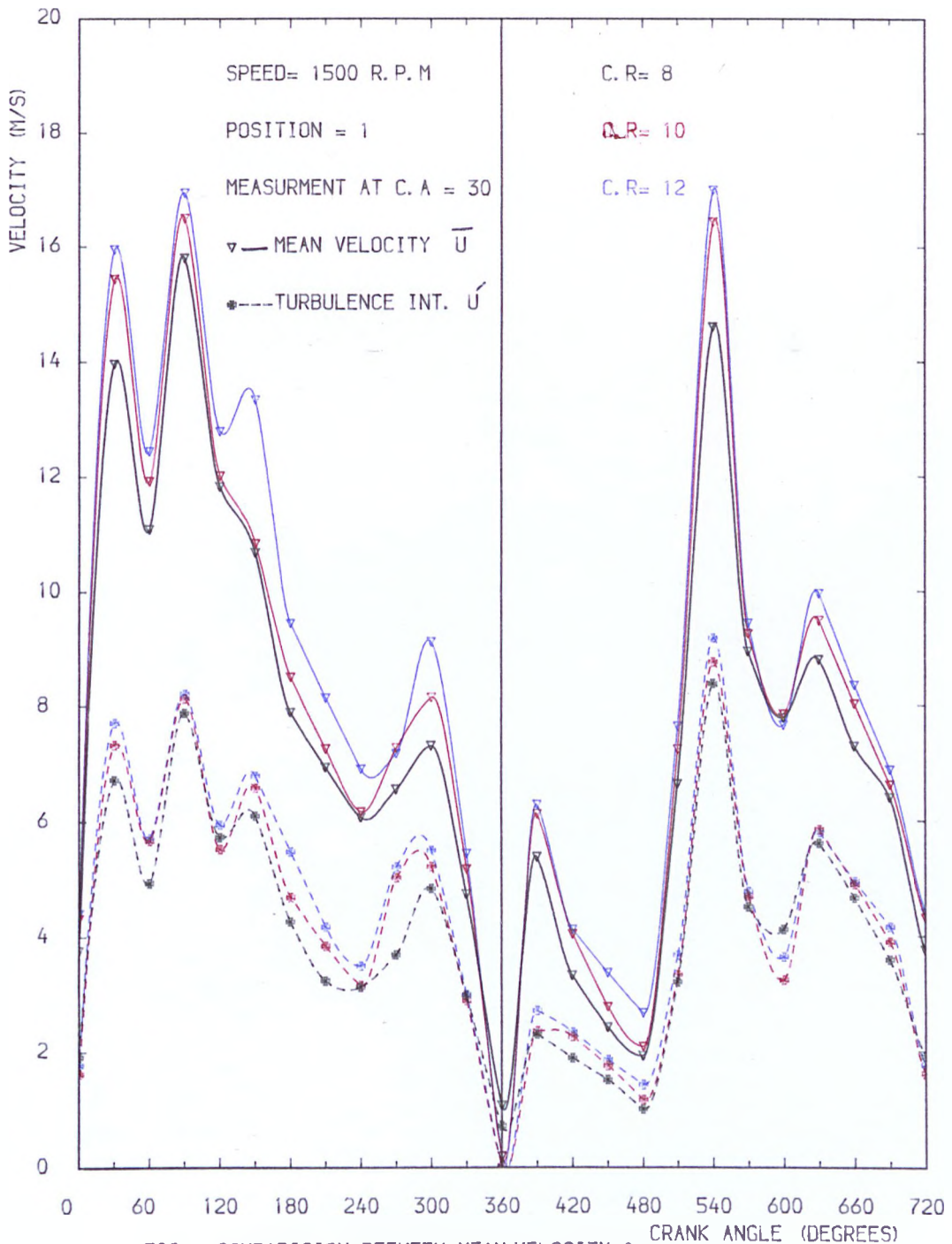


FIG. COMPARISON BETWEEN MEAN VELOCITY & TURBULENCE INT. AT DIFFERENT C.R

FIG. 9.49

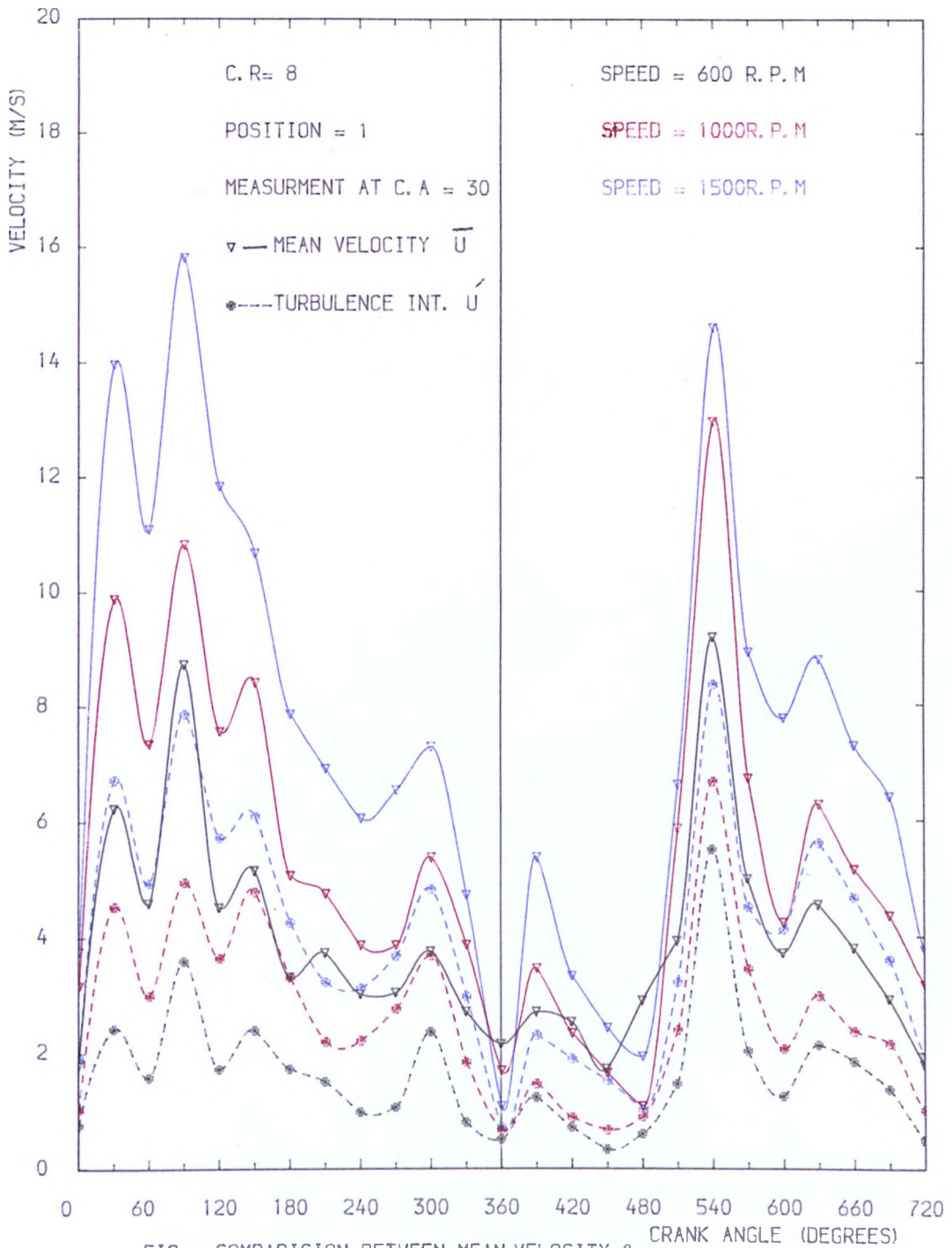


FIG. COMPARISON BETWEEN MEAN VELOCITY & TURBULENCE INT. AT DIFFERENT SPEED

FIG. 9.50

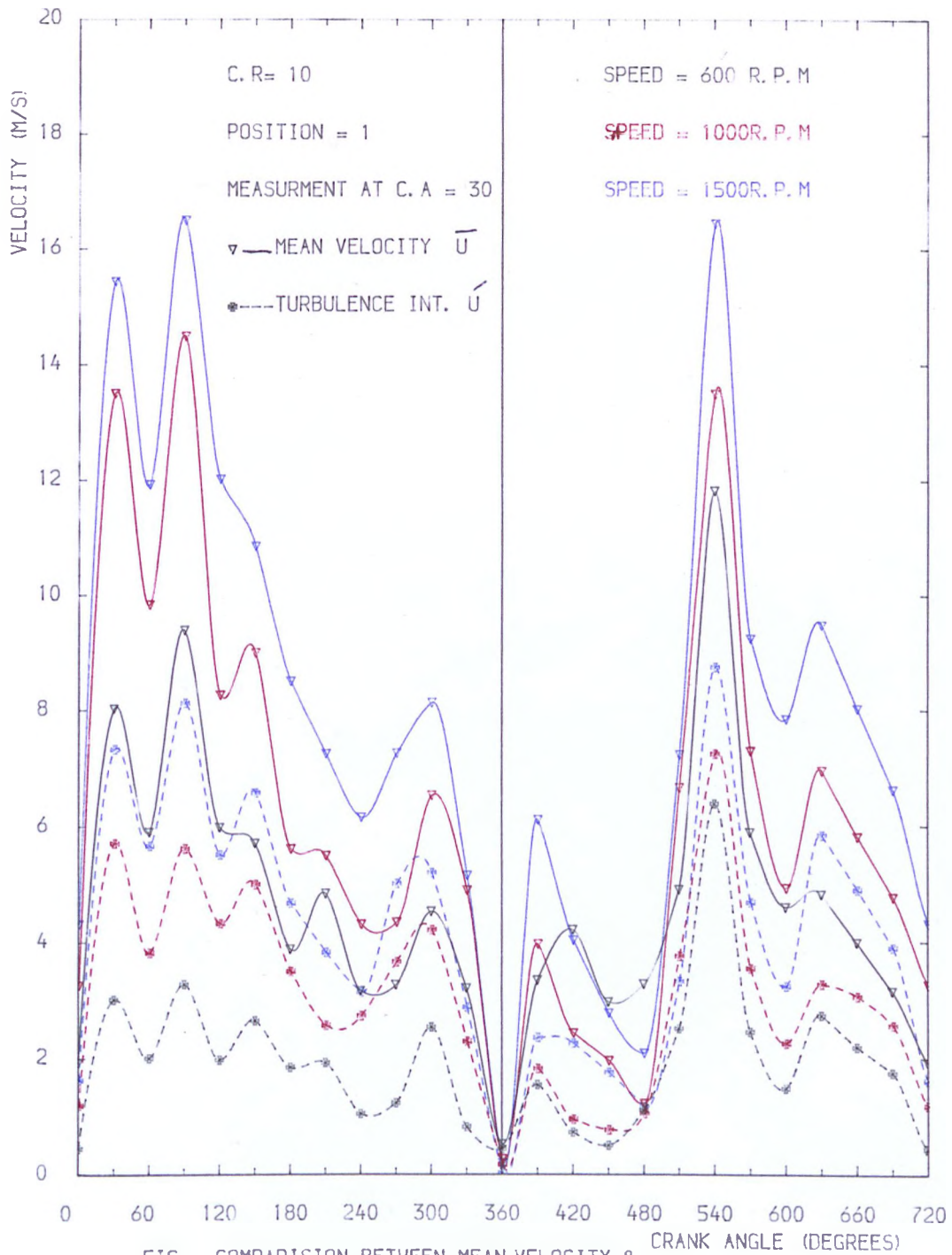


FIG. COMPARISON BETWEEN MEAN VELOCITY & TURBULENCE INT. AT DIFFERENT SPEED

FIG. 9.51

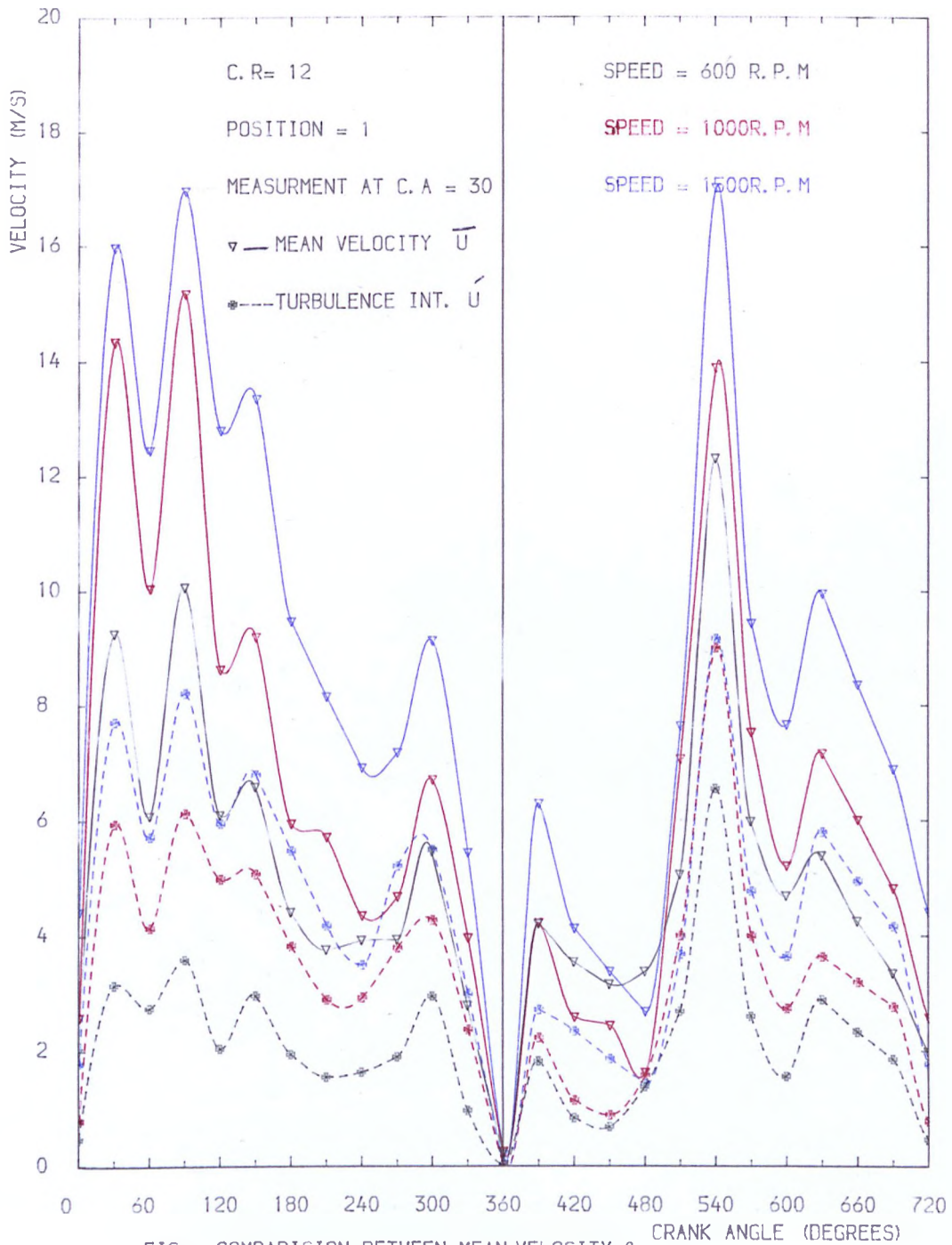


FIG. COMPARISON BETWEEN MEAN VELOCITY & TURBULENCE INT. AT DIFFERENT SPEED

FIG. 9.52

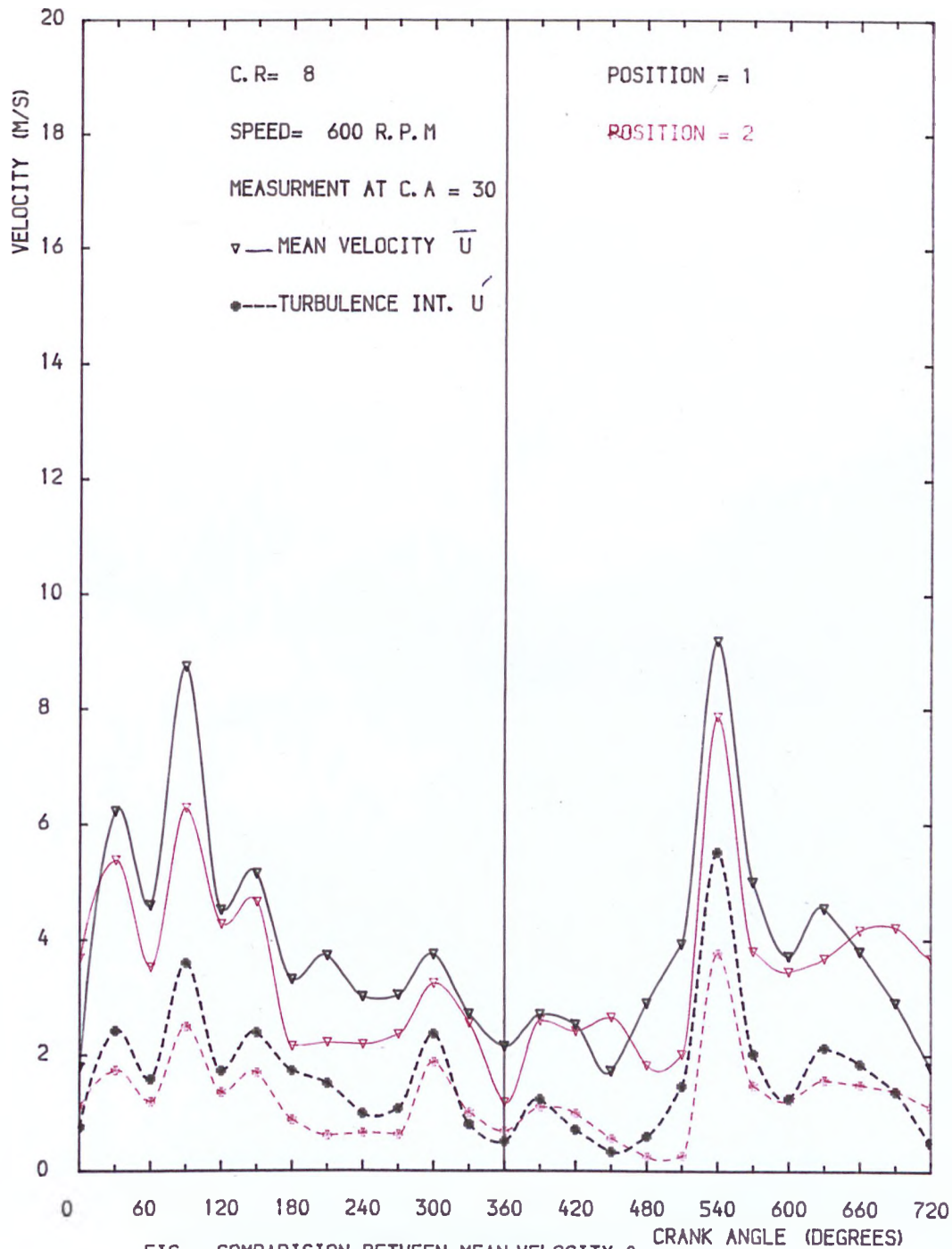


FIG. COMPARISON BETWEEN MEAN VELOCITY & TURBULENCE INT. AT DIFFRENT POSITION

FIG. 9.53

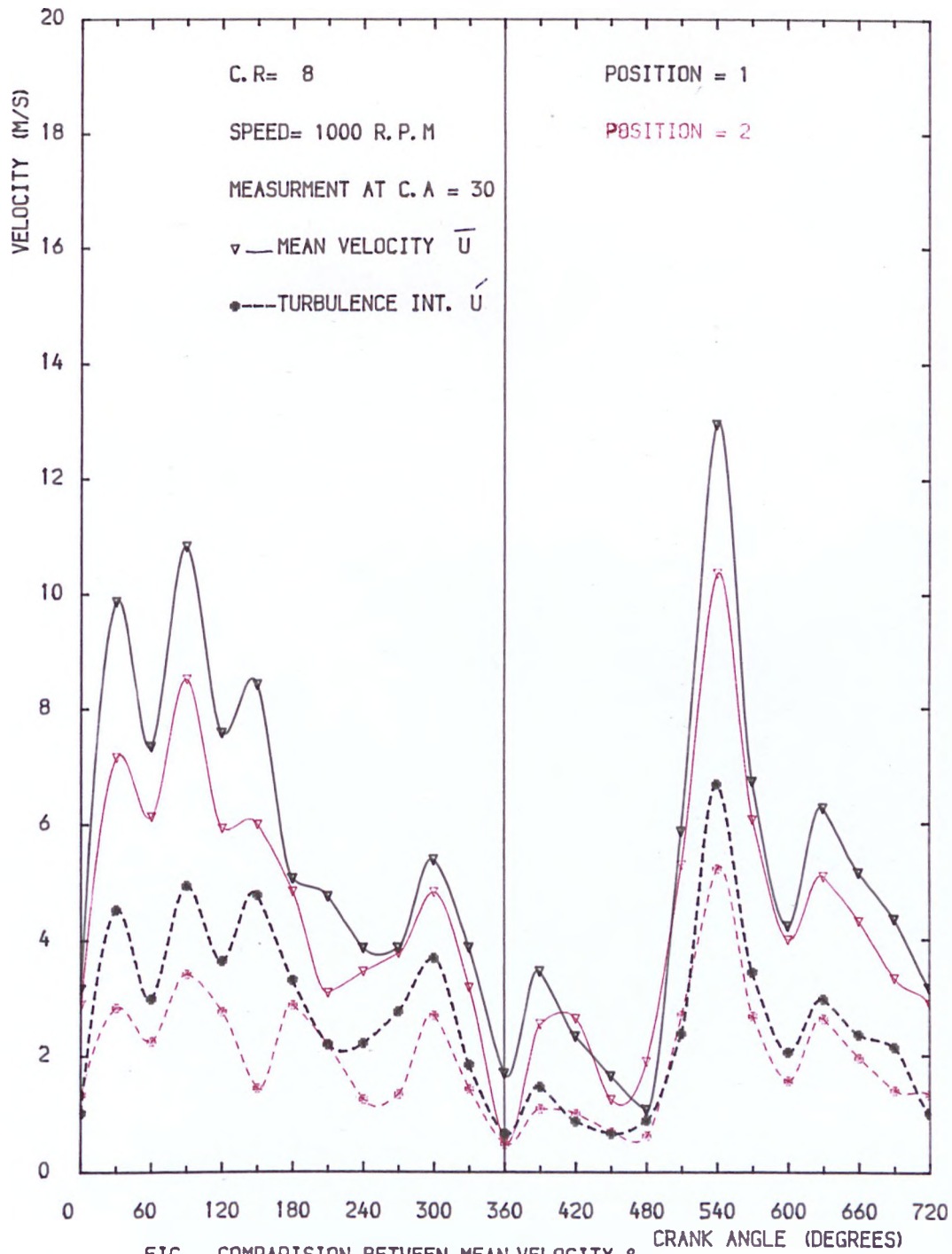


FIG. COMPARISON BETWEEN MEAN VELOCITY & TURBULENCE INT. AT DIFFRENT POSITION

FIG. 9.54

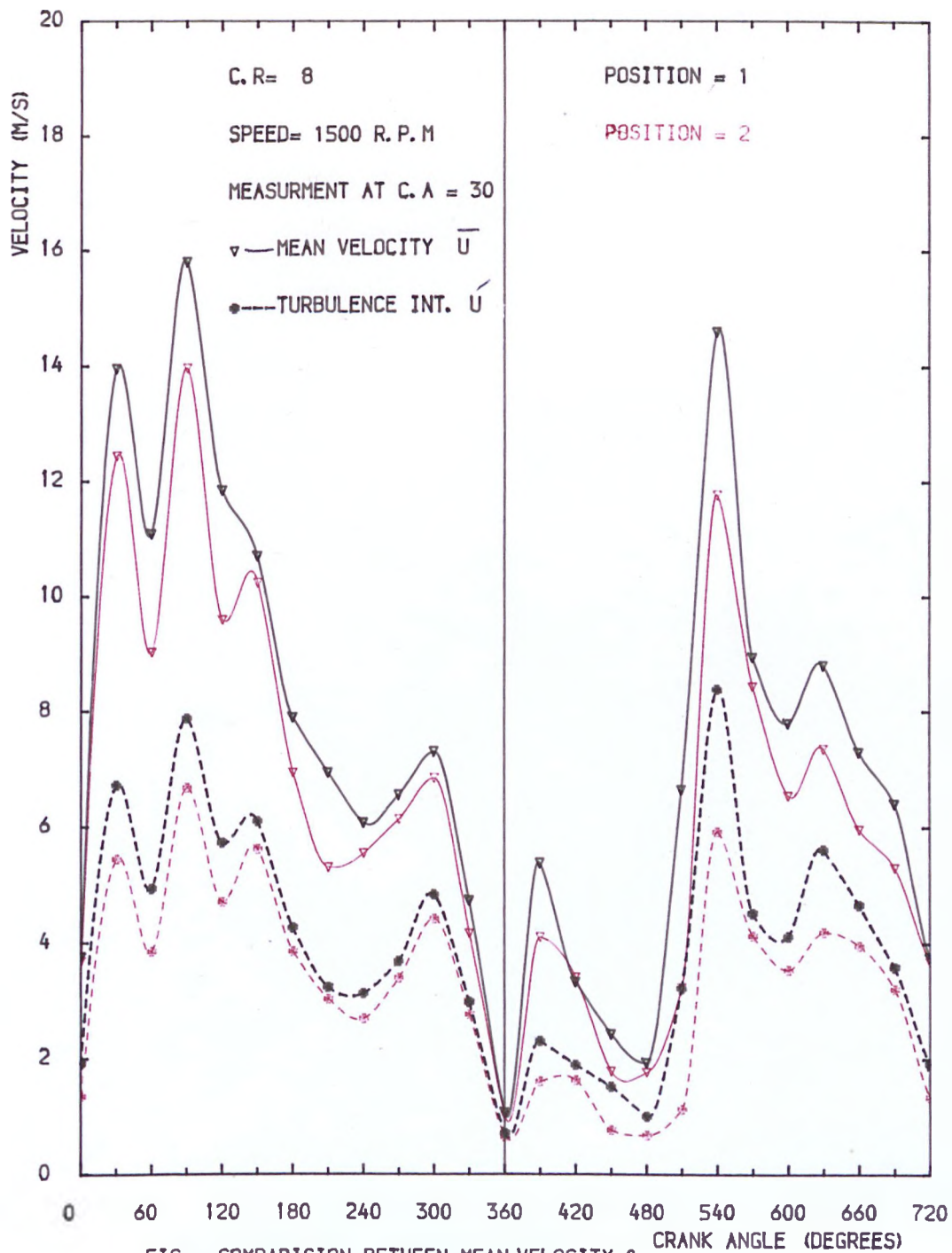


FIG. COMPARISON BETWEEN MEAN VELOCITY & TURBULENCE INT. AT DIFFERENT POSITION

FIG. 9.55

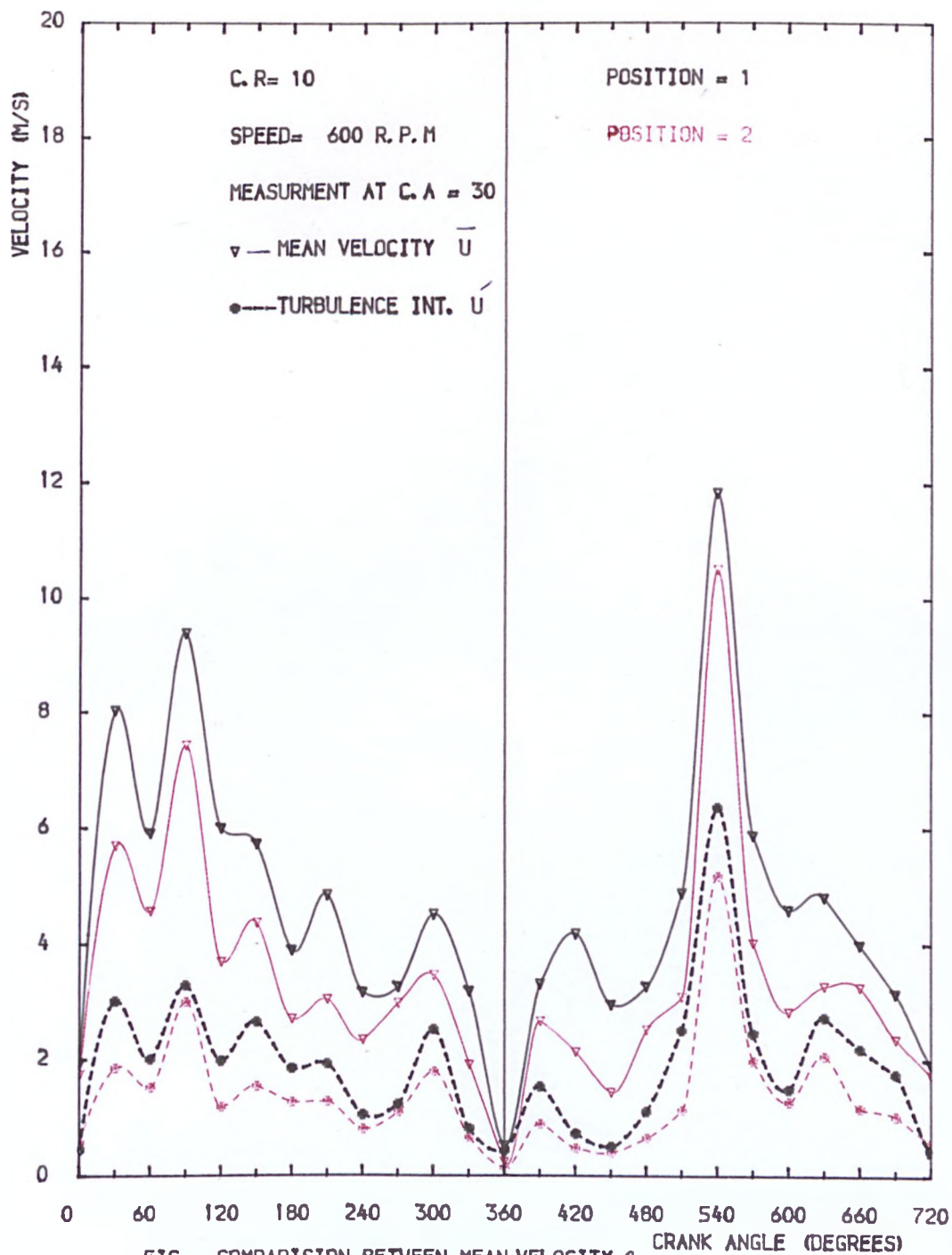


FIG. COMPARISON BETWEEN MEAN VELOCITY & TURBULENCE INT. AT DIFFRENT POSITION

FIG. 9.56

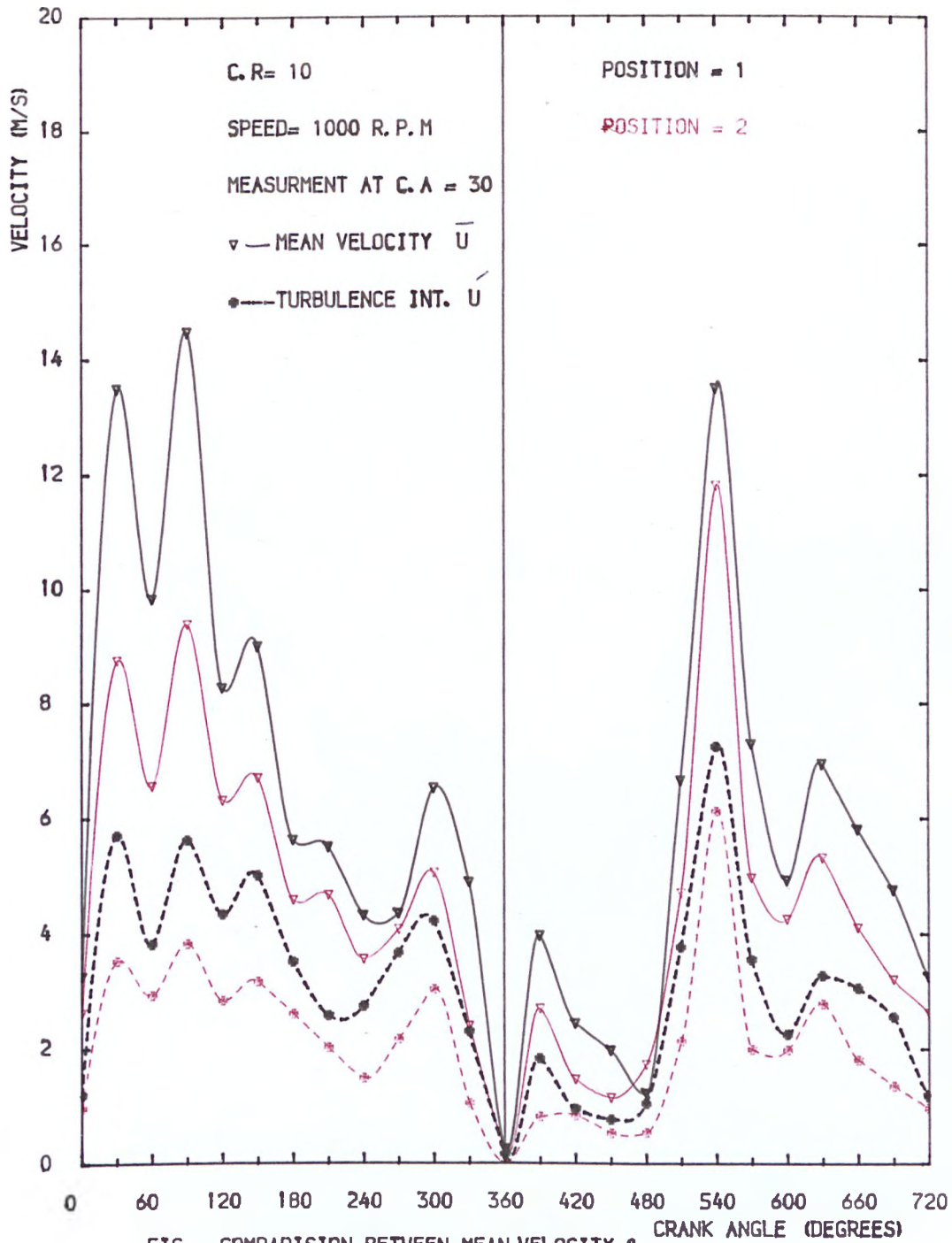


FIG. COMPARISON BETWEEN MEAN VELOCITY & TURBULENCE INT. AT DIFFERENT POSITION

FIG. 9.57

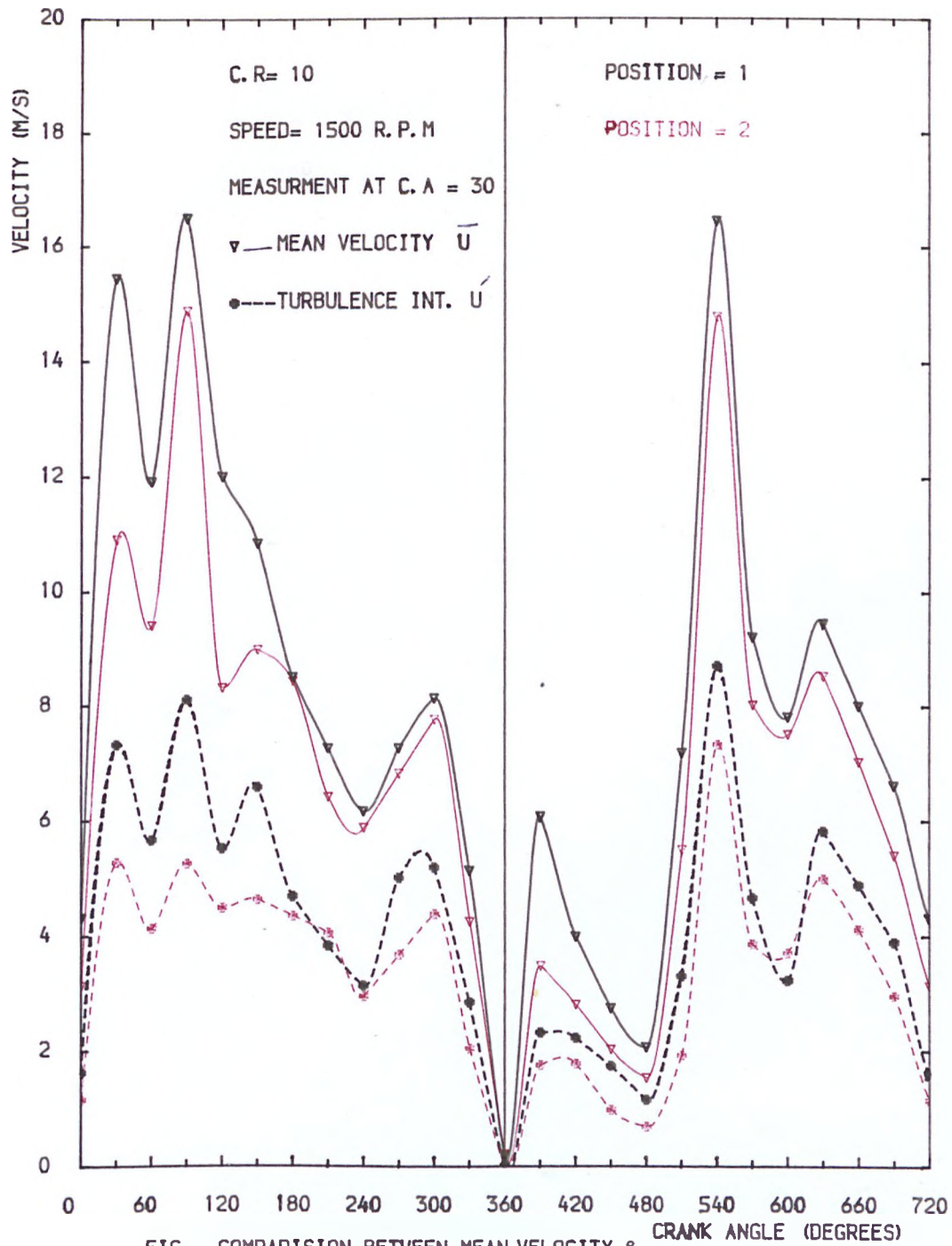


FIG. COMPARISON BETWEEN MEAN VELOCITY & TURBULENCE INT. AT DIFFERENT POSITION

FIG. 9.58

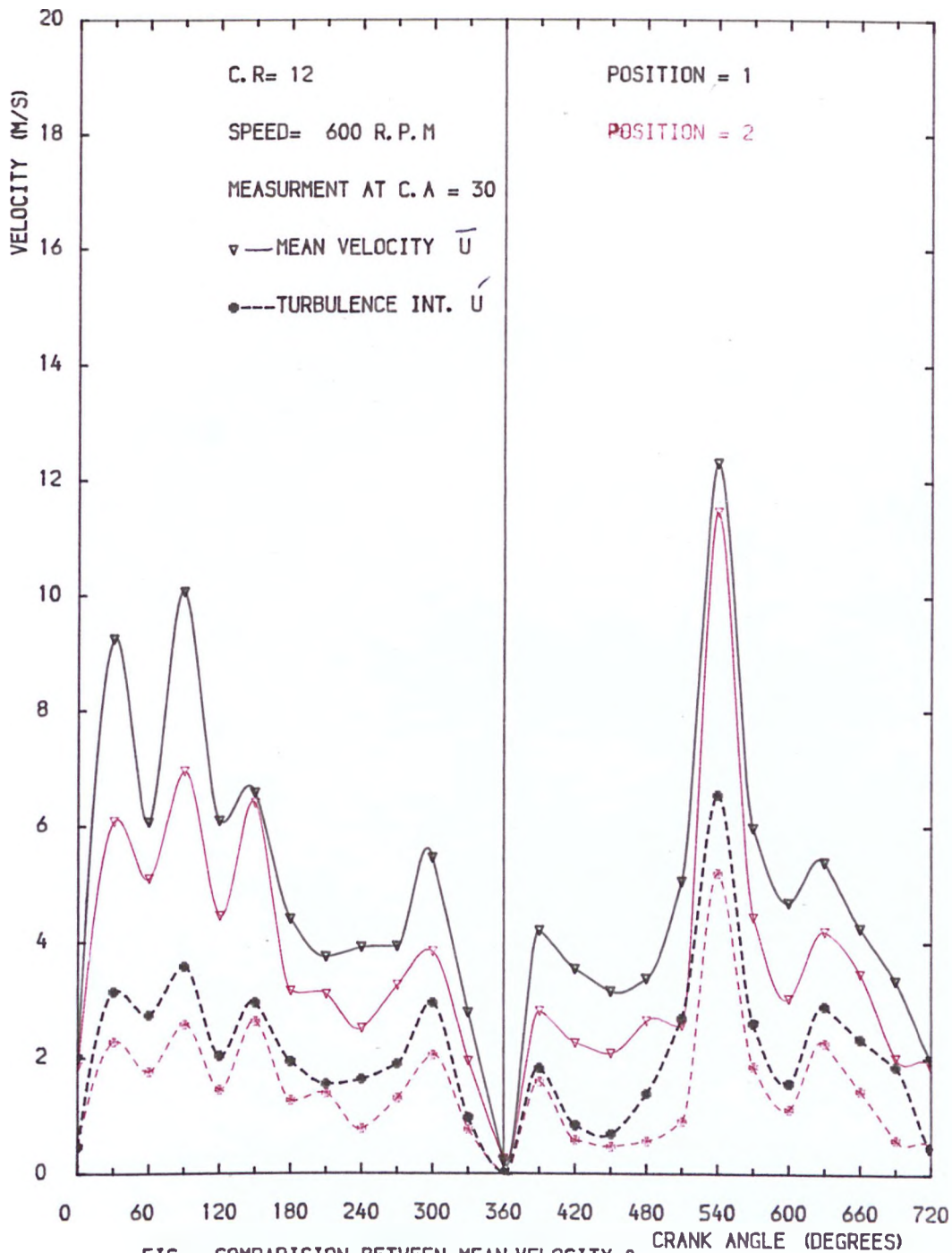


FIG. COMPARISON BETWEEN MEAN VELOCITY & TURBULENCE INT. AT DIFFERENT POSITION

FIG. 9.59

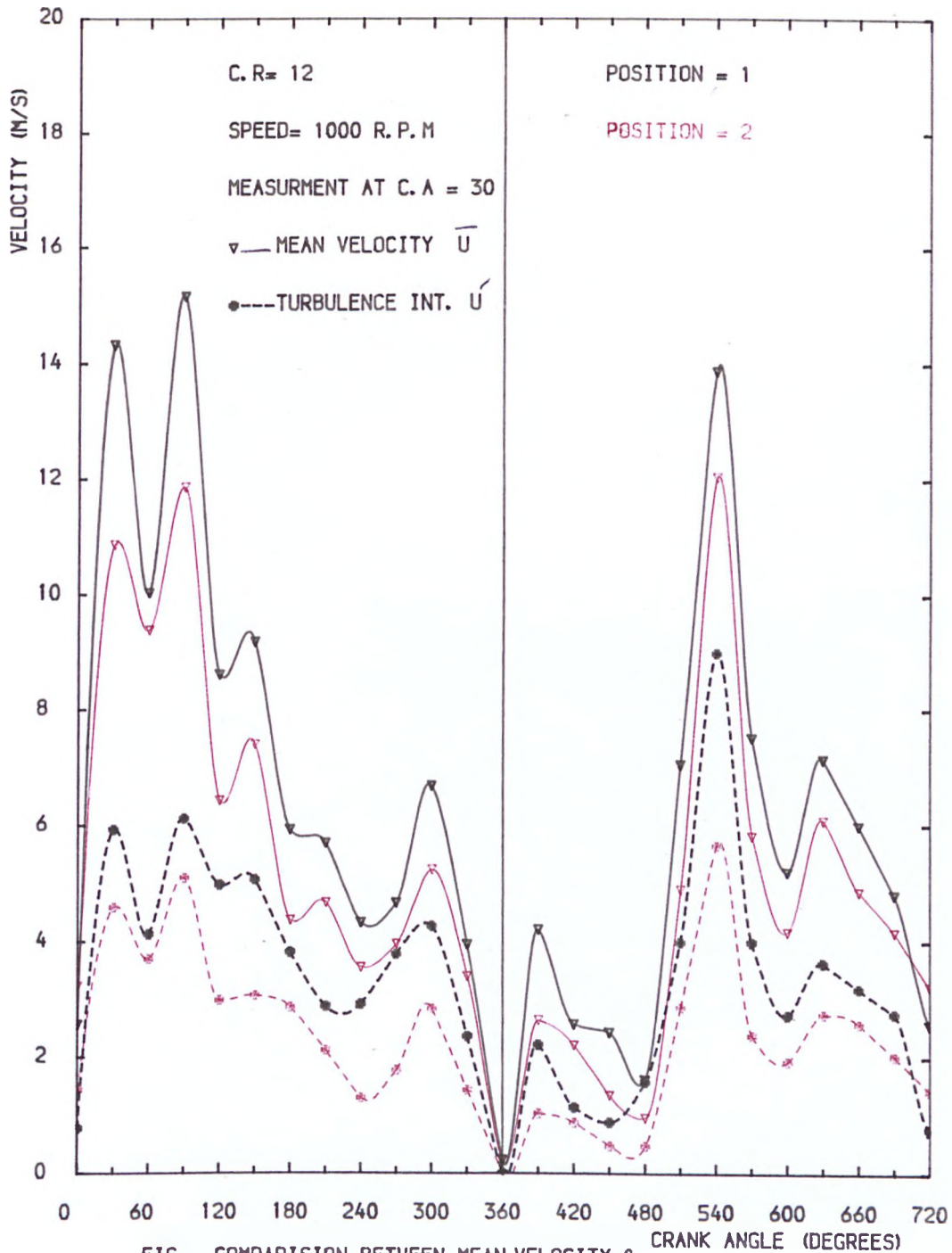


FIG. COMPARISON BETWEEN MEAN VELOCITY & TURBULENCE INT. AT DIFFERENT POSITION

FIG. 9.60

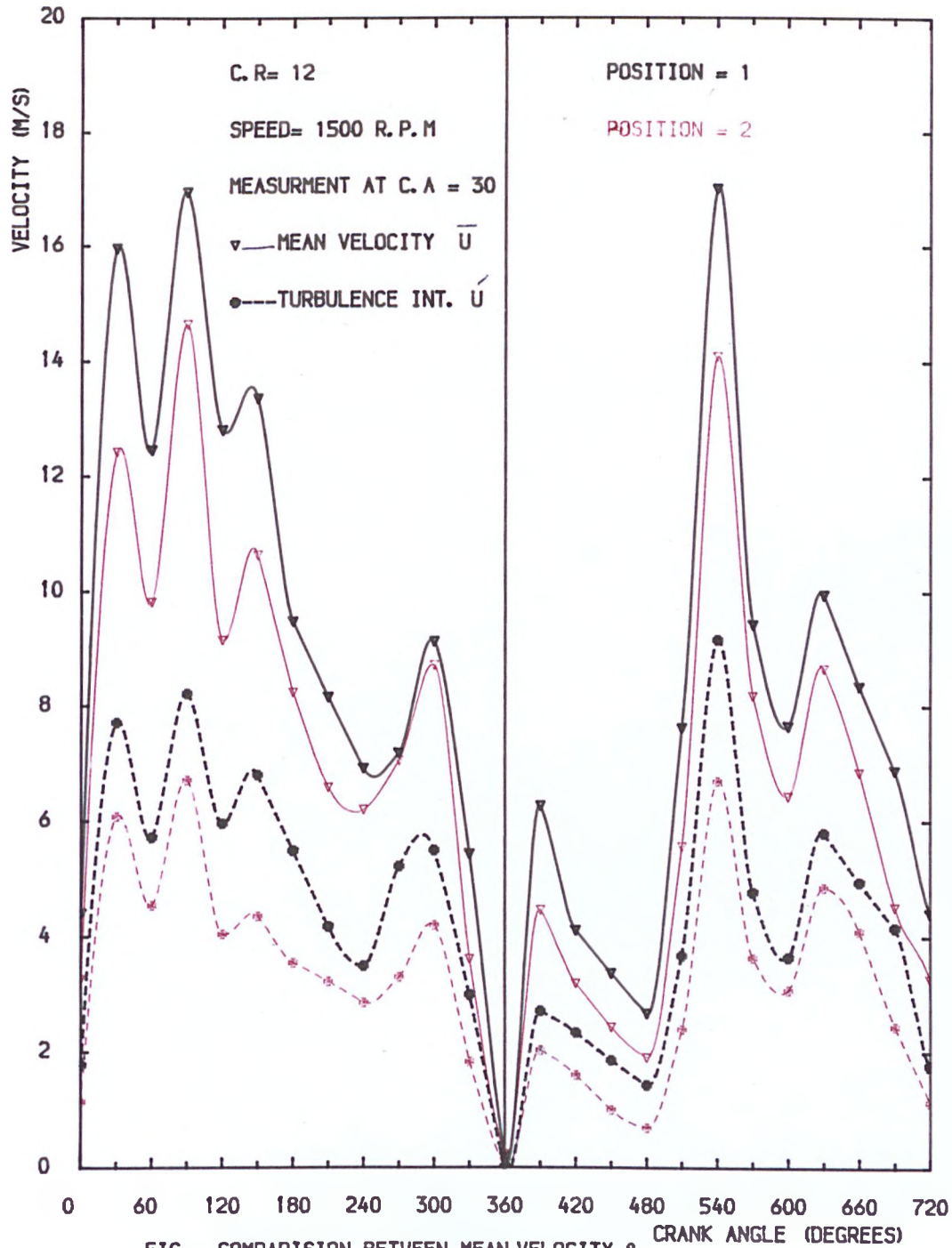


FIG. COMPARISON BETWEEN MEAN VELOCITY & TURBULENCE INT. AT DIFFERENT POSITION

FIG. 9.61

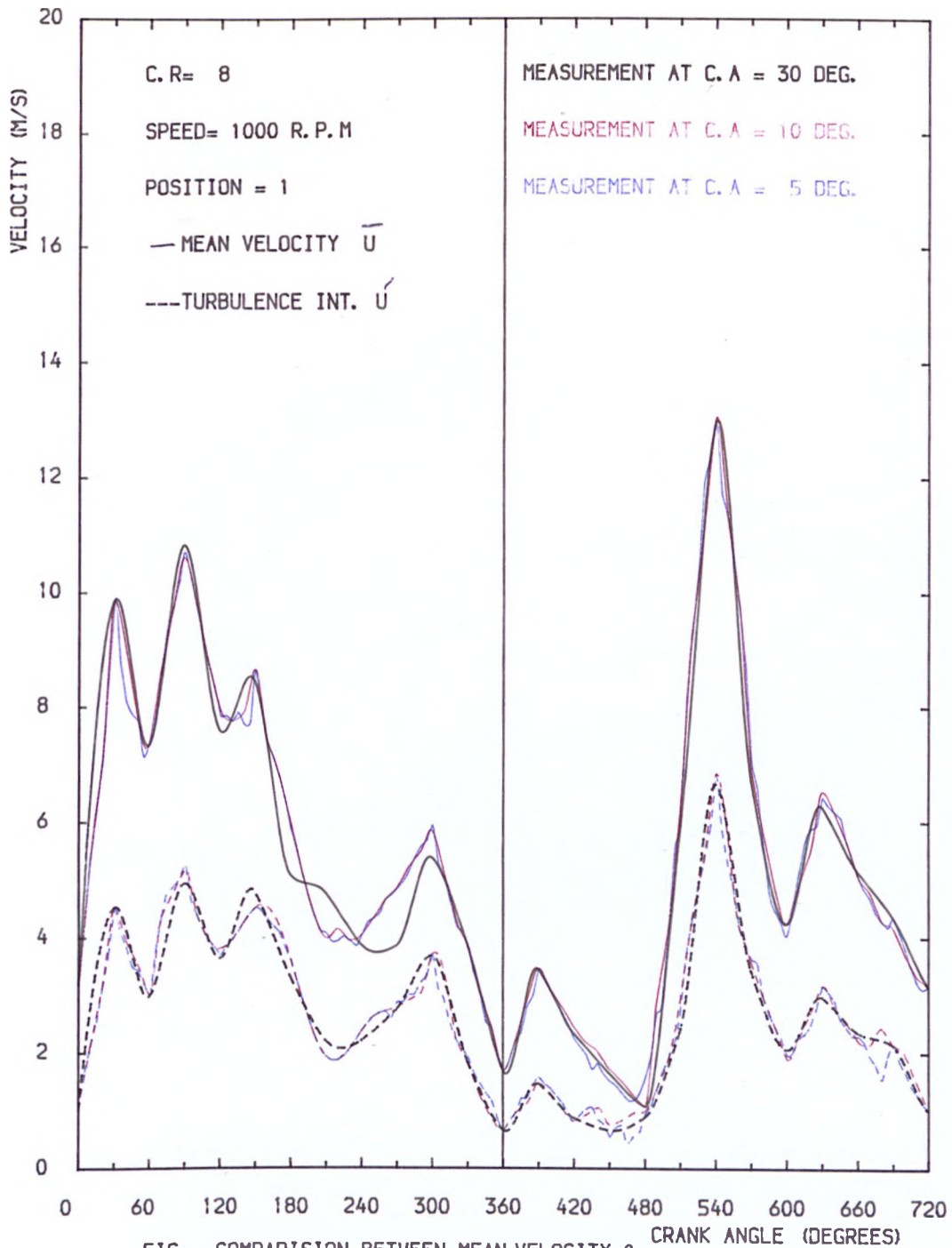


FIG. COMPARISON BETWEEN MEAN VELOCITY & TURBULENCE INT. AT DIFFRENT C.A MEASUREMENT

FIG. 9.62

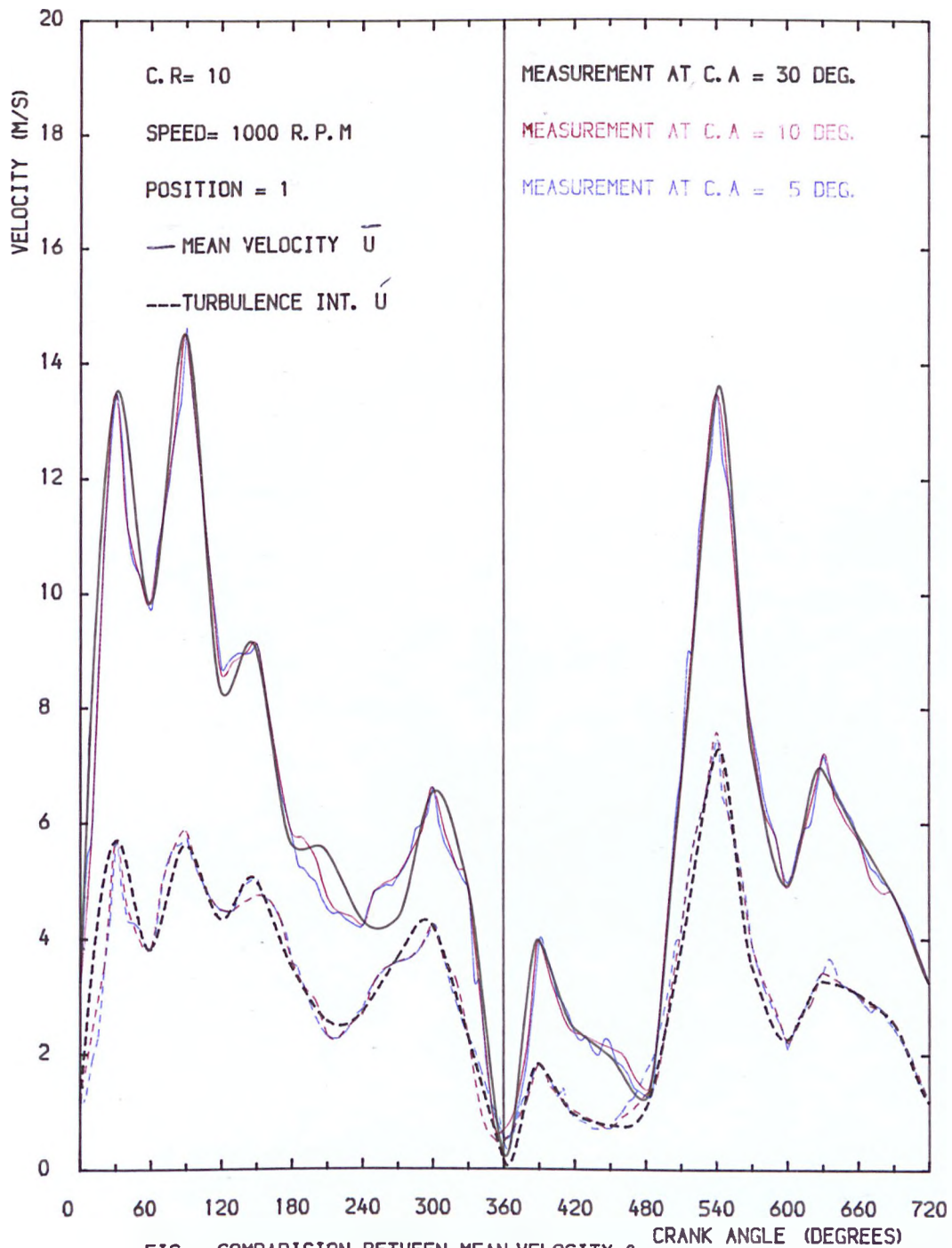


FIG. COMPARISON BETWEEN MEAN VELOCITY & TURBULENCE INT. AT DIFFERENT C.A MEASUREMENT

FIG. 9.63

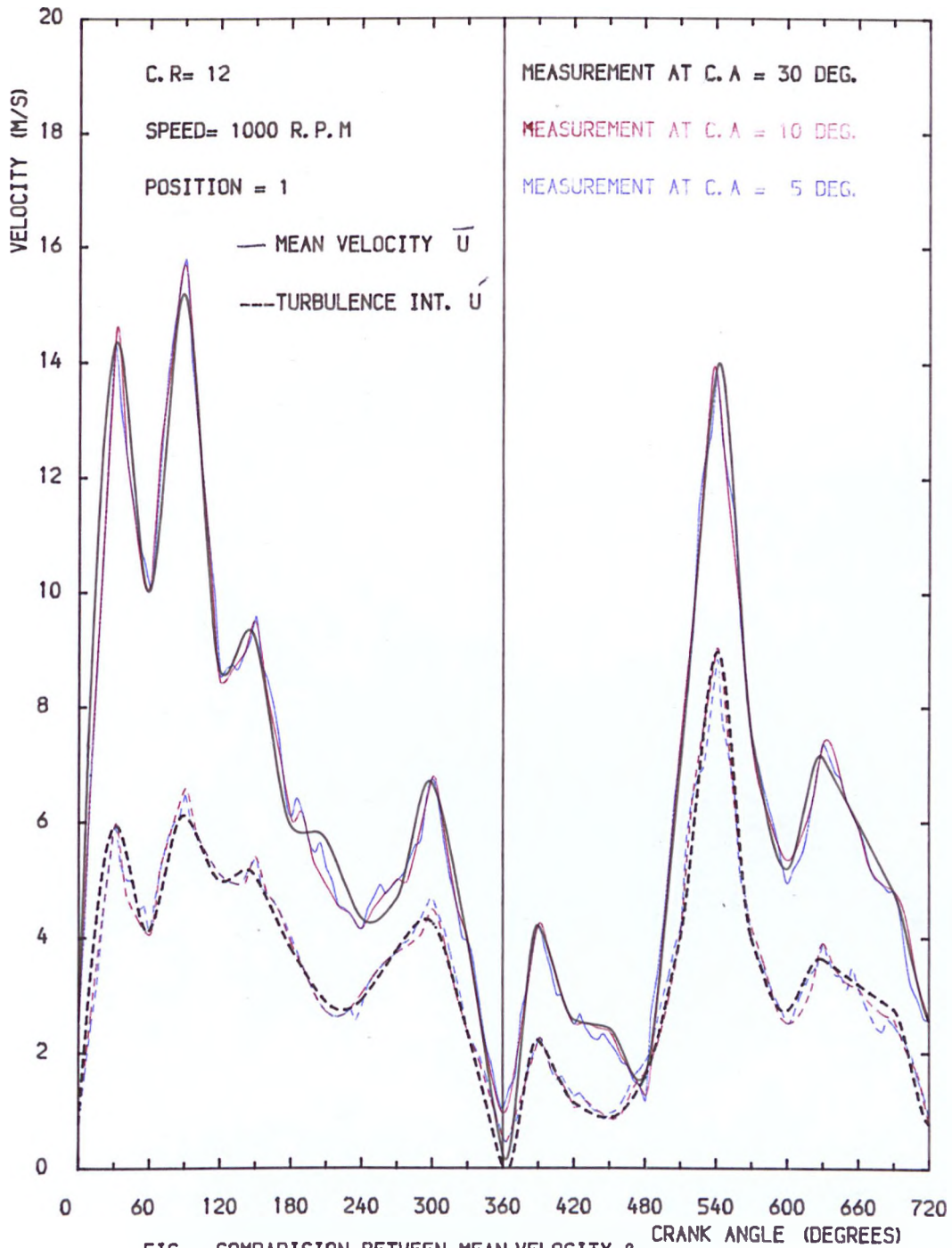


FIG. COMPARISON BETWEEN MEAN VELOCITY & TURBULENCE INT. AT DIFFRENT C.A MEASUREMENT

FIG. 9.64

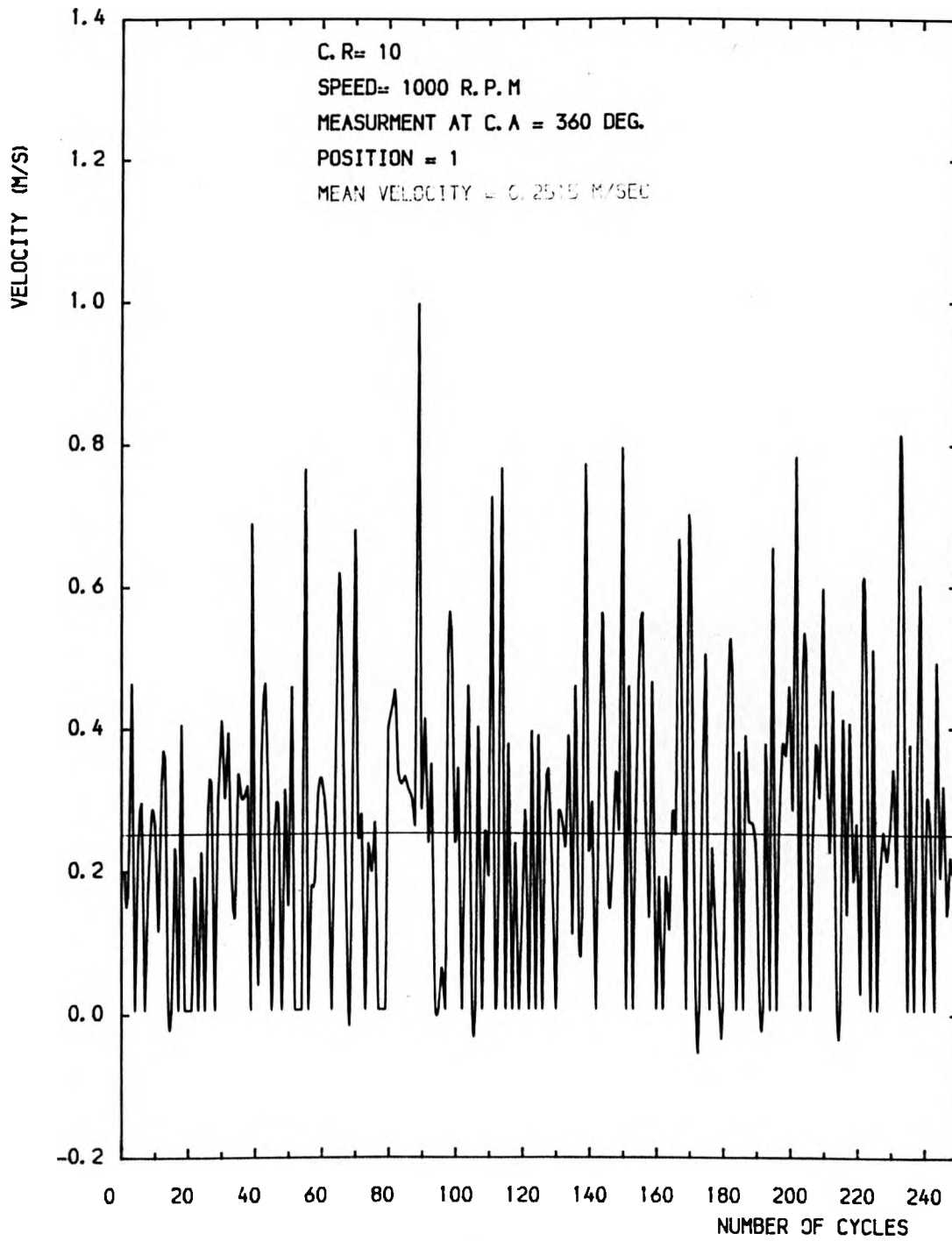


FIG. INSTANTANEOUS VELOCITY OVER MANY CYCLES

FIG. 9.65

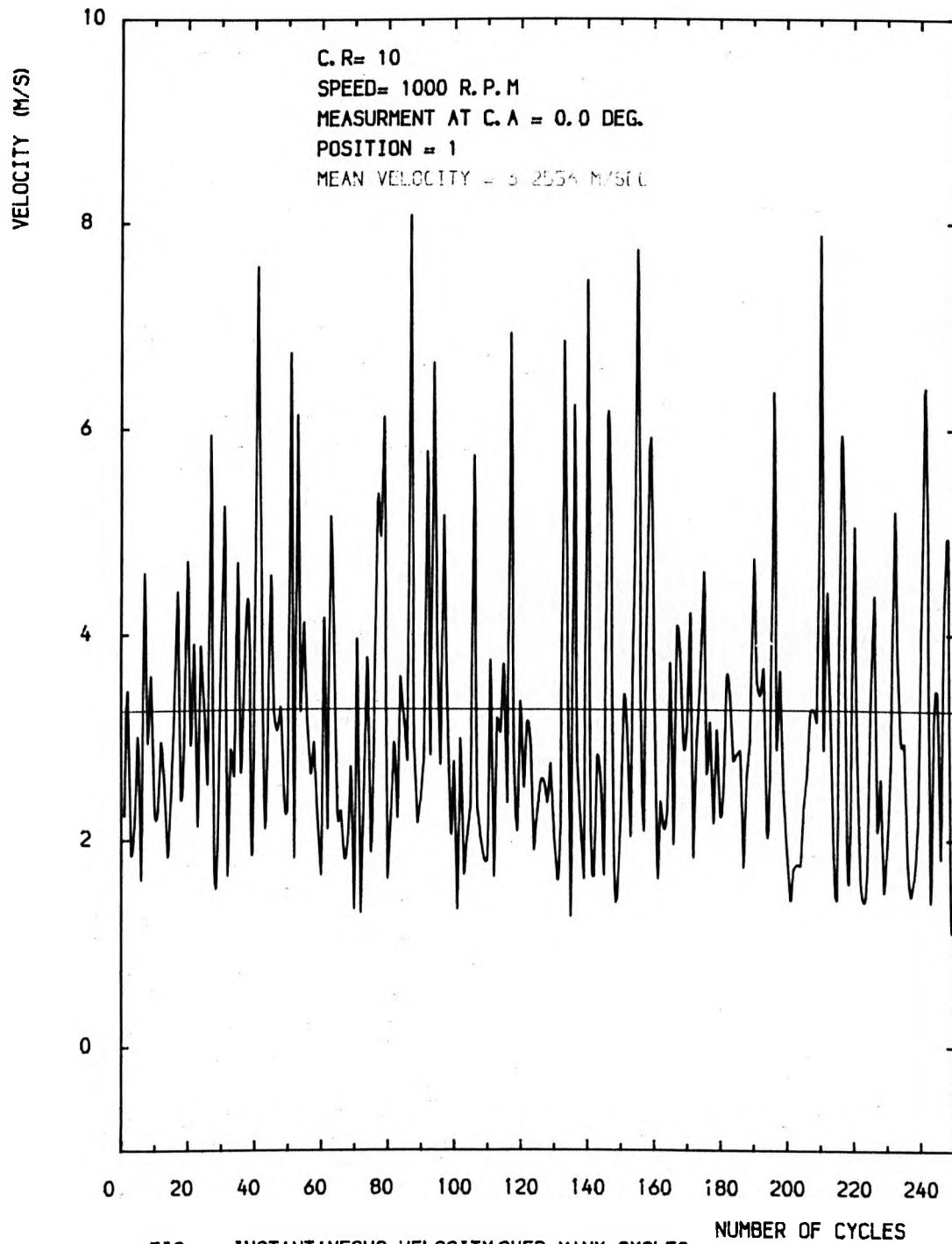


FIG. 9.66

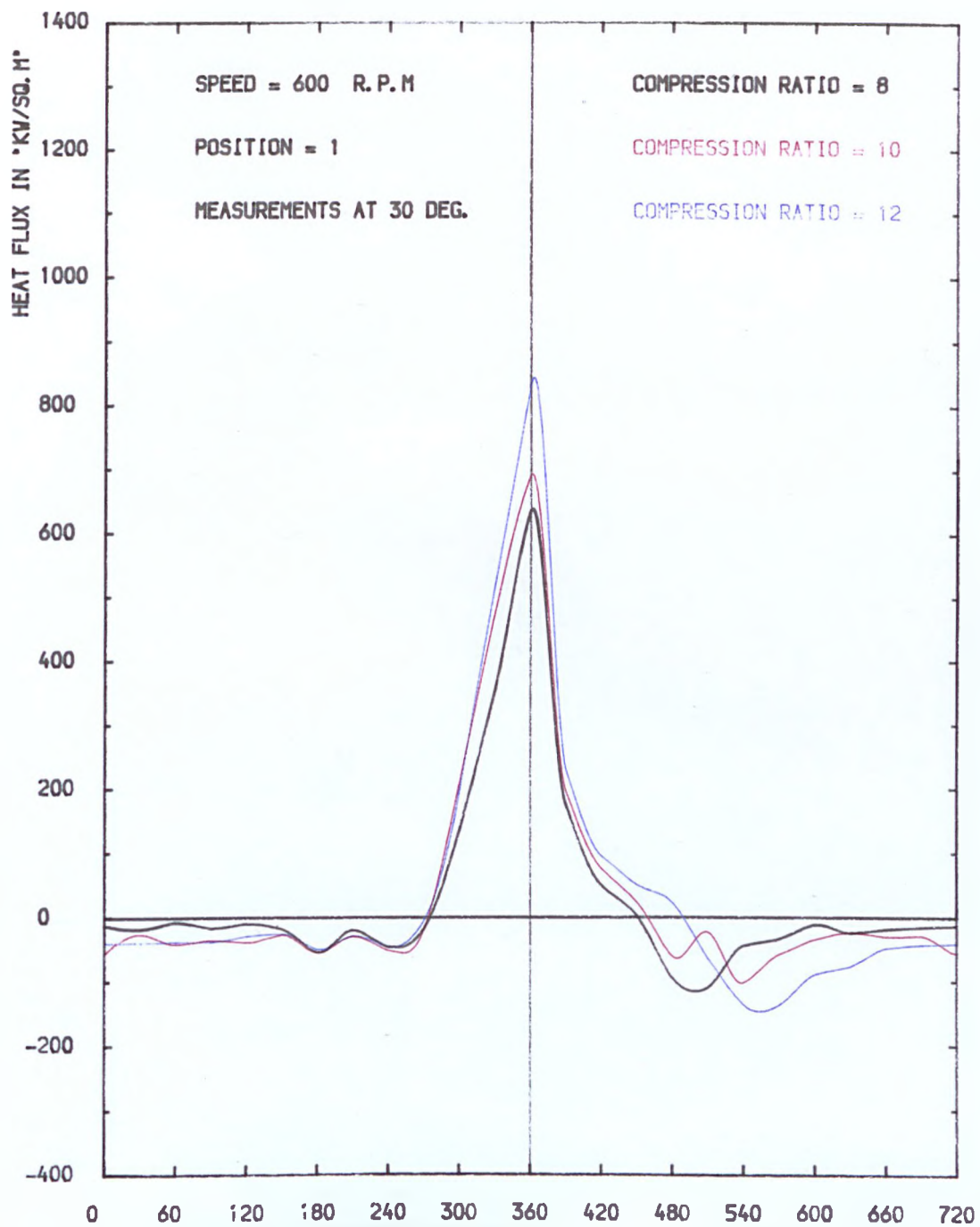


FIG. 9.66 COMPARASSION BETWEEN
HEAT FLUX AT DIFFERENT C. R

FIG. 9.67

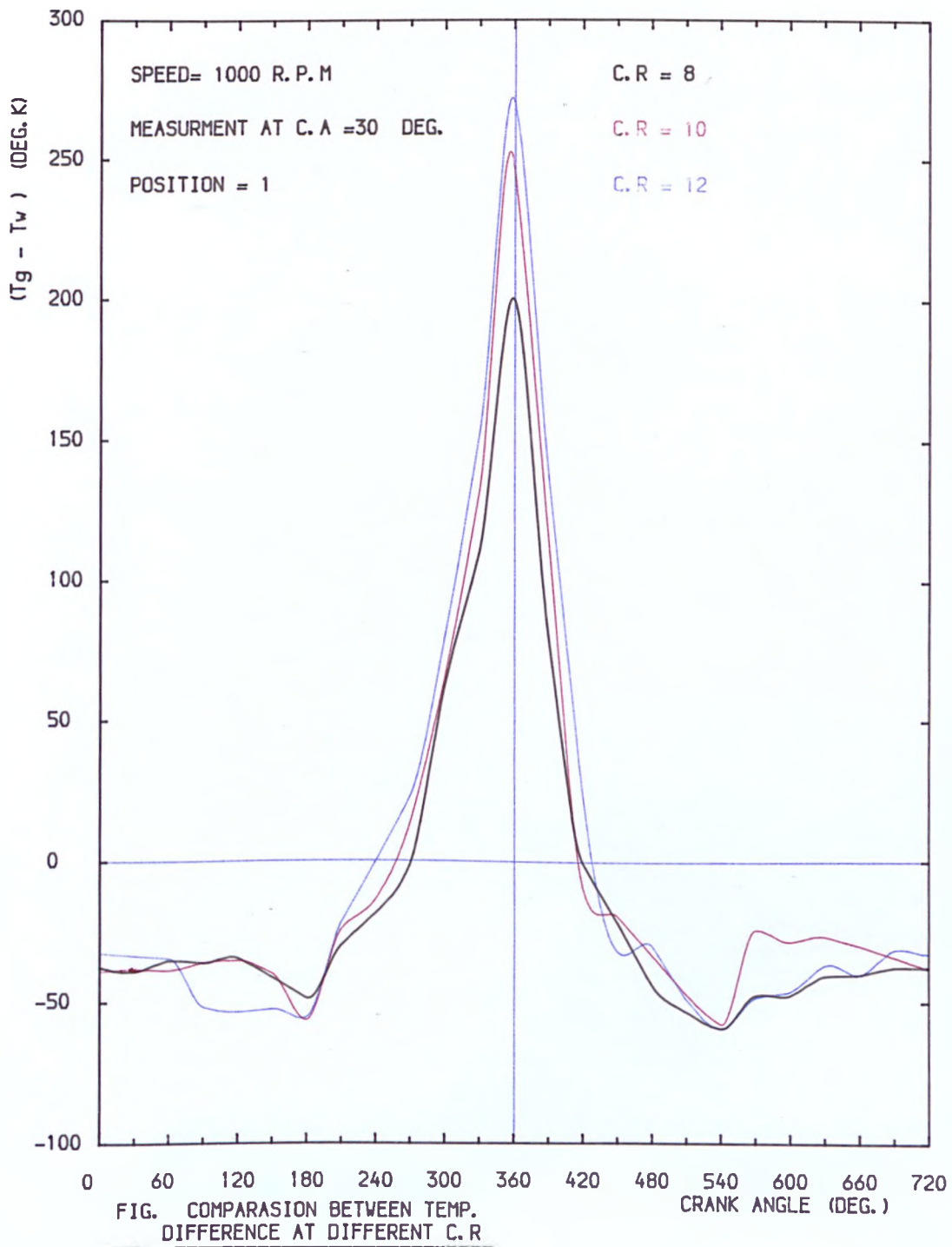


FIG. 9.68

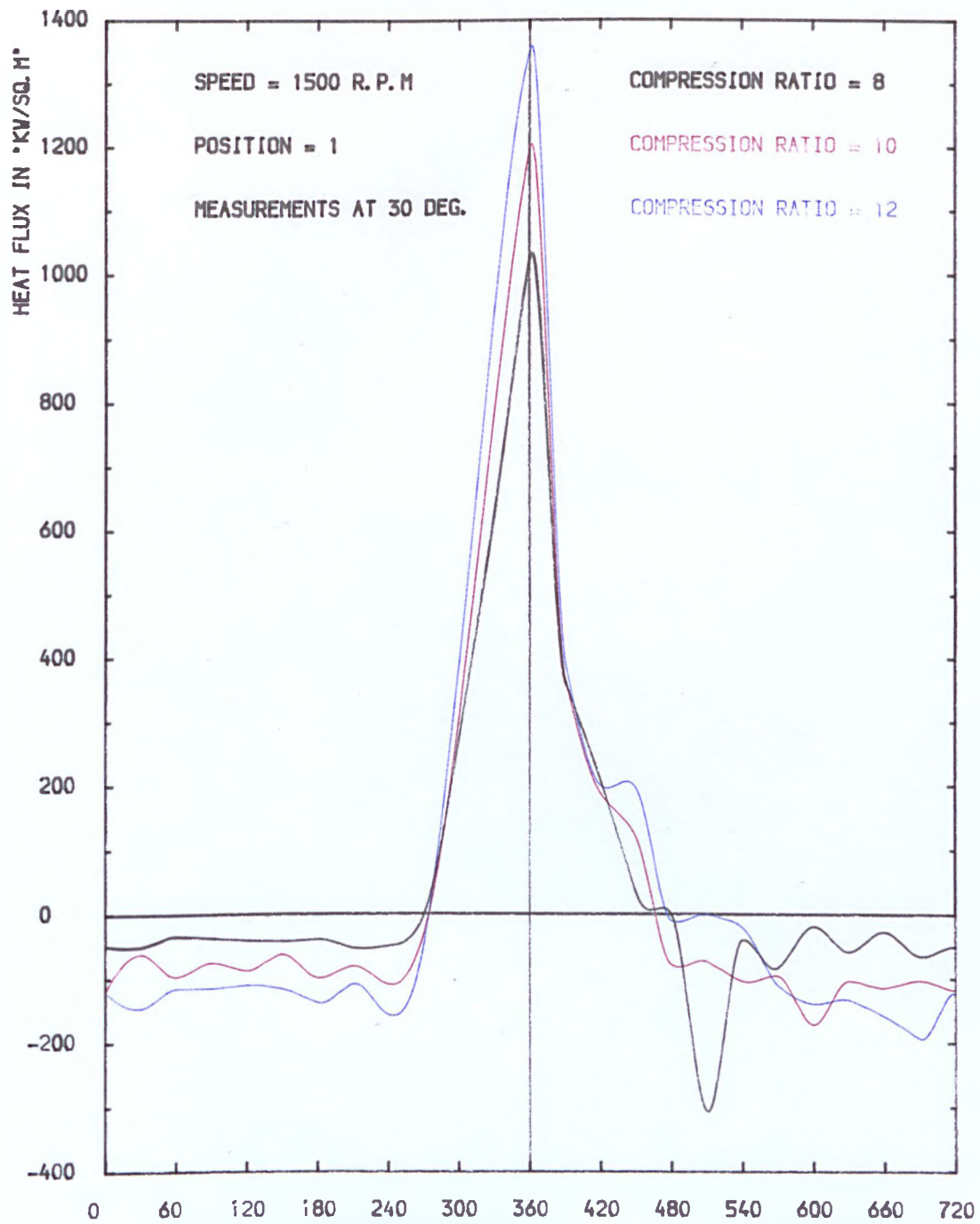


FIG. 9.68 COMPARASSION BETWEEN
HEAT FLUX AT DIFFERENT C. R.

CRANK ANGLE (DEGREES)

FIG. 9.69

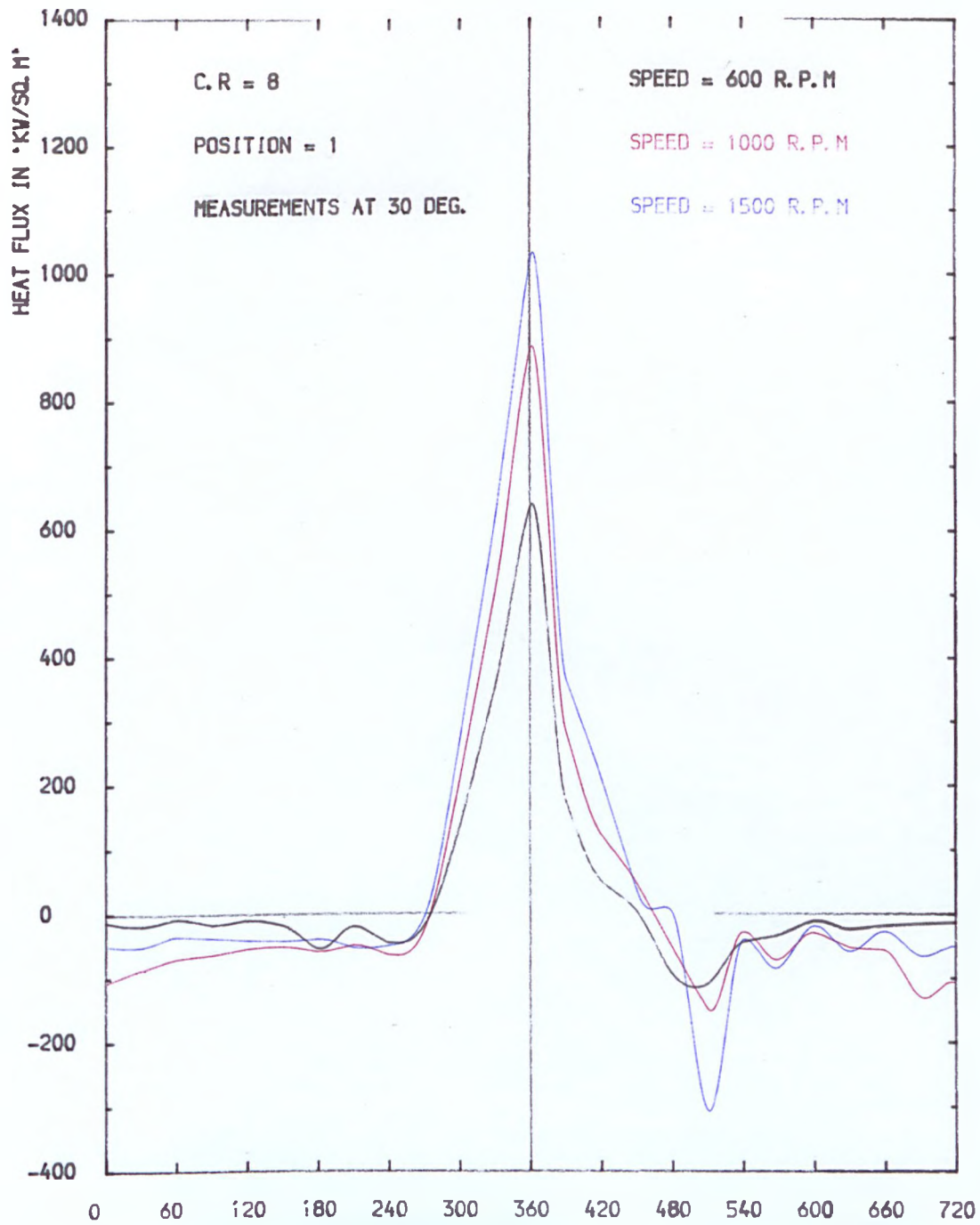


FIG. 9.69 COMPARASSION BETWEEN
HEAT FLUX AT DIFFERENT SPEEDS

CRANK ANGLE (DEGREES)

FIG. 9.70

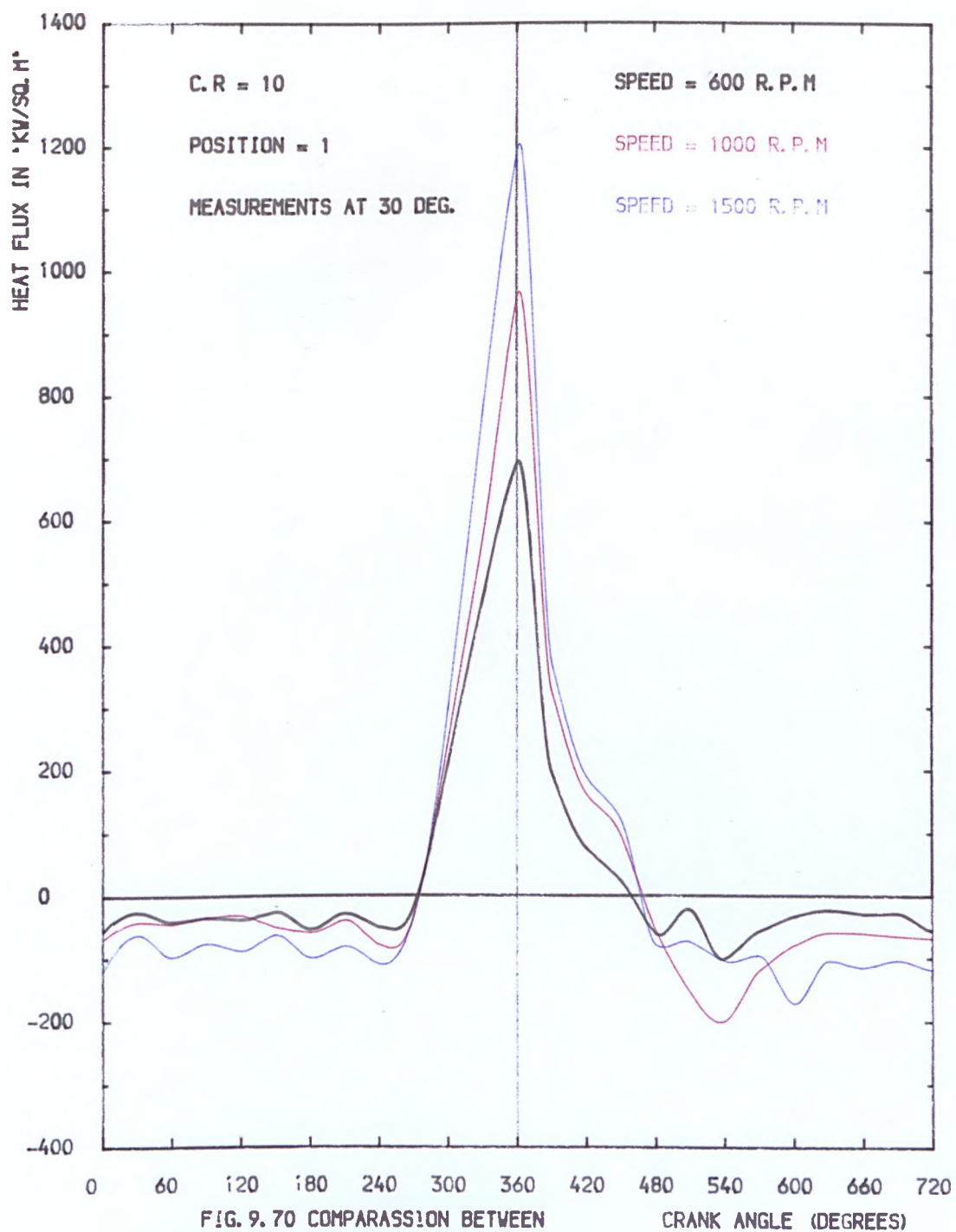


FIG. 9.70 COMPARASSION BETWEEN
HEAT FLUX AT DIFFERENT SPEEDS

FIG. 9.71

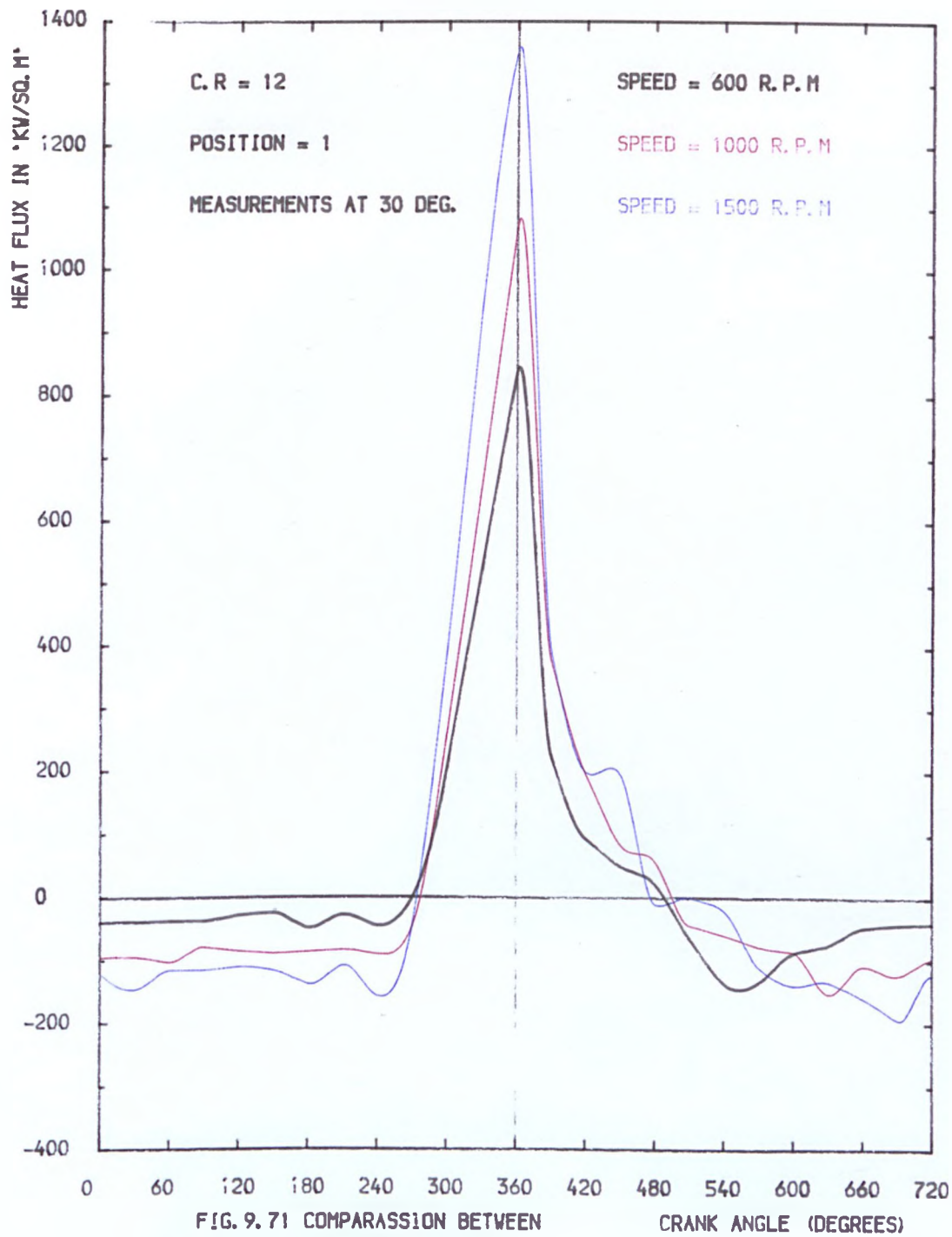


FIG. 9.71 COMPARASSION BETWEEN
HEAT FLUX AT DIFFERENT SPEEDS

FIG. 9.72

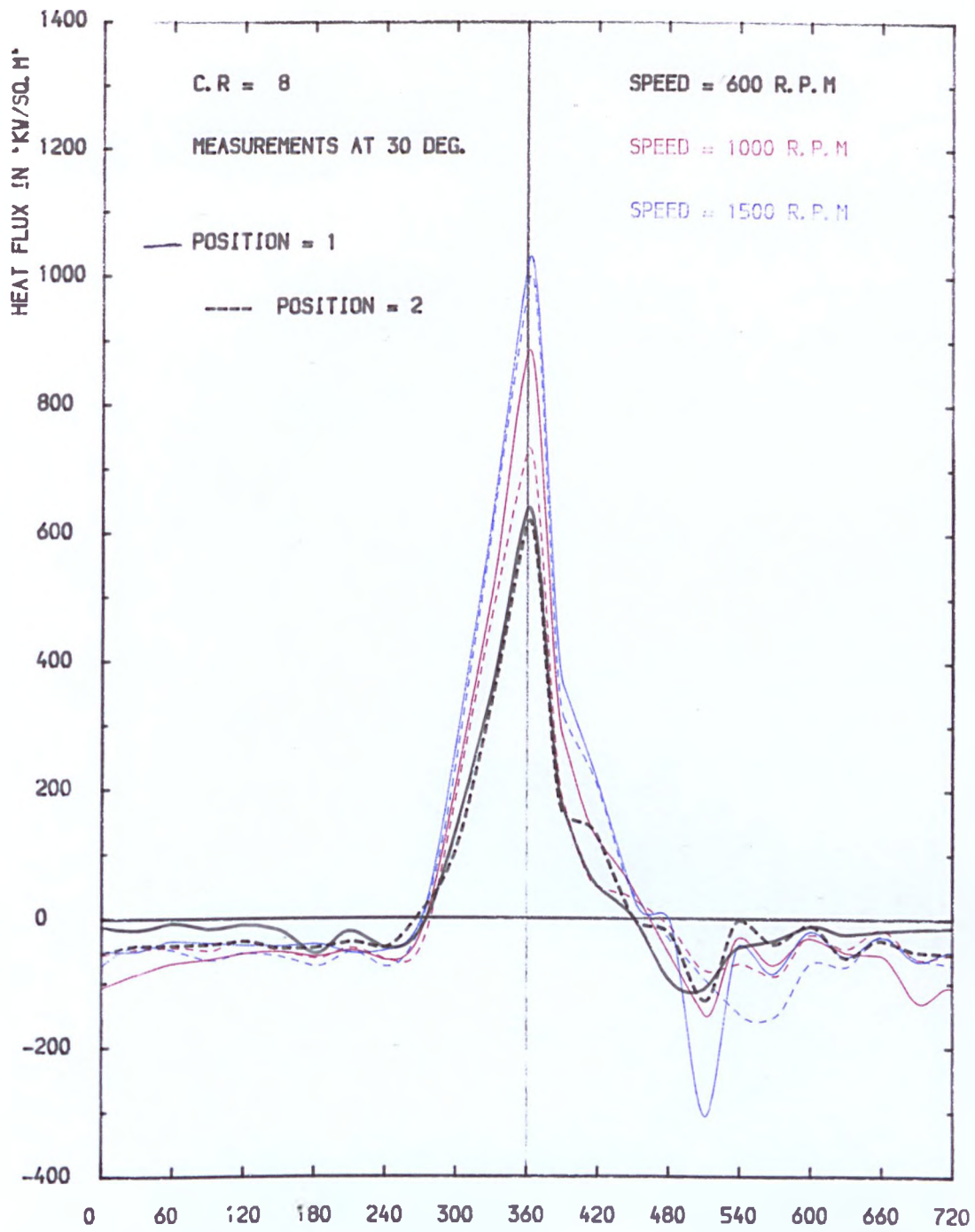


FIG. 9.72 COMPARASSION BETWEEN
HEAT FLUX AT DIFFERENT POSITION

CRANK ANGLE (DEGREES)

FIG. 9.73

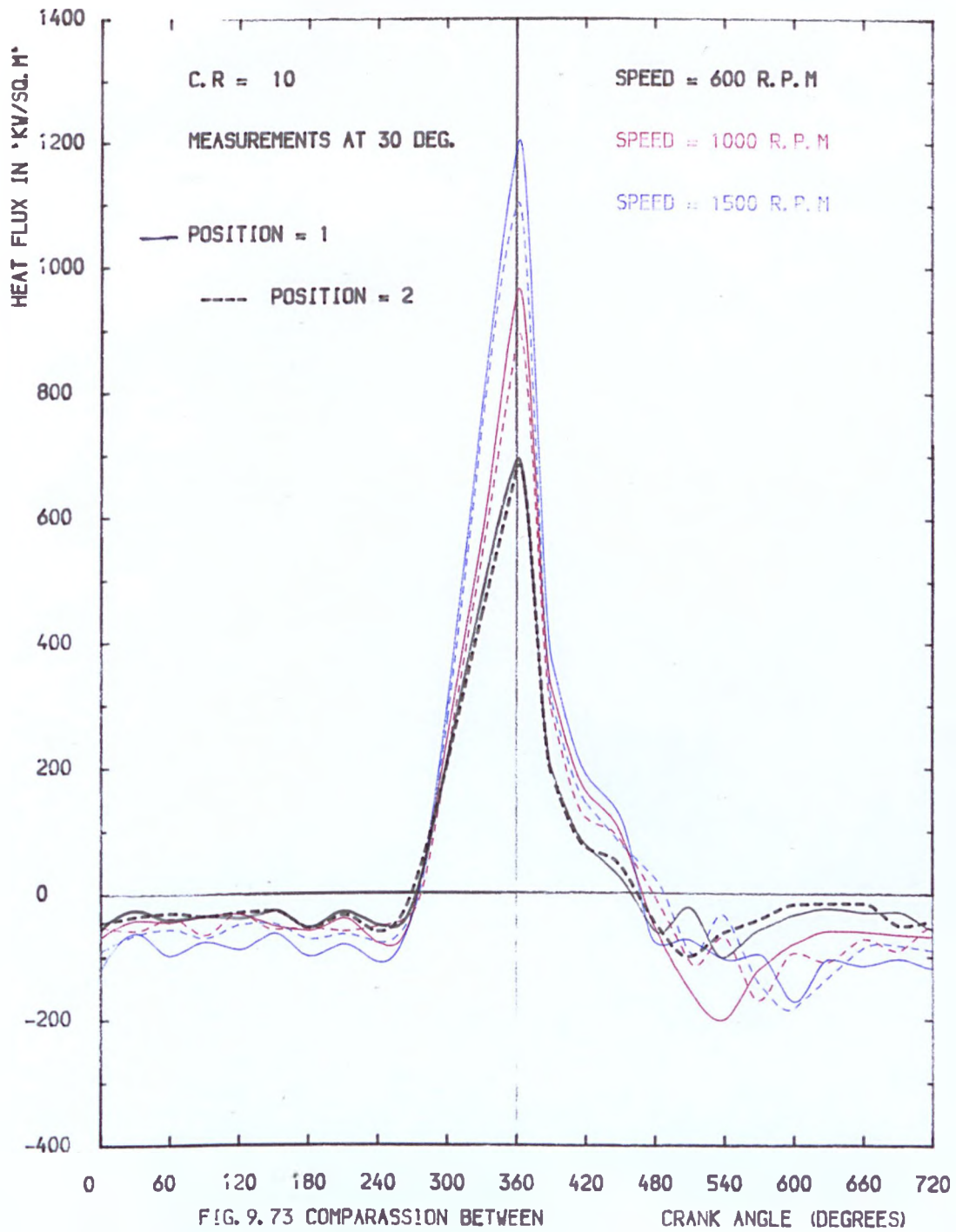


FIG. 9.74

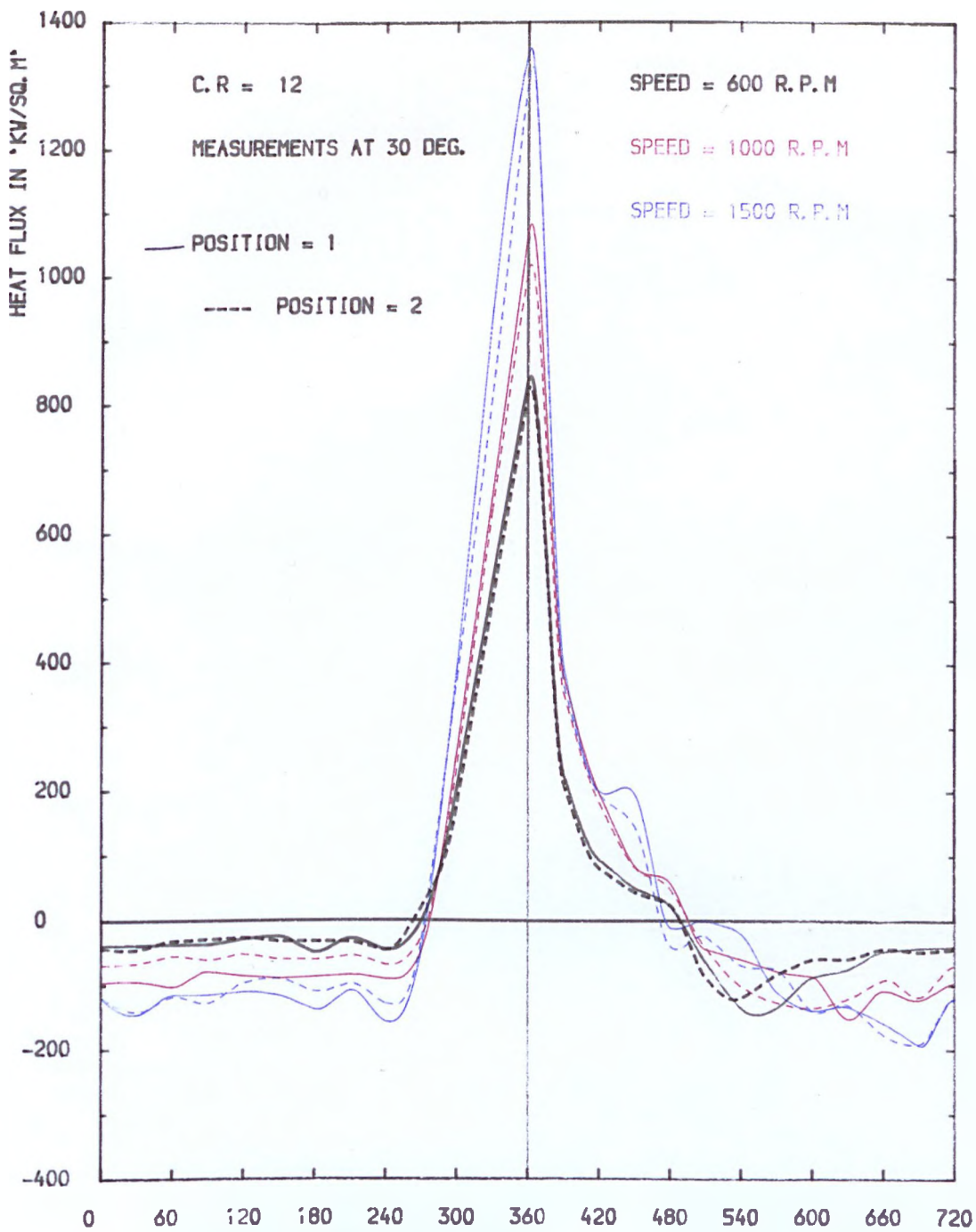


FIG. 9.74 COMPARASSION BETWEEN HEAT FLUX AT DIFFERENT POSITION

FIG. 9.75

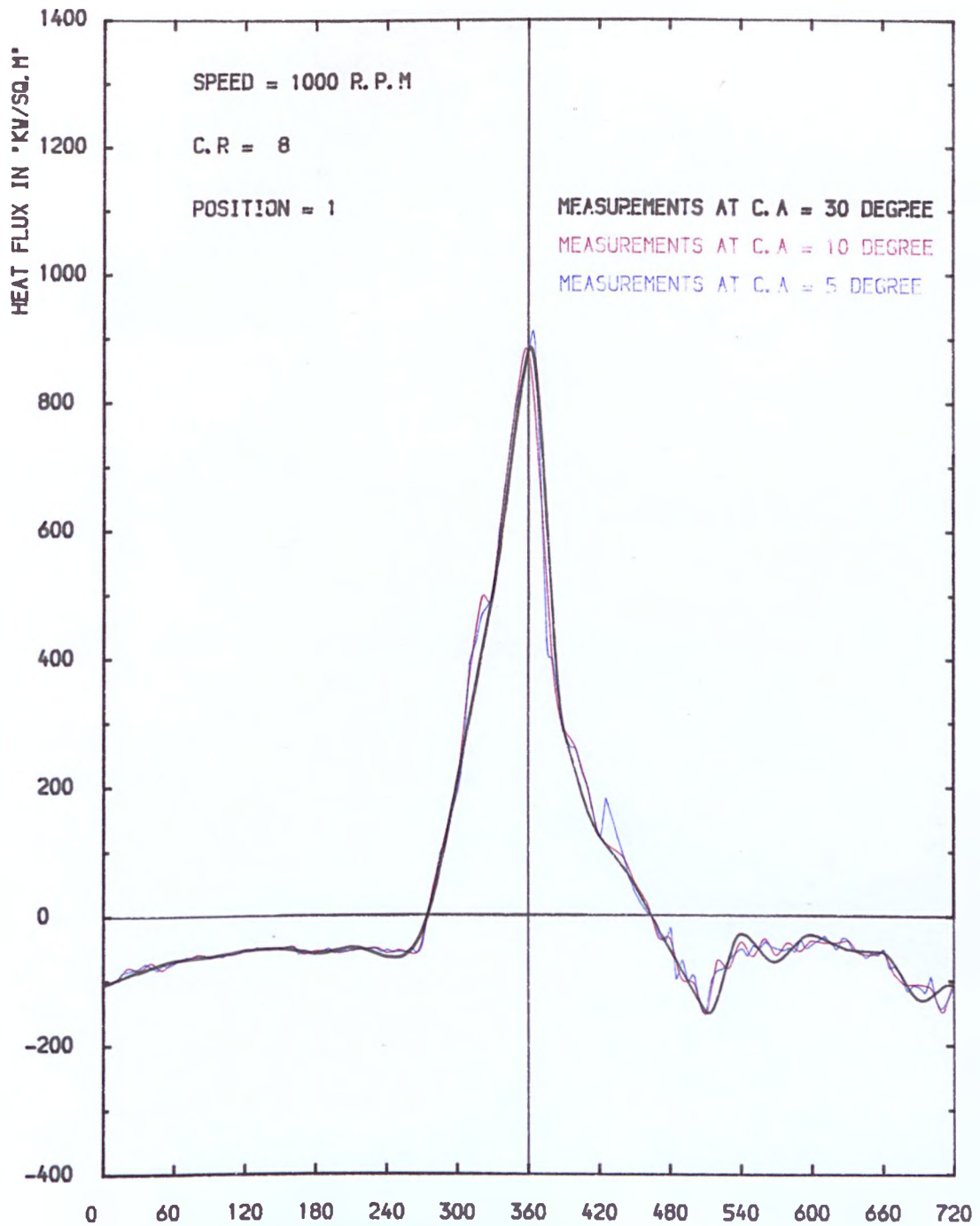


FIG. 9.75 COMPARASSION BETWEEN HEAT FLUX AT DIFFERENT C. A MEASUREMENTS

CRANK ANGLE (DEGREES)

FIG. 9.76

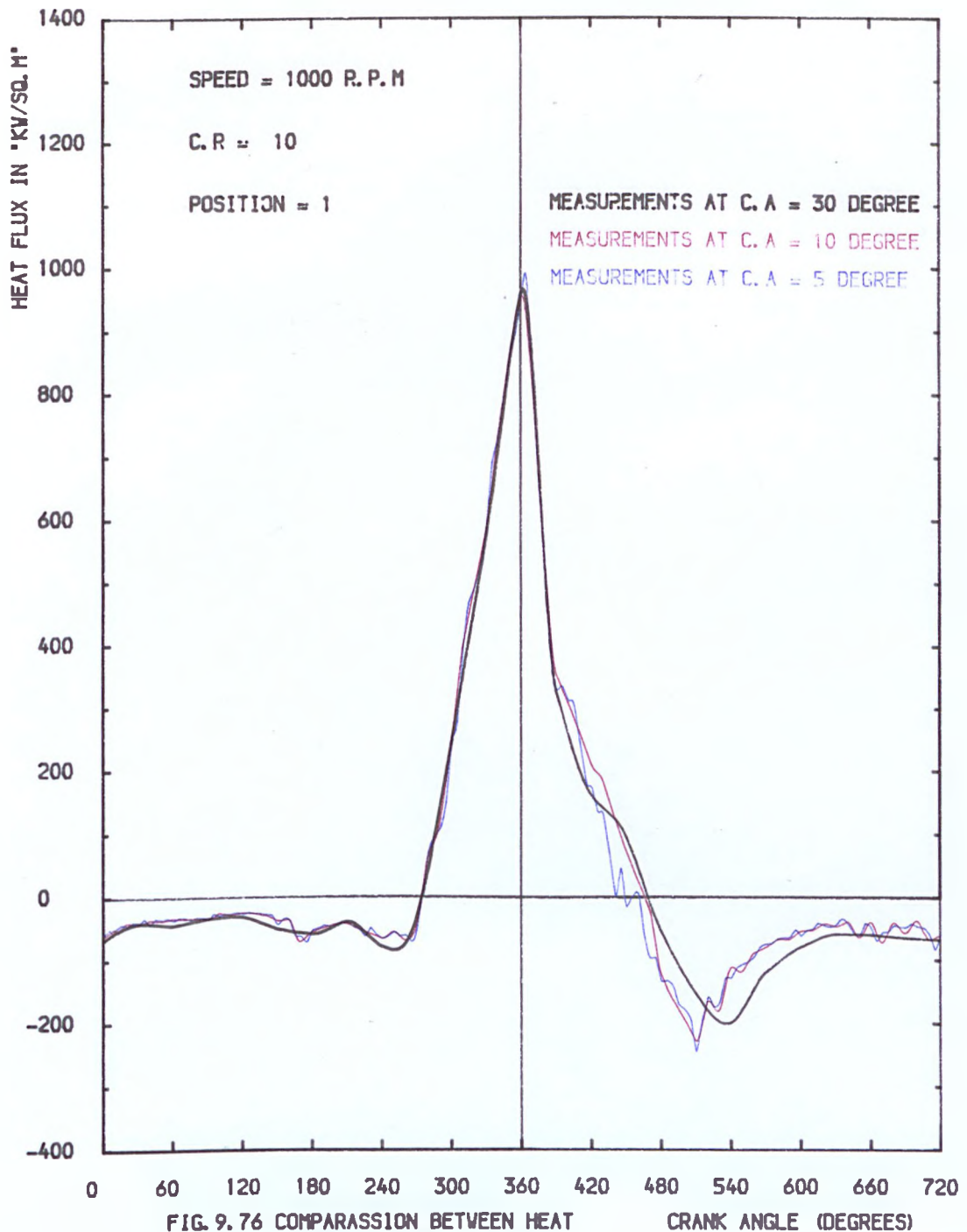


FIG. 9.76 COMPARASSION BETWEEN HEAT FLUX AT DIFFERENT C. A MEASUREMENTS

FIG. 9.77

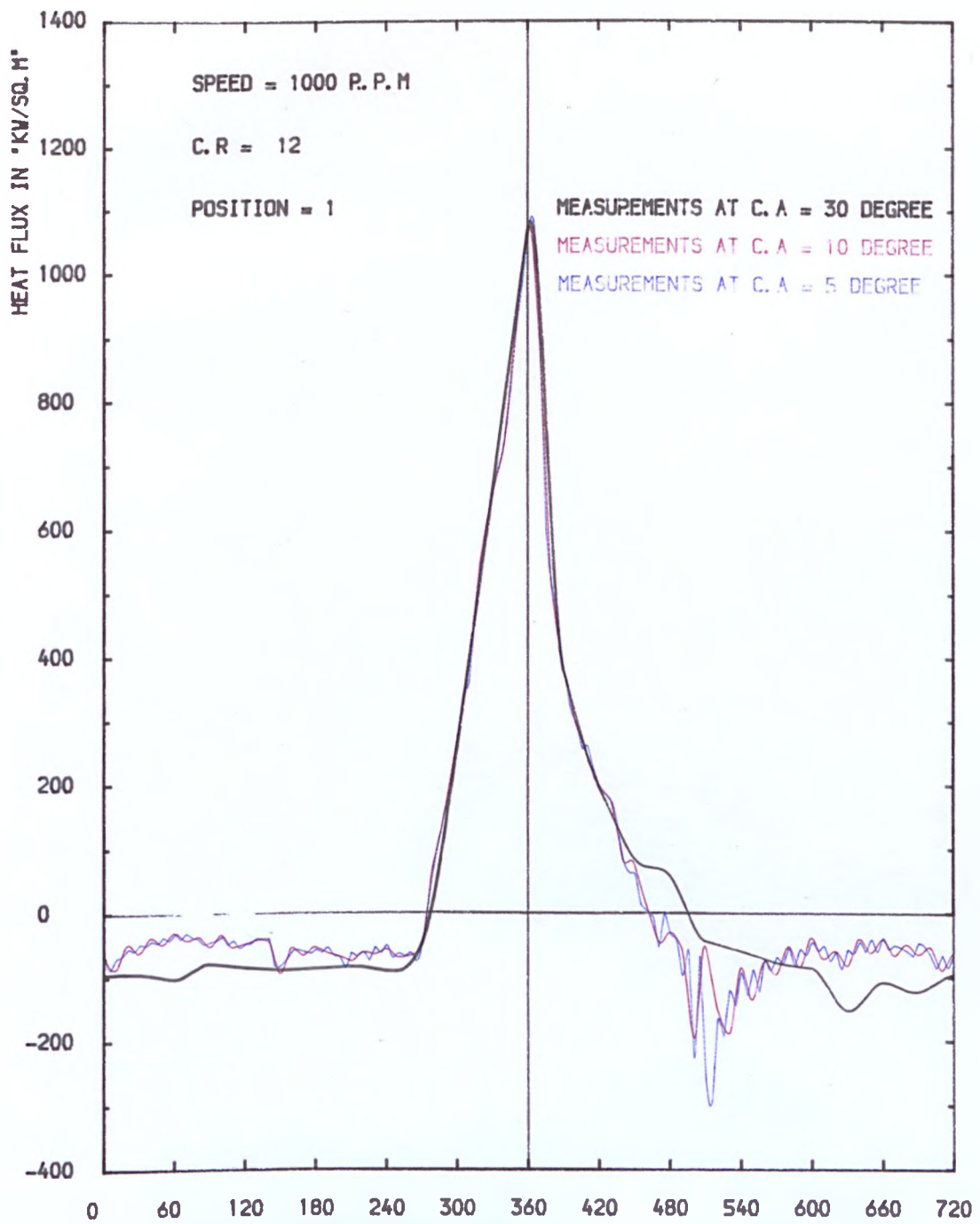


FIG. 9.77 COMPARASSION BETWEEN HEAT FLUX AT DIFFERENT C. A MEASUREMENTS

CRANK ANGLE (DEGREES)

FIG. 9.78

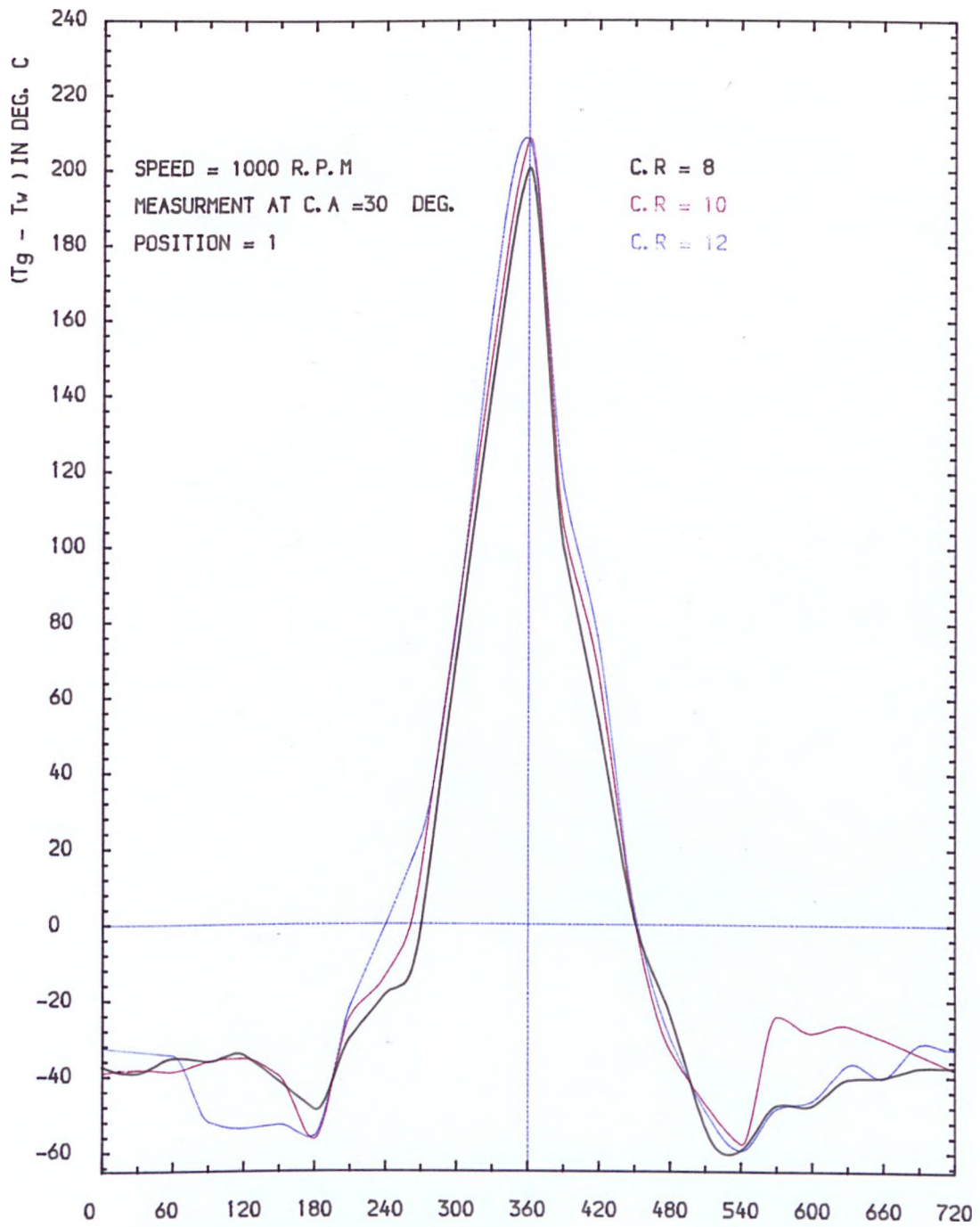


FIG. COMPARASION BETWEEN $(T_g - T_w)$ AT DIFFERENT COMPRESSION RATIOS

FIG. 9.79

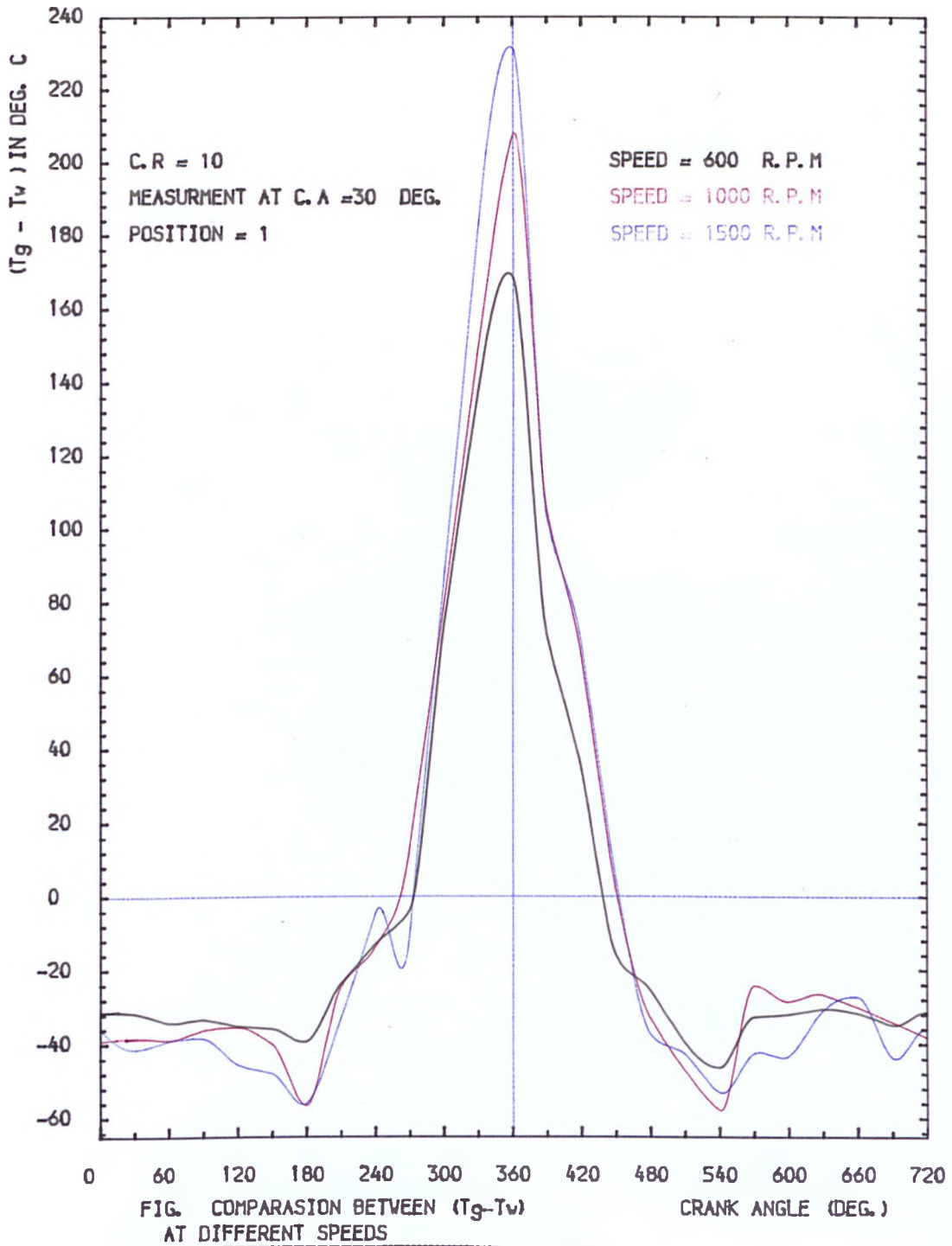


FIG. 9.80

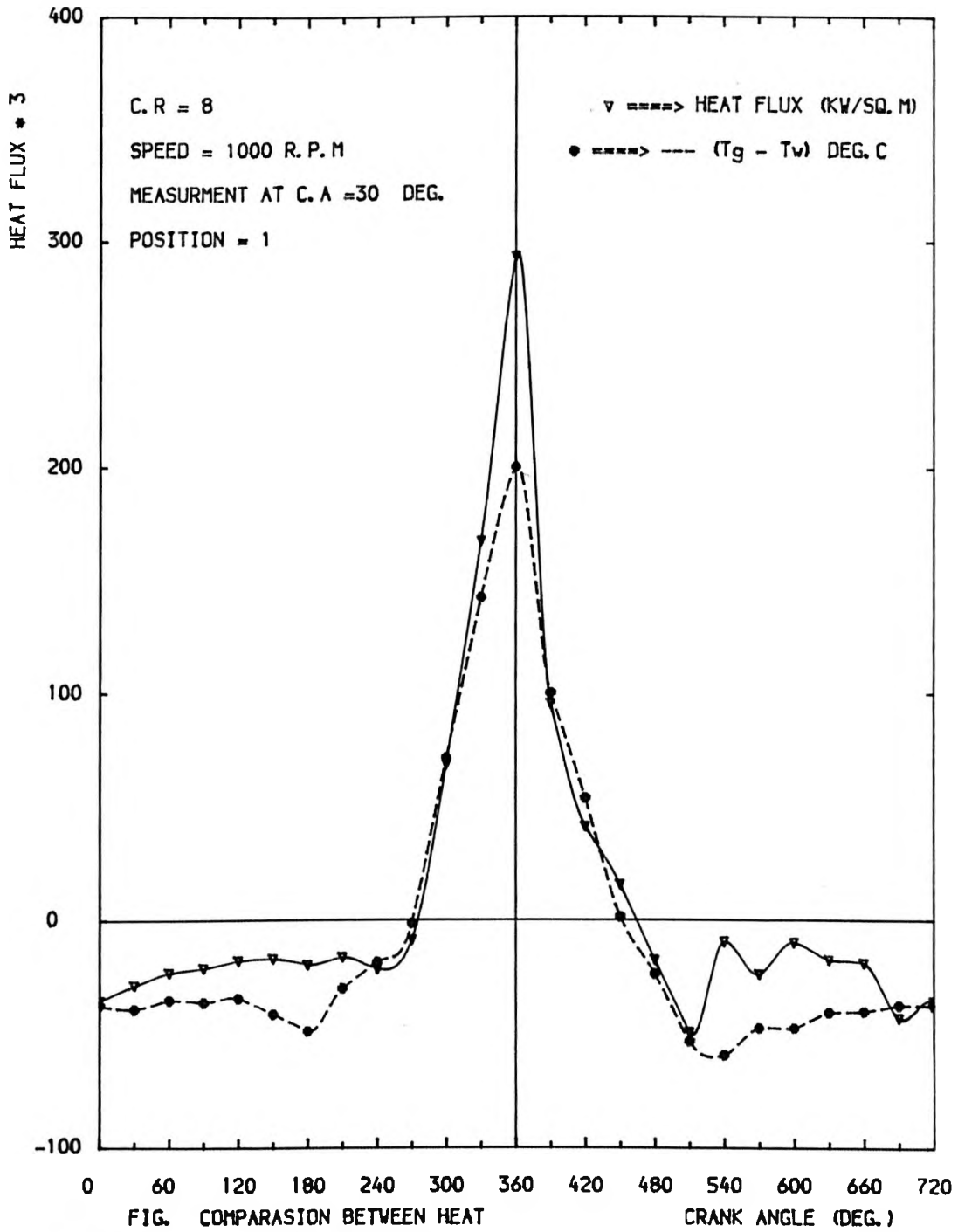


FIG. 9.81

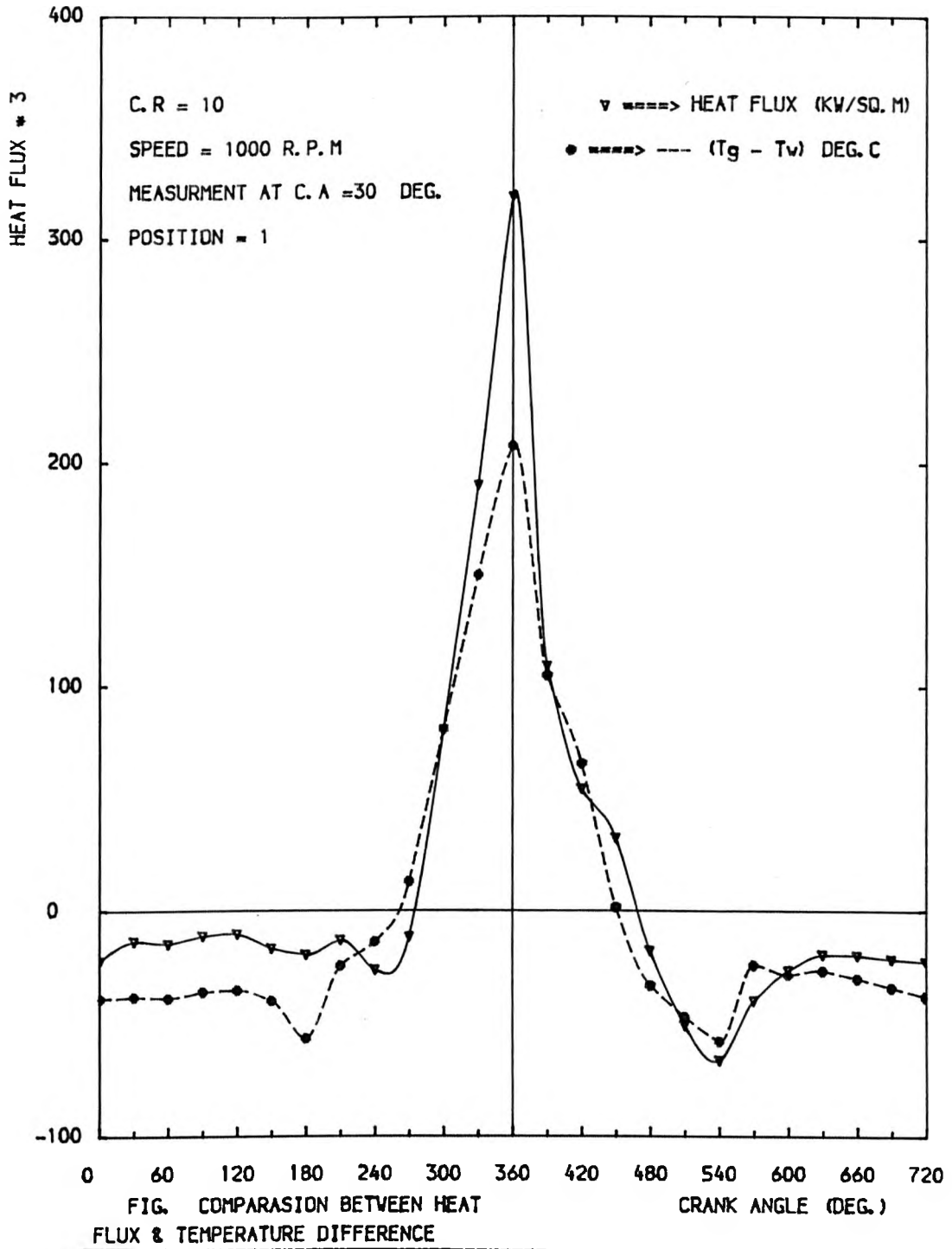


FIG. 9.82

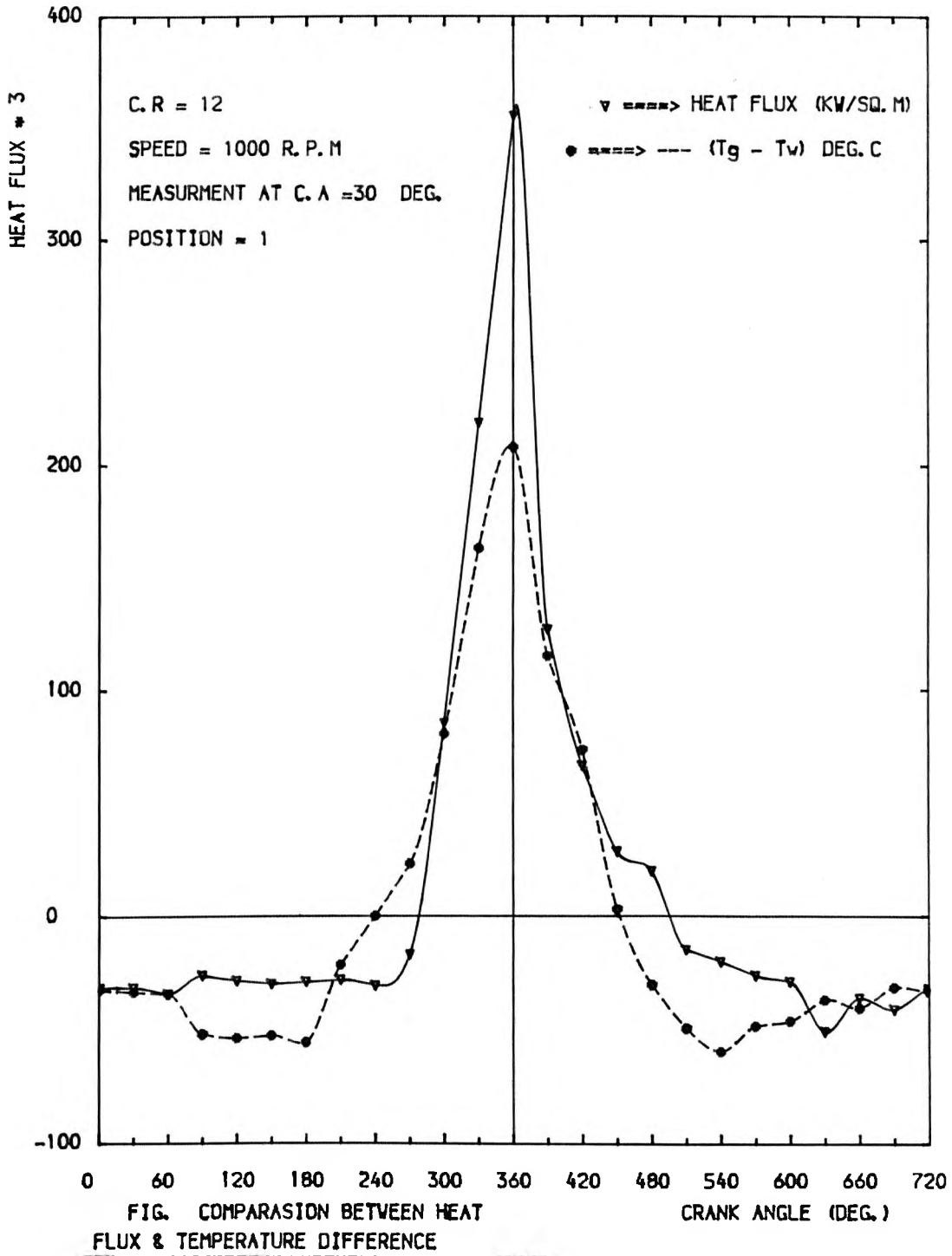


FIG. 9.83

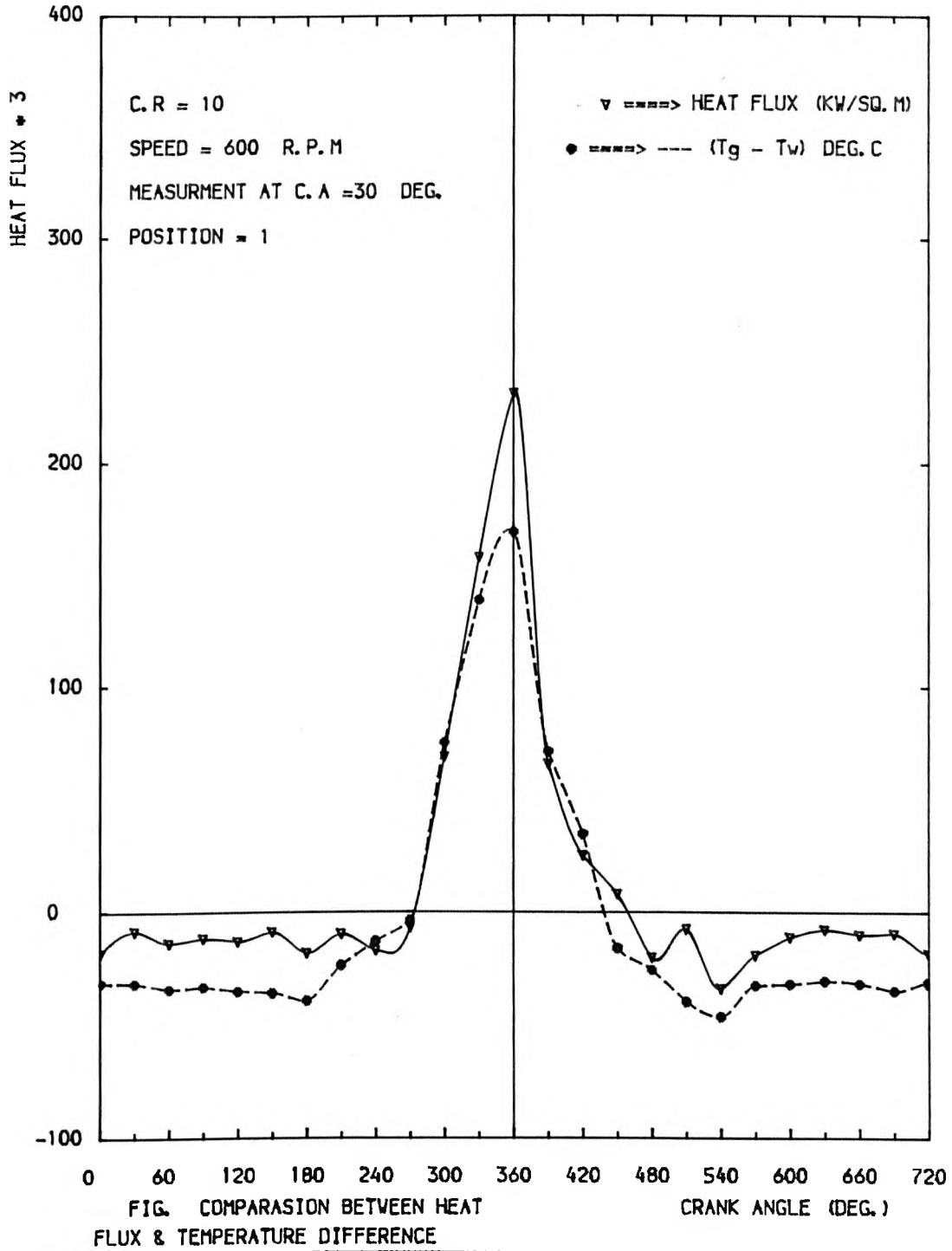


FIG. 9.84

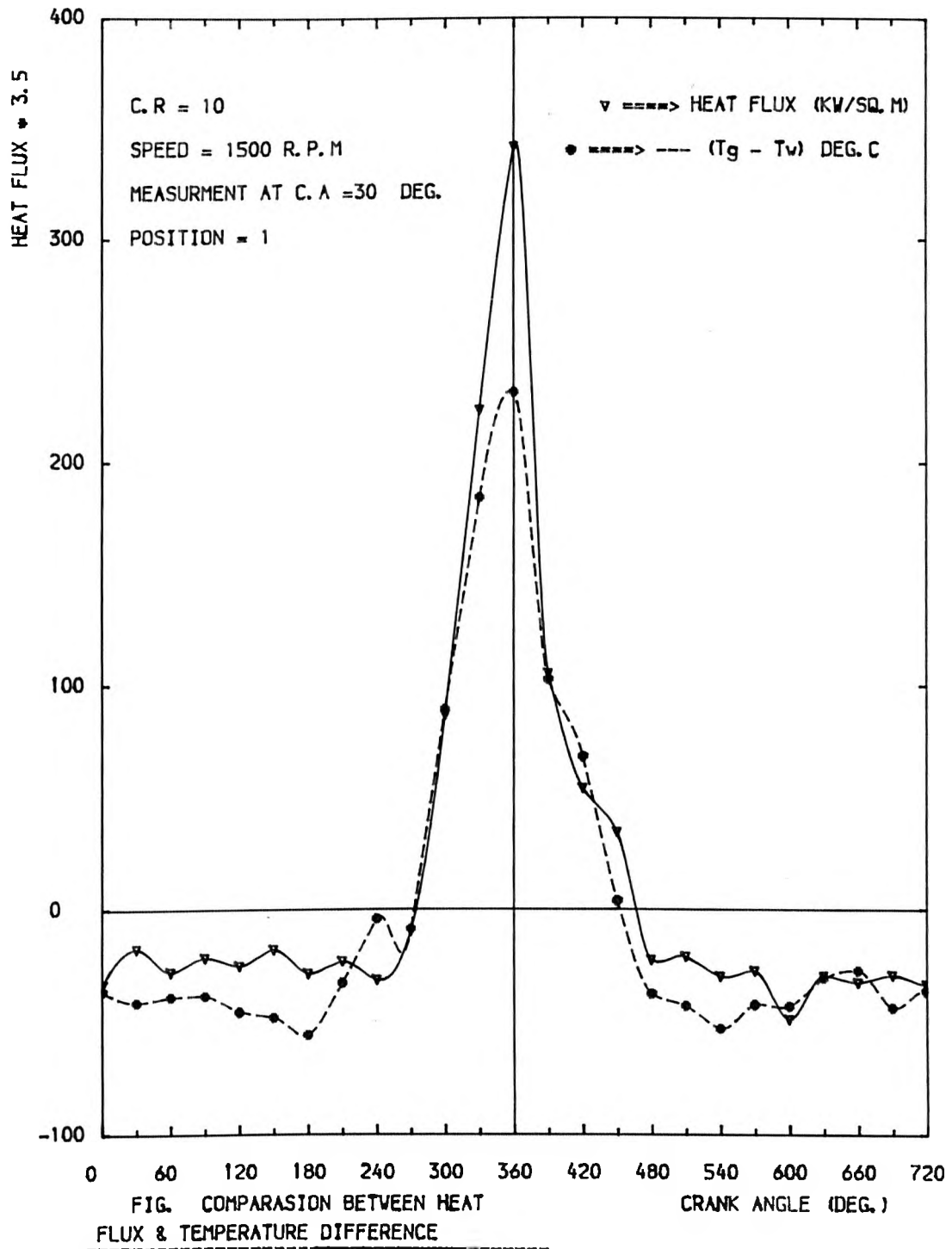


FIG. 9.85

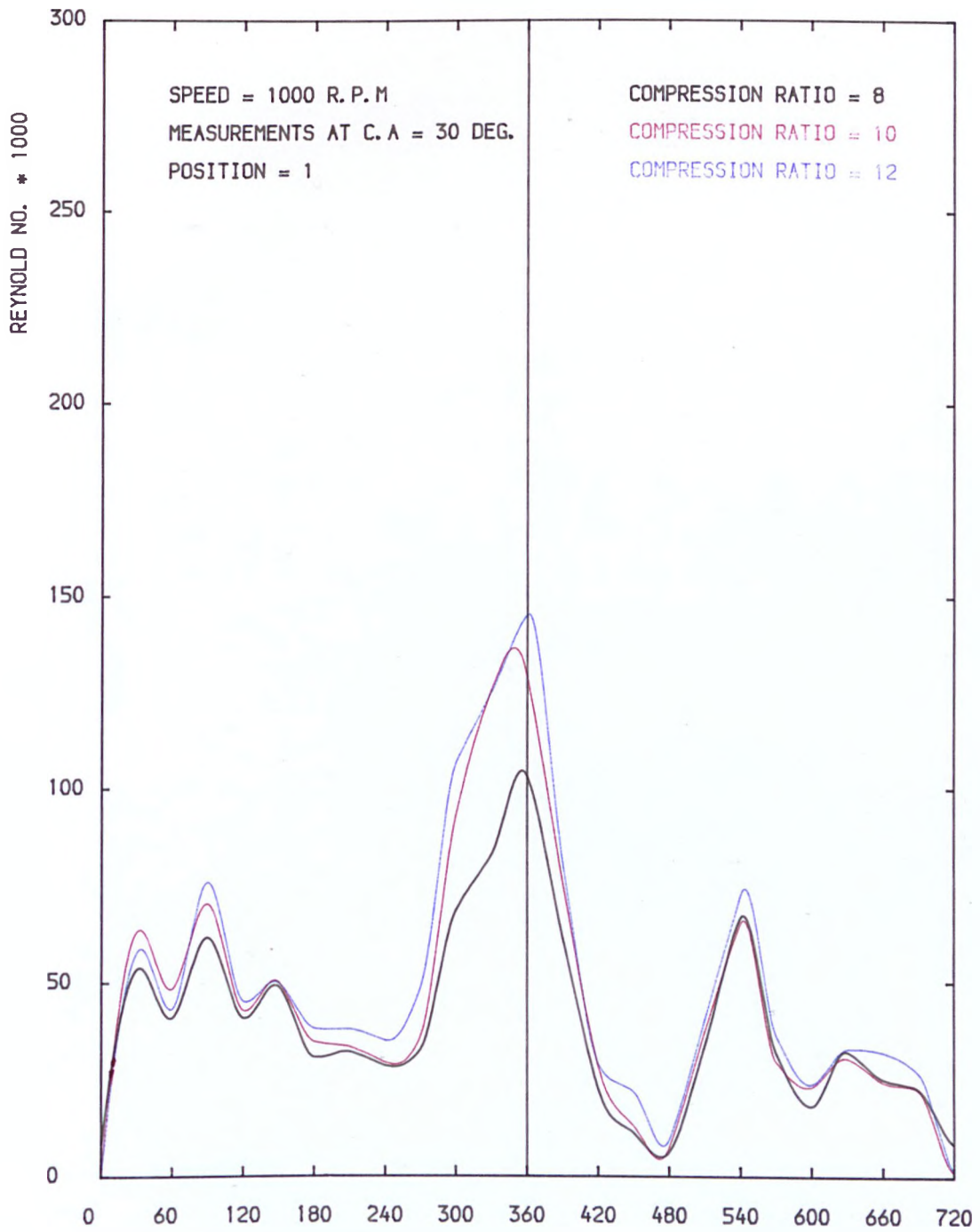


FIG. COMPARISON BETWEEN RE
NO. AT DIFFERENT COMPRESSION RATIO

FIG. 9.86

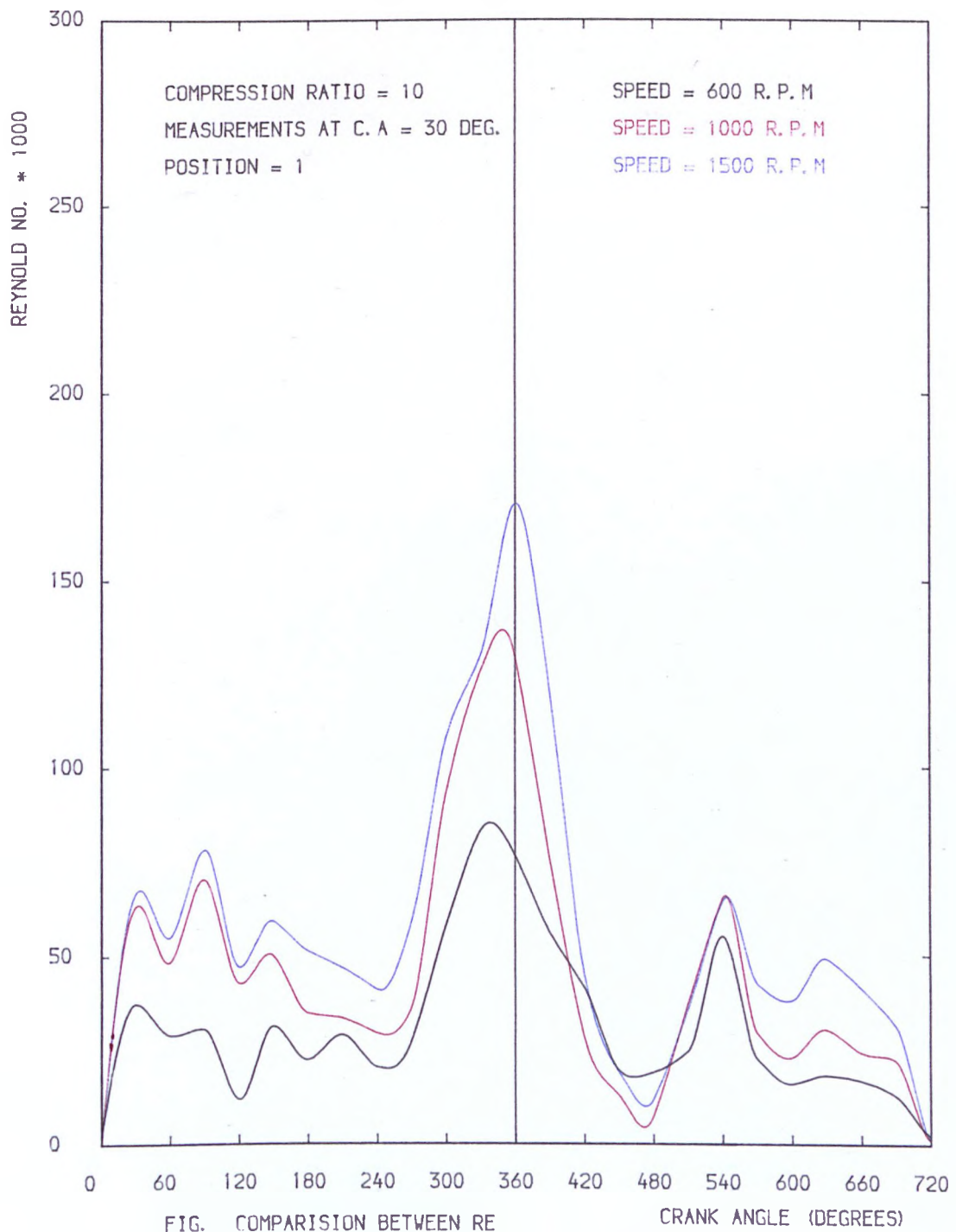


FIG. 9.87

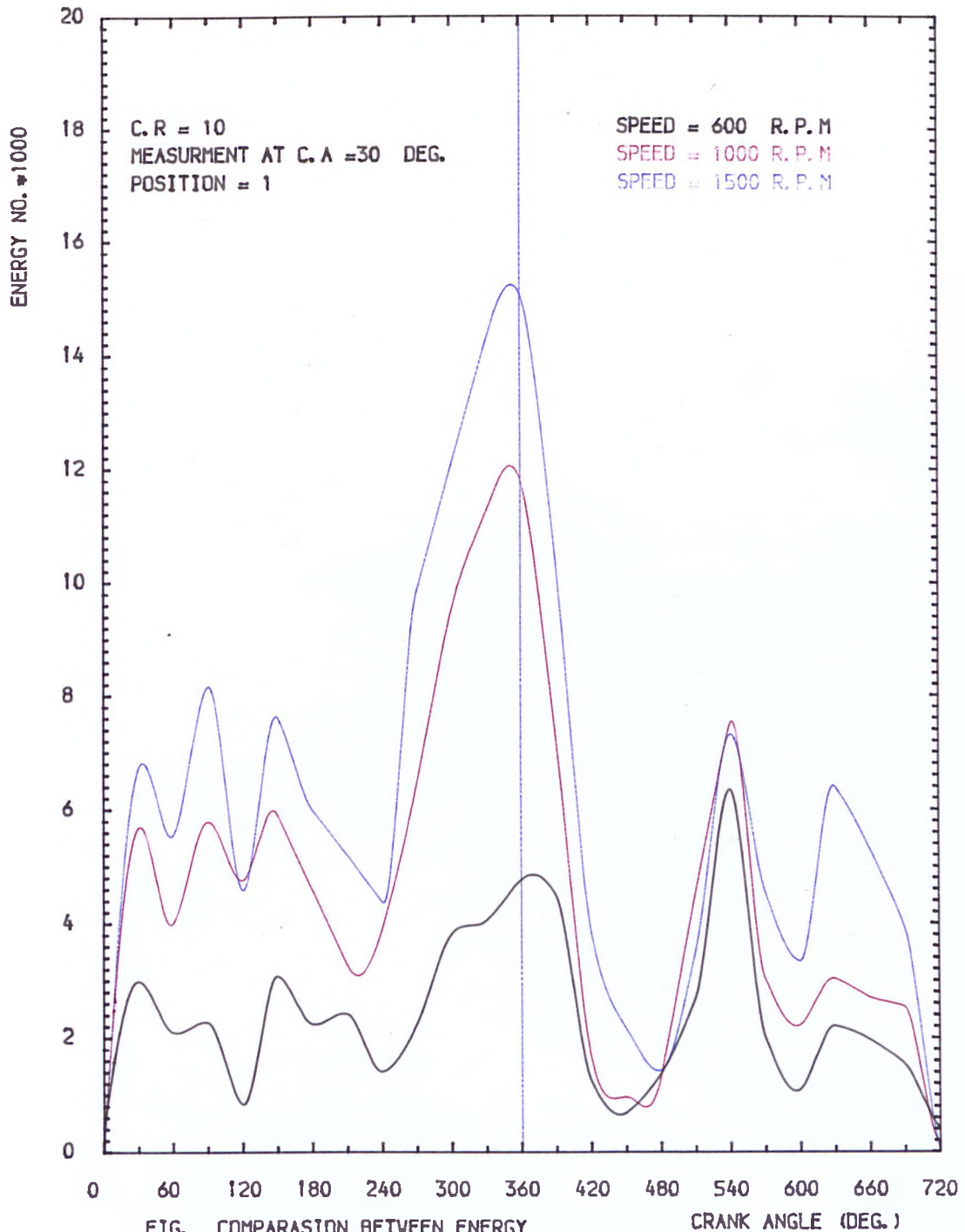


FIG. COMPARASION BETWEEN ENERGY
NO. AT DIFFERENT SPEEDS

CRANK ANGLE (DEG.)

FIG. 9.88

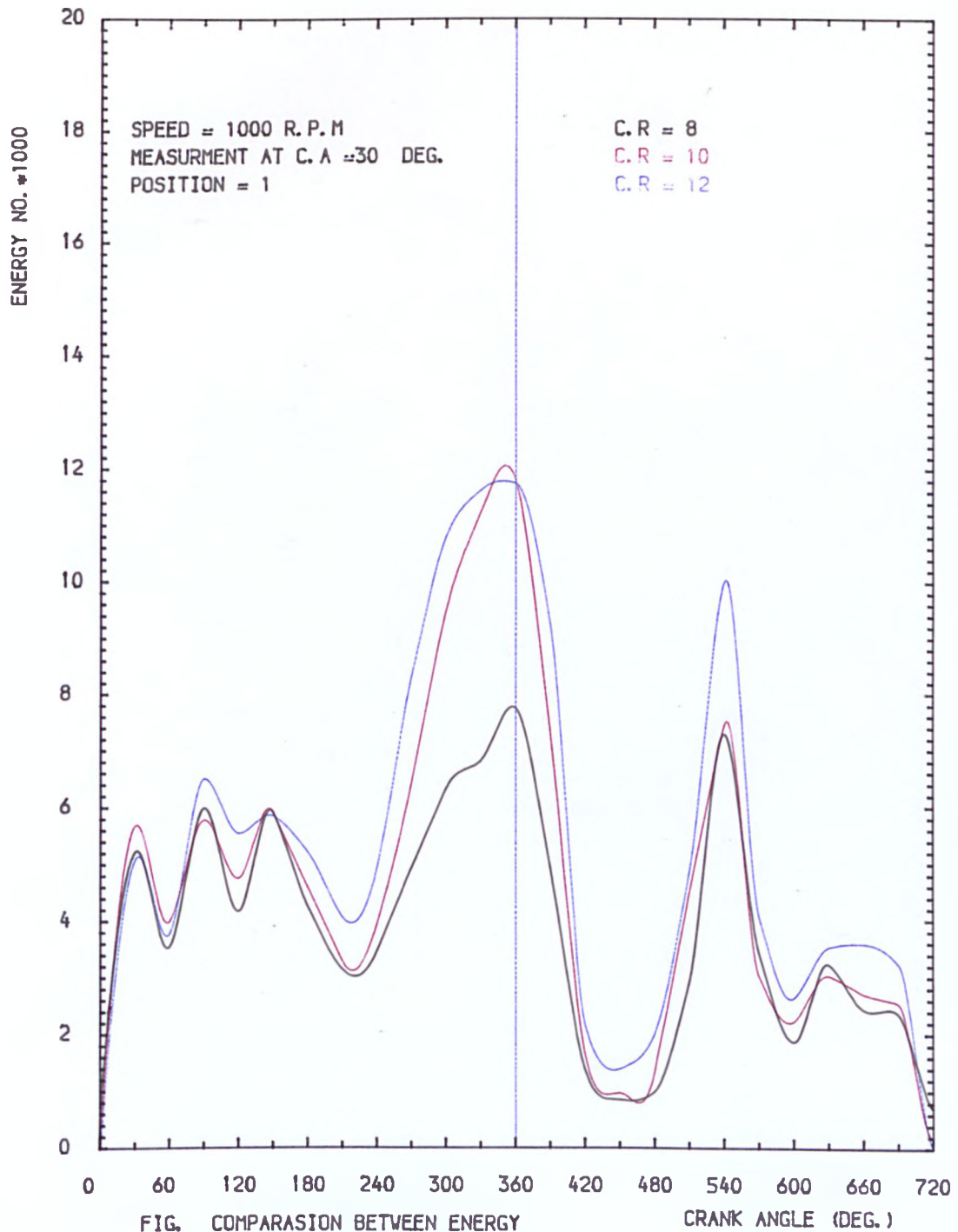


FIG. COMPARASION BETWEEN ENERGY
NO. AT DIFFERENT COMPRESSION RATIOS

FIG. 9.89

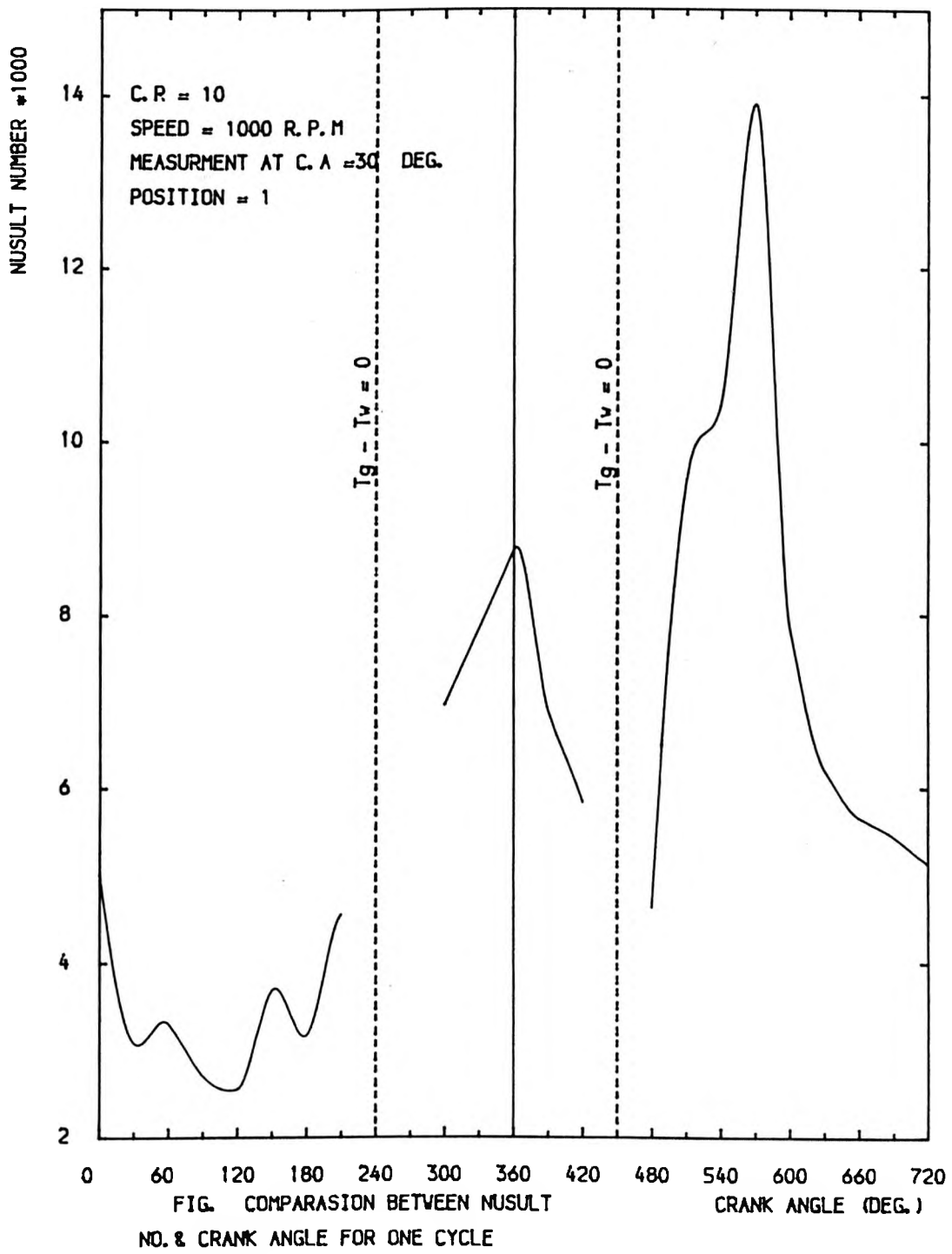


FIG. 9.90

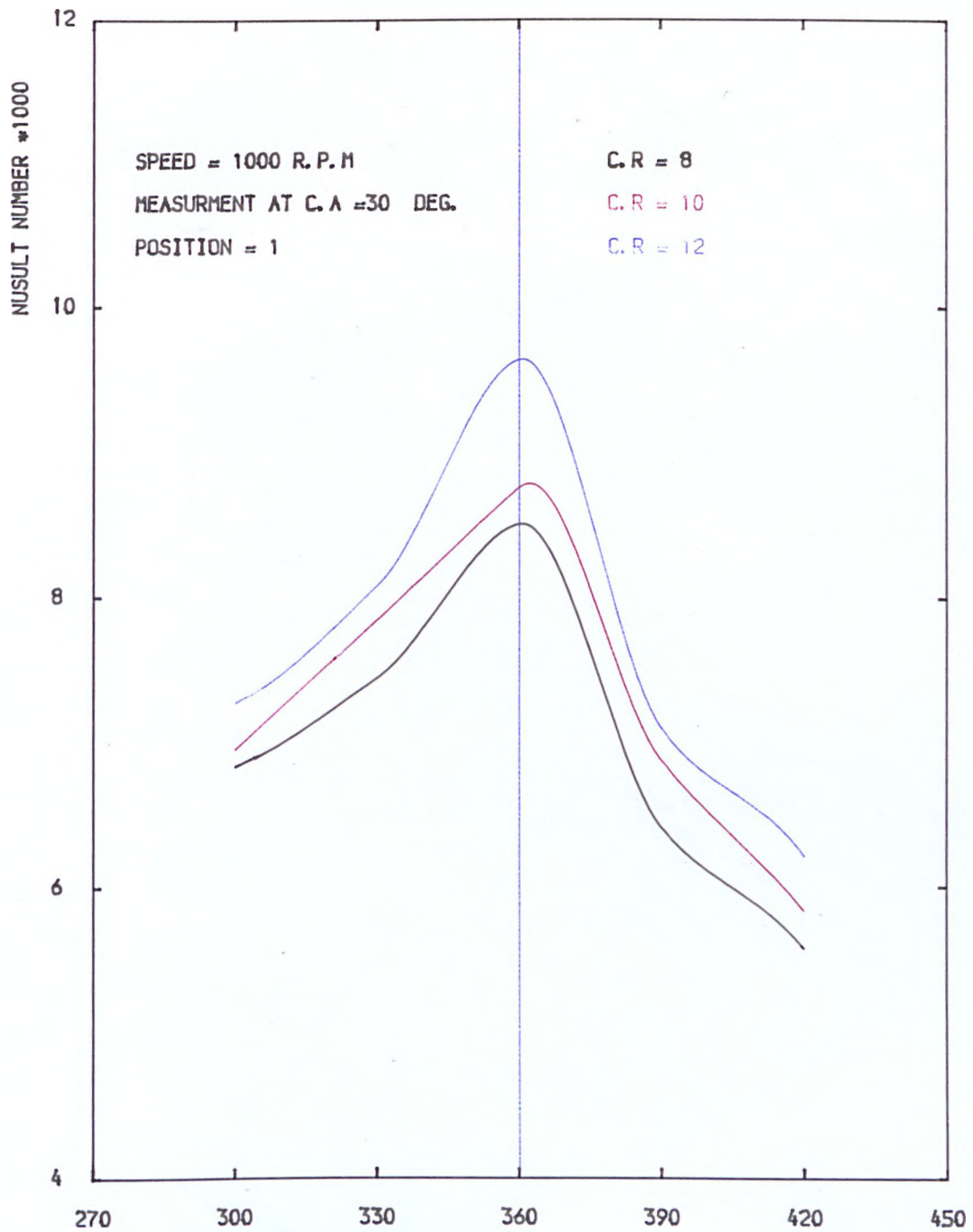


FIG. COMPARASION BETWEEN NUSULT NO. AT DIFFERENT COMPRESSION RATIO

CRANK ANGLE (DEG.)

FIG. 9.91

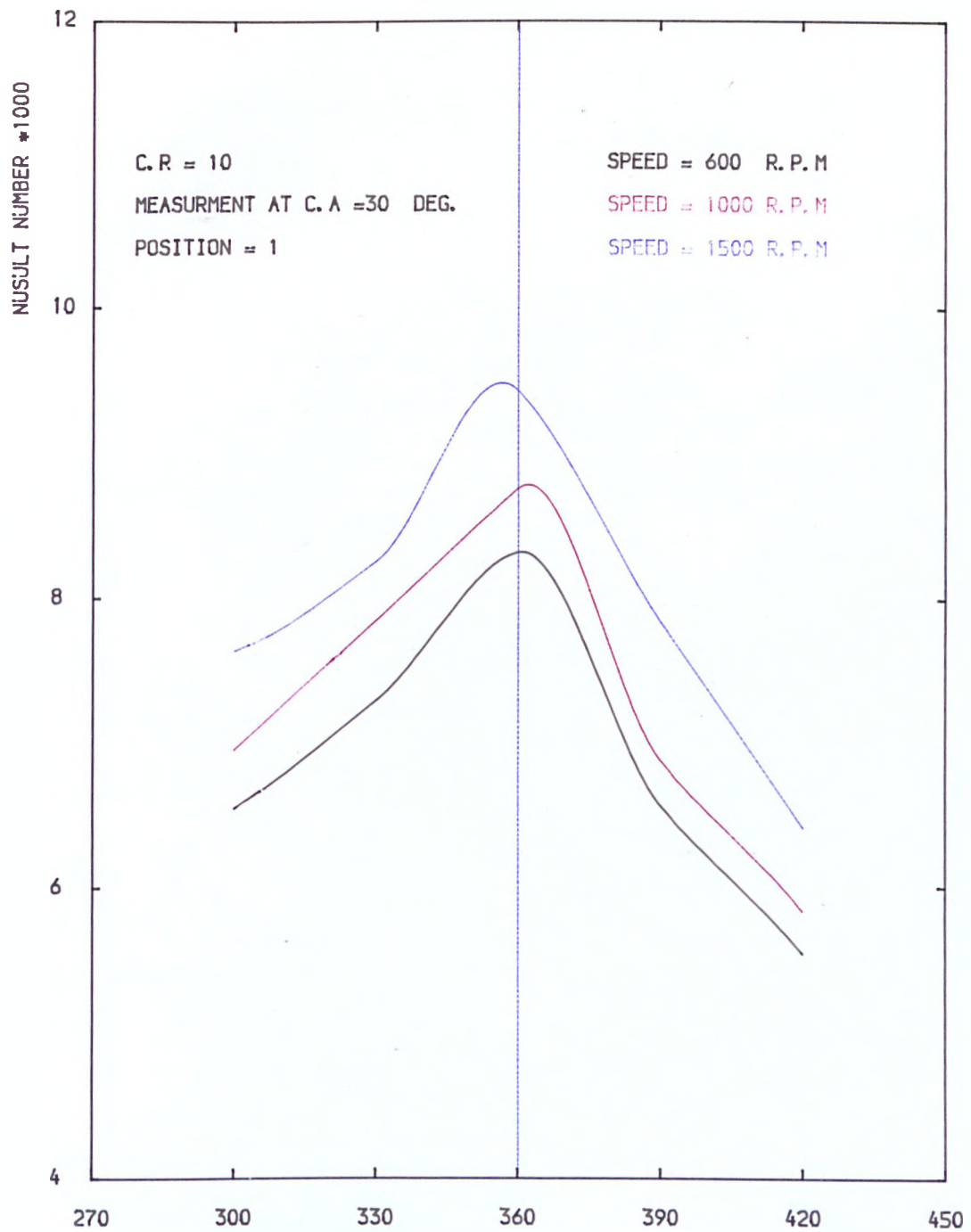


FIG. COMPARASION BETWEEN NUSULT NO. AT DIFFERENT SPEEDS

CRANK ANGLE (DEG.)

FIG. 9.92

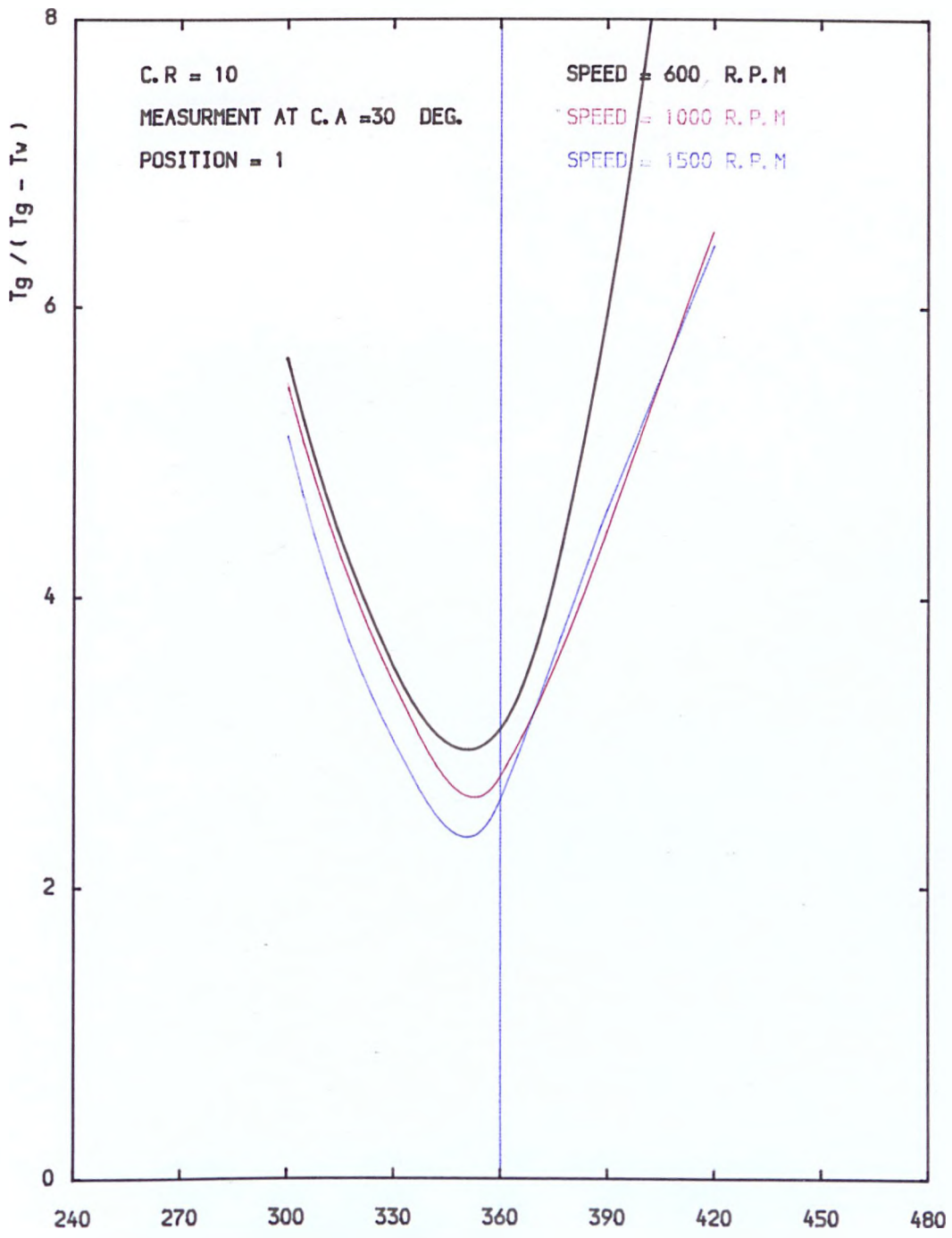


FIG. COMPARASION BETWEEN GAS RA-
TIO AT DIFFERENT SPEEDS

FIG. 9.93

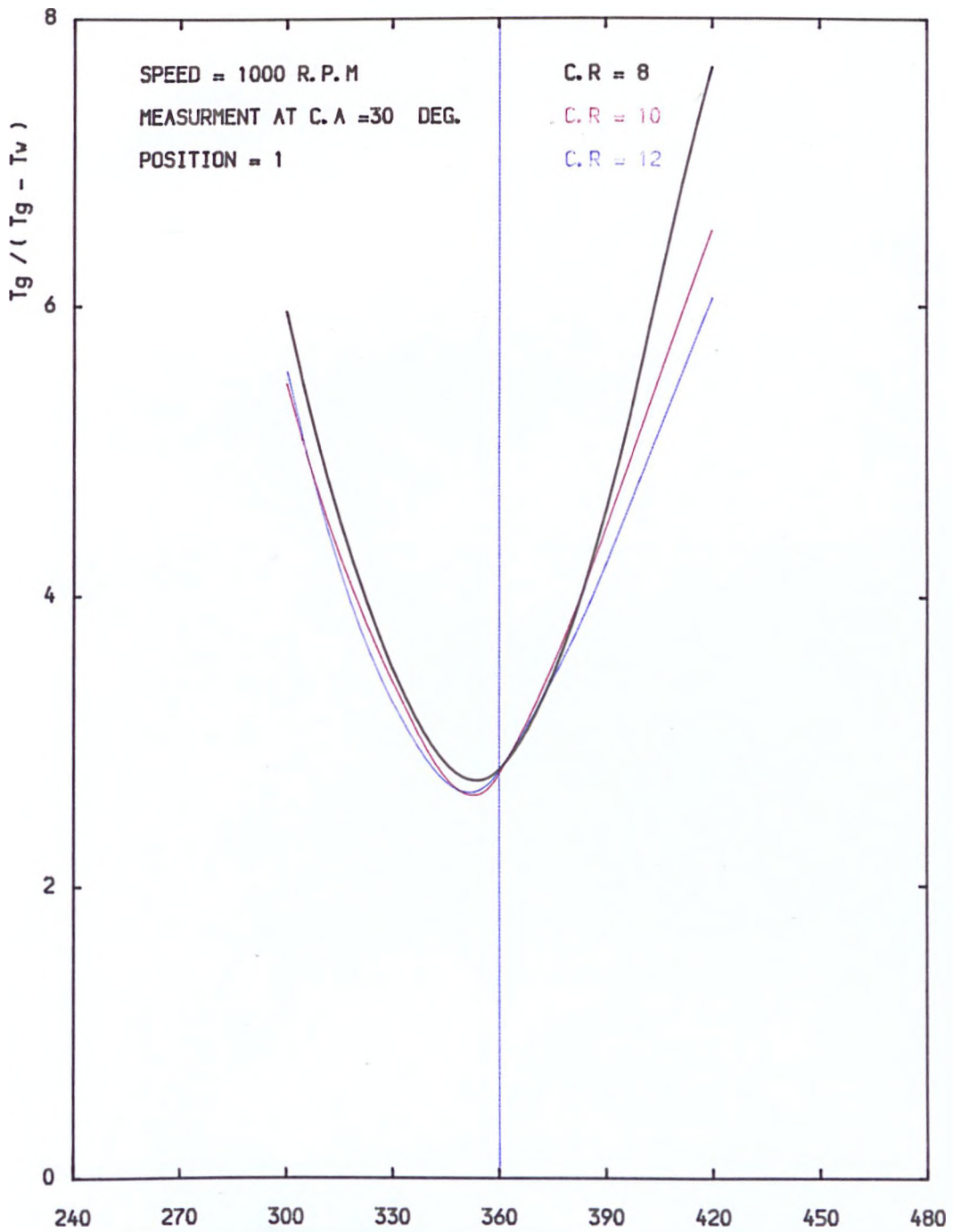


FIG. COMPARISON BETWEEN GAS RATIO AT DIFFERENT COMPRESSION RATIOS

FIG. 9.94

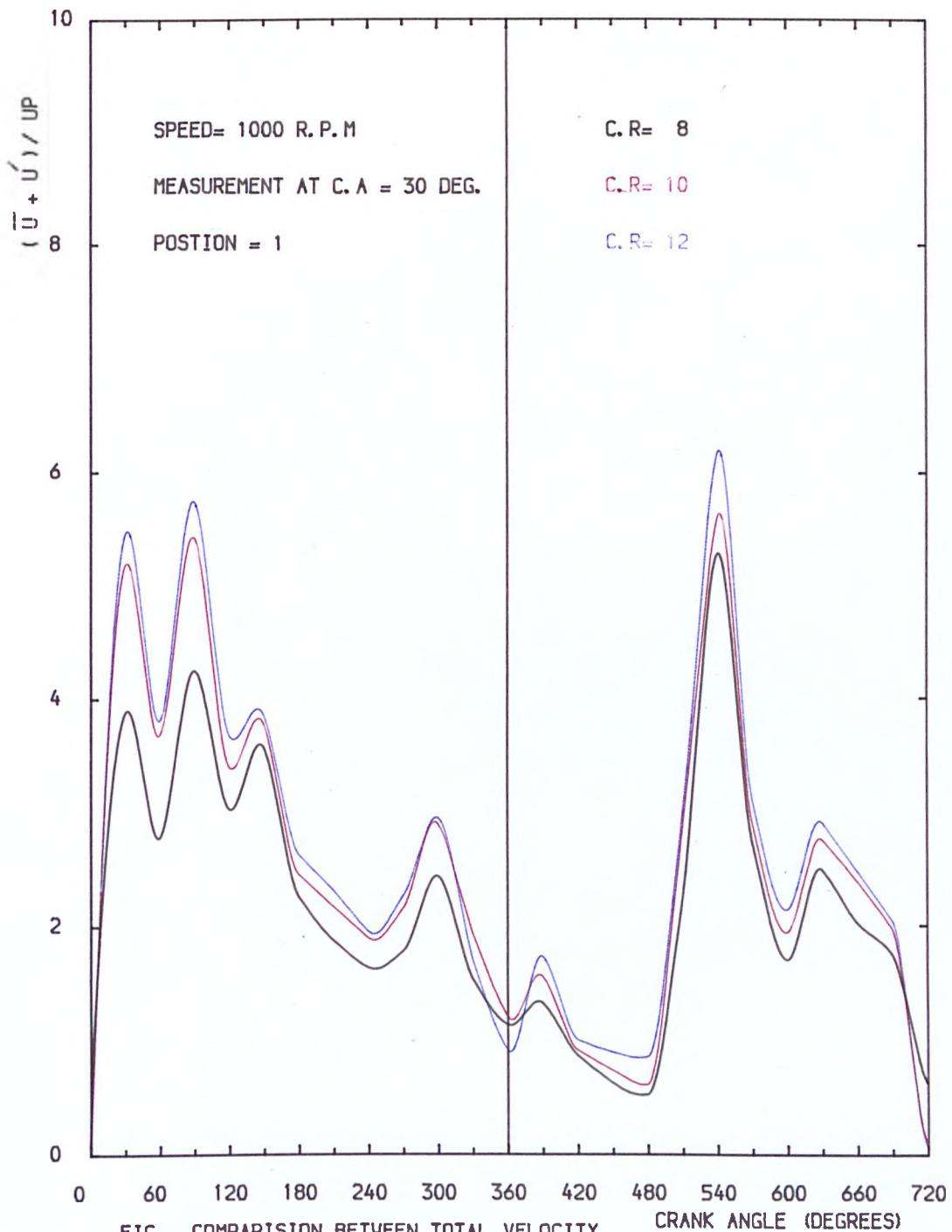


FIG. COMPARISON BETWEEN TOTAL VELOCITY RATIO AT DIFFERENT COMPRESSION RATIOS

FIG. 9.95

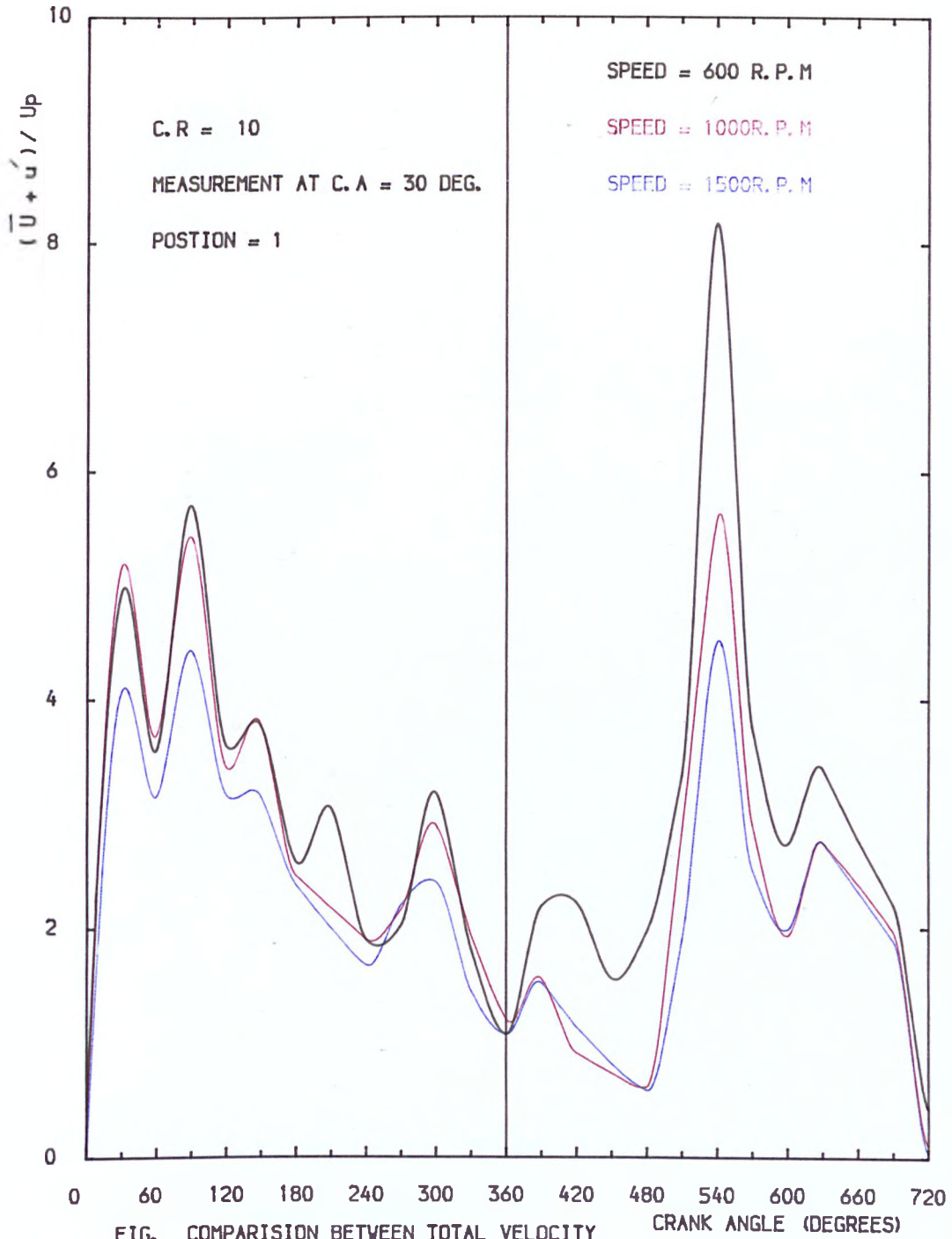


FIG. COMPARISON BETWEEN TOTAL VELOCITY RATIO AT DIFFERENT SPEEDS

FIG. 9.96

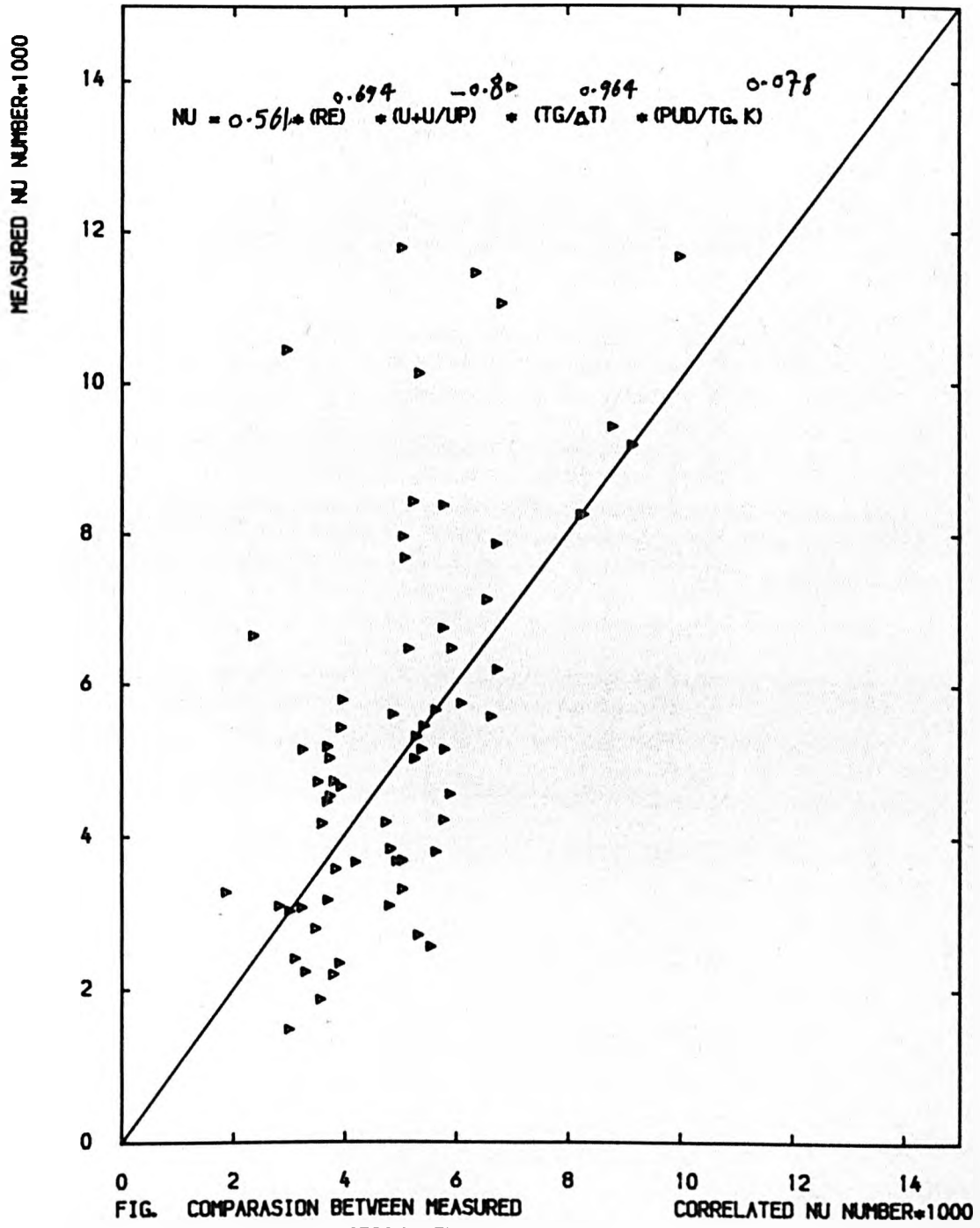


FIG. 9.97

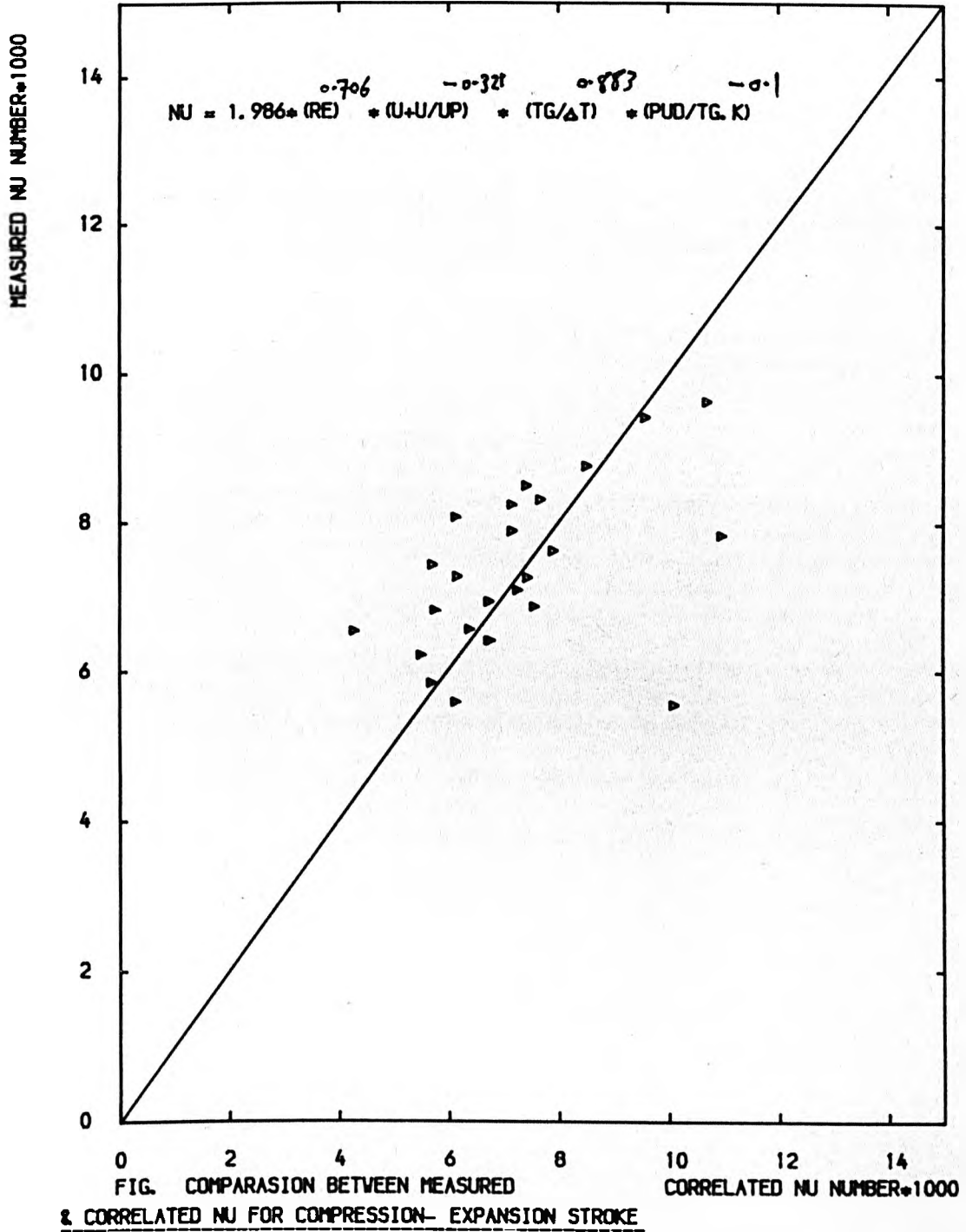


FIG. 9.98

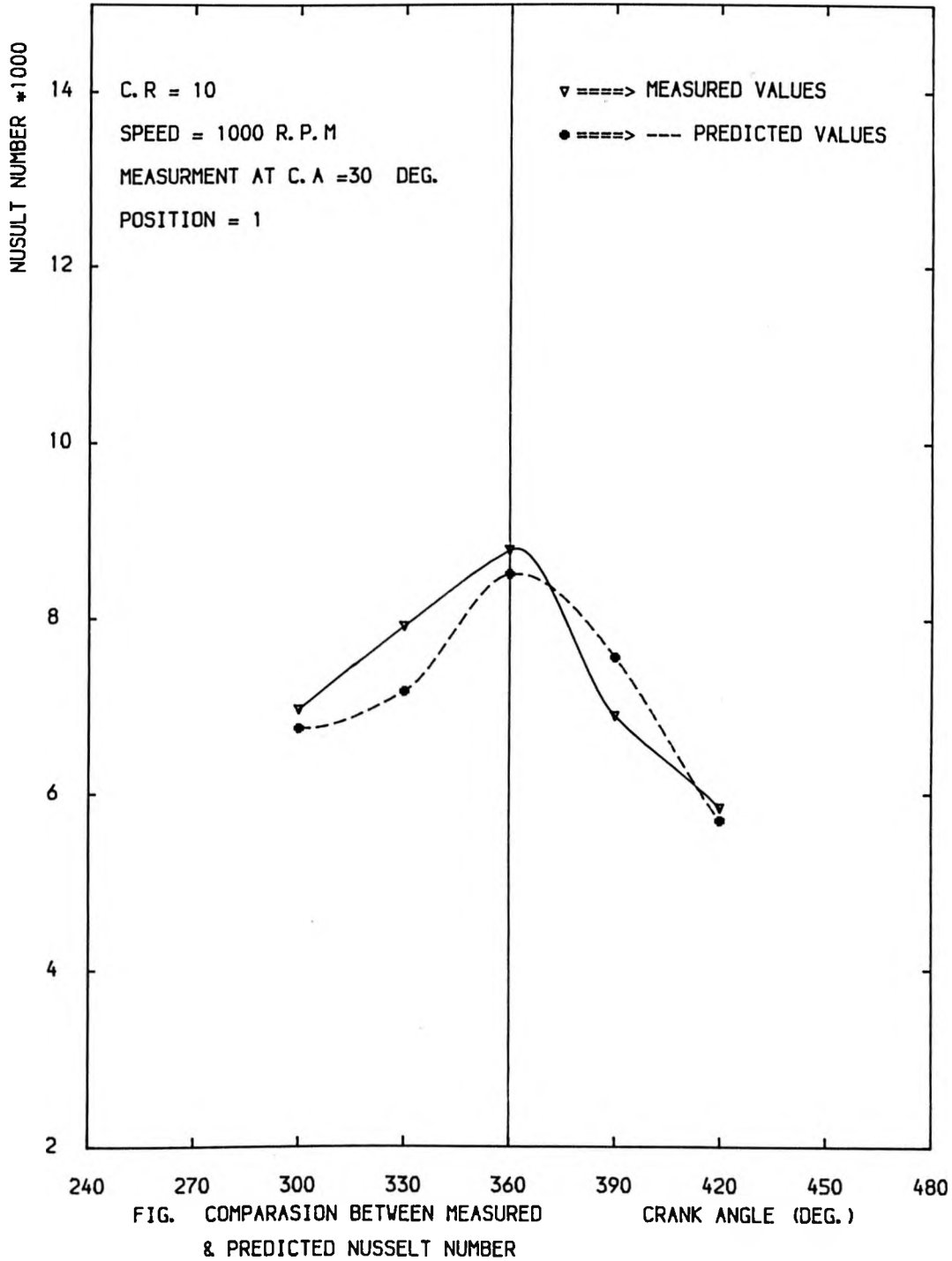


FIG. 9.99

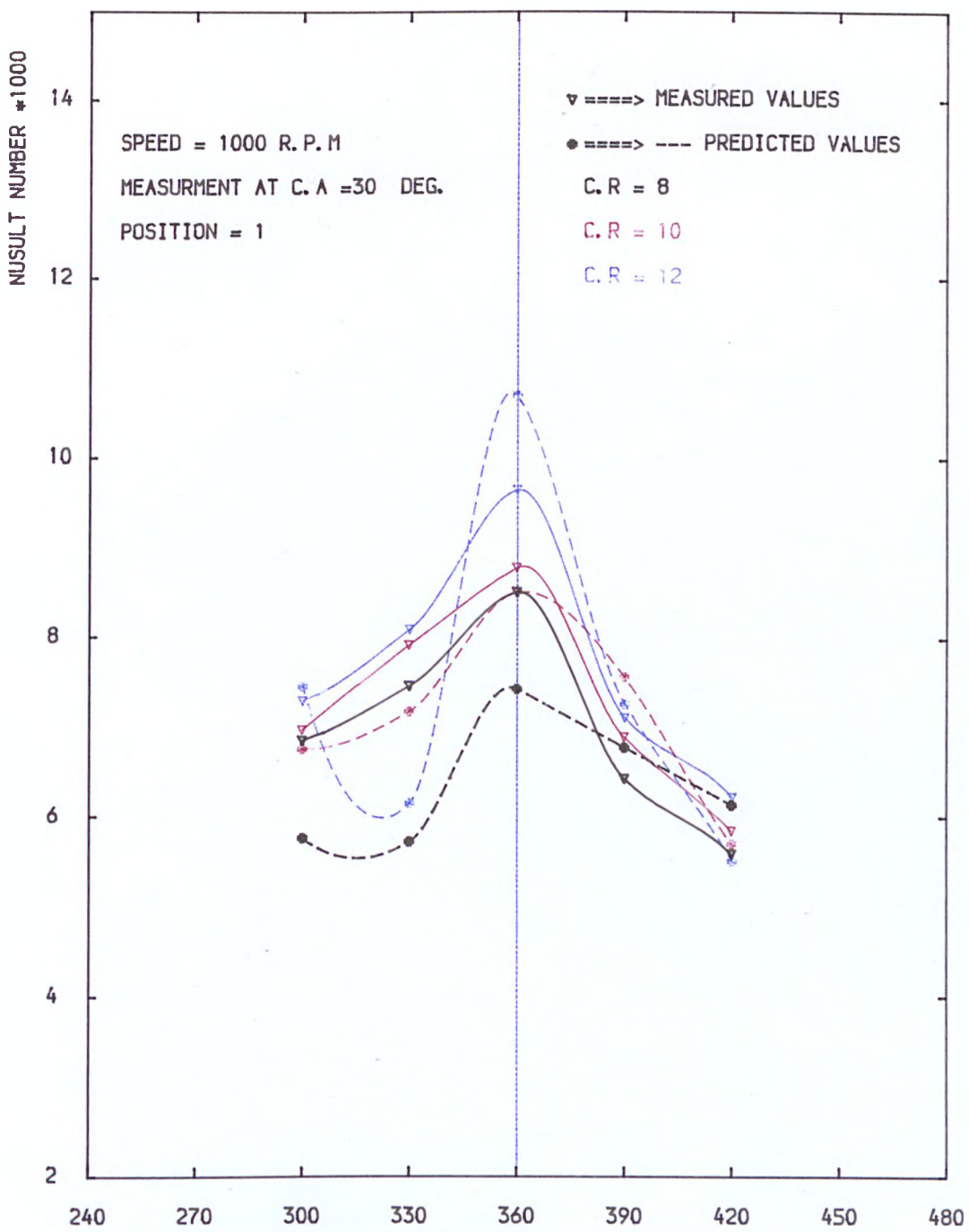


FIG. COMPARASION BETWEEN MEASURED & PREDICTED NUSSELT NUMBER AT DIFFERENT C. R

FIG. 9.100

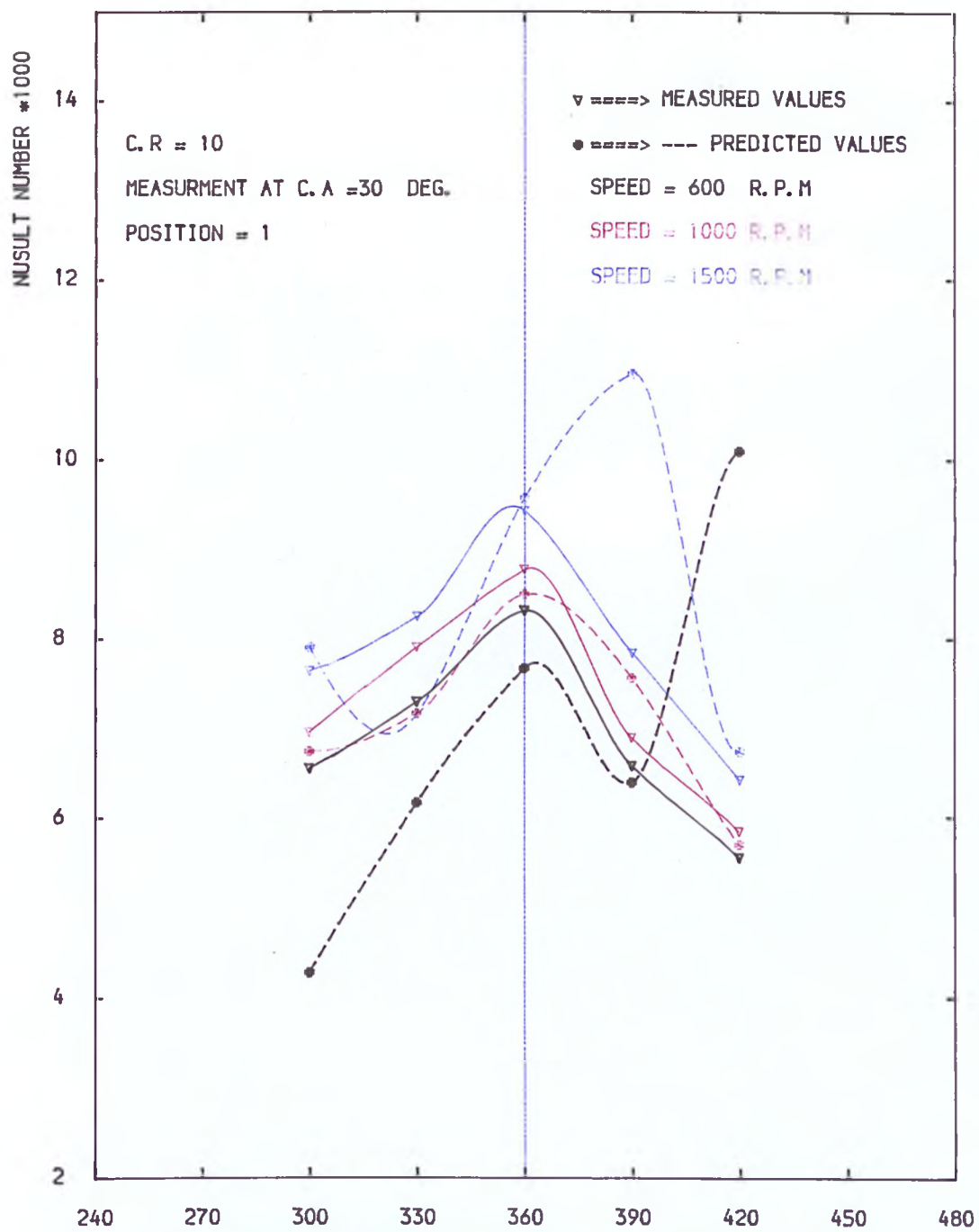


FIG. COMPARISON BETWEEN MEASURED & PREDICTED NUSSLETT NUMBER AT DIFFERENT SPEEDS

FIG. 9.101

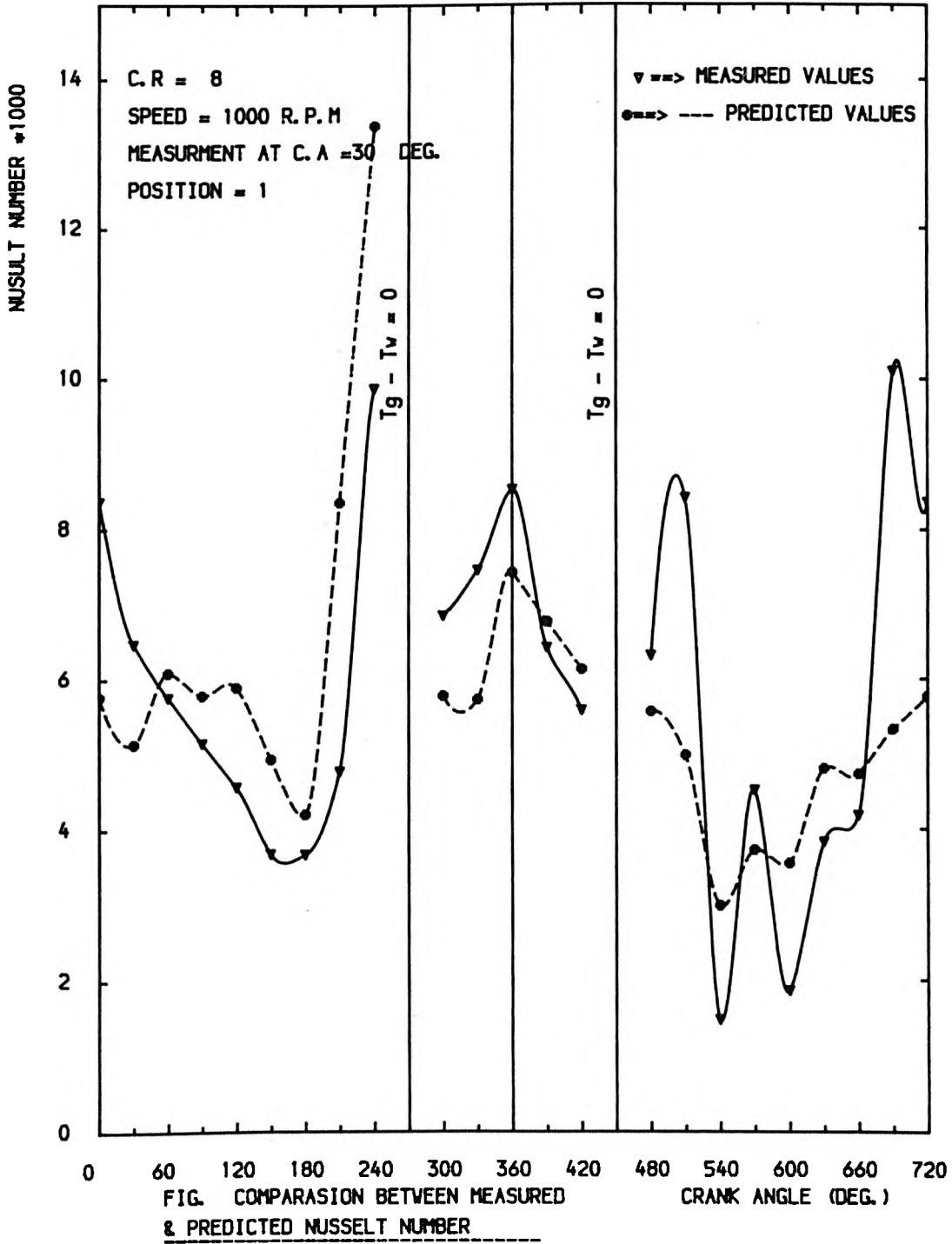


FIG. 9.102

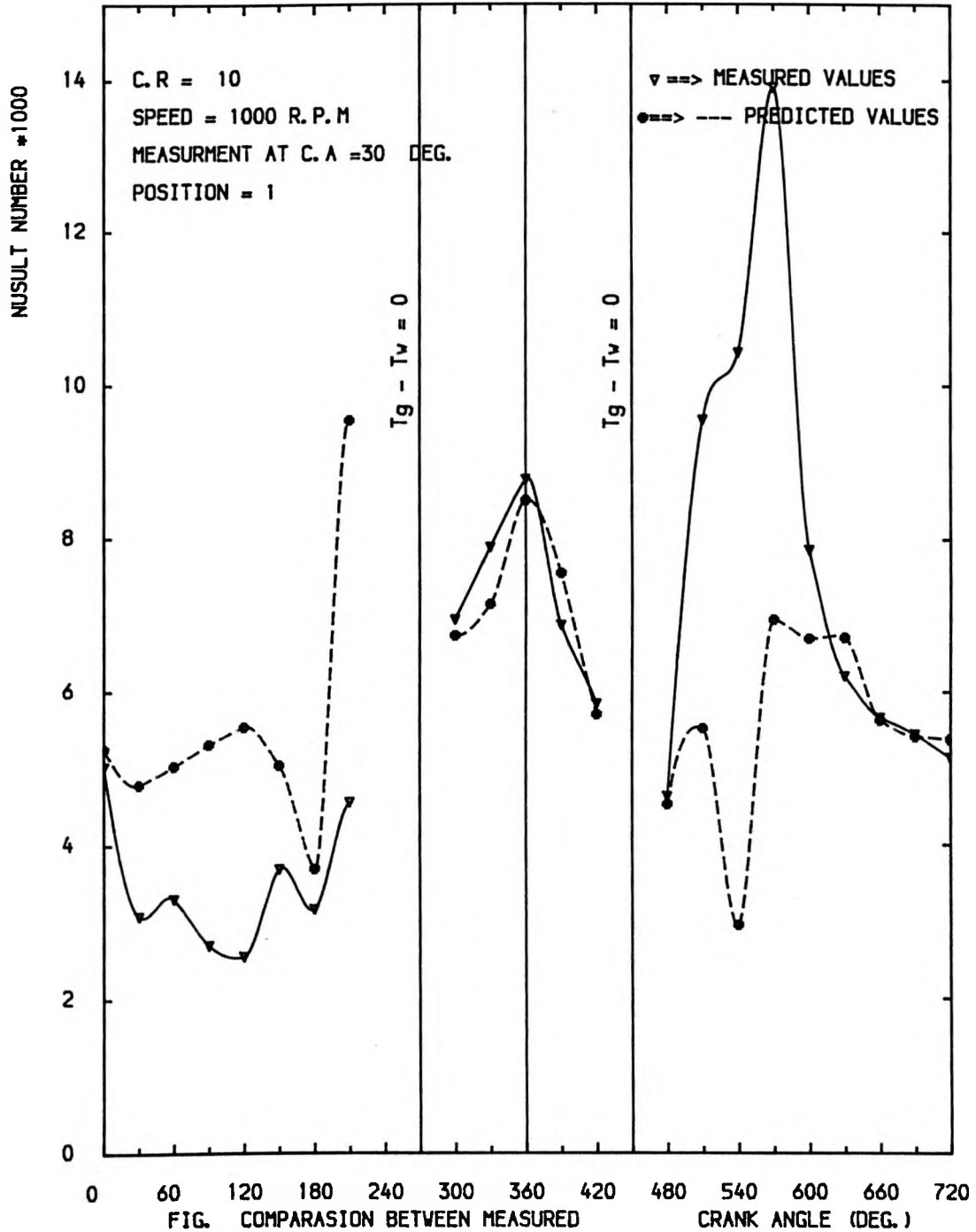


FIG. 9.103

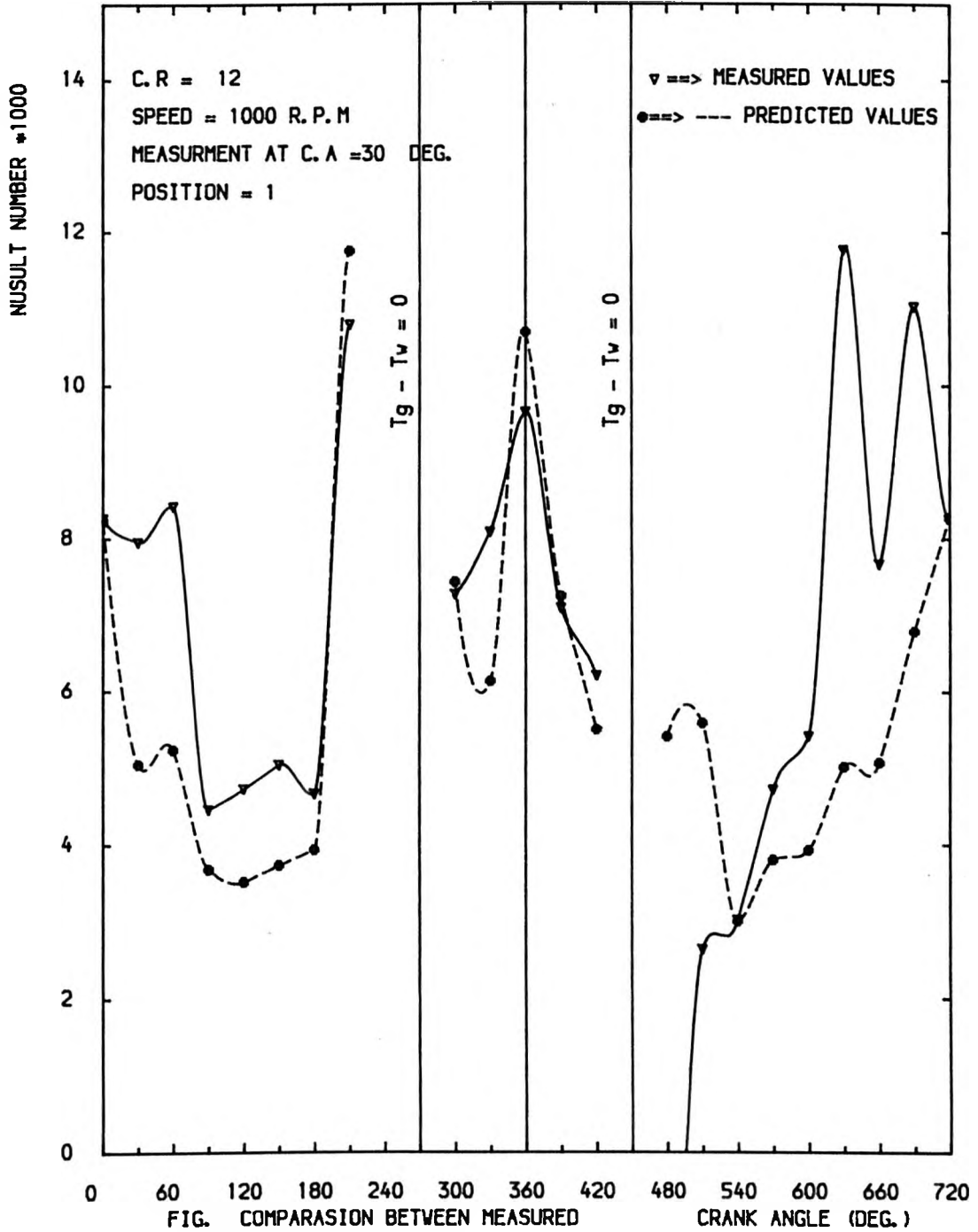


FIG. COMPARISON BETWEEN MEASURED & PREDICTED NUSSELT NUMBER

FIG. 9.104

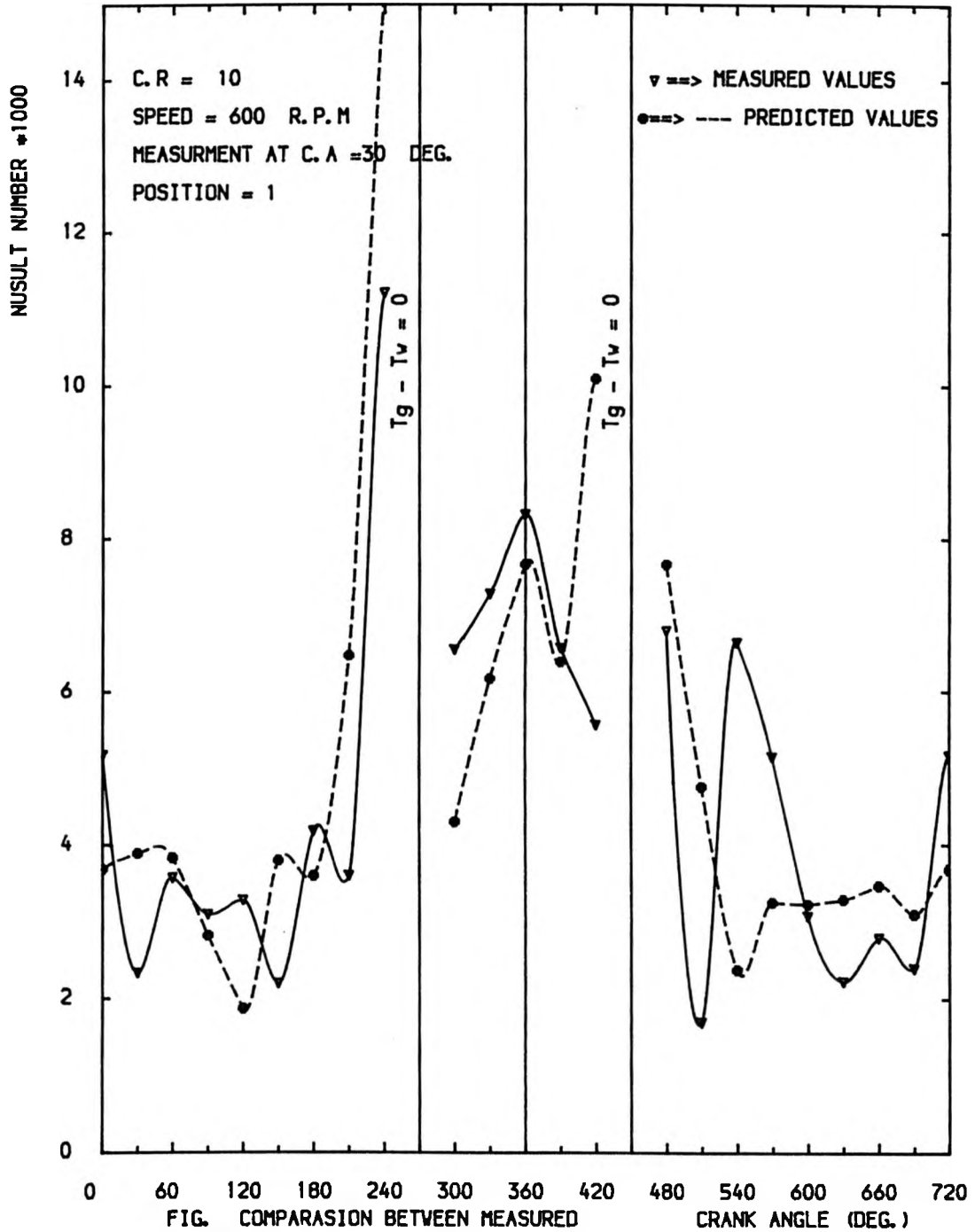


FIG. COMPARASION BETWEEN MEASURED & PREDICTED NUSSULT NUMBER

FIG. 9.105

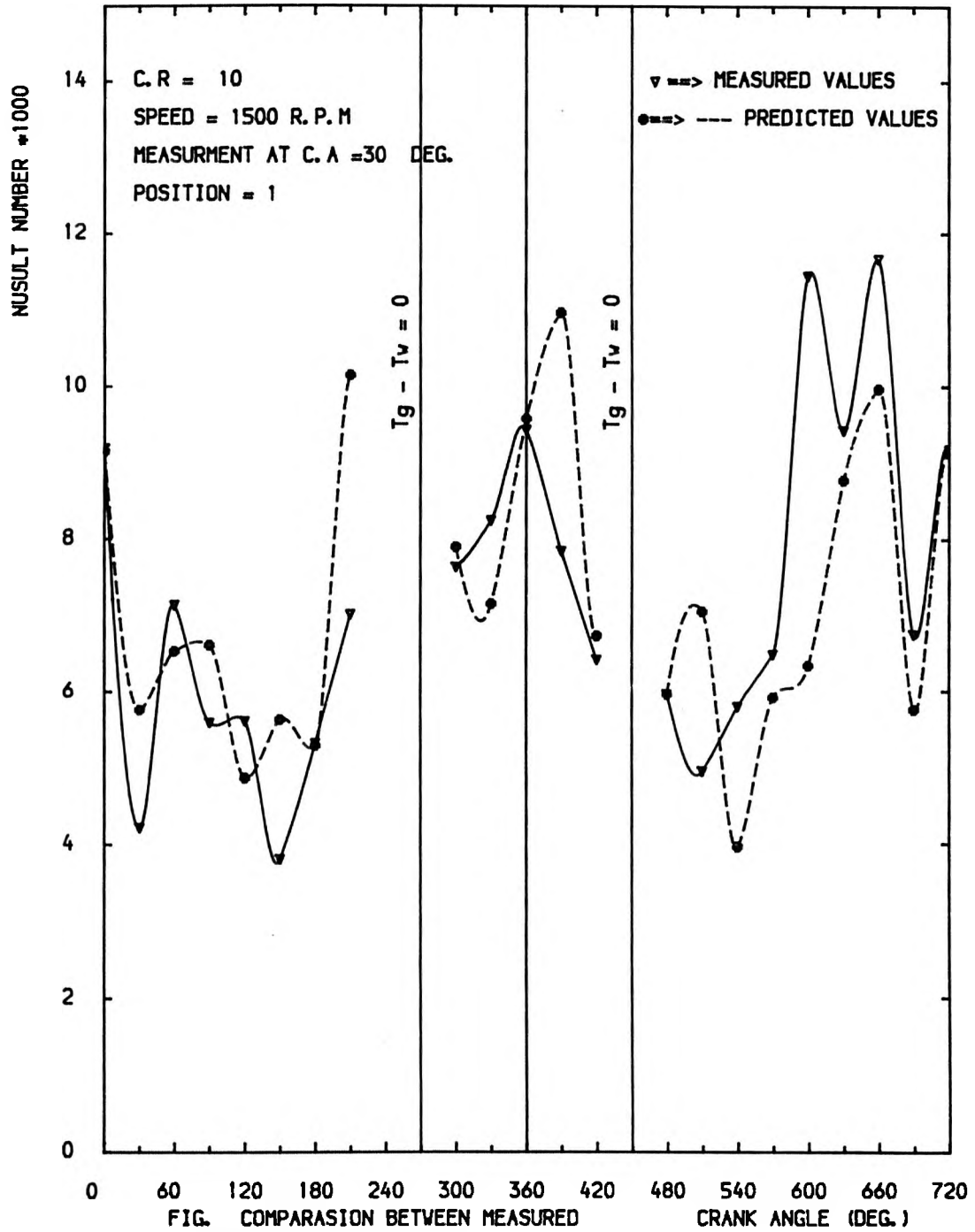


FIG. COMPARASION BETWEEN MEASURED & PREDICTED NUSSELT NUMBER

FIG. 9.106

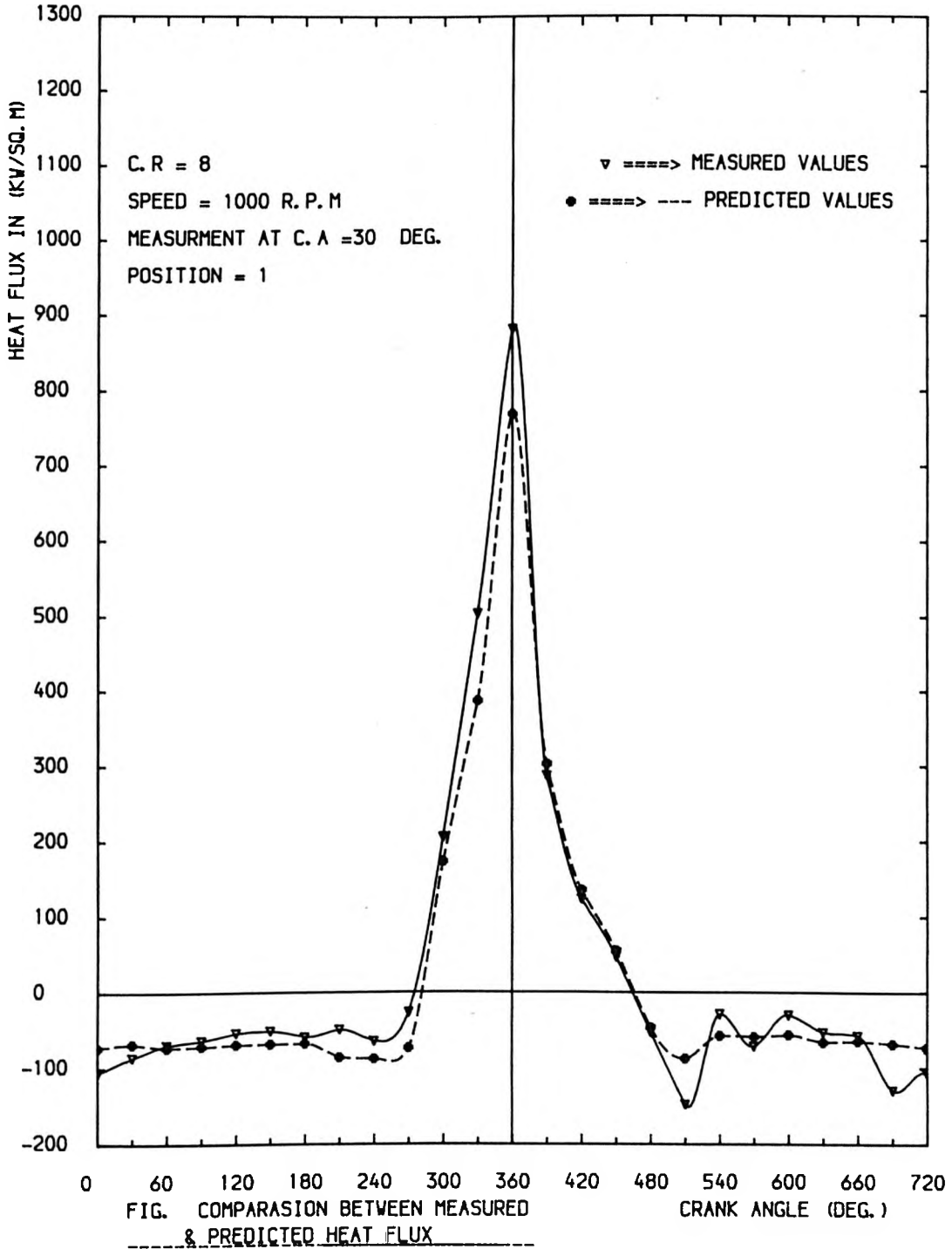


FIG. 9.107

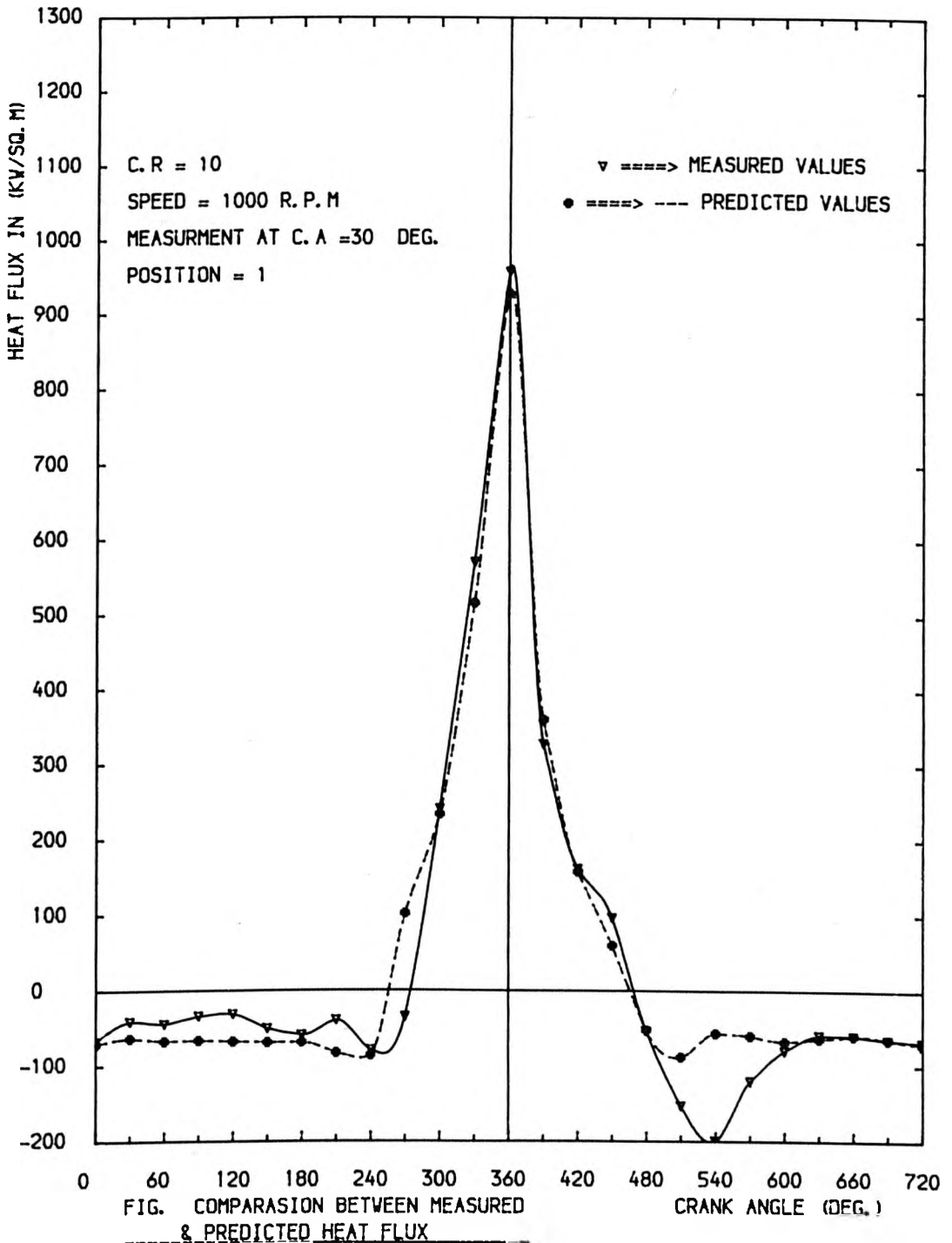


FIG. 9.108

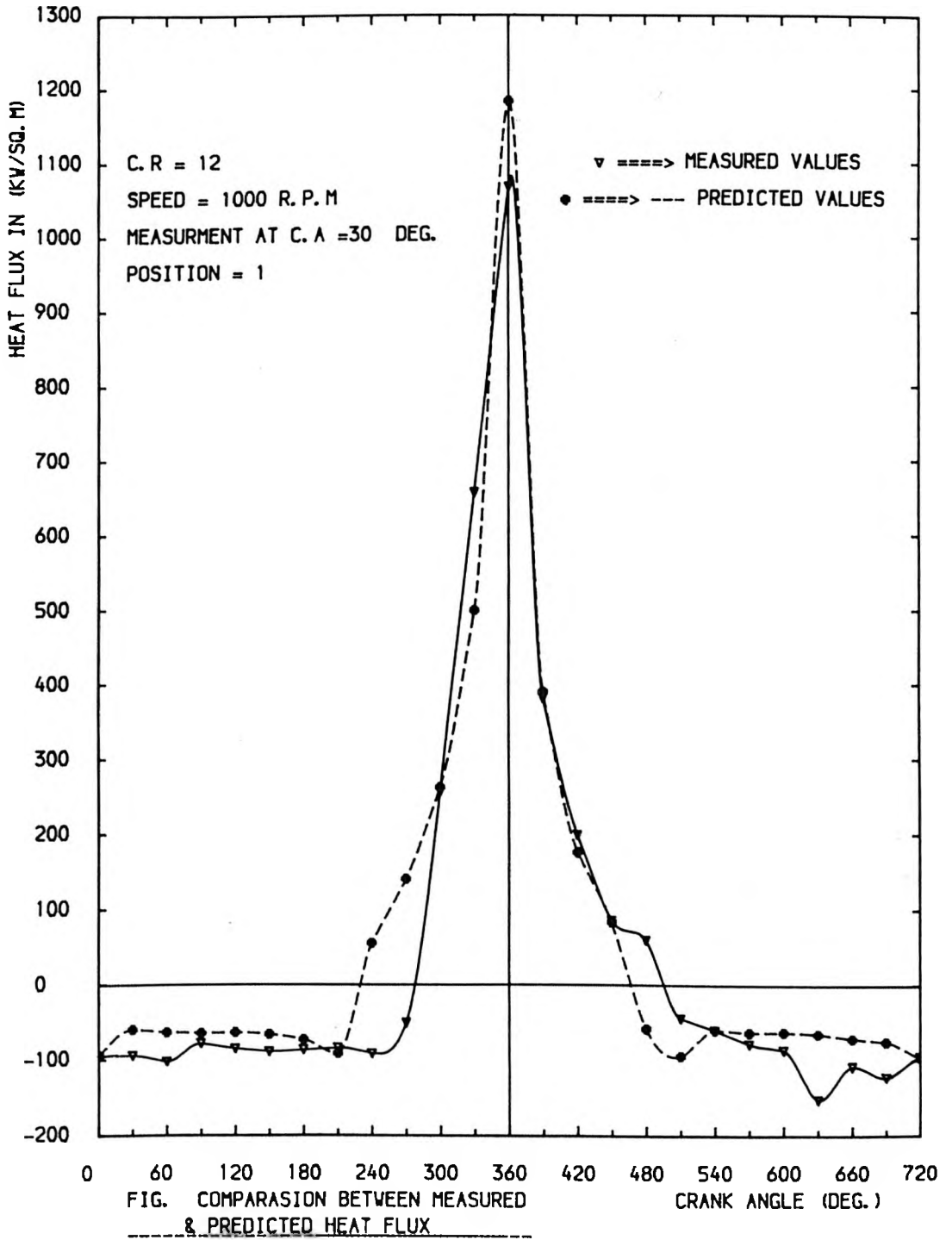


FIG. 9.109

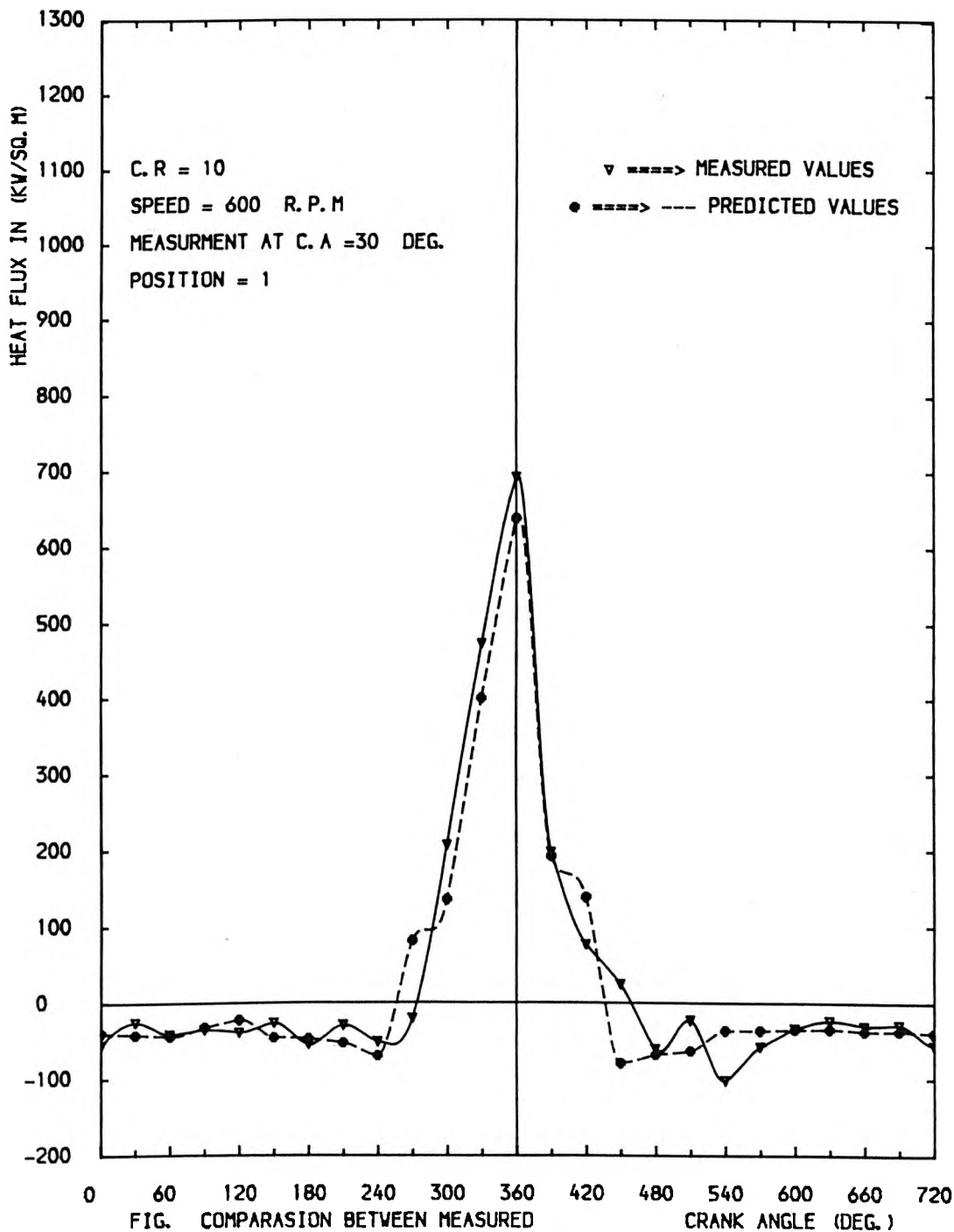


FIG. COMPARISON BETWEEN MEASURED & PREDICTED HEAT FLUX

FIG. 9.110

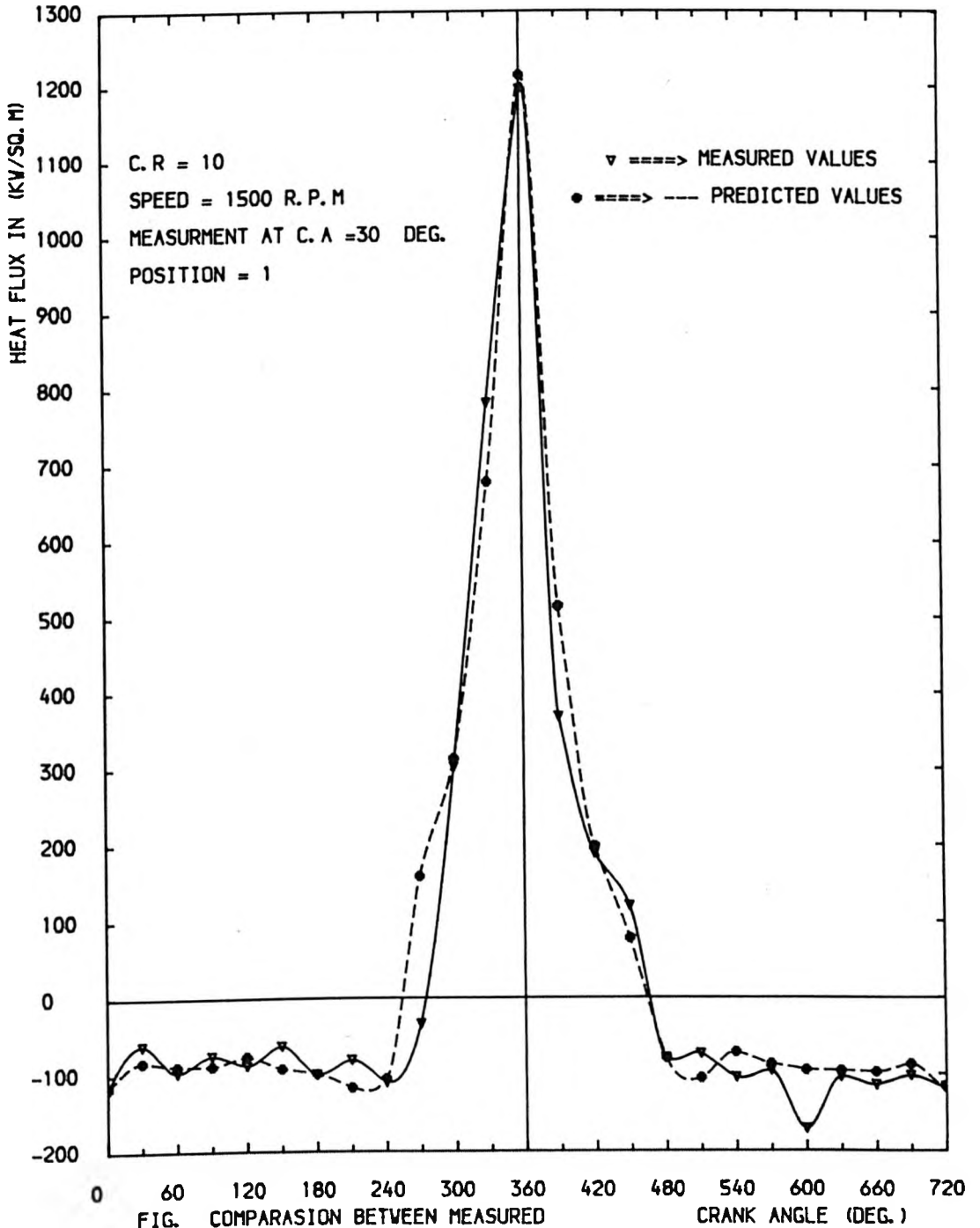


FIG. COMPARASION BETWEEN MEASURED & PREDICTED HEAT FLUX

FIG. 9.111

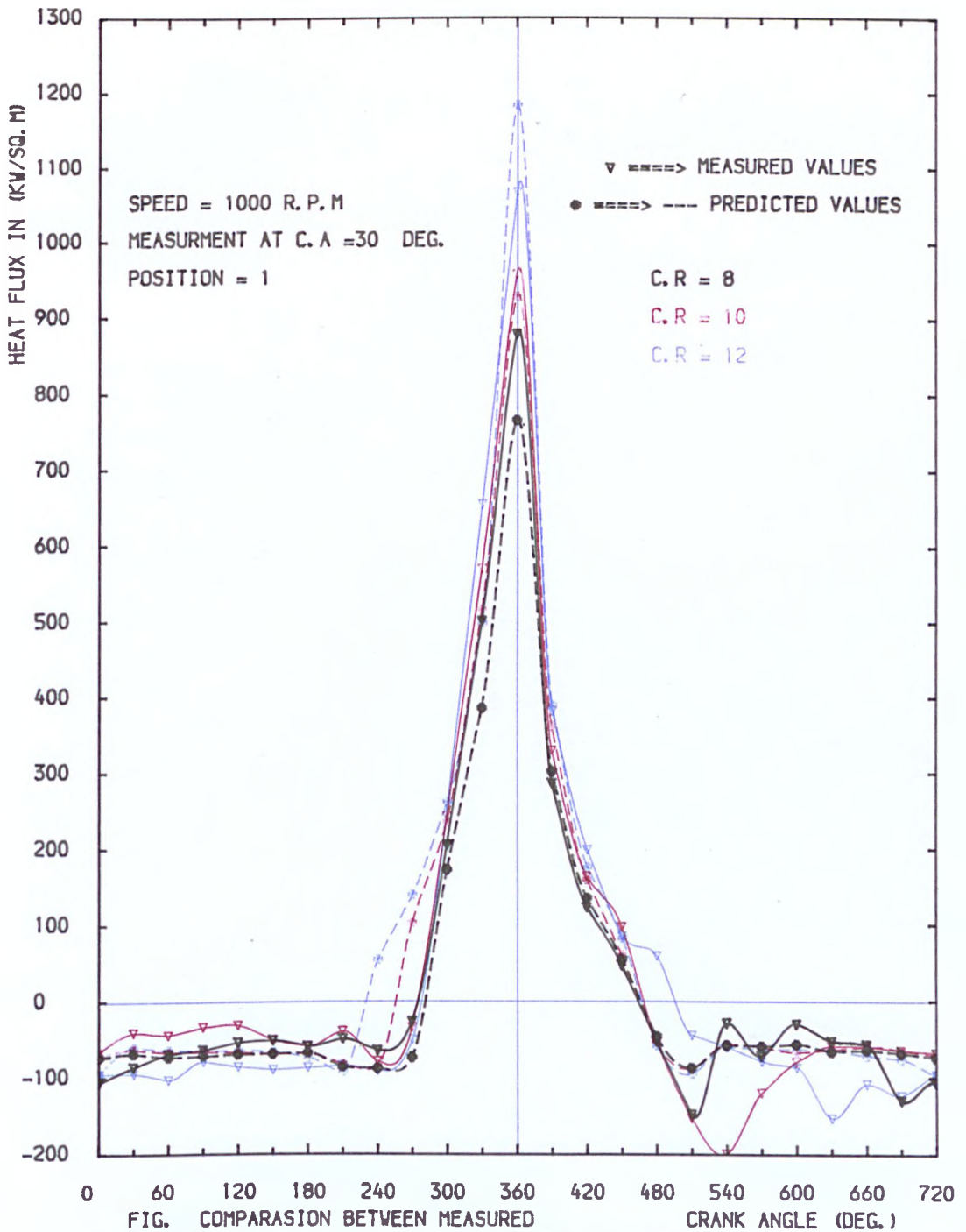


FIG. COMPARASION BETWEEN MEASURED & PREDICTED HEAT FLUX AT DIFFERENT COMPRESSION RATIOS

FIG. 9.112

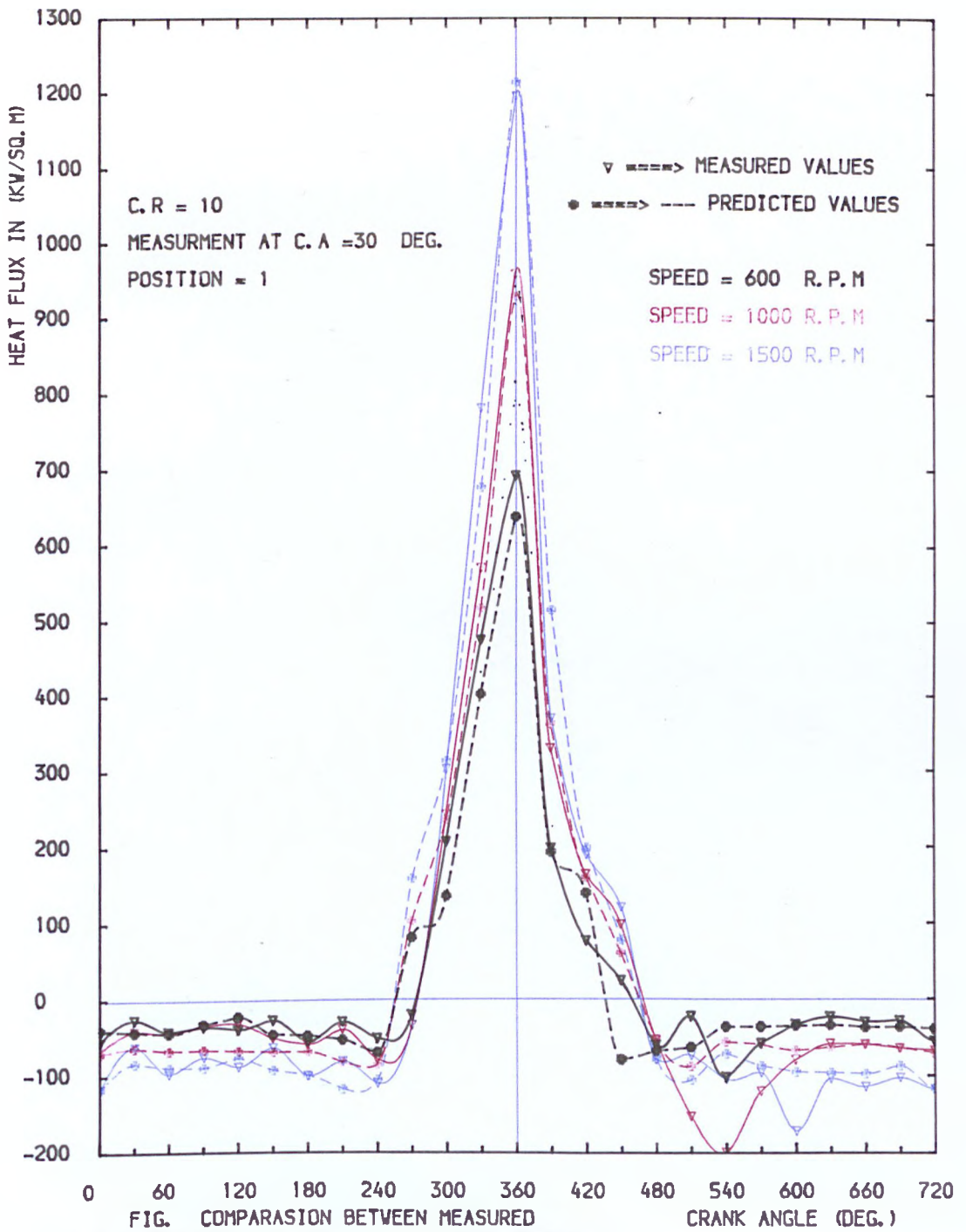


FIG. COMPARISON BETWEEN MEASURED & PREDICTED HEAT FLUX AT DIFFERENT SPEEDS

FIG. 9.113

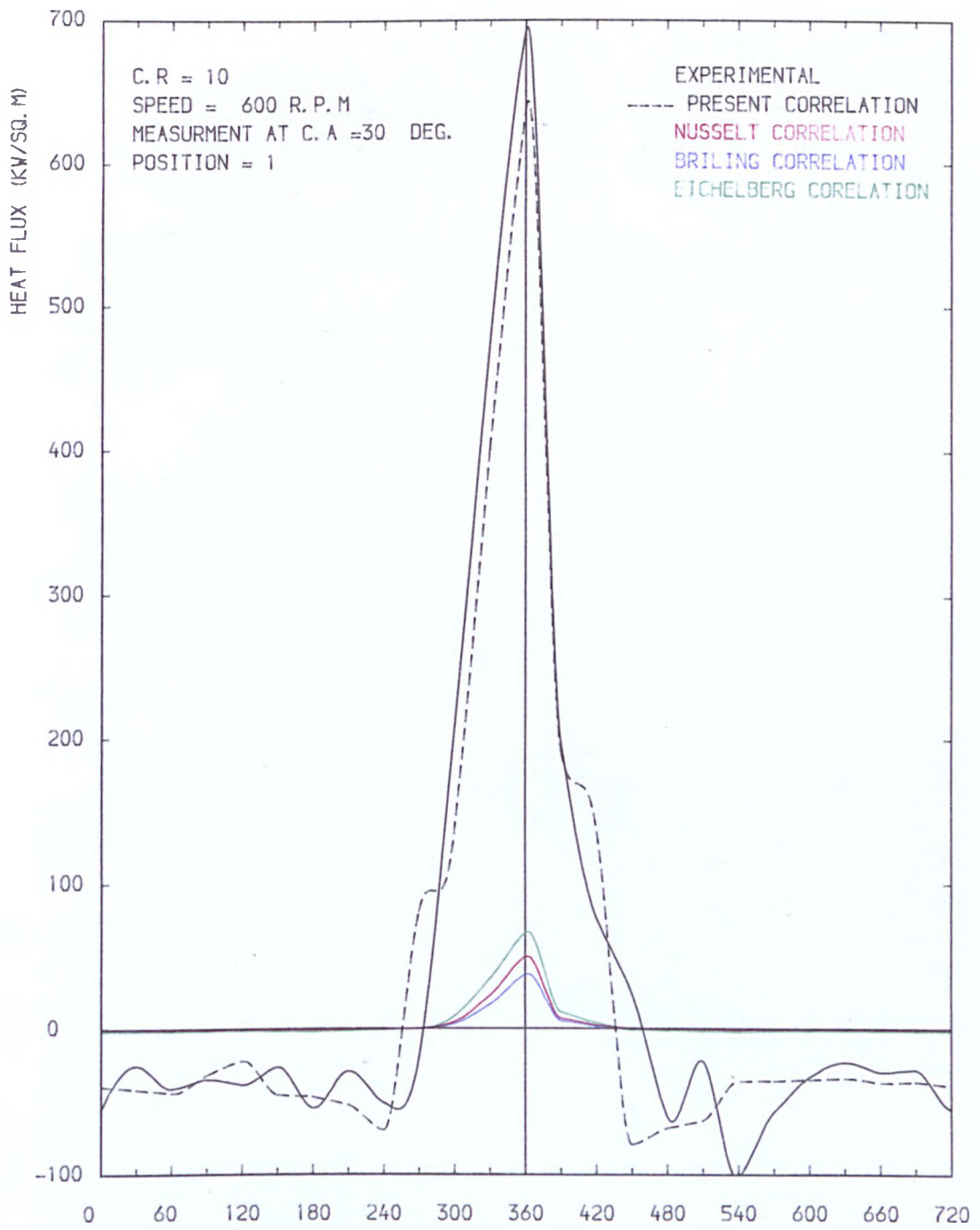


FIG. COMPARASION BETWEEN HEAT FLUX UNDER DIFFERENT CORRELATIONS

FIG. 9.114

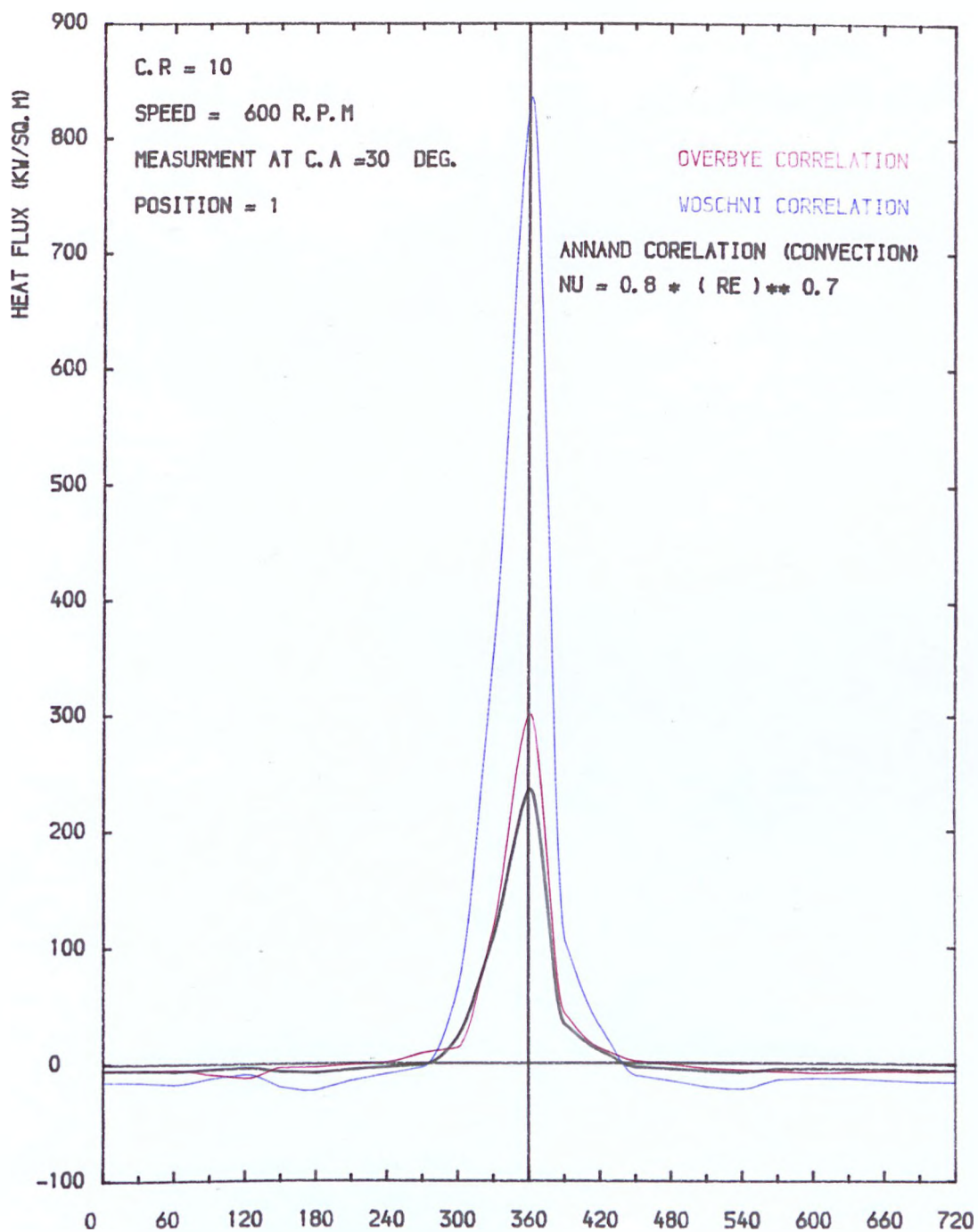


FIG. 9.114 COMPARASION BETWEEN HEAT FLUX UNDER DIFFERENT CORRELATIONS

CRANK ANGLE (DEG.)

FIG. 9.115

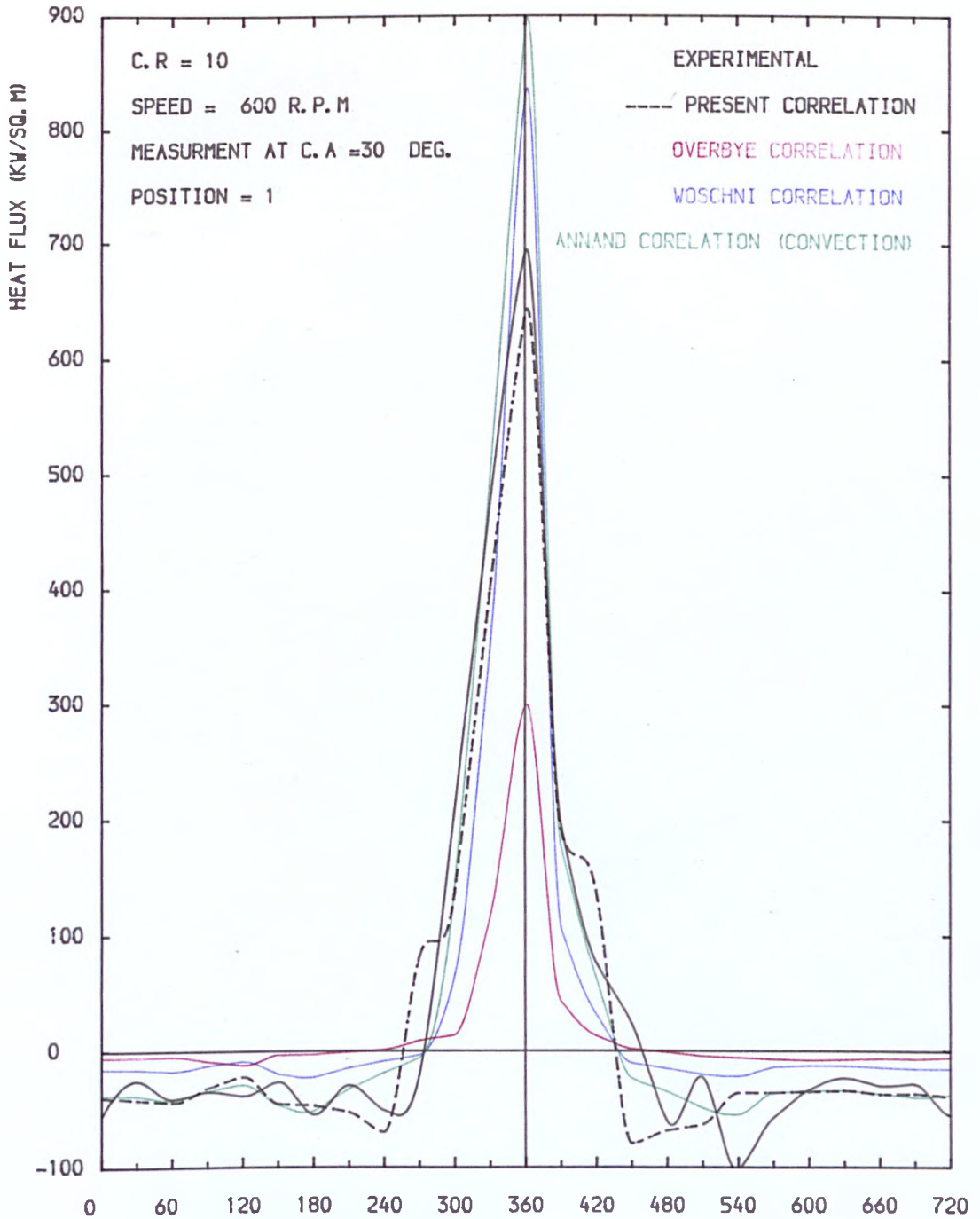


FIG. COMPARISON BETWEEN HEAT FLUX UNDER DIFFERENT CORRELATIONS

C H A P T E R 1 0

CONCLUSION AND SUGGESTIONS FOR FURTHER WORK

10.1 Conclusion

10.2 Suggestion for Further Work

10.1 CONCLUSION

From the present investigations the following conclusions are reached:-

1. The present design of surface thermocouple is adequate for measuring surface wall temperature under motoring condition, although there is an error due to the three dimensional situation.
2. Significant cycle-to-cycle variations in the surface temperature measurements, and consequently in the heat flux results, are observed at each location of measurement.
3. Large negative heat flux is observed during induction and expansion strokes, and this is due to the cold cylinder wall. This effect is not reproduced by other correlations.
4. The peak heat flux at each position investigated in the cylinder increases with increasing engine speed.
5. A significant influence of engine speed and compression ratio on the heat flux and the other measuring parameters is observed although the compression has less effect than the speed.
6. There is no significant phase lag between gas - wall temperature difference and heat flux, and the peak heat flux coincide with the peak temperature differences.
7. Heat transfer rate due to the radiation plays a negligible part in a motored reciprocating engine.
8. Any measured value of the parameters represents the value at a point in the combustion chamber at which the sensor is placed, i.e. the location has significant effect on the measuring parameters.

This explains why the heat transfer coefficient is different from one point to another in the combustion chamber. The differences may be explained in terms of differences in the fluid adjacent to the point.

9. The use of a data logging system improves the accuracy of the results and allows many parameters to be measured at the same time.
10. The method of averaging the measured values in the present work is different from the one used by other workers and shows reliable results.
11. The introduction of turbulence and instantaneous velocity into the correlation should improve the heat transfer prediction. The correlation does however need to be checked with different engine geometries under different operating conditions.
12. Ensemble average velocity and turbulence is increased as the engine speed is increased.
13. In this investigation the heat transfer coefficient was calculated at a point in the combustion chamber where the instantaneous velocity and turbulence were measured. At some points in the cycle the heat transfer coefficient has infinite value, but fortunately this occurs at these points where the heat flux is small.
14. The introduction of new dimensionless numbers is thought to be significant.
15. The present correlation shows an agreement with the experimental result under different conditions, although there is a discrepancy

due to the experimental errors of measuring parameters at a few points in the cycle.

16. Splitting the engine cycle into two separate periods, the valve closed revolution and the valve open revolution produces a better correlation between heat transfer and local fluid condition than if the cycle were treated as a single period.
17. The early existing correlations of Nusselt, Eichelberg and PFLAUM do not agree with both the experimental investigation and the correlation in the present work.
18. Annand, Woschni and Overbye correlations do agree with the present work, although some discrepancy is apparent. The discrepancy is explained by incorporating local velocity and turbulence into the correlation.

10.2 SUGGESTIONS FOR FURTHER WORK

The following points should be considered for further work in this field:-

1. Development of an improved heat flux meter.
2. Development of an engine cylinder with improved access for coincidental measurement in time and space.
3. Improved calibration in the hot wire anemometer under variable gas pressure and temperature is desirable.
4. Results should be obtained from engines with varying velocity and turbulence, together with other geometries.
5. Extend the work to a running engine.

6. Use improved anemometry to obtain the components of velocity and turbulence.

R E F E R E N C E S

1. ALCOCK, J. F.
"Air swirl in oil engines."
proc.I.Mech.Eng., Vol. 128, 1934
2. ALCOCK, J. F. and SCOTT, W. M.
"Some more light on diesel combustion."
proc.I.Mech.Eng. (A.D.), No.5, 1962-63
3. ALKIDAS, A. C.
"Thermal Loading of the cylinder head of a spark-ignition engine."
Heat transfer eng. Volume 3, No.3-4, pp.66-75, Coden HTEN D2
TSSN 01457632, Jan-June 1982
4. ALKIDAS, A. C.
"Heat transfer characteristics of a spark-ignition engine."
Transactions of the ASME, Journal of heat transfers, Vol.102,
p.189, 1980
5. ALKIDAS, A. C. and COLE, R. M.
"The distribution of heat rejection from a single-cylinder divided
chamber diesel engine."
SAE Spec. Publ. Sp-495 diesel cumbus. and Emiss., Part 3, Highway
and Expo. Milwaukee, U.S.A., 1981
6. ALKIDAS, A. C. and MYERS, J. P.
"Transient heat-flux measurements in the combustion chamber of a
spark-ignition engine."
ASME pap. 81-WA/HT-1 for meeting Nov. 15th-28th 1981.
7. ALPHA mini computer instruction manual.

8. ANNAND, W. J. D.
"Heat transfer in the cylinders of reciprocating internal combustion engines."
Proc.Instn.Mech.Engrs. Vol. 177, No.36, 1963
9. ANNAND, W. J. D. and MA, T. H.
"Instantaneous heat transfer rates to the cylinder head surface of a small compression-ignition engine."
proc.Instn.Mech.Engrs., Vol. 185, p.976, 1970-71
10. ANON,
"Measurement of gun barrel temperatures."
Instrum.Automat. Vol.2 (2), pp.71-73, 1955
11. ARNOLD, M. J., TINDAL, M. J. and WILLIAMS, T. J.
"Measurement of induction gas velocities in a reciprocating engine cylinder."
SAE Paper No. 720115, Autom.Eng. Congress, Detroit Jan. 1972.
12. ATESMEN, K. M.
"Heat transfer in rotary combustion engines."
ASME Transactions, May 1975.
13. BARTON, R. K., LESTZ, S. S. and MEYER, W. E.
"An empirical model for correlating cycle-by-cycle cylinder gas motion and combustion variations of a spark-ignition engine."
SAE Paper 710163, Jan. 1971.
14. BENDERSKY, D.
"A special thermocouple for measuring transient temperatures."
ASME, Vol. 75, pp.117-121, 1953

15. BENSON, R. S. and BRUNDRETT, W. G.
"Development of a resistance wire thermometer for measuring transient temperature in exhaust systems of internal combustion engines."
Temperature, its measurements and control in Science and Industry, Vol.3, Part. 2, editor Dahl, Reinhold publishing corporation N.Y. pp 117-144, 1964
16. BENSON, R. S. and PICK, R.
"Recent advances in internal combustion engine instrumentation with particular reference to high-speed data acquisition and automated test bed."
SAE, Paper No. 740695, National Combined Farm, construction and industrial machinery and power plant meetings Milwaukee, Wis. Sept. 9-12, 1974.
17. BERNARD, P. S.
"Computation of the turbulent flow in an internal combustion engine during compression."
Transaction of the ASME, Jour. of fluids Eng. Vol. 103/75, March 1981
18. BONE, W. A. and TOWNEND, D. T. A.,
"Flame and combustion in gases."
Published by Longmans, Green and Co. Ltd., London 1927
19. BORGNAKKE, C., ARPACI, V.S. and TABACZYNSKI, R. J.
"A model for the instantaneous heat transfer and trubulence in a spark ignition engine."
SAE Technical paper series, Congress and exposition cobo hall, Detroit, Feb 25-29, 1980.

- 20 BOYER, R. L., CRAIG, D. R. and MILLER, C. D.
"A photographic study of events in a 14 inch two stroke engine."
A.S.M.E., Vol.76, pp.97-108, 1954
21. BOYES, J.
A guide to the ALPHA LSI-2 computer.
Internal report of mechanical Engineering department, Liverpool
University, 1981
22. BRIMLEY and BREVOORT
"Correlation of engine cooling data."
NACA MR-LSA17, Jan., 1945.
23. BRADSHAW, P.
"An Introduction to turbulence and its measurement".
Pergamon Press, Oxford (1971).
24. BRYDSON, J. A.
"Plastic Materials"
London ILIFFE Books Ltd.
25. CARSLAW, H. S. and JAEGER, J. C.
"Conduction of heat in solids."
Second edition, OXFORD, Clarendon press.
26. CATON, J. A. and HEYWOOD, J. B.
"Models for heat transfer mixing and hydrocarbon oxidation in a
exhaust port of a spark-ignited engine."
SAE Tech. Paper. Series No. 800290. Congress and Exposition, cobo
hall, Detroit, Feb. 25-29, 1980.

27. CHEBYSHEV, P. V.
"Design of hot-wire anemometer for the investigation of ventilation of electrical equipment."
Otchet Vsesoyunznogo Elektrotekhnicheskogo Instituta imene Lenina. 1952.
28. CHIRKOV, A. A. and STEFANOVSKI, B. S.
"O dominiruyushchem sposobe pyerysdachi tepla v tsilindrach dvigatyelyei vnutryennyeto sgoraniya."
Trudy Rostovkova Instituta Inj'yenyeror Zyelyeznodorotnota Transporta 1958 21.
29. COLE, M. and SWORDS, M. D.
"Laser Doppler anemometry measurements in an engine."
Applied optics, Vol. 18, No.10, 15th May, 1979
30. DAHL, A. I. (Ed.)
Applied methods and instruments
Part 2 of Temperature: Its Measurement and Control in Science and Industry, Vol.3. New York, Reinhold: London, Chapman and Hall, 1962.
31. DAO, K., UYEHARA, O. A. and MYERS, P. S.
"Heat transfer rates at gas-wall interfaces in motored piston engine."
SAE, combined commercial vehicle Engineering and operations and powerplant meetings, Chicago, Paper No. 730632, June 18-22, 1973
32. DENT, J. C. and DERHAM, J. A.
"Air motion in a four-stroke direct injection diesel engine."
Proc.I.Mech.E. Vol. 188, 21/74, 1974.

33. DENT, J. C. and SALAMA, N. S.
"Turbulence Structure in the spark ignition Engine,"
Paper No. C83/75, I.MECH.E. Conference on combustion in engines,
Cranfield, 1975.
34. DENT, J. C. and SALAMA, N. S.
"The measurement of the turbulence characteristics in an internal
combustion engine."
SAE paper No. 750886, 1975
35. DENT, J. C. and SULIAMAN, S. J.
"Convective and radiative heat transfer in a high swirl direct
injection diesel engine."
SAE, International Automotive Engineering, Congress and Exposition
Cobo Hall, Detroit, Paper No. 770407, Feb. 28 - March 4, 1977
36. DISA "Technical DATA"
37. DIWAKAR, R.
"Direct injection stratified-charge engine computations with
improved submodels for turbulence and wall heat transfer."
SAE Tech. Paper. Series. International congress and Exposition,
Detroit, Michigan Feb 22-26, 1982.
38. EBERSOLE, G. D., MYERS, P. S. and UYEHARA, O. A.
"The radiant and convective components of Diesel engine heat
transfer."
SAE, Meeting Canada, 701C, Paper No. 639235, 1963
39. EICHELBERG, G.
"Temperaturverlauf und Warmespannung in Verbrennung Motoren."
VDI (Berlin) Forsch., 263, 1923

40. EICHELBERG, G.
"Some new investigations in old internal-combustion engine problem."
Engineering, London. 1939, 148, 463 and 547.
41. EICHELBERG, G. and PFLAUM, W.
"Untersuchung eines hochaufgeladene dieselmotors."
z.ver.dtsch.Ing. 1951 93, 1113. English translation in Mot. ship
1952 33, 18 and 58.
42. EL-KHAFAJI, A. H. A.
"Gas flow measurement in receprocatng engines cylinder."
Ph.D. Thesis, King's College, London, 1972.
43. EL-KHAFAJI, A. H. A., TINDAL, M. J. and WILLIAMS, T. J.
"Engine cylinder gas flow measurements by hot-wire anemometry."
Internal report, King's College, London, 1971.
44. ELSER, K.
"Der instationaire Wärmeübergang in diesel motoren."
Mitt. Inst. Thermodyn. Zürich No. 15, 1954
45. FALCUS, M.
Heat release in a highly pressure charged two-stroke diesel engine,
M.Sc. Thesis, U.M.I.S.T., 1970
46. FRENCH, C. C. J. and HARTLESS, E. R.
"The cooling of piston in marien diesel engines."
Proc. of the third international heat transfer conference.
Chicago, Illinois, papers 1 - 40, volume I, Aug. 7-12, 1966

47. FURUHAMA, S. and SUZUKI, H.
"Temperature distribution of piston rings and piston in high speed diesel engine."
Bulletin of the JSME, Vol.22, No. 174, Dec. 1979.
48. GEORGE, W. K.
"Limitations on the measurement of unsteady flow velocities with a laser doppler velocimeter."
Ordinance Research Laboratory, The Pennsylvania State University
U.S.A., 1971
49. GHIRLANDO, R.
"Radial flow in an engine cylinder near the end of compression."
Ph.D. Thesis, Liverpool University, 1973
50. GIEDT, W. H.
The determination of transient temperatures and heat transfer at a gas-metal interface applied to a 40mm gun barrel.
Jet propulsion, 25 (4), pp.158-162, 1955
51. GOSMAN, A. D. and JOHNS, R. J. R.
"Development of a predictive tool for in-cylinder gas motion in engines."
SAE, Technical paper series No. 780315, Congress and Exposition, Cobo Hall, Detroit, Feb. 27 - March 3, 1978
52. GOSMAN, A. D., JOHNS, R. J. R. TIPLER, W. and WATKINS, A. P.
"Computer simulation of in-cylinder flow, heat transfer and combustion." A Progress Report.
13th International Congress on combustion engines. VIENNA.
Session A4. D21. 1979

53. GOSMAN, A. D., MELLING, A., WHITELAW, J. H. and WATKINS, P.
"Axisymmetric flow in a motored reciprocating engine."
proc.Instn.Mech.Eng., Vol. 192, 1978
54. GOSMAN, A. D. and WATKINS, . P.
"A computer prediction method for turbulent flow and heat transfer
in piston cylinder assemblies."
proc. of Symposium of turbulent shear flow PENN. State University,
pp.5.23-5.30, 1977
55. GUERNIGOU, J., INDRIGO, C., MAISONNEUVE, Y. and MENTRE, P. G.
"Development of surface temperature fluxmeters."
Rech. Aerosp. - No. 3, May-June 1980.
56. HACKEMANN, P.
A method for measuring reapidly changing surface temperatures and
its application to gun barrels.
Theoretical Res. Transl., 1/46 arm. Res. Dept.
57. HADLEY, H. E.
Magnetism and Electricity for students
MacMillan and Co., Ltd., 1950
58. HANDBOOK OF CHEMISTRY AND PHYSICS
59th Edition, published by chemical Rubber Company, 1978-1979.
59. HASSAN, H.
"Unsteady heat transfer in a motored I.C. Engine Cylinder."
proc.Instn.Mech.Engrs., Volume. 185 80/71, 1970-71
60. HASSAN, H.
"Unsteady heat transfer in a motores internal combustion-engine."
Ph.D. Thesis, Loughborough University, 1968.

61. HASSAN, H. and DENT, J. C.
The measurement of air velocity in a motored Internal Combustion engine using a hot-wire anemometer.
proc.I.Mech.E., Vol. 185, 1970-71
62. HENEIN, N. A.
"Instantaneous heat transfer rates and coefficients between the gas and combustion chamber of a diesel engine."
SAE, International Automotive engineering Congress. Detroit, Michigan, No. 969B, Jan 11-15 1965.
63. HIRAKI, H. and RIFE, J. M.
"Performance and No_x Model of a Direct injection stratified charge engine."
SAE Technical paper series, No. 800050. Congress and Exposition, Cobo Hall, Detroit, Feb. 25-29, 1980.
64. HOHENBERG, G. F.
"Advanced approaches for heat transfer calculations."
SAE Spec. Publ. Sp.449 Diesel Eng. thermal loading off highw. VEH.meet and expo Milwaukee, Wiss. Paper No. 790825, 1979
65. HORVATIN, M.
Some problems concerning the analytical evaluation of the characteristics of hot-wire immersed in a fluid of variable pressures and temperatures.
DISA Information, No.8, July, 1969.
66. HORVATIN, M. and HUSSMAN, A. W.
"Measurement of air movements in internal combustion engine cylinders."
DISA Information, No.8, July, 1969.

67. HUEBNER, K. H. and McDONALD, A. T.
"A dynamic model and measurement technique for studying induction air swirl in an engine cylinder."
Journal of Engineering for Power, A.S.M.E., A92,2, pp.189-197, April, 1970.
68. HUG, K.
"Messung und Berchnung von kolbentemperaturen in dieselmotoren."
Mitt.Inst. Thermodyn. Zürich 1937 No. 1
69. HUTCHINSON, P., MORSE, A. and WHITELAW, J. H.
"Velocity measurements in motored engines experience and prognosis."
SAE. Technical paper series, Congress and Exposition, Cobo Hall, Detroit, Feb 27 - March 3, 1978
70. IHAN, I. M., GREEVES, G. and PROBERT, D. M.
"Prediction of soot and nitric oxide concentrations in diesel engine exhaust."
I.Mech.E., Conference on Air pollution control in Transport Engines, paper C142/71, 1971.
71. KAMEL, M. and WATSON, N.
"Heat transfer in the indirect injection diesel engine."
SAE Spec. Publ. Sp-449 Diesel Eng. thermal loading off highw.
VEH.meet and Expo. Milwaukee, Wiss. Paper No. 790826, 1979
72. KAMM, MITT
"Results of experiments with geometrically - similar cylinders of different size."
Deutschen Academy der luftfahrtforschung, Mar. 3, 1939.

73. KASTNER, L. J., TINDEL, M. J. and WILLIAMS, T. J.
"Velocity and rate of flow measurements in internal combustion engines".
Proc.I.Mech.E., Vol. 180, pt. 3G, 1965-66
74. KHAN, I. M.
"Contribution to discussion."
Proc.I.Mech.E. Vol. 184, pt. 3J, p.269, 1969-70
75. KHAN, I. M., GREEVES, G. and WANG, C. H. T.
"Factors affecting smoke and gaseous emissions from direct injection engines and a method of calculation."
SAE paper No. 730169, 1971
76. KHAN, I. M. and WANG, C. H. T.
"Factors affecting emissions of smoke and gaseous pollutants from direct injection diesel engines".
I.Mech.E. conference on Air Pollution, Control in Transport Engines (C151/71) 1971.
77. KNEEN, C. and WOOD, W. A.
"Charge motion and turbulence in an engine cylinder."
First progress report for the Ford Motor Company, Mech.Eng., Liverpool University, 1976.
78. KNIGHT, B. E.
"The problem of predicting heat transfer in diesel engines."
Proc.I.Mech.E. London, 179 pt. 3C, 1964-5.

79. KREYSZIG, E.
"Advanced Engineering Mathematics."
Third edition, Wiley International edition.
80. KRIEGER, R. B. and BORMAN, G. L.
"The computation of apparent heat release for Internal Combustion Engines."
ASME publication, paper 66-WA/DGP, 1966.
81. KU, P. M.
"Factors effecting heat transfer in the Internal Combustion Engine."
NACA TN 787, 1940.
82. KUETHE, A. M. and SCHETZER, J. D.
"Turbulence."
Foundation of Aerodynamics, New York. Wiley & Sons, Inc.,
Dept. of Aero. Eng. Univeristy of Michigan.
83. LANCASTER, D. R.
"Effect of engine variables on trubulence in a spark-ignition Engine."
S.A.E., Automotive Eng. Congress and Exposition Detroit,
Michigan, Feb. 23-27, 1976.
84. LARSENG, J. T., PRESTJORD, O., SANDTORV, H. and ISDAL, B.
Faster Engine testing with computer. Diesel and gas Turbine
Progress Worldwide, July-August 1976.

85. LAW, A. G.
Instantaneous heat transfer in an opposed-piston two-stroke Diesel engine.
Ph.D. Thesis, U.M.I.S.T., 1968

86. LEE, D. W.
"A study of air flow in an engine cylinder."
N.A.C.A. report No. 653, 1939.

87. LE FEUVRE, T., MYERS, P. S. and UYEHARA, O. A.
Experimental Instantaneous heat fluxes in a Diesel engine and their calculation.
Soc. Automat. Engrs., No. 690464, 1969

88. LOBO, P. C.
"The determination of Velocity patterns in engine cylinders by means of the hot-wire anemometer."
University of London, Ph.D. thesis, 1966.

89. LOBO, P. C.
"The hot-wire anemometer in engine research."
ASME paper 70-DGP-3 for meeting April 12-16, 1970.

90. LYN, W. T., STOCKWELL, A. J. and WANG, C. H. T.
Accuracy in cylinder pressure measurement
Proc.Instn.Mech.Eng., Vol. 180, 1969, pp.8-16.

91. LYN, W. T. and VALDMANIS, E.
"The application of high-speed schlieren photography to diesel combustion research."
Jrn1. Photo. Science. Vol. 10, 1962.

92. MATTAVI, J. N.
A miniature sensor for measuring heat-transfer rates in engines
Soc. Aut. Engrs., Paper No. 741078, pp.1-10, 1974.

93. MAULARD, J.
"Etude du fluxmeter a temperature superficielle pour mesures dans les tubes a choc-N.T. Onera, no. 139 (1969).

94. McADAMS, W. H.
"Heat transmission."
McGraw Hill Book Company, Inc.
Third Edition, 1954.

95. MELLING, A. and WHITELAW, J. H.
"Design of laser doppler anemometers for reciprocating engines."
Internal Report, Imperial College, Mech.Eng. Dept., London, 1976.

96. MOELLER, C. E.
"Thermocouples for the measurement of transient surface temperatures."
Temperature its measurement and control in science and industry,
Volume 3, Part 2, 1962

97. MONAGHAN, M. L. and PETTIFER, H. F.
"Air motion and its effect on diesel performance and emission."
SAE 810255.

98. MORSE, A. P., WHITELAW, J. H. and YIANNESKIS, M.
"Turbulent flow measurement by Laser-Doppler anemometry in motored piston-cylinder assemblies."
Transaction of the ASME, Vol. 101, No. 2, June, 1979.

99. MOSS, H.
"Heat transfer in internal combustion engines."
REP.MEMDR. AERO RES. COMM. LONDON, No. 1129, 1927.

100. NAGAO, F., IKEGAMI, M., MIWA, K., OKAZAKI, G., SUGIMOTO, H. and NANBA, T.
"Measurement of air flows by means of repetitive spark method."
J.S.E.M., Vol. 14, No. 78, pp.1340-1351, Dec. 1971.

101. NAGAO, F. and KAKIMOTO, H.
"Swirl and combustion in divided combustion chamber type diesel engines."
Trans. S.A.E., Vol. 70, pp.680-699, 1962.

102. NISHIWAKI, K., SHIMAMOTO, Y. and MIYAKE, K.
"Average heat transfer coefficients on a cylinder wall in the Intake and Exhaust processes of motoring test."
Bulletin of the JSME, Vol. 22, No. 174, Paper No. 174-13- Dec. 1979.

103. NUSSELT, W.
"Die warmeubergang in den Verbrennungs-kraftmaschinen."
z.ver.dtsch.Ing. 1923 67, 692 and 708.
104. OGURI, T.
"On the coefficient of heat transfer between gases and cylinder walls of the spark-ignition engine."
Bull.Jap.Soc.Mech.Engrs 1960 3,363.
105. OHIGASHI, S., HAMAMOTO, Y. and TANABE, S.
"A new digital method for measuring gas flow velocity by electric discharge."
SAE paper 690180, 1969.
106. OHIGASHI, S., HAMAMOTO, Y. and TANABE, S.
"Swirl - its measurement and effect on combustion in a diesel engine."
I.M.E. Conference on air pollution control in transport engines,
Nov., 1971.
107. OVERBYE, V. D., BENNETHUM, J. E. UYEHARA, O. A. and MYERS, P. S.
"Unsteady Heat transfer in Engines."
SAE Transactions, N.Y. Vol. 69, 461, 1961.
108. OZISIK, M. N.
"Heat conduction."
Wiley-interscience publ. New York, 1980.

109. PFLAUM, W.
Warmeubergang bei dieselmaschinen mit und ohne Aufladung.
M.T.Z. 1961 22, 70. English abstract in Engrs. Dig., N.Y. 1961
22.86.
110. PINKEL, Et.A1.
"Heat transfer processes in liquid-cooled engine cylinders."
NACA L-131, ARR E5 J31, Nov., 1945.
111. PINKEL and ELLERBROOK.
"Correlation of cooling data from an Air-cooled cylinder and
several multi-cylinder engines."
NACA TR 683, 1940.
112. POVOLNY Et.A1.
"Cylinder head temperatures and coolant heat rejection of a 1650
Cu In. liquid-cooled engine."
NACA TN 2069, Apr., 1950.
113. RAMOS, J. I., HUMPHREY, J. A. C. and SIRIGNANO, W. A.
"Numerical prediction of axisymmetric laminar and turbulent flows
in motored, reciprocating internal combustion engines."
SAE paper No. 790356.
114. RASK, R. B.
"Laser doppler anemometer measurements in an internal combustion
engine."
SAE Technical paper series, congress and exposition Cobo Hall,
Detroit, Feb. 26 - March 2, 1979.

115. RICARDO, H. R.
"Highspeed internal combustion engine."
Blackwell London 1955.
116. RICARDO, H. R.
"Combustion in diesel engines"
Proc.Inst. of Auto. Engrs., Vol. 24, pp.645-682.
117. ROGERS, G. F. C. and MAYHEW, Y. R.
Thermodynamic and transport properties of fluids, SI Units.
Third Edition, published by Basil Blackwell, Oxford, 1980.
118. ROHSENOW, W. M. and CHOI, H. Y.
"Heat, Mass and momentum transfer."
Prentice-Hall. International, London, 1961
119. ROTHROCK, A. M. and SPENCER, R. C.
"The influence of directed air flow on combustion in an S.I.
engine."
N.A.C.A. Report No. 657, 1939.
120. SAFFMAN, P. G. and WILCOX, D. C.
"Turbulence Model Prediction for turbulent boundary layers."
AIAA Journal, 12, No. 4., P.541, 1974.
121. SARSTEN, Arthur
Survey of theoretical and experimental evaluation of thermal
loading of diesel engines in Norway. Diesel Engine thermal
loading, off - highway vehicle meeting and exposition, MECCA,
Milwaukee, 1979.

122. SCHOCK, H. J., REGAN, C. A., RICE, W. J. and CHLEBECEK, R. A.
"Multicomponent Velocity measurement in a piston-cylinder
configuration using laser velocimetry."
TSI Quarterly, Volume IX, Issue 4. Oct - Dec 1983.
123. SEMENOV, E. S.
"Apparatus for investigation of turbulence in piston engines."
Pribory i Tekhnika Eksperimenta, No. 1, 1958.
124. SEMENOV, E. S.
"Studies of turbulent gas flow in piston engines."
Combustion in turbulent flow, ed. I.W. Khitrin,
Moscow 1959, translated by the Isreal program for scientific
translations, Ipst cat. No. 812, 1963.
125. SCHLICHTING, H.
"Boundary-Layer theory." Translated by J. Kestin
6th Edition, New York, McGraw Hill, 1968.
126. SIHLING, K. and WOSCHNI, G.
Experimental investigation of the instantaneous heat transfer in
the cylinder of a high speed diesel engine.
SAE Spec. Publ. sp-449 Diesel Eng. Thermal loading off-highway
vehicle meeting and exposition Milwaukee Wiss., Paper No. 790833
pp.95-103, 1979

127. SMYTH, R.
"Transient heat flow investigations using an on-line computer."
Thermodynamics and fluid mechanics convention, Institution of
Mech.Engrs., London 1968.
128. SPALDING, D. B.
"Convective Mass Transfer."
London, Edward Arnold Publ. Ltd., 1963
129. STAMBULEANU, A.
"Contribution to the study of the distribution of heat transfer
co-efficients during the phase of the working cycle of an internal
combustion engine."
Proceeding of the third international heat transfer conference.
Chicago, Illinois, Papers 1-40, Volume I, Aug 7-12, 1966.
130. TABACZYNSKI, R. J., BORGNAKKE, C. and ARPACI, V. S.
"A model for the instantaneous heat transfer and turbulence in
a spark ignition engine."
SAE Technical paper, congress and Exposition Cobo Hall, Detroit
Paper No. 8 002087, Feb. 25-29, 1980.
131. TAYLOR and TAYLOR INT.
"The internal combustion engines."
Text book company, 1938, rev. 1948.
132. TAYLOR, C. F.
"Heat transmission in Internal Combustion engine."
Proc. general discussion on heat transfer. INST.MECH.ENGINEERS,
London, Vol. 397, 1951.

133. TAYLOR, C. F.
"The internal combustion engine in theory and practice."
MIT Press, Volume 1, 1978.
134. TAYLOR, D. H. C.
"The application of a double pass schlieren system to a small
high speed diesel engine."
Proc. of 7th Int. Cong. on high-speed photography, Zurich, Sept.
1965.
135. TINDAL, M. J.
"An investigation of the induction process in four-stroke engines."
London University Ph.D.thesis, 1963.
136. TINDAL, M. J., WILLIAMS, T. J. and EL-KHAFAJI, A. H. A.
"Gas flow measurements in Engine Cylinder."
S.A.E., National combined Farm, construction and industrial,
Machinery and power plant meetings, Milwaukee, Wis. Paper No. 740719
Sept. 9-12, 1974.
137. TSU, T. C.
"A mathematical analysis of the intake and Exhaust processes of
the internal combustion engine."
Ph.D. Thesis, Massachusetts Institute of Technology, 1944.
138. WAKEFIELD, S. B.
Heat transfer in a two-stroke diesel engine
M.Sc. Thesis, Victoria University of Manchester, 1971.

139. WAKISAKA, T., HAMAMOTO, Y., OHIGASHI, S. and HASHIMOTO
"Measurements of air swirl and its turbulence characteristics
in the cylinder of an internal combustion engine."
I.Mech.E. paper No. C91/79, 1979.
140. WALLACE, F. J., WAY, R. J. B. and VOLLMERT, H.
"Effect of partial suppression of heat loss to coolant on the
high output diesel engine cycle."
SAE Spec. Publ. sp.449, Diesel Engine Thermal Loading off-highway
Vehicle. Meeting and Exposition Milwaukee Wis., 1979, pp.43-53.
141. WALZ, A.
"Boundary layers of flow and temperature."
Edited and Translated from the German by Oser, H.J. The M.I.T.
Press, England.
142. WATTS, R. and SCOTT, W. M.
"Air motion and fuel distribution requirements in high-speed
direction injection diesel engines."
Proc. I.Mech.E., Vol. 184, pt. 3J, 1969-70.
143. WAY, R. J. B. and WALLACE, F. J.
"Results of matching calculations for turbocharged and compound
engines with reduced heat loss."
SAE Spec. Publ sp.449. Diesel Engine Thermal Loading off-highway,
1979, pp.53-61.
144. WEIDENMULLER, M.
"Velocities in the combustion chamber of a motored diesel engine."
M.T.Z., April 1970, Vol. 31, No. 4, p.137-144.

145. WENGER, H.
Luftfahrtforschung, 19(2), 1939, translation supplied by King's
College, London.
146. WHITEHOUSE, N. D.
Heat Transfer in a quiescent chamber diesel engine.
Proc.Instn.Mech.Engrs., Volume 185, First Paper, p.963, 1970-71
147. WIGLEY, G. and HAWKINS, M. G.
"Three dimensional velocity measurements by laser anemometry in
a diesel engine cylinder under steady state inlet flow conditions."
SAE, Technical paper series, congress and exposition Cobo Hall
Detroit, Feb. 27 - March 3, 1978.
148. WILLIAMS, T. J.
"Cylinder gas flow and combustion in compression ignition engines."
Inst.Mech.Eng. Conference combustion in engines July 1975.
149. WITZE, P. O.
"Measurements of the spatical distribution and engine speed
dependence of turbulent air motion in I.C. Engine."
SAE paper No. 770220, 1977.
150. WITZKY, J. E. and CLARK, J. M.
"A study of the swirl stratified combustion principle."
S.A.E., paper 660092, Jan. 1966.
151. WONG, H. Y.
"Heat transfer for engineers."
Handbook of Essential Formulae and Data Longman, London and New
York, 1977.

152. WOSCHNI, G.

"A universally applicable equation for the instantaneous heat transfer coefficient in the internal combustion engine."

SAE Transaction, Volume 76, 1967, pp.3065-3065.

153. WOSCHNI, G.

"Prediction of thermal loading of supercharged diesel engines."

SAE Spec. Publ. sp.449. Diesel Engine Thermal Loading off-highway vehicle meeting and exposition Milwaukee Wis., 1979, pp.33-43.

154. WOSCHNI, G. and FIEGER, J.

"Determination of local heat transfer coefficients at the piston of a high speed diesel engine by evaluation of measured temperature distribution."

SAE Spec. Publ. sp.449. Diesel Engine Thermal Loading off-Highway Vehicle meeting and Exposition Milwaukee, Wis., 1979, pp.105-115.


155. YEH, Y. and CUMMINS, H. Z.

"Localized flow measurements with an He-Ne laser spectrometer."

Applied physics letters, 4, pp.176-178.

APPENDIX 8.1

Bootstrapping the ALPHA LSI-2 Disk Operating System

- (i) Load the BOOTSTRAP paper tape into the Teletype paper tape reader and set the control lever to "FREE"
- (ii) Move the tape to the start of the BINARY section. (This may be marked "  "). Set tape reader control lever to "START"
- (iii) Make sure a SYSTEM diskette is loaded into drive 0 (F0)
- (iv) Press "STOP" on computer so that light above the switch is LIT
- (v) Press $\frac{\text{"SREG"}}{\text{DATA}}$ switch so that the light above it is LIT
- (vi) Press 0 on the HEXADECIMAL keypad on the computer
- (vii) Press $\frac{\text{"SREG"}}{\text{DATA}}$ again so that the light above it goes OUT
- (viii) Press "SENSE" switch so that the light above it is LIT
- (ix) Press "RESET"
- (x) Press "STOP" switch again so that the light above it goes OUT
- (xi) Press switch marked "AUTO"

If computer fails to respond within 20 secs. re-try from instruction

- (i). If it still fails try switching the computer off for a minute or so then re-try from (i).

APPENDIX 8.2

Machine Language (ML) Codes Used in Programs WS1 and WS2

CODE INSTRUCTION	EXPLINATION
ADD	Add to Accumulator (ACC) (A-register)
AND	And with ACC
CAR or CAX	Complement A or complement A and put in X
DAR or DXR	Decrement (subtract 1) ACC. or X-register
DIN or EIN	Disable or Enable interrupts
EMA	Exchange ACC. with memory
EXTR	External and this can be used for any subroutines from Basic which the ML program is likely to call should be declared as External
HLT	Stop the computer
IAR or IXR	Increment (add 1) ACC. or X-register
ICA or ICX	Input console register to ACC. or X-register
IMS	Increment memory, skip on zero
IOR	OR with ACC
JMP	Unconditional jump to lable or $\$ \pm N$
JST	Jump and store program counter (used for subroutines)
JAL or JAG	Jump if $ACC \leq 0$ or if $ACC > 0$
JAM or JXM	Jump if ACC or X-register is minus
JAZ or JXZ	Jump if ACC or X-register is zero
JAN or JXN	Jump if ACC. or X-register is not zero
JSS or JSR	Jump if SENSE light is ON or OFF respectively

CODE INSTRUCTION	EXPLANATION
LAP or LXP	Load ACC or X-register with +Ve byte (0→ FF)
LAM or LXM	Load ACC or X-register with -VE byte (0→ FF)
LDA or LDX	Load into ACC or X-register from memory
LLA or LLX	Shift the A or X-register left
LRA or LRX	The number of places specified (Maximum = 8)
NAR or NXR	Negate ACC or X-register
NOP	No operation
OCA or OCX	Output ACC or X-register to console register
OTA or OTX	Output ACC or X-register to device selected
RLA or RLX	Shift the A or X-register right
RRA or RRX	Number of places specified (Maximum = 8)
RDA or RDX	Read from device to ACC or X-register
STA or STX	Store ACC or X-register into memory
SUB	Subtract from ACC
SBM or SWM	Set BYTE or word mode
SEL	Select device with code
SEN	Sense device and skip on response
XOR	Exclusive or with ACC
ZAR or ZXR	Zero (clear) ACC or X-register
ZAX	Zero (clear) ACC or X-register
SEN : 11,4	Sence if a disk controller is present and skip the next instruction if it is

CODE INSTRUCTION

EXPLANATION

OTX : 11,0	Send a command to the disk. The address of the control information is in the X-register
SEN : 11,0 JMP : \$-1	Wait in this loop until the disk has finished its input/output (I/O)
SEL : 12,0	Initialise A to D convertor
SEL : 12,7	Prepare for mode
SEL : 12,6	Prepare for channel
OTA or OTX : 12,2	ACC or X-register sent to control A/D convertor
RDA or RDX : 12,6	Get an A/D convertor in ACC or X-register
SEL : 12,3	Initialise D/A convertor

APPENDIX 8.3

Machine Language Program Name WS1

This machine language program was written in Macro assembler instructions and the main explanation of the program runs briefly as follows:-

<u>Instruction No.</u>	<u>Illustration</u>
7 - 9	Cylinder start
10 - 12	Cylinder finish
15 - 18	Low channel
19 - 24	High channel
25 - 28	Make sure the disk controller is properly connected
29 - 47	These instructions guarantee that the head is left over cylinder zero
52 - 123	Read and load the parameter into the Buffer 1 and 2
124 - 153	Subroutine called GPAR which will take the next parameter and convert it to binary number
154 - 182	Finish and error message

/EX OS:MAC,NB

MACR02 (A2)

PAGE 0001 MM/DD/YY 00:39:08

MACR02 (A2) SI = WS1:S B0=

```
0001          *NEWENG.  DISK DATA COLLECTION.
0002          *MODIFIED FOR PARAMETER INPUT
0003          *JTB.  7:82.
0004          EXTR      SPND:, SUPV:, MSG:, TERM:
0005  0000  F900  0000  ENTRY  JST      SPND:
0006  0001  00A3          DATA  MSG1
0007  0002  FA73  0076          JST      GPAR
0008  0003  B290  0094          LDA      SORB+5
0009  0004  9A93  0098          STA      SYLNO
0010  0005  FA70  0076          JST      GPAR
0011  0006  B28D  0094          LDA      SORB+5
0012  0007  9290  0098          SUB      SYLNO
0013  0008  0210          CAR
0014  0009  9A8B  0095          STA      MCKNT
0015  000A  FA6B  0076          JST      GPAR
0016  000B  C6FF          LAP      :FF
0017  000C  8287  0094          AND      SORB+5
0018  000D  9A88  0096          STA      CHANS
0019  000E  FA67  0076          JST      GPAR
0020  000F  C6FF          LAP      :FF
0021  0010  8283  0094          AND      SORB+5
0022  0011  1357          LLA      :8
0023  0012  8A83  0096          ADD      CHANS
0024  0013  9A82  0096          STA      CHANS
0025  0014  498C          SEN      :11,4
0026  0015  F28A  00A0          JMP      NO CONT
0027  0016  4988          SEN      :11,0
0028  0017  F601  0016          JMP      $-1
0029  0018  E239  0052          LDX      IOBP
0030  0019  C609          LAP      9
0031  001A  9C00  0000          STA      @0
0032  001B  C602          LAP      2
0033  001C  9C03  0003          STA      @3
0034  001D  0110          ZAR
```

MACRO2 (A2) SI = WS1:S B0=

0035	001E	9A78	0097	STA	SSW
0036	001F	9A79	0099	STA	PC
0037	0020	9C07	0007	STA	@7
0038	0021	6E88		OTX	:11,0
0039	0022	4988		SEN	:11,0
0040	0023	F601	0022	JMP	\$\$-1
0041	0024	C750		LAM	80
0042	0025	9C03	0003	STA	@3
0043	0026	6E88		OTX	:11,0
0044	0027	4988		SEN	:11,0
0045	0028	F601	0027	JMP	\$\$-1
0046	0029	C602		LAP	2
0047	002A	9C00	0000	STA	@0
0048	002B	B26E	009A	LDA	PDINT
0049	002C	9C07	0007	STA	@7
0050	002D	B22F	005D	LDA	PBUF1
0051	002E	9A6D	009C	STA	POINT
0052	002F	4097		SEL	:12,7
0053	0030	C402		NXTCY LXP	2
0054	0031	6E92		OTX	:12,2
0055	0032	4096		SEL	:12,6
0056	0033	E262	0096	LDX	CHANS
0057	0034	6E92		OTX	:12,2
0058	0035	B265	009B	MORE LDA	M1664
0059	0036	9A66	009D	STA	COUNT
0060	0037	5996		HERE RDA	:12,6
0061	0038	9B63	009C	STA	*POINT
0062	0039	DA62	009C	IMS	POINT
0063	003A	DA62	009D	IMS	COUNT
0064	003B	F604	0037	JMP	HERE
0065	003C	B25A	0097	LDA	SSW
0066	003D	3105	0043	JAN	\$\$+6
0067	003E	B21E	005D	LDA	PBUF1
0068	003F	9A19	0059	STA	DBUFF
0069	0040	B21D	005E	LDA	PBUF2
0070	0041	9A5A	009C	STA	POINT
0071	0042	F204	0047	JMP	\$\$+5
0072	0043	B21A	005E	LDA	PBUF2

MACRO2 (A2) SI = WS1:S B0=

0073	0044	9A14	0059		STA	DBUFF
0074	0045	B217	005D		LDA	PBUF1
0075	0046	9A55	009C		STA	POINT
0076	0047	B24F	0097		LDA	SSW
0077	0048	0210			CAR	
0078	0049	9A4D	0097		STA	SSW
0079	004A	E207	0052		LDX	IOBP
0080	004B	B24C	0098		LDA	SYLNO
0081	004C	9C02	0002		STA	@2
0082	004D	924B	0099		SUB	PC
0083	004E	9C03	0003		STA	@3
0084	004F	6E88			OTX	:11,0
0085	0050	0A00			EIN	
0086	0051	F61C	0035		JMP	MORE
0087	0052	0053		IOBP	DATA	IOB
0088	0053	0000		IOB	DATA	0
0089	0054	0001			DATA	1
0090	0055	0000			DATA	0
0091	0056	0000			DATA	0
0092	0057	0001			DATA	1
0093	0058	0680			DATA	1664
0094	0059	073F		DBUFF	DATA	BUFF2
0095	005A	005F			DATA	DINT
0096	005B	0000			DATA	0
0097	005C	0000			DATA	0
0098	005D	00BF		PBUF1	DATA	BUFF1
0099	005E	073F		PBUF2	DATA	BUFF2
0100	005F	FA02	0062	DINT	JST	DO
0101	0060	0000			NOP	
0102	0061	F20E	0070		JMP	DONT
0103	0062	0800		DO	ENT	
0104	0063	9A3A	009E		STA	STORA
0105	0064	EA3A	009F		STX	STORX
0106	0065	DA32	0098		IMS	SYLNO
0107	0066	E614	0052		LDX	IOBP
0108	0067	B402	0002		LDA	@2
0109	0068	9A30	0099		STA	PC
0110	0069	B234	009E		LDA	STORA

MACRO2 (A2) SI = WS1:S BO=

0111	006A	E234	009F		LDX	STORX
0112	006B	DA29	0095		IMS	MCKNT
0113	006C	F70A	0062		JMP	*D0
0114	006D	F900	0000		JST	MSG:
0115	006E	00A9			DATA	MSG2
0116	006F	F100	0000		JMP	TERM:
0117	0070	C6FF		DONT	LAP	:FF
0118	0071	8615	005C		AND	DBUFF+3
0119	0072	4404			ØCA	
0120	0073	F900	0000		JST	SPND:
0121	0074	00B4			DATA	MSG4
0122	0075	F675	0000		JMP	ENTRY
0123	0076	0800		GPAR	ENT	
0124	0077	F900	0000		JST	SUPV:
0125	0078	008F			DATA	SORB
0126	0079	E601	0078		LDX	\$-1
0127	007A	C600			LAP	0
0128	007B	9C05	0005		STA	@:5
0129	007C	B402	0002		LDA	@:2
0130	007D	0310			NAR	
0131	007E	9C03	0003		STA	@:3
0132	007F	0E00		BACK	SBM	
0133	0080	B30F	0090		LDA	*SORB+1
0134	0081	0F00			SWM	
0135	0082	8404	0004		AND	@:4
0136	0083	8C05	0005		ADD	@:5
0137	0084	9C05	0005		STA	@:5
0138	0085	DC03	0003		IMS	@:3
0139	0086	F201	0088		JMP	\$+2
0140	0087	F711	0076		JMP	*GPAR
0141	0088	9C05	0005		STA	@:5
0142	0089	1351			LLA	:2
0143	008A	8C05	0005		ADD	@:5
0144	008B	1350			LLA	:1
0145	008C	9C05	0005		STA	@:5
0146	008D	DA02	0090		IMS	SORB+1
0147	008E	F60F	007F		JMP	BACK

MACRO2 (A2) SI = WS1:S B0=

0148	008F	0005		SORB	DATA	:5
0149	0090	0000			DATA	:0
0150	0091	0000			DATA	:0
0151	0092	0000			DATA	:0
0152	0093	000F			DATA	:F
0153	0094	0000			DATA	:0
0154	0095	0000		MCKNT	DATA	0
0155	0096	0000		CHANS	DATA	0
0156	0097	0000		SSW	DATA	0
0157	0098	0000		SYLNO	DATA	0
0158	0099	0000		PC	DATA	0
0159	009A	005F		PDINT	DATA	DINT
0160	009B	F980		M1664	DATA	-1664
0161	009C	0000		POINT	DATA	0
0162	009D	0000		COUNT	DATA	0
0163	009E	0000		STORA	DATA	0
0164	009F	0000		STORX	DATA	0
0165	00A0	F900	0000	NOCONT	JST	SPND:
0166	00A1	00AF			DATA	MSG3
0167	00A2	F6A2	0000		JMP	ENTRY
0168	00A3	0BA0		MSG1	DATA	FIN1-\$*2-1%8+' '
0169	00A4	D2C5			TEXT	'READY F1.'
	00A5	C1C4				
	00A6	D9A0				
	00A7	C6B1				
	00A8	AFA0				
0170		00A9		FIN1	EQU	\$
0171	00A9	0BA0		MSG2	DATA	FIN2-\$*2-1%8+' '
0172	00AA	C6C9			TEXT	'FINISHED.'
	00AB	CEC9				
	00AC	D3C8				
	00AD	C5C4				
	00AE	AEA0				
0173		00AF		FIN2	EQU	\$
0174	00AF	09A0		MSG3	DATA	FIN3-\$*2-1%8+' '
0175	00B0	CECF			TEXT	'NO D.C.'

PAGE 0006 MM/DD/YY 00:39:08

MACRO2 (A2) SI = WS1:S B0=

	00B1	A0C4			
	00B2	AEC3			
	00B3	AEA0			
0176		00B4	FIN3	EQU	\$
0177	00B4	15A0	MSG4	DATA	FIN4-\$*2-1%8+' '
0178	00B5	C4C1		TEXT	'DATA TRANSFER ERROR'
	00B6	D4C1			
	00B7	A0D4			
	00B8	D2C1			
	00B9	CED3			
	00BA	C6C5			
	00BB	D2A0			
	00BC	C5D2			
	00BD	D2CF			
	00BE	D2A0			
0179		00BF	FIN4	EQU	\$
0180	00BF		BUFF1	RES	1664
0181	073F		BUFF2	RES	1664
0182				END	
0000	ERRORS				

PAGE 0007 MM/DD/YY 00:39:08

MACRO2 (A2) SI = WS1:S B0=

0000 WARNING

MACRO2 (A2) END

A P P E N D I X 8.4

MACHINE LANGUAGE PROGRAM NAME WS2

This ML program was modified to control the number of data points required. The explanation is the same as in ML WS1 except the instructions from 25 to 32 is added in order to control the number of data points required. The rest of the instructions are the same as in ML WS1

/EX OS:MAC,NB

MACRO2 (A2)

PAGE 0001 MM/DD/YY 01:00:25

MACRO2 (A2) SI = WS2:S BO=

0001				*NEW ENG. DISK DATA COLLECTION.	
0002				*MODIFIED FOR PARAMETER INPUT	
0003				*J.B. 7:82.	
0004				EXTR	SPND: ,SUPV: ,MSG: ,TERM:
0005	0000	F900	0000	ENTRY JST	SPND:
0006	0001	00A7		DATA	MSG1
0007	0002	FA77	007A	JST	GPAR
0008	0003	B294	0098	LDA	SORB+5
0009	0004	9A97	009C	STA	SYLNO
0010	0005	FA74	007A	JST	GPAR
0011	0006	B291	0098	LDA	SORB+5
0012	0007	9294	009C	SUB	SYLNO
0013	0008	0210		CAR	
0014	0009	9A8F	0099	STA	MCKNT
0015	000A	FA6F	007A	JST	GPAR
0016	000B	C6FF		LAP	:FF
0017	000C	828B	0098	AND	SORB+5
0018	000D	9A8C	009A	STA	CHANS
0019	000E	FA6B	007A	JST	GPAR
0020	000F	C6FF		LAP	:FF
0021	0010	8287	0098	AND	SORB+5
0022	0011	1357		LLA	:8
0023	0012	8A87	009A	ADD	CHANS
0024	0013	9A86	009A	STA	CHANS
0025	0014	FA65	007A	JST	GPAR
0026	0015	B282	0098	LDA	SORB+5
0027	0016	0310		NAR	
0028	0017	9A87	009F	STA	M1664
0029	0018	498C		SEN	:11,4
0030	0019	F28A	00A4	JMP	NO CONT
0031	001A	4988		SEN	;11.0
0032	001B	F601	001A	JMP	\$-1
0033	001C	E239	0056	LDX	IOBP

PAGE 0002 MM/DD/YY 01:00:25

MACRO2 (A2) SI = WS2:S B0=

0034	001D	C609		LAP	9	
0035	001E	9C00	0000	STA	@0	
0036	001F	C602		LAP	2	
0037	0020	9C03	0003	STA	@3	
0038	0021	0110		ZAR		
0039	0022	9A78	009B	STA	SSW	
0040	0023	9A79	009D	STA	PC	
0041	0024	9C07	0007	STA	@7	
0042	0025	6E88		OTX	:11,0	
0043	0026	4988		SEN	:11,0	
0044	0027	F601	0026	JMP	-\$-1	
0045	0028	C750		LAM	80	
0046	0029	9C03	0003	STA	@3	
0047	002A	6E88		OTX	:11,0	
0048	002B	4988		SEN	:11,0	
0049	002C	F601	002B	JMP	-\$-1	
0050	002D	C602		LAP	2	
0051	002E	9C00	0000	STA	@0	
0052	002F	B26E	009E	LDA	PDINT	
0053	0030	9C07	0007	STA	@7	
0054	0031	B22F	0061	LDA	PBUF1	
0055	0032	9A6D	00A0	STA	POINT	
0056	0033	4097		SEL	:12,7	
0057	0034	C402	NXTCY	LXP	2	
0058	0035	6E92		OTX	:12,2	
0059	0036	4096		SEL	:12,6	
0060	0037	E262	009A	LDX	CHANS	
0061	0038	6E92		OTX	12,2	
0062	0039	B265	009F	MORE	LDA	M1664
0063	003A	9A66	00A1	STA	COUNT	
0064	003B	5996	HERE	RDA	:12,6	
0065	003C	9B63	00A0	STA	*POINT	
0066	003D	DA62	00A0	IMS	POINT	
0067	003E	DA62	00A1	IMS	COUNT	
0068	003F	F604	003B	JMP	HERE	
0069	0040	B25A	009B	LDA	SSW	

MACRO2 (A2) SI = WS2:S BO=

0070	0041	3105	0047		JAN	\$+6
0071	0042	B21E	0061		LDA	PBUF1
0072	0043	9A19	005D		STA	DBUFF
0073	0044	B21D	0062		LDA	PBUF2
0074	0045	9A5A	00A0		STA	POINT
0075	0046	F204	004B		JMP	\$+5
0076	0047	B21A	0062		LDA	PBUF2
0077	0048	9A14	005D		STA	DBUFF
0078	0049	B217	0061		LDA	PBUF1
0079	004A	9A55	00A0		STA	POINT
0080	004B	B24F	009B		LDA	SSW
0081	004C	0210			CAR	
0082	004D	9A4D	009B		STA	SSW
0083	004E	E207	0056		LDX	IOBP
0084	004F	B24C	009C		LDA	SYLNO
0085	0050	9C02	0002		STA	@2
0086	0051	924B	009D		SUB	PC
0087	0052	9C03	0003		STA	@3
0088	0053	6E88			OTX	:11,0
0089	0054	0A00			EIN	
0090	0055	F61C	0039		JMP	MORE
0091	0056	0057		IOBP	DATA	IOB
0092	0057	0000		IOB	DATA	0
0093	0058	0001			DATA	1
0094	0059	0000			DATA	0
0095	005A	0000			DATA	0
0096	005B	0001			DATA	1
0097	005C	0680			DATA	1664
0098	005D	0743		DBUFF	DATA	BUFF2
0099	005E	0063			DATA	DINT
0100	005F	0000			DATA	0
0101	0060	0000			DATA	0
0102	0061	00C3		PBUF1	DATA	BUFF1
0103	0062	0743		PBUF2	DATA	BUFF2
0104	0063	FA02	0066	DINT	JST	DO
0105	0064	0000			NOP	
0106	0065	F20E	0074		JMP	DONT

PAGE 0004 MM/DD/YY 01:00:25

MACRO2 (A2) SI = WS2:S B0=

0107	0066	0800		DO	ENT	
0108	0067	9A3A	00A2		STA	STORA
0109	0068	EA3A	00A3		STX	STORX
0110	0069	DA32	009C		IMS	SYLNO
0111	006A	E614	0056		LDX	IOBP
0112	006B	B402	0002		LDA	@2
0113	006C	9A30	009D		STA	PC
0114	006D	B234	00A2		LDA	STORA
0115	006E	E234	00A3		LDX	STORX
0116	006F	DA29	0099		IMS	MCKNT
0117	0070	F70A	0066		JMP	*DO
0118	0071	F900	0000		JST	MSG:
0119	0072	00AD			DATA	MSG2
0120	0073	F100	0000		JMP	TERM:
0121	0074	C6FF		DONT	LAP	:FF
0122	0075	8615	0060		AND	DBUFF+3
0123	0076	4404			OCA	
0124	0077	F900	0000		JST	SPND:
0125	0078	00B8			DATA	MSG4
0126	0079	F679	0000		JMP	ENTRY
0127	007A	0800		GPAR	ENT	
0128	007B	F900	0000		JST	SUPV:
0129	007C	0093			DATA	SORB
0130	007D	E601	007C		LDX	\$\$-1
0131	007E	C600			LAP	0
0132	007F	9C05	0005		STA	@:5
0133	0080	B402	0002		LDA	@:2
0134	0081	0310			NAR	
0135	0082	9C03	0003		STA	@:3
0136	0083	0E00		BACK	SBM	
0137	0084	B30F	0094		LDA	*SORB+1
0138	0085	0F00			SWM	
0139	0086	8404	0004		AND	@:4
0140	0087	8C05	0005		ADD	@:5
0141	0088	9C05	0005		STA	@:5
0142	0089	DC03	0003		IMS	@:3
0143	008A	F201	008C		JMP	\$\$+2
0144	008B	F711	007A		JMP	*GPAR

MACRO2 (A2) SI = WS2:S B0=

0145	008C	9C05	0005		STA	@:5
0146	008D	1351			LLA	:2
0147	008E	8C05	0005		ADD	@:5
0148	008F	1350			LLA	:1
0149	0090	9C05	0005		STA	@:5
0150	0091	DA02	0094		IMS	SORB+1
0151	0092	F60F	0083		JMP	BACK
0152	0093	0005		SORB	DATA	:5
0153	0094	0000			DATA	:0
0154	0095	0000			DATA	:0
0155	0096	0000			DATA	:0
0156	0097	000F			DATA	:F
0157	0098	0000			DATA	:0
0158	0099	0000		MCKNT	DATA	0
0159	009A	0000		CHANS	DATA	0
0160	009B	0000		SSW	DATA	0
0161	009C	0000		SYLNO	DATA	0
0162	009D	0000		PC	DATA	0
0163	009E	0063		PDINT	DATA	DINT
0164	009F	F980		M1664	DATA	-1664
0165	00A0	0000		POINT	DATA	0
0166	00A1	0000		COUNT	DATA	0
0167	00A2	0000		STORA	DATA	0
0168	00A3	0000-		STORX	DATA	0
0169	00A4	F900	0000	NOCONT	JST	SPND:
0170	00A5	00B3			DATA	MSG3
0171	00A6	F6A6	0000		JMP	ENTRY
0172	00A7	OBA0		MSG1	DATA	FIN1-\$*2-1%8+' '
0173	00A8	D2C5			TEXT	'READY F1.'
	00A9	C1C4				
	00AA	D9A0				
	00AB	C6B1				
	00AC	AEA0				
0174		00AD		FIN1	EQU	\$
0175	00AD	OBA0		MSG2	DATA	FIN2-\$*2-1%8+' '
0176	00AE	C6C9			TEXT	'FINISHED.'

PAGE 0006 MM/DD/YY 01:00:25

MACRO2 (A2) SI = WS2:S B0=

	00AF	CEC9			
	00B0	D3C8			
	00B1	C5C4			
	00B2	AEA0			
0177		00B3	FIN2	EQU	\$
0178	00B3	09A0	MSG3	DATA	FIN3-\$*2-1%8+' '
0179	00B4	CECF		TEXT	'NO D.C.'
	00B5	AOC4			
	00B6	AEC3			
	00B7	AEA0			
0180		00B8	FIN3	EQU	\$
0181	00B8	15A0	MSG4	DATA	FIN4-\$*2-1%8+' '
0182	00B9	C4C1		TEXT	'DATA TRANSFER ERROR'
	00BA	D4C1			
	00BB	A0D4			
	00BC	D2C1			
	00BD	CED3			
	00BE	C6C5			
	00BF	D2A0			
	00C0	C5D2			
	00C1	D2CF			
	00C2	D2A0			
0183		00C3	FIN4	EQU	\$
0184	00C3		BUFF1	RES	1664

PAGE 0007 MM/DD/YY 01:00:25

MACRO2 (A2) SI = WS2:S B0=

0185	0743		BUFF2	RES	1664
0186				END	

0000 ERRORS
0000 WARNING

MACRO2 (A2) END

A P P E N D I X 8 . 5

DATA LOGGING PROCEDURE

After loading the disks into the disk drive, the light protect of the right unit must be on, a command was typed on the Teletype to start the conversion process (the command varies with test to be carried out) as in Appendix 8.6. The method of starting the conversion was as follows:-

1. Select the required crank angle degree for reading.
2. Connect the pulse trigger of the T.D.C. and its required degree to the real-time clock input
3. Type the required command on the Teletype to start the conversion process. This includes the number of the cylinder to be filled, the number of the channels to be loaded and the number of the data points to be logged.
4. The computer must respond and give a message after each command if not, the command was typed again until the correct message appeared.
5. A message of "Ready" appears on the Teletype, then the required cylinder, channel and the number of data was typed into the computer before pressing "Return" function the protect light of the data disk must be off.
6. A message of "Finish" must be appear, i.e. the Logging process is finished, if the data was not logged properly a message of "DATA transfer error" appeared on the Teletype.

A P P E N D I X 8 . 6

THE INSTRUCTIONS TO START THE LOADING AND CONVERSION PROCESS

The following commands are typed on the Teletyped in order to start the loading and conversion process. They are as follows:-

1. /As BI = F0. WS2:B (As binary input is equal to the number of the drive unit zero and the name of ML programme.)
2. /Ex OS:LDR,NL,TE (Excute the loading instruction, this maintains the operating system monitor in core and re-locates any programmes it loads so that they start at the first address after the monitor. The no-list (NL) and terminate (TE) parameters simply supress unwanted output.)

The computer replies:

OS:LDR (Co)

OS:LDR (Co) END (Confirming successful loading)

3. /BE 17DA (This is the first address after monitor and starts program)

The computer replies:

READY - F1

4. /RE a, b, c, d, e
 - a = 1st Cylinder (numbered 0-76)
 - b = Last Cylinder
 - c = 1st Channel

d = Last Channel

e = Number of readings

The computer replies either

FINISHED

and now another crank angle degree can be selected OR

DATA TRANSFER ERROR

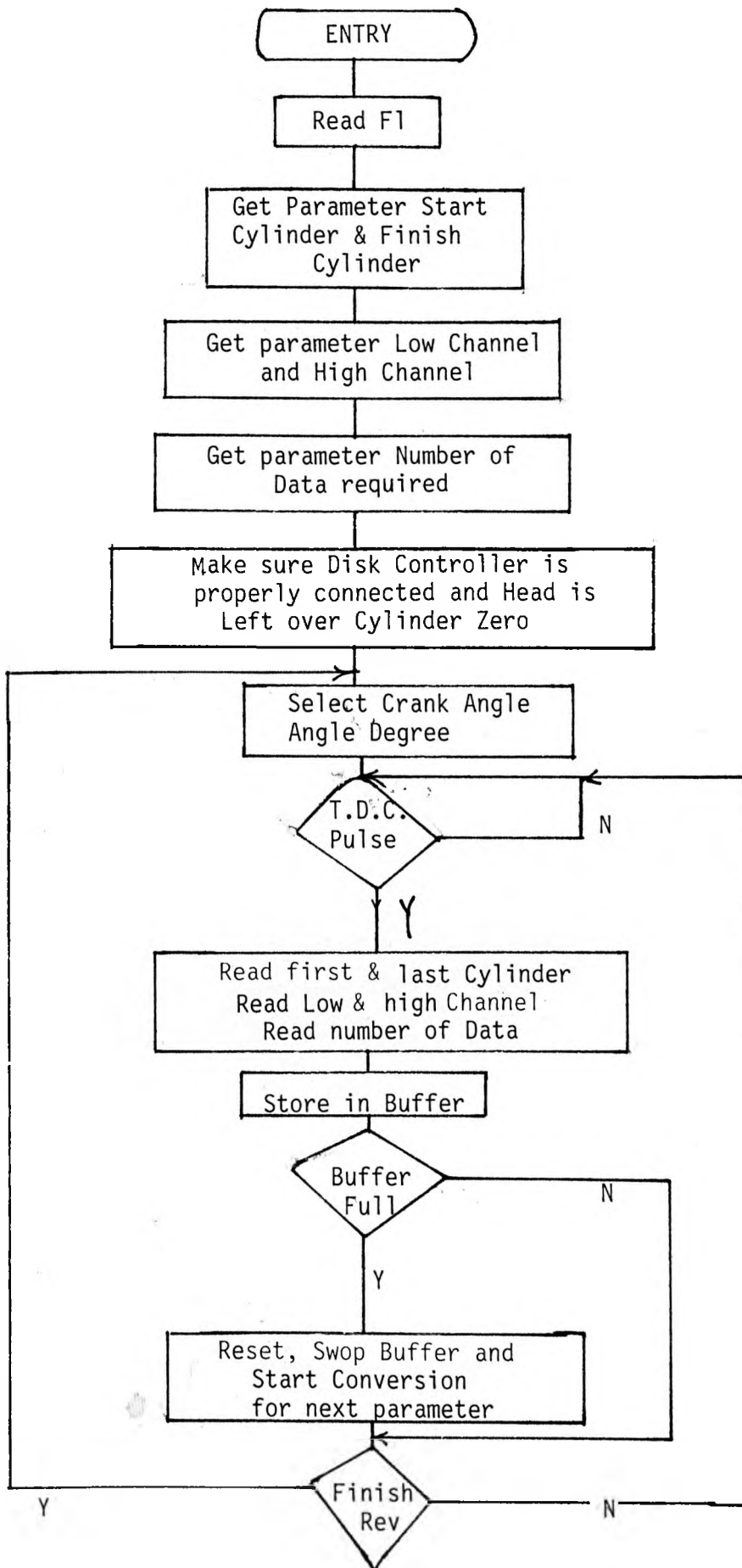
and in this case re-started from command 1. It should

be pointed out that after each command return must

be pressed.

A P P E N D I X 8.7

FLOW CHART OF DATA LOGGING



A P P E N D I X 8.8

THE PROCEDURE TO READ THE ALPHA-DISK ON PDP11 COMPUTER

To run the ALPHA program, place the ALPHA disketter to be read in one of the floppy disk drives and type ALPHA at a logged-in terminal. To the prompt ALF the name of the file to be created must be entered and must include the version number. e.g. ALF filename DAT;1. The program then requests the drive number 0 or 1 it depends if the left or right-hand drive was used.

The first and last cylinder must be entered separated by a comma. When the sign (>) appears the diskette should be removed from the drive.

To access the data using Basic, declare a virtual array in the following manner:

```
DIM n, I% (m) OPEN "filename.DAT;1" As FILE n
```

where 'n' is the logical unit number associated with file, and m is calculated as follows:

$$m = (\text{number of cylinder}) * 1664 - 1$$

e.g. for the maximum number of cylinder (19) "m" would be:

$$19 * 1664 - 1 = 31615$$

The array elements are integer Basic variables.

Example:

To convert one such value to volts:

$$V = I\% (j) * 2.5/1024.$$

CV400010

APPENDIX 8.9

CV400020

CV400030

COMPUTER PROGRAMM TO CALCULATE GAS TEMPERATURE

CV400040

FROM PRESSURE

CV400050

CV400060

CV400070

CV400080

REAL X1(200),X2(200),X3(200),X4(200),VO(200),T(200)

CV400090

REAL Y(200),Y1(200),P(200)

CV400100

1000 FORMAT(F8.1,F8.3,F13.3,F8.3)

CV400110

READ(1,1000)(X1(I),X2(I),X3(I),X4(I),I=1,145)

CV400120

VC=46.0909

CV400130

N1=24.1978

CV400140

L1=11.1125

CV400150

D1=253.3854

CV400160

B1=((0.790-0.369)*(552.8614))/(49.060)

CV400170

DO 31 I=1,145

CV400180

P(I)=X4(I)-1.000

CV400190

Y(I)=SIN((4.0*ATAN(1.0)/180)*X1(I))

CV400200

Y1(I)=COS((4.0*ATAN(1.0)/180)*X1(I))

CV400210

VO(I)=VC+D1*(1.0+N1-(((N1)**2)-((Y(I))**2))**0.5-Y1(I))

CV400220

T(I)=(P(I)*VO(I))/B1

CV400230

T(I)=T(I)+273.0

CV400240

31 CONTINUE

CV400250

WRITE(2,100)(X1(I),P(I),VO(I),T(I),I=1,145)

CV400260

100 FORMAT(F8.1,F8.3,F10.4,F8.3)

CV400270

STOP

CV400280

END

CV400290

Appendix 8.10

Computer Programm to obtain the corrected
gas temperature

```

10 DIM S(200),T(200),V(200),X(200),S(200),R(200)
20 OPEN "LP:" FOR OUTPUT AS FILE #1
30 OPEN "DATA,S1;1" FOR INPUT AS FILE #9
40 PRINT "NUMBER OF DATA POINTS" \ INPUT N9
50 PRINT "READING DATA ORDINATES" \ FOR I=1 TO N9
60 INPUT #9,T(I),V(I),X(I) \ NEXT I
70 PRINT "FINISHED READING"
80 A0=.654 \ B0=.26 \ N=.48 \ D=10*(10^-6) \ T0=290.8
90 R0=21.61*(10^3) \ S1=133.888 \ U0=1.7919*(10^-5)
100 K0=2.5389*(10^-2) \ T1=755.456 \ R1=14.854
110 FOR I=1 TO N9
120 G(I)=T(I)
130 L=(T1*(B0^2,3))/(T0+T1) \ M=(B0^2,3)/(T0+T1)
140 J=(T1*(A0^1,25))/(T0+T1) \ K=(A0^1,25)/(T0+T1)
150 F1=(L+M*G(I))^(,208/N)
160 C1=(,573*4*K0)/(R0*S1*X(I)*(D^2)*(T0^,8))
170 C2=(,3*4*K0*(D^,48)*(T0^,365))/(R0*S1*X(I)*(D^2)*(T0^,8)*(U0^,48))
180 F2=C1*(G(I)^,8)*(L+M*G(I))^(,208/N)
190 R(I)=T1/(R1*(V(I)^2)) \ S(I)=1/(R1*(V(I)^2))
200 F3=C2*(G(I)^(,435))*((R(I)-S(I)*G(I))^(,-1))-((J+K*G(I))^(,8))^(,48/N)
210 F4=F2+F3
220 F5=T(I)-G(I)+(F1/F4)
230 F6=(,208/N)*M*(L+M*G(I))^(,208/N)-1)
240 F7=C1*,8*(G(I)^(,-2))*((L+M*G(I))^(,208/N))
250 F8=C1*(G(I)^,8)*M*(,208/N)*((L+M*G(I))^(,208/N)-1)
260 F9=F7+F8
270 F0=C2*(,435)*(G(I)^(,-,565))
280 P=((R(I)-S(I)*G(I))^(,-1))-((J+K*G(I))^(,8))^(,48/N)
290 Q=F0*P
300 A1=C2*(G(I)^(,435))*((,48/N)
310 A2=((R(I)-S(I)*G(I))^(,-1))-((J+K*G(I))^(,8))^(,48/N)-1)
320 A=A1*A2
330 B=(S(I)*((R(I)-S(I)*G(I))^(,-2)))-(.8*K*((J+K*G(I))^(,-,2)))
340 Z=-1+((F4*F6)-F1*(F9+Q+(A*B)))/(F4^2)
350 PRINT "Z=";Z \ PRINT #1,"Z=";Z
360 PRINT "G(I)=";G(I) \ PRINT #1,"G(I)=";G(I)
370 G1=G(I)-(F5/Z)
380 PRINT "G1=";G1 \ PRINT #1,"G1=";G1
390 PRINT "ABS(G1-G(I))="; (G1-G(I))
400 REM IF ABS(G1-G(I))>10^-5 GOTO 130
410 REM IF ABS(G1-G(I))<10^-5 GO TO 470
420 PRINT "ABS(G1-G(I))="; (G1-G(I))
430 PRINT #1,"ABS(G1-G(I))="; (G1-G(I))
440 PRINT "G1=";G1 \ PRINT "G(I)=";G(I)
450 PRINT #1,"G1=";G1 \ PRINT #1,"G(I)=";G(I)
460 NEXT I
470 CLOSE

```

APPENDIX 8.11

Computer Program to Calculate Heat Flux

This program is written in BASIC language and calculates the Heat Flux at various crank angles using equation (3.11) to (3.18) CAPTER THREE.

The various notations used are given below:

- A(K),b(K)- Fourier Coefficients in equation(3.13)
- C - Specific heat of the cylinder material
- D - Density of the cylinder wall material
- K - Harmonic number in equation (3.15)
- L - Thickness of wall
- N - Number of data points
- Q - Heat Flux in equation (3.18)
- R - Constant in equation (3.16)
- T1 - Coolent side wall temperature
- U - Thermal diffusivity in equation (3.11)
- W - Angular frequency which is equal to 2π times the cycle repetition rate
- Z - Thermal conductivity of the cylinder wall material

Data for this program was taken from [Grey Cast Iron grade 17,b.s. 1452 1961

]

D= 7233.79 Kg/m³ for Cast Iron

C= 544.31 J/Kg.C°

L= 0.033m, surface thermocouple length

N= varies between 24,72 and 144 at 30,10 and 5 degree intervals respectively

T1= It depends on the test conditions

W= It depends on the test speed

Z= 58.618 watt/m.C°

The output calculated the Heat Flux in watt/m²

Appendix 8.11

```
1 OPEN 'LP:' FOR OUTPUT AS FILE #1
5 DIM A(80),B(80),Y(80)
10 J=0
15 PRINT "NUMBER OF DATA POINTS" \ INPUT N \ IF N/2-INT(N/2)<>0 GO TO 25
20 J=1
25 N=N-1 \ PRINT "INPUT DATA ORDINATES"
30 FOR I=0 TO N \ INPUT Y(I) \ NEXT I
35 PRINT "FOURIER COEFFICIENTS" \ PRINT "A(K)", "B(K)", "K"
40 FOR K=0 TO INT(N/2)+J \ A(K)=0 \ B(K)=0 \ FOR I=0 TO N
45 A(K)=A(K)+2*Y(I)*COS(6.28318*K*I/(N+1))/(N+1)
50 IF K=0 GO TO 60 \ IF J<>1 GO TO 55 \ IF K=INT(N/2)+1 GO TO 60
55 B(K)=B(K)+2*Y(I)*SIN(6.28318*K*I/(N+1))/(N+1)
60 NEXT I \ PRINT A(K),B(K),K
61 PRINT #1,A(K),B(K),K
62 NEXT K
65 PRINT "INPUT D,C,Z,L,T1,W" \ INPUT D,C,Z,L,T1,W
70 U=Z/(D*C) \ PRINT "U";U
72 PRINT #1,"U";U
75 FOR I=0 TO N
80 Y(I)=A(0)/2/L-T1/L \ PRINT "Y(I)=";Y(I)
81 PRINT #1,"Y(I)=";Y(I)
85 FOR K=1 TO INT(N/2)+1
90 R=((K*W)/(2*U))^.5
92 PRINT #1,"R=";R \ PRINT "R=";R
95 Y(I)=Y(I)+R*((B(K)-A(K))*SIN(K*I*6.28318/(N+1)))
96 PRINT "Y(I)=";Y(I) \ PRINT #1,"Y(I)=";Y(I)
100 Y(I)=Y(I)+R*((B(K)+A(K))*COS(K*I*6.28318/(N+1)))
105 NEXT K
110 PRINT "HEAT FLUX" \ Q=2*Y(I)
115 PRINT Q
118 PRINT "Y(I)=";Y(I)
119 PRINT #1,"Y(I)=";Y(I)
125 PRINT "HEAT FLUX=";Q
130 PRINT #1,"HEAT FLUX=";Q
132 NEXT I
133 PRINT "MORE=? (1 OR 9)"
134 INPUT S \ IF S=1 GO TO 25 \ IF S=9 GO TO 135
135 CLOSE
```

APPENDIX 8.12

00010		RN
00020		RN
00030	COMPUTER PROGRAM TO SOLVE EQUATION 5.21	RN
00040		RN
00050	-----	RN
00060	RE = REYNOLD NUMBER	RN
00070	RO = DENSITY	RN
00080	UM = DYNAMIC VISCOSITY	RN
00090	UN1= EXPERIMENTAL NUSSELT NUMBER	RN
00100	UN2= PREDICTED NUSSELT NUMBER	RN
00110	T1 = TEMPERATURE DIFFERENCE	RN
00120	S = SPECIFIC HEAT	RN
00130	P = THERMAL CONDUCTIVITY OF THE GAS	RN
00140	Z = VELOCITY RATIO	RN
00150	Z1 = GAS RATIO	RN
00160	EN = ENERGY NUMBER	RN
00170	D = CYLINDER BORE DIAMETER	RN
00180		RN
00190	-----	RN
00200	MIAN PROGRAM	RN
00210	-----	RN
00220		RN
00230	INTEGER IWORK(450)	RN
00240	REAL X1(500),X2(500),X3(500),X4(500),X5(500),X6(500),X7(500),	RN
00250	* RE(500),RO(500),UM(500),UN(500),A(452,7),XX(50),F1(500),	RN
00260	* T1(500),P(500),Z(500),Q1(500),Q2(500),Q3(200),ZZ(500),	RN
00270	* UN1(500),EN(500),Z1(500),UN2(500),QS(500),S(500),	RN
00280	* PI1(500),PI2(500),PI3(500),PI4(500),PI5(500)	RN
00290	D=7.62E-2	RN
00300	N1=452	RN


```

00310 READ(1,100)(X1(I),X2(I),X3(I),X4(I),X5(I),X6(I),X7(I),I=1,234) RN
00320 C WRITE(3,100)(X1(I),X2(I),X3(I),X4(I),X5(I),X6(I),X7(I),I=1,234) RN
00330 N=0 RN
00340 DO 99 I=1,234 RN
00350 IF(I.LE.26) GOTO 1 RN
00360 IF(I.LE.52) GOTO 2 RN
00370 IF(I.LE.78) GOTO 3 RN
00380 IF(I.LE.104) GOTO 1 RN
00390 IF(I.LE.130) GOTO 2 RN
00400 IF(I.LE.156) GOTO 3 RN
00410 IF(I.LE.182) GOTO 1 RN
00420 IF(I.LE.208) GOTO 2 RN
00430 IF(I.LE.234) GOTO 3 RN
00440 1 X=2.225 RN
00450 GO TO 170 RN
00460 2 X=3.708 RN
00470 GO TO 170 RN
00480 3 X=5.563 RN
00490 170 T1(I)=X5(I)-X2(I) RN
00500 UM(I)=(3.16*(X5(I)**0.645))/(10000000.0) RN
00510 S(I)=0.224+(0.471*(X5(I)-273.0)/10000.0) RN
00520 P(I)=(UM(I)*S(I)*6234.0)/(0.7) RN
00530 UN1(I)=(X3(I)*0.0762)/(P(I)*T1(I)) RN
00540 EN(I)=((X4(I)*100000.0*X7(I)*0.0762)/(P(I)*X5(I))) RN
00550 IF(UN1(I) .LE. 0.0) GO TO 99 RN
00560 IF(EN(I) .LE. 0.0) GO TO 99 RN
00570 N=N+1 RN
00580 UM(N)=UM(I) RN
00590 T1(N)=T1(I) RN
00600 S(N)=S(I) RN
00610

```

00620	P(N)=P(I)	RN
00630	EN(N)=EN(I)	RN
00640	UN1(N)=UN1(I)	RN
00650	RO(N)=(X4(I)*100000.0)/(287.0*X5(I))	RN
00660	UN(N)=(UM(N)/RO(N))*1.488	RN
00670	RE(N)=X6(I)*D/UN(N)	RN
00680	Z(N)=(X6(I)+X7(I))/X	RN
00690	Z1(N)=X5(I)/T1(N)	RN
99	CONTINUE	RN
00700	DO 700 I= 1,N	RN
00710	IF(Z1(I) .LE. 0.0) Z1(I)=-Z1(I)	RN
00720	PI2(I)=ALOG10(RE(I))	RN
00730	PI3(I)=ALOG10(Z(I))	RN
00740	PI4(I)=ALOG10(Z1(I))	RN
00750	PI5(I)=ALOG10(EN(I))	RN
00760	PI1(I)=ALOG10(UN1(I))	RN
00770	A(I,1)=1.0	RN
00780	A(I,2)=PI2(I)	RN
00790	A(I,3)=PI3(I)	RN
00800	A(I,4)=PI4(I)	RN
00810	A(I,5)=PI5(I)	RN
00820	F1(I)=PI1(I)	RN
00830	WRITE(3,305)A(I,1),A(I,2),A(I,3),A(I,4),A(I,5),F1(I),I	RN
00840	700 CONTINUE	RN
00850	305 FORMAT(6F10.3,I6)	RN
00860	C STOP	RN
00870	306 IFAIL=1	RN
00880	CALL E02GAF(N,A,N1,F1,7,0.0,XX,RESID,RANK,ITER,IWORK,IFAIL)	RN
00890	WRITE(3,301)(XX(I),I=1,5)	RN
00900	301 FORMAT(5F10.3)	RN
00910	SUM=0	RN

```

00920      SUM1=0                                RN
00930      DO 302 I=1,N                          RN
00940      UNG2=((10.)**XX(1))*(RE(I)**XX(2))*(Z(I)**XX(3))*(Z1(I)**XX(4))RN
00950      UNG2=UNG2*(EN(I)**XX(5))              RN
00960      RES=UNG2-UN1(I)                       RN
00970      RES1=RES*100./UN1(I)                 RN
00980      SUM=SUM+RES**2                       RN
00990      SUM1=SUM1+RES1                      RN
01000      WRITE(3,303)UN1(I),UNG2,RES,RES1     RN
01010      302  CONTINUE                        RN
01020      SD= SQRT(SUM)/N                      RN
01030      AVER=SUM1/N                          RN
01040      WRITE(3,*)SD,AVER                    RN
01050      303  FORMAT(4F15.5)                  RN
01060      100  FORMAT(F8.1,F10.3,F13.3,F8.3,F10.3,2F10.4) RN
01070      200  FORMAT(F8.1,F7.3,2F9.3,2F10.4) RN
01080      300  FORMAT(5F12.4,I6)              RN
01090      C400 FORMAT(F7.1,2F10.3)           RN
01100      STOP                                RN
01110      END                                  RN
01120

```

APPENDIX 8.13

SET OF DATA & RESULTS

C.R = 8
 SPEED = 1000 R.P.M
 POSITION = 1
 MEASUREMENT AT CA = 30 DEG.

CA DEG. DEG.	WALL TEMP. DEG.K	ABS. PRESSURE BAR	THERMO. TEMP. DEG.K	GAS TEMP. DEG.K	AVERAGE VELOCITY M/SEC	TURBULENCE INTENSITY M/SEC
0.0	351.860	1.175	314.430	314.430	1.676	0.652
30.0	351.790	1.225	313.315	312.763	9.877	4.532
60.0	351.701	1.285	315.630	316.595	7.345	2.990
90.0	351.660	1.305	315.551	315.521	10.825	4.948
120.0	351.608	1.245	316.730	317.231	7.571	3.639
150.0	351.570	1.295	312.189	310.256	8.415	4.771
180.0	351.490	1.295	305.800	302.701	5.053	3.294
210.0	351.420	1.595	316.495	321.432	4.738	2.183
240.0	351.360	1.845	327.574	332.760	3.842	2.200
270.0	351.290	2.295	342.970	349.743	3.842	2.743
300.0	352.140	3.065	406.410	423.126	5.359	3.665
330.0	354.120	8.763	479.150	496.181	3.849	1.824
360.0	356.670	21.985	535.025	556.620	3.160	1.014
390.0	356.450	6.945	481.450	456.305	3.436	1.451
420.0	355.820	2.694	439.284	409.254	2.317	0.864
450.0	355.200	1.715	376.770	356.570	1.635	0.653
480.0	354.370	1.305	348.080	330.675	1.058	0.880
510.0	353.470	1.205	308.930	300.108	5.850	2.367
540.0	353.270	1.045	298.030	293.892	12.947	6.666
570.0	353.080	1.025	303.256	305.635	6.717	3.424
600.0	352.900	0.925	304.700	305.429	4.226	2.052
630.0	352.790	1.155	309.894	312.265	6.264	2.964
660.0	352.570	1.095	314.868	312.475	5.144	2.352
690.0	352.190	1.185	314.777	314.733	4.347	2.139
720.0	351.860	1.175	314.430	314.430	1.676	0.652

CONTINUED ---->

C.R = 12
 SPEED = 1000 R.P.M
 POSITION = 1
 MEASUREMENT AT CA = 30 DEG.

CA DEG. DEG.	WALL TEMP. DEG.K	ABS. PRESSURE BAR	THERMO. TEMP. DEG.K	GAS TEMP. DEG.K	AVERAGE VELOCITY M/SEC	TURBULENCE INTENSITY M/SEC
0.0	365.250	1.491	332.720	332.720	0.234	0.002
30.0	365.160	1.011	331.950	331.654	14.329	5.931
60.0	364.950	1.071	330.889	330.487	10.032	4.132
90.0	364.880	1.131	318.070	312.915	15.161	6.114
120.0	364.790	1.171	313.250	311.084	8.602	4.972
150.0	364.630	1.221	312.410	312.029	9.163	5.053
180.0	364.550	1.421	310.060	308.952	5.911	3.799
210.0	364.410	1.751	333.050	342.887	5.677	2.867
240.0	364.350	2.341	355.060	364.407	4.313	2.903
270.0	364.240	3.371	375.438	387.226	4.647	3.766
300.0	365.350	4.959	429.119	445.556	6.665	4.248
330.0	367.690	13.091	512.298	530.669	3.931	2.349
360.0	370.670	46.521	557.466	578.671	2.567	0.778
390.0	370.430	9.461	510.220	485.327	4.198	2.206
420.0	369.510	3.641	482.939	442.608	2.556	1.129
450.0	368.950	2.271	407.050	371.860	2.415	0.871
480.0	368.420	1.561	351.050	338.297	1.598	1.560
510.0	367.840	1.341	329.000	318.598	7.041	3.976
540.0	367.240	1.151	313.480	307.713	13.871	8.996
570.0	366.860	1.111	316.989	318.569	7.504	3.978
600.0	366.490	1.071	319.270	320.348	5.189	2.726
630.0	365.970	1.131	326.177	329.204	7.137	3.623
660.0	365.660	1.281	325.662	325.423	5.990	3.186
690.0	365.450	1.391	331.370	334.218	4.808	2.762
720.0	365.250	1.501	332.720	332.720	0.234	0.002

CONTINUE =====>

C.R = 10
 SPEED = 600 R.P.M
 POSITION = 1
 MEASUREMENT AT CA = 30 DEG.

CA DEG. DEG.	WALL TEMP. DEG.K	ABS. PRESSURE BAR	THERMO. TEMP. DEG.K	GAS TEMP. DEG.K	AVERAGE VELOCITY M/SEC	TURBULENCE INTENSITY M/SEC
0.0	347.250	1.050	315.930	315.930	0.519	0.432
30.0	347.190	1.070	315.697	315.643	8.031	3.020
60.0	347.100	1.110	313.627	313.013	5.906	2.009
90.0	346.980	0.741	313.840	313.900	9.389	3.284
120.0	346.900	0.450	312.317	311.866	5.980	1.975
150.0	346.850	1.230	311.340	311.062	5.701	2.645
180.0	346.700	1.260	308.350	307.431	3.874	1.839
210.0	346.610	1.421	319.595	323.030	4.834	1.921
240.0	346.560	1.611	330.330	333.624	3.156	1.041
270.0	346.420	2.280	347.730	352.677	3.258	1.229
300.0	347.490	2.680	413.600	422.267	4.520	2.532
330.0	349.510	11.369	474.499	488.394	3.196	0.815
360.0	351.840	27.220	505.090	521.026	1.927	0.447
390.0	351.530	5.210	435.528	422.758	3.333	1.538
420.0	350.410	2.600	413.906	385.149	4.206	0.724
450.0	349.950	1.650	343.500	333.923	2.958	0.499
480.0	349.030	1.390	328.220	323.387	3.267	1.104
510.0	348.760	1.110	313.553	309.141	4.896	2.502
540.0	348.130	0.990	304.040	301.755	11.827	6.379
570.0	347.810	0.880	312.540	315.205	5.879	2.447
600.0	347.760	0.801	315.870	315.823	4.588	1.485
630.0	347.700	0.880	317.870	317.245	4.812	2.736
660.0	347.580	0.970	316.350	315.890	3.986	2.190
690.0	347.490	0.931	313.510	312.615	3.152	1.755
720.0	347.250	1.050	315.930	315.930	0.519	0.432

CONTINUE =====>

C.R = 10
 SPEED = 1000 R.P.M
 POSITION = 1
 MEASUREMENT AT CA = 30 DEG.

CA DEG. DEG.	WALL TEMP. DEG.K	ABS. PRESSURE BAR	THERMO. TEMP. DEG.K	GAS TEMP. DEG.K	AVERAGE VELOCITY M/SEC	TURBULENCE INTENSITY M/SEC
0.0	358.310	1.110	320.182	319.173	0.252	0.156
30.0	358.280	1.100	320.069	320.036	13.496	5.706
60.0	358.240	1.150	319.601	319.415	9.828	3.819
90.0	358.190	1.150	321.500	322.213	14.486	5.612
120.0	358.180	1.230	322.450	322.849	8.247	4.323
150.0	358.060	1.290	319.360	318.051	8.975	4.987
180.0	357.920	1.310	307.230	301.249	5.592	3.486
210.0	357.880	1.520	325.322	333.339	5.471	2.552
240.0	357.730	1.790	338.080	343.929	4.290	2.716
270.0	357.020	2.464	360.550	369.929	4.325	3.644
300.0	358.570	4.270	424.170	438.820	6.510	4.197
330.0	360.850	12.210	493.290	510.043	4.875	2.274
360.0	363.350	29.905	545.417	570.521	3.255	1.189
390.0	363.190	8.680	492.639	468.267	3.948	1.806
420.0	362.250	3.220	475.770	427.876	2.413	0.936
450.0	361.830	1.740	383.480	363.353	1.944	0.756
480.0	360.950	1.440	341.419	327.713	1.206	1.038
510.0	360.030	1.260	323.722	312.783	6.648	3.741
540.0	359.140	1.020	307.450	301.200	13.482	7.231
570.0	358.830	1.020	326.540	334.658	7.278	3.532
600.0	358.750	1.150	329.000	330.141	4.911	2.247
630.0	358.690	1.090	331.080	331.976	6.938	3.264
660.0	358.590	1.020	329.230	328.443	5.800	3.053
690.0	358.460	1.120	325.880	324.326	4.759	2.556
720.0	358.310	1.110	320.182	320.182	0.252	0.156

CONTINUE ==>>>>

C.R = 10
 SPEED = 1500 R.P.M
 POSITION = 1
 MEASUREMENT AT CA = 30 DEG.

CA DEG. DEG.	WALL TEMP. DEG.K	ABS. PRESSURE BAR	THERMO. TEMP. DEG.K	GAS TEMP. DEG.K	AVERAGE VELOCITY M/SEC	TURBULENCE INTENSITY M/SEC
0.0	365.630	1.072	329.430	329.430	0.181	0.013
30.0	365.620	1.042	326.146	324.308	15.440	7.326
60.0	365.510	1.122	326.486	326.682	11.919	5.663
90.0	365.400	1.152	326.880	327.087	16.497	8.117
120.0	365.320	0.917	322.440	319.816	12.006	5.508
150.0	365.260	1.260	319.200	317.310	10.834	6.564
180.0	365.150	1.332	313.181	309.332	8.482	4.663
210.0	365.010	1.602	325.223	332.361	7.232	3.813
240.0	364.920	1.892	347.577	360.686	6.135	3.128
270.0	364.860	2.602	372.551	385.980	7.240	4.994
300.0	365.920	4.712	430.290	454.911	8.114	5.181
330.0	368.030	14.102	534.897	552.382	5.135	2.865
360.0	370.760	30.712	570.850	601.981	4.312	1.620
390.0	370.550	9.642	504.048	473.259	6.095	2.338
420.0	369.490	3.222	482.450	437.551	4.019	2.243
450.0	369.190	1.762	413.400	372.960	2.761	1.743
480.0	368.210	1.442	355.200	330.599	2.069	1.155
510.0	367.670	1.196	337.375	324.804	7.223	3.308
540.0	367.170	0.892	316.956	314.084	16.449	8.740
570.0	366.890	1.096	321.695	324.506	9.241	4.669
600.0	366.360	1.158	322.592	323.177	7.835	3.229
630.0	366.160	1.312	330.498	335.449	9.478	5.832
660.0	365.990	1.322	335.690	338.717	8.016	4.887
690.0	365.830	1.123	327.345	322.075	6.616	3.897
720.0	365.630	1.072	329.430	329.430	0.181	0.013

CONTINUE ==>>>

C.R = 8
 SPEED = 1000 R.P.M
 POSITION = 1
 MEASUREMENT AT CA = 30 DEG.

CA DEG	RE NO. 1000	(U+U)/VP	TG/ T	ENERGY NO. 1000	EXP. NU NO. 1000	PRED. NU NO. 1000	EXP.Q KW/SQ.M	PRED.Q KW/SQ.M
0.0	8.66	0.63	-8.40	0.71	8.37	5.76	-106.69	-73.50
30.0	53.69	3.89	-8.01	5.23	6.47	5.14	-85.75	-68.03
60.0	41.05	2.79	-9.02	3.54	5.75	6.08	-69.10	-73.10
90.0	61.79	4.25	-8.73	5.99	5.14	5.77	-63.41	-71.24
120.0	40.86	3.02	-9.23	4.17	4.55	5.87	-53.68	-69.22
150.0	49.00	3.56	-7.51	5.90	3.67	4.91	-51.14	-68.52
180.0	30.64	2.25	-6.20	4.25	3.66	4.18	-59.16	-67.66
210.0	32.06	1.87	-10.72	3.13	4.75	8.32	-49.28	-86.34
240.0	28.41	1.63	-17.89	3.44	9.84	13.38	-64.90	-88.27
270.0	32.56	1.78	-226.08	4.90	46.74	129.92	-26.58	-73.88
300.0	44.33	2.43	5.96	6.29	6.82	5.75	204.27	172.08
330.0	70.06	1.53	3.49	6.79	7.43	5.70	501.03	384.39
360.0	119.45	1.13	2.78	7.75	8.50	7.41	879.46	766.13
390.0	56.89	1.32	4.57	4.95	6.41	6.76	285.40	300.90
420.0	17.80	0.86	7.66	1.38	5.57	6.12	122.65	134.68
450.0	10.03	0.62	260.27	0.84	91.18	107.27	46.55	54.77
480.0	5.59	0.52	-13.96	0.98	6.31	5.57	-52.83	-46.59
510.0	33.48	2.22	-5.62	2.88	8.41	4.99	-147.92	-87.71
540.0	66.51	5.29	-4.95	7.30	1.48	2.99	-28.43	-57.59
570.0	31.73	2.74	-6.44	3.44	4.52	3.73	-71.61	-59.03
600.0	18.04	1.69	-6.43	1.86	1.86	3.55	-29.54	-56.22
630.0	32.19	2.49	-7.71	3.23	3.83	4.81	-52.66	-66.06
660.0	25.04	2.02	-7.79	2.43	4.18	4.73	-56.88	-64.37
690.0	22.62	1.75	-8.40	2.36	10.11	5.33	-129.07	-68.05
720.0	8.66	0.63	-8.40	0.71	8.37	5.76	-106.69	-73.50

CONTINUE =====>

C.R = 12
 SPEED = 1000 R.P.M
 POSITION = 1
 MEASUREMENT AT CA = 30 DEG.

CA DEG	RE NO. 1000	(U+U)/VP	TG/ T	ENERGY NO. 1000	EXP. NU NO. 1000	PRED. NU NO. 1000	EXP.Q KW/SQ.M	PRED.Q KW/SQ.M
0.0	1.40	0.06	-10.23	0.00	8.26	8.23	-95.28	-94.95
30.0	58.37	5.46	-9.90	5.11	7.95	5.04	-94.23	-59.75
60.0	43.55	3.82	-9.59	3.79	8.41	5.22	-102.35	-63.53
90.0	76.03	5.74	-6.02	6.51	4.45	3.67	-78.42	-64.77
120.0	45.10	3.66	-5.79	5.53	4.71	3.51	-85.54	-63.73
150.0	49.84	3.83	-5.93	5.84	5.02	3.72	-89.46	-66.33
180.0	38.04	2.62	-5.56	5.19	4.64	3.92	-86.86	-73.35
210.0	37.92	2.30	-15.93	4.04	10.79	11.76	-84.19	-91.72
240.0	34.85	1.95	6393.10	4.93	4253.49	2530.08	-91.78	54.59
270.0	48.92	2.27	16.85	8.29	-5.56	15.34	-50.55	139.44
300.0	81.94	2.94	5.55	10.79	7.26	7.43	255.32	260.98
330.0	95.70	1.69	3.26	11.62	8.07	6.13	656.42	498.31
360.0	192.59	0.90	2.78	11.74	9.64	10.68	1067.79	1183.78
390.0	85.56	1.73	4.22	9.21	7.09	7.25	380.41	388.58
420.0	23.32	0.99	6.05	2.13	6.21	5.50	197.99	175.31
450.0	18.31	0.89	127.79	1.39	76.11	74.16	85.07	82.90
480.0	9.73	0.85	-11.23	2.01	-5.47	5.41	59.15	-58.49
510.0	40.64	2.97	-6.47	4.87	2.63	5.59	-44.56	-94.66
540.0	72.77	6.17	-5.17	10.03	3.02	3.00	-60.23	-59.86
570.0	35.89	3.10	-6.60	4.03	4.72	3.80	-78.34	-63.09
600.0	23.71	2.14	-6.94	2.64	5.42	3.93	-86.34	-62.53
630.0	32.92	2.90	-8.95	3.54	11.77	5.01	-152.28	-64.89
660.0	31.90	2.48	-8.09	3.59	7.67	5.07	-107.75	-71.24
690.0	26.61	2.04	-10.70	3.23	11.03	6.80	-122.53	-75.56
720.0	1.41	0.06	-10.23	0.00	8.26	8.27	-95.28	-95.44

CONTINUE =====>

C.R = 10
SPEED = 600 R.P.M
POSITION = 1
MEASURMENT AT CA = 30 DEG.

CA DEG	RE NO. 1000	(U+U)/VP	TG/ T	ENERGY NO. 1000	EXP. NU NO. 1000	PRED. NU NO. 1000	EXP.Q KW/SQ.M	PRED.Q KW/SQ.M
0.0	2.38	0.43	-10.09	0.42	5.17	3.68	-55.36	-39.44
30.0	37.56	4.97	-10.00	3.00	2.33	3.89	-25.13	-41.91
60.0	29.05	3.56	-9.18	2.10	3.57	3.83	-41.34	-44.31
90.0	30.69	5.70	-9.49	2.28	3.08	2.81	-34.72	-31.64
120.0	12.00	3.57	-8.90	0.84	3.27	1.87	-38.79	-22.13
150.0	31.40	3.75	-8.69	3.09	2.19	3.78	-26.47	-45.76
180.0	22.28	2.57	-7.83	2.25	4.17	3.58	-54.85	-47.19
210.0	28.91	3.04	-13.70	2.43	3.59	6.46	-29.37	-52.90
240.0	20.29	1.89	-25.79	1.42	11.20	15.20	-51.48	-69.85
270.0	28.36	2.02	-91.55	2.26	15.36	34.86	-20.82	80.65
300.0	32.81	3.17	5.65	3.81	6.54	4.28	205.98	134.74
330.0	77.46	1.80	3.52	4.04	7.28	6.15	473.95	400.74
360.0	100.52	1.07	3.08	4.75	8.32	7.66	692.61	637.95
390.0	46.94	2.19	5.94	4.50	6.56	6.38	197.07	191.49
420.0	34.45	2.22	11.09	1.24	5.54	10.08	75.85	138.02
450.0	19.45	1.55	-20.84	0.69	-4.22	13.96	24.07	-79.56
480.0	19.07	1.96	-12.61	1.36	6.79	7.66	-60.53	-68.28
510.0	24.58	3.32	-7.80	2.67	1.69	4.74	-22.47	-63.17
540.0	55.11	8.18	-6.51	6.32	6.64	2.36	-101.89	-36.24
570.0	22.67	3.74	-9.67	2.00	5.13	3.24	-57.08	-36.02
600.0	16.05	2.73	-9.89	1.10	3.06	3.22	-33.40	-35.11
630.0	18.36	3.39	-10.42	2.21	2.22	3.28	-23.20	-34.26
660.0	16.88	2.78	-9.97	1.97	2.79	3.46	-30.21	-37.53
690.0	13.03	2.21	-8.96	1.54	2.40	3.10	-28.34	-36.62
720.0	2.38	0.43	-10.09	0.42	5.17	3.68	-55.36	-39.44

CONTINUE =====>

C.R = 10
 SPEED = 1000 R.P.M
 POSITION = 1
 MEASURMENT AT CA = 30 DEG.

CA DEG	RE NO. 1000	(U+U)/VP	TG/ T	ENERGY NO. 1000	EXP. NU NO. 1000	PRED. NU NO. 1000	EXP.Q KW/SQ.M	PRED.Q KW/SQ.M
0.0	1.20	0.11	-8.16	0.16	5.02	5.25	-67.61	-70.74
30.0	63.44	5.18	-8.37	5.69	3.08	4.78	-40.66	-63.12
60.0	48.45	3.68	-8.23	3.99	3.30	5.02	-44.21	-67.16
90.0	70.39	5.42	-8.96	5.78	2.70	5.30	-33.67	-66.05
120.0	42.72	3.39	-9.14	4.74	2.55	5.52	-31.29	-67.70
150.0	49.98	3.76	-7.95	5.89	3.68	5.02	-50.60	-69.01
180.0	34.58	2.45	-5.32	4.59	3.16	3.68	-59.16	-68.92
210.0	33.23	2.16	-13.58	3.28	4.54	9.53	-39.59	-83.06
240.0	29.14	1.89	-24.92	3.89	15.81	17.20	-79.25	-86.19
270.0	35.88	2.15	28.66	6.34	-7.06	20.59	-34.87	101.70
300.0	70.67	2.89	5.47	9.43	6.94	6.73	241.31	233.92
330.0	117.81	1.93	3.40	11.20	7.83	7.14	570.27	516.29
360.0	160.52	1.20	2.75	11.81	8.75	8.50	957.67	927.93
390.0	78.30	1.55	4.46	7.37	6.87	7.55	328.24	360.70
420.0	20.59	0.90	6.52	1.66	5.83	5.68	162.77	158.70
450.0	11.73	0.73	238.58	0.96	168.50	103.86	96.95	59.75
480.0	7.14	0.60	-9.86	1.30	4.62	4.52	-53.85	-52.66
510.0	37.17	2.80	-6.62	4.44	9.55	5.51	-153.17	-88.32
540.0	64.92	5.59	-5.20	7.41	10.43	2.95	-199.69	-56.45
570.0	29.47	2.92	-13.84	3.02	13.91	6.96	-119.76	-59.87
600.0	22.93	1.93	-11.54	2.22	7.86	6.70	-79.35	-67.65
630.0	30.42	2.75	-12.43	3.03	6.21	6.72	-58.70	-63.55
660.0	24.22	2.39	-10.90	2.70	5.66	5.62	-59.93	-59.57
690.0	22.28	1.97	-9.50	2.53	5.44	5.41	-64.71	-64.31
720.0	1.19	0.11	-8.40	0.16	5.14	5.38	-67.61	-70.76

CONTINUE =====>

C.R = 10
 SPEED = 1500 R.P.M
 POSITION = 1
 MEASURMENT AT CA = 30 DEG.

CA DEG	RE NO. 1000	(U+U)/VP	TG/ T	ENERGY NO. 1000	EXP. NU NO. 1000	PRED. NU NO. 1000	EXP.Q KW/SQ.M	PRED.Q KW/SQ.M
0.0	0.79	0.03	-9.10	0.01	9.18	9.14	-117.05	-116.56
30.0	67.26	4.09	-7.85	6.76	4.22	5.76	-60.66	-82.83
60.0	55.25	3.16	-8.41	5.56	7.14	6.53	-96.99	-88.79
90.0	78.35	4.43	-8.54	8.16	5.58	6.61	-74.91	-88.69
120.0	47.09	3.15	-7.03	4.58	5.60	4.86	-87.85	-76.23
150.0	59.16	3.13	-6.62	7.60	3.80	5.62	-62.41	-92.35
180.0	51.05	2.36	-5.54	5.96	5.31	5.28	-99.77	-99.15
210.0	46.52	1.99	-10.18	5.19	7.00	10.14	-81.04	-117.28
240.0	40.74	1.67	-85.19	4.37	69.15	66.39	-110.02	-105.63
270.0	67.56	2.20	-40.09	9.81	10.21	18.98	-33.75	158.17
300.0	91.61	2.39	5.11	12.06	7.63	7.89	302.02	312.51
330.0	126.07	1.44	3.00	14.22	8.24	7.14	781.54	677.26
360.0	200.13	1.07	2.60	15.06	9.43	9.57	1196.38	1214.86
390.0	131.94	1.52	4.61	10.40	7.84	10.94	368.84	514.96
420.0	33.08	1.13	6.43	3.82	6.41	6.72	188.60	197.90
450.0	16.16	0.81	98.93	2.14	82.61	53.39	119.89	77.48
480.0	12.09	0.58	-8.79	1.43	5.95	5.95	-78.98	-78.95
510.0	36.03	1.89	-7.58	3.49	4.93	7.05	-73.74	-105.38
540.0	64.66	4.53	-5.92	7.29	5.79	3.95	-104.56	-71.38
570.0	42.30	2.50	-7.66	4.53	6.49	5.91	-95.77	-87.23
600.0	38.15	1.99	-7.48	3.33	11.43	6.33	-171.47	-95.02
630.0	49.18	2.75	-10.92	6.39	9.42	8.77	-103.22	-96.13
660.0	41.25	2.32	-12.42	5.31	11.66	9.96	-114.27	-97.62
690.0	31.42	1.89	-7.36	3.92	6.75	5.75	-102.35	-87.23
720.0	0.79	0.03	-9.10	0.01	9.18	9.14	-117.05	-116.56

CONTINUE =====>